INFN

A
N
N
U
A
L

R
E
P
O
R
T

2
0
1
3

Annual Report 2013

Laboratori Nazionali del Gran Sasso

Cover image: GERDA Experiment

© Markus Knapp - Univ. of Tübingen

Annual Report 2013

LNGS Director   Prof. Stefano Ragazzi

Editor   Dr. Roberta Antolini

Technical Assistants   Dr. Alessia Giampaoli
                                 Mr. Marco Galeota

INFN

Laboratori Nazionali del Gran Sasso

Annual Report 2013

Contents

THE BOREXINO EXPERIMENT

The Borexino collaboration
Spoke-persons: C. Galbiati, M. Pallavicini, G. Ranucci

G. Bellini[h], J. Benziger[k], D. Bick[s], G. Bonfini[e], D. Bravo[q], B. Caccianiga[h], F. Calaprice[l], A. Caminata[c], P. Cavalcante[e], A. Chavarria[l], A. Chepurnov[r], D. D'Angelo[h], S. Davini[t], A. Derbin[m], A. Empl[t], A. Etenko[g], K. Fomenko[b,e], D. Franco[a], C. Galbiati[l], S. Gazzana[e], C. Ghiano[c], M. Giammarchi[h], M. Göger-Neff[n], A. Goretti[l], C. Hagner[s], E. Hungerford[t], Aldo Ianni[e], Andrea Ianni[l], V. Kobychev[f], D. Korablev[b], G. Korga[t], D. Kryn[a], M. Laubenstein[e], T. Lewke[n], E. Litvinovich[g], F. Lombardi[e], P. Lombardi[h], L. Ludhova[h], G. Lukyanchenko[g], I. Machulin[g], S. Manecki[q], W. Maneschg[i], S. Marcocci[c], Q. Meindl[n], E. Meroni[h], M. Meyer[s], L. Miramonti[h], M. Misiaszek[d], P. Mosteiro[l], V. Muratova[m], L. Oberauer[n], M. Obolensky[a], F. Ortica[j], K. Otis[p], M. Pallavicini[c], L. Papp[q], L. Perasso[c], A. Pocar[p], G. Ranucci[h], A. Razeto[e], A. Re[h], A. Romani[j], N. Rossi[e], R. Saldanha[l], C. Salvo[c], S. Schönert[n], H. Simgen[i], M. Skorokhvatov[g], O. Smirnov[b], A. Sotnikov[b], S. Sukhotin[g], Y. Suvorov[u,g], R. Tartaglia[e], G. Testera[c], D. Vignaud[a], R.B. Vogelaar[q], F. von Feilitzsch[n], H. Wang[u], J. Winter[n], M. Wojcik[d], A. Wright[l], M. Wurm[s], O. Zaimidoroga[b], S. Zavatarelli[c], and G. Zuzel[d].

[a] APC, Univ. Paris Diderot, CNRS/IN2P3, CEA/Irfu, Obs. de Paris, Sorbonne Paris Cité, France
[b] Joint Institute for Nuclear Research, Dubna 141980, Russia
[c] Dipartimento di Fisica, Università e INFN, Genova 16146, Italy
[d] M. Smoluchowski Institute of Physics, Jagellonian University, Crakow, 30059, Poland
[e] INFN Laboratori Nazionali del Gran Sasso, Assergi 67010, Italy
[f] Kiev Institute for Nuclear Research, Kiev 06380, Ukraine
[g] NRC Kurchatov Institute, Moscow 123182, Russia
[h] Dipartimento di Fisica, Università degli Studi e INFN, Milano 20133, Italy
[i] Max-Plank-Institut für Kernphysik, Heidelberg 69029, Germany
[j] Dipartimento di Chimica, Università e INFN, Perugia 06123, Italy
[k] Chemical Engineering Department, Princeton University, Princeton, NJ 08544, USA
[l] Physics Department, Princeton University, Princeton, NJ 08544, USA
[m] St. Petersburg Nuclear Physics Institute, Gatchina 188350, Russia
[n] Physik Department, Technische Universität München, Garching 85747, Germany
[p] Physics Department, University of Massachusetts, Amherst MA 01003, USA

[q] Physics Department, Virginia Polytechnic Institute and State University, Blacksburg, VA 24061, USA

[r] Lomonosov Moscow State University Skobeltsyn Institute of Nuclear Physics, Moscow 119234, Russia

[s] Institut für Experimentalphysik, Universität Hamburg, Germany

[t] Department of Physics, University of Houston, Houston, TX 77204, USA

[u] Physics ans Astronomy Department, University of California Los Angeles (UCLA), Los Angeles, CA 90095, USA

Abstract

Borexino is a large liquid–scintillator detector located in the Laboratori Nazionali del Gran Sasso. The main goal of the experiment is the study of solar neutrinos, in particular those coming from the so-called ^{7}Be reaction. The exceptionally high levels of radiopurity of the scintillator have made it possible to accomplish not only its primary goal, but also produce a number of other significant results. Among these, we are going to discuss those published in 2013, regarding, in particular, an updated measurement of geo–neutrinos, measurement of cosmogenic background, new limits on heavy sterile neutrino mixing in ^{8}B-decay. In 2013, Borexino collaboration has also published new results about the lifetime measurements of ^{214}Po and ^{212}Po with CTF liquid scintillator detector and a description of the SOX: Short distance neutrino Oscillations project, being currently in progress.

1   Introduction

Neutrinos from the Sun have been studied by several experiments in the past 40 years and these studies have led to the discovery of solar neutrino oscillations. However, the investigation of the solar neutrino spectrum is far from being complete, especially in the energy region below 1 MeV where experiments can be severely affected by background due to natural radioactivity. The Borexino experiment has been specifically designed to study the low–energy solar neutrinos, in particular those coming from the so-called ^{7}Be reaction. The success of Borexino comes as a result of a 15-year long R& D study carried out by the collaboration to develop the best techniques of purification to reach the required levels of radiopurity. Thanks to this, Borexino succeeded in measuring ^{7}Be, ^{8}B ($T > 3$ MeV), and *pep* solar neutrinos and set the best limit to date for the CNO solar neutrinos. Moreover, Borexino achieved important scientific results out of the field of solar neutrinos. In the following, we briefly describe the Borexino detector. Then, we briefly summarize the status of the Borexino project and its main past scientific results, while we concentrate on the results published in the calendar year 2013. We conclude with the description of the ongoing and future Borexino activity.

2   The Borexino detector

The Borexino detector is located under the Gran Sasso mountain in the Laboratori Nazionali del Gran Sasso, Italy. It detects solar neutrinos via their elastic scattering on the

electrons of 300 tons of liquid scintillator. The scintillator (PC + 1.5 g/l of PPO) is contained in a large spherical nylon vessel (R = 4.25 m). The scintillation light is viewed by 2214 photomultiplier tubes (defining the so called Inner Detector, ID) mounted on a Stainless Steel Sphere (SSS) concentric with the vessel at a radius of 6.85 m (see Fig. 1). In order to reduce external background, the design of Borexino is based on the principle of graded shielding, with the inner core scintillator at the center of a set of concentric shells of increasing radiopurity. Besides keeping external backgrounds at a low level, the key requirement for measuring low energy neutrinos with Borexino is the exceptional radiopurity of the scintillator itself. Based on extensive R&D studies and on the tests performed with the Borexino prototype, so called Counting Test Facility (CTF), the Borexino collaboration developed a successful purification strategy which proved to be effective in removing the most dangerous contaminants from the scintillator. The Inner Detector (ID) described above is contained in a tank filled with $2000\,\mathrm{m}^3$ of ultra-pure water which provides further shielding from background from the rocks and also acts as a Cherenkov muon detector (Outer Detector, OD) to tag residual cosmic muons. For more details concerning the Borexino detector see [1], [2]. Borexino detector was extensively calibrated with radioactive sources [3], an essential ingredient in understanding the detector response function and reducing the systematic errors on all Borexino results.
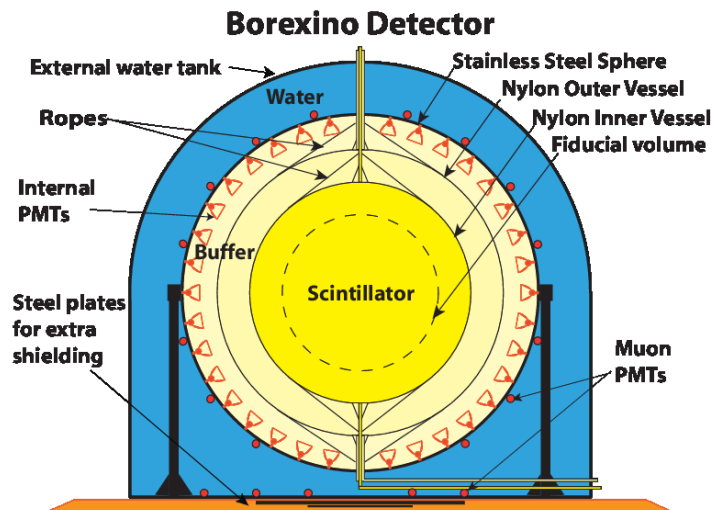

Figure 1: Schematic view of the Borexino detector.

3   Status of the project

The Borexino experiment started taking data in May 2007. Since then, it has produced a considerable amount of results. It reached the aim for which it was build: after the first ^{7}Be neutrino measurements [4], [5], the precision measurement of the ^{7}Be solar neutrino rate with a total error of less than 5% [6] has been reached. A possible day–night asymmetry

of the [7]Be neutrino interaction rate, predicted by some models, has been excluded [7]. Borexino provided the first measurement of the *pep* solar neutrino flux and gave the best to-date upper limit on the CNO solar neutrino flux [8]. It also performed the measurement of the [8]B solar neutrino rate with an unprecedented low energy threshold of $T > 3\,\mathrm{MeV}$ [9]. Borexino has also published significant results on non-solar neutrino physics, such as the first observation of anti-neutrinos from the Earth (geo–neutrinos) [10] and several limits on rare or forbidden processes [11], [12], [13]. These important results have been discussed in previous reports and won't be addressed here. In this report we are going to focus on the articles published in year 2013.

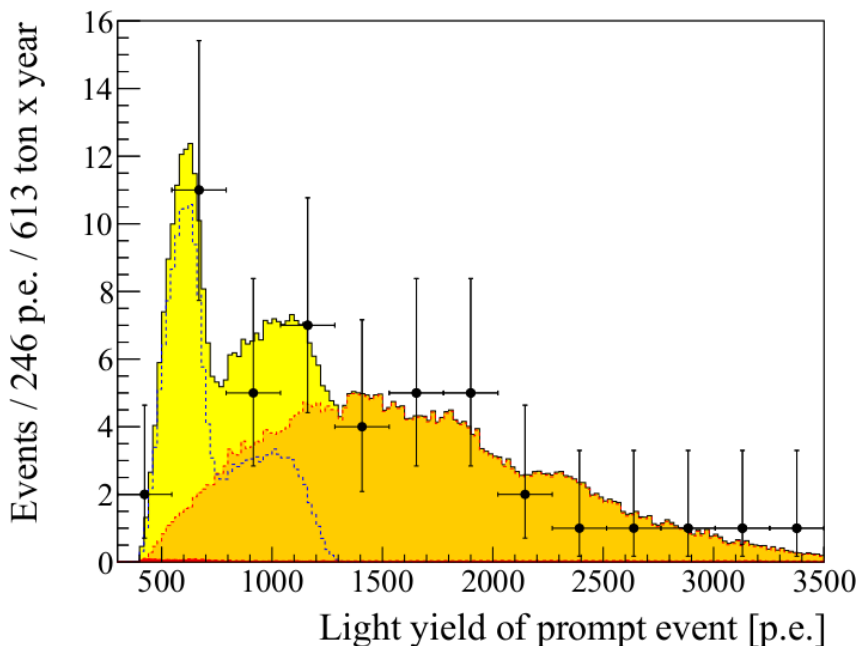## 3.1   Measurement of geo–neutrinos from 1353 days of Borexino

Figure 2: Light yield spectrum of the 46 prompt golden anti–neutrino candidates and the best fit. The yellow area isolates the contribution of the geo–$\bar{\nu}_e$ in the total signal. Dashed red line/orange area: reactor–$\bar{\nu}_e$ signal from the fit. Dashed blue line: geo–$\bar{\nu}_e$ signal resulting from the fit. The contribution of other background is almost negligible and is shown by the small red filled area in the lower left part. The conversion from p.e. to energy is approximately 500 p.e./MeV.

We reported a measurement of the geo–neutrino signal obtained from 1353 days of data with the Borexino detector [14]. This analysis was performed with 2.4 times larger exposure with respect to the first geo–neutrino observation that Borexino published in 2010 [10]. With a fiducial exposure of $(3.69 \pm 0.16) \times 10^{31}$ proton $\times$ year after all selection cuts and background subtraction, we detected (14.3 ± 4.4) geo–neutrino events assuming a fixed chondritic mass Th/U ratio of 3.9. This corresponds to a geo–neutrino

signal $S_{geo} = (38.8 \pm 12.0)$ TNU[1] with just a 6×10^{-6} probability for a null geo–neutrino measurement. The data and the best fit are shown in Fig. 2. The main background for the geo–neutrino measurement is due to reactor anti–neutrinos. The systematic error on the expected background from the reactor anti–neutrinos is at the level of 5.8%. The fit results in the $S_{\mathrm{react}} = 84.5^{+19.3}_{-16.9}$ TNU (there is no penalty on the reactor signal in the fit), in a complete accordance with the expectations. Thanks to the extreme radiopurity of the Borexino detector, the non anti–neutrino background is almost negligible, only 0.7 ± 0.18 events within the 46 golden candidates.

With U and Th left as free parameters in the fit, the relative signals are $S_{\mathrm{Th}} = (10.6 \pm 12.7)$ TNU and $S_{\mathrm{U}} = (26.5 \pm 19.5)$ TNU. Borexino data alone are compatible with a mantle geo–neutrino signal of (15.4 ± 12.3) TNU, while a combined analysis with the KamLAND data allows to extract a mantle signal of (14.1 ± 8.1) TNU. The current precision of the existing geo–neutrino measurements (both Borexino and KamLAND results [15]) is not sufficient to discriminate among different geological models.

3.2 Cosmogenic backgrounds in Borexino

The solar neutrino experiment Borexino is in a unique position to study muon-induced backgrounds in an organic liquid scintillator. In the study [16] published in 2013, a large sample of cosmic muons is identified and tracked by a muon veto detector external to the liquid scintillator, and by the specific light patterns observed when muons cross the scintillator volume. The yield of muon-induced neutrons is found to be $Y_n = (3.10 \pm 0.11) \cdot 10^{-4} \, n/(\mu \cdot (\mathrm{g/cm^2}))$. The distance profile between the parent muon track and the neutron capture point has the average value $\lambda = (81.5 \pm 2.7)$ cm. Additionally, the yields of a number of cosmogenic radioisotopes are measured for ^{12}N, ^{12}B, ^{8}He, ^{9}C, ^{9}Li, ^{8}B, ^{6}He, ^{8}Li, ^{11}Be, ^{10}C, and ^{11}C, see Table 1. All results are compared with Monte Carlo simulation predictions using the Fluka and Geant4 packages. General agreement between data and simulation is observed for the cosmogenic production yields with a few exceptions, the most prominent case being ^{11}C yield for which both codes return about 50% lower values. The predicted μ-n distance profile and the neutron multiplicity distribution are found to be overall consistent with data.

3.3 New limits on heavy sterile neutrino mixing in ^{8}B decay

If heavy neutrinos with mass $m_{\nu_H} \geq 2m_e$ are produced in the Sun via the decay $^8\mathrm{B} \to \,^8\mathrm{Be} + e^+ + \nu_H$ in a side branch of pp-chain, they would undergo the observable decay into an electron, a positron and a light neutrino ν_L:

$$\nu_H \to \nu_L + e^+ + e^-. \tag{1}$$

Borexino data are used to set a bound on the existence of such decays [18].

The emission of a heavy neutrino in the β^+-decay of ^{8}B is suppressed by the mixing

---

[1] 1 TNU = 1 Terrestrial Neutrino Unit = 1 event / year / 10^{32} protons

	Geant4 Model III	Geant4 Model IV	Fluka	Borexino	KamLAND
$\langle E_\mu \rangle$		—— 283 ± 19 GeV ——			260 ± 8 GeV
Isotopes		Yield $[10^{-7}\,(\mu\,\mathrm{g/cm^2})^{-1}]$			
^{12}N	(1.11 ± 0.13)	(3.0 ± 0.2)	(0.5 ± 0.2)	<1.1	(1.8 ± 0.4)
^{12}B	(30.1 ± 0.7)	(29.7 ± 0.7)	(28.8 ± 1.9)	(56 ± 3)	(42.9 ± 3.3)
^{8}He	<0.04	(0.18 ± 0.05)	(0.30 ± 0.15)	<1.5	(0.7 ± 0.4)
^{9}Li	(0.6 ± 0.1)	(1.68 ± 0.16)	(3.1 ± 0.4)	(2.9 ± 0.3)	(2.2 ± 0.2)
^{8}B	(90.52 ± 0.09)	(1.44 ± 0.15)	(6.6 ± 0.6)	(14 ± 6)	(8.4 ± 2.4)
^{6}He	(18.5 ± 0.5)	(8.9 ± 0.4)	(17.3 ± 1.1)	(38 ± 15)	not reported
^{8}Li	(27.7 ± 0.7)	(7.8 ± 0.4)	(28.8 ± 1.0)	(7 ± 7)	(12.2 ± 2.6)
^{9}C	$90.16 \pm 0.05)$	(0.99 ± 0.13)	(0.91 ± 0.10)	<16	(3.0 ± 1.2)
^{11}Be	(0.24 ± 0.06)	(0.45 ± 0.09)	(0.59 ± 0.12)	<7.0	(1.1 ± 0.2)
^{10}C	(15.0 ± 0.5)	(41.1 ± 0.8)	(14.1 ± 0.7)	(18 ± 5)	(16.5 ± 1.9)
^{11}C	(315 ± 2)	(415 ± 3)	(467 ± 23)	(886 ± 115)	(866 ± 153)
Neutrons		Yield $\mathrm{m}[10^{-4}\,(\mu\,\mathrm{g/cm^2})^{-1}]$			
	(3.01 ± 0.05)	(2.99 ± 0.03)	(2.46 ± 0.12)	(3.10 ± 0.11)	(2.79 ± 0.31)

Table 1: Predicted yields for cosmogenic products obtained from Geant4 (Model III and IV) and Fluka are compared to data from Borexino. Also shown are results from the KamLAND experiment [17]. Note that the production yields depend on the number of carbon atoms per weight and the muon energy spectrum. Thus, a $10-20\,\%$ difference between KamLAND and Borexino results is expected.

parameter $|U_{eH}|^2$ and a phase-space factor as:

$$\Phi(E_{\nu_H}) = |U_{eH}|^2 \sqrt{1 - \left(\frac{m_{\nu_H}}{E_{\nu_H}}\right)^2} \Phi_{^8\mathrm{B}}(E_\nu), \tag{2}$$

where E_{ν_H} is the total energy of the heavy neutrino. We use the standard ^{8}B solar neutrino spectral shape for $\Phi_{^8\mathrm{B}}$.

The search for $\nu_H \to \nu_L + e^+ + e^-$ decay is performed by comparing the measured energy spectrum with that expected from ν_H-decays. The latter requires the knowledge of the heavy neutrino flux $\Phi(E_{\nu_H})$ through the detector, of the kinetic energy of the e^+e^- pairs produced (eq. 1), and the response function of Borexino to energy released by e^+e^- pairs in the scintillator. The fit was performed in the range of 4.8 –12.8 MeV and had 76 degrees of freedom. We constrain the mixing of a heavy neutrino with mass 1.5 MeV $\leq m_{\nu_H} \leq 14$ MeV to be $|U_{eH}|^2 \leq (10^{-3} - 4 \times 10^{-6})$, respectively, see Fig. 3. These are tighter limits on the mixing parameters than obtained in previous experiments at nuclear reactors [19] and accelerators [20].
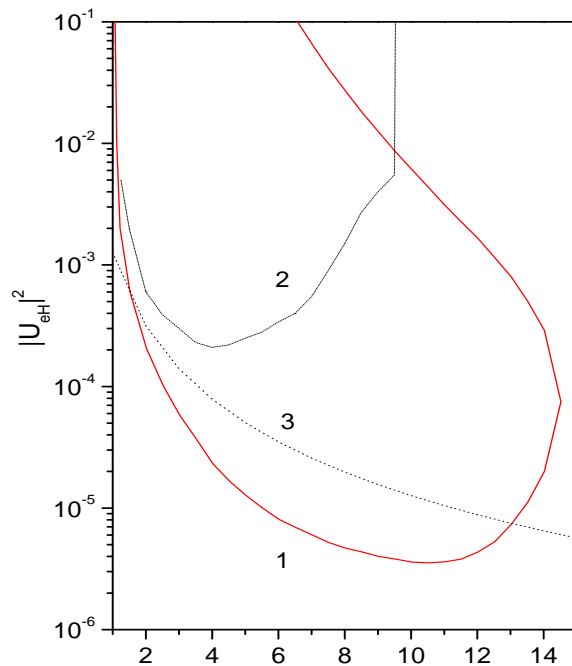
Figure 3: Limits on the mixing parameter $|U_{eH}|^2$ as a function of neutrino mass m_ν (90% c.l.). 1: Borexino work [18] excludes values of $|U_{eH}|^2$ and m_ν inside region 1. 2: upper limits from reactor experiments on the search for $\nu_H \to \nu_L + e^+ + e^-$ decay due to W-exchange mode [19]. 3: upper limits from $\pi \to e + \nu$ decay [20].

3.4 Lifetime measurements of ^{214}Po and ^{212}Po with CTF liquid scintillator detector

The data collected with CTF detector have been already used by Borexino collaboration in past to set some important limits on physics beyond the standard model. But the main goal of CTF was to serve as an ultrasensitive tool for measuring the radioactivity levels unreachable by any other existing method. At the end of 2012 the Counting Test Facility (CTF) was dismounted to host Dark Side experiment.

A series of measurements with radioactive sources ^{222}Rn, ^{232}Th, and ^{220}Rn sealed inside transparent quartz vials and inserted in CTF detector were performed in 2011-2012 [21], the main goal of the measurement was to establish the spectral shape of electron spectra of ^{212}Bi and ^{214}Bi of importance for precision geo–neutrino studies. Collected data allowed us to study the decay time of ^{214}Po and of ^{212}Po isotopes.

Both ^{214}Po and ^{212}Po are unstable isotopes, characterized by short mean-lives ($\tau_{214\text{Po}} \approx 235\mu$s, $\tau_{212\text{Po}} \approx 430$ns) and by emission of alpha particles with energies $E_{214\text{Po}} \approx 7.833$~MeV and $E_{212\text{Po}} \approx 8.954$~MeV and 100\% branching ratios (BR). They belong to the ^{238}U and ^{232}Th chains, respectively. In both measurements, we look for the fast coincidence be-

7

tween the β-decay of the father isotope (^{214}Bi or ^{212}Bi) and the ^{214}Po or ^{212}Po α-decay, respectively. The ^{214}Po lifetime measurement is characterized by an unprecedented large statistics ($\approx 10^5$ events), and both the ^{212}Po and ^{214}Po ones exploit a very long acquisition window, correspondent to ≈ 7 mean-lives. Moreover, the high purity of the detector materials allows to reach a signal–to–background ratio three orders of magnitude better than any other existing measurement,

We find that the mean lifetime of ^{214}Po is $(236.00 \pm 0.42(\text{stat}) \pm 0.15(\text{syst}))\mu s$ and that of ^{212}Po is $(425.1 \pm 0.9(\text{stat}) \pm 1.2(\text{syst}))\,\text{ns}$. Our results, obtained from data with signal–to–background ratio larger than 1000, reduce the overall uncertainties and are compatible with previous measurements.

3.5 SOX: Short distance neutrino Oscillations project

The Borexino detector offers a unique opportunity to perform a short-baseline neutrino oscillation test, which will be able of exploring the sterile neutrino hypothesis in the range of ($\sin^2 \theta_{14}$, Δm_{14}^2) currently allowed by several experimental anomalies. Since the currently preferred value for Δm_{14}^2 is of the order of $1\,\text{eV}^2$, and the neutrino energies are of the order of $\sim 1\,\text{MeV}$, the resulting oscillation lengths is of the order of meters. In this case, it would be even possible to observe a spatial oscillation pattern emerging inside the target volume.

The Borexino–collaboration paper [22] describes the possible layouts of ^{51}Cr (ν_e) and ^{144}Ce–^{144}Pr ($\bar{\nu}_e$) source experiments in Borexino and shows the expected sensitivity to eV mass sterile neutrinos for three possible different phases of the experiment 4. The experiment (named SOX - Short distance neutrino Oscillations with BoreXino) will be carried out by using in a first instance (Phase A) a ^{51}Cr ν_e source of 200-400 PBq activity deployed at 8.25 m from the detector center; in a second phase (Phase B) by deploying a ^{144}Ce–^{144}Pr $\bar{\nu}_e$ source with 2-4 PBq activity at 7.15 m from the detector center, and, finally, in a possible Phase C, a similar ^{144}Ce–^{144}Pr $\bar{\nu}_e$ source located right in the center of the liquid scintillator volume. Expected results on neutrino magnetic moment, electroweak mixing angle, and couplings to axial and vector currents are shown too.

In its current form, the SOX project doesn't require any modifications of the Borexino experimental apparatus. The project has recently received a Advances ERC European grant of 5-years duration.

4 Conclusions and perspectives

The first phase of Borexino started in 2007 and ended in 2010. Borexino collaboration reviewed the solar neutrino program of Phase 1 in [24]. This work contains all details about the analysis methods used in the ^{7}Be, *pep*, and CNO neutrino studies and for the first time shows the results about the seasonal modulation of the ^{7}Be neutrino signal. This work is currently under revision and will be submitted shortly to the journal.

Between 2010 and 2011 several purification cycles using the water extraction technique have been performed in order to increase even further the scintillator radiopurity. These purification campaigns have brought the ^{85}Kr content to values consistent with zero, and
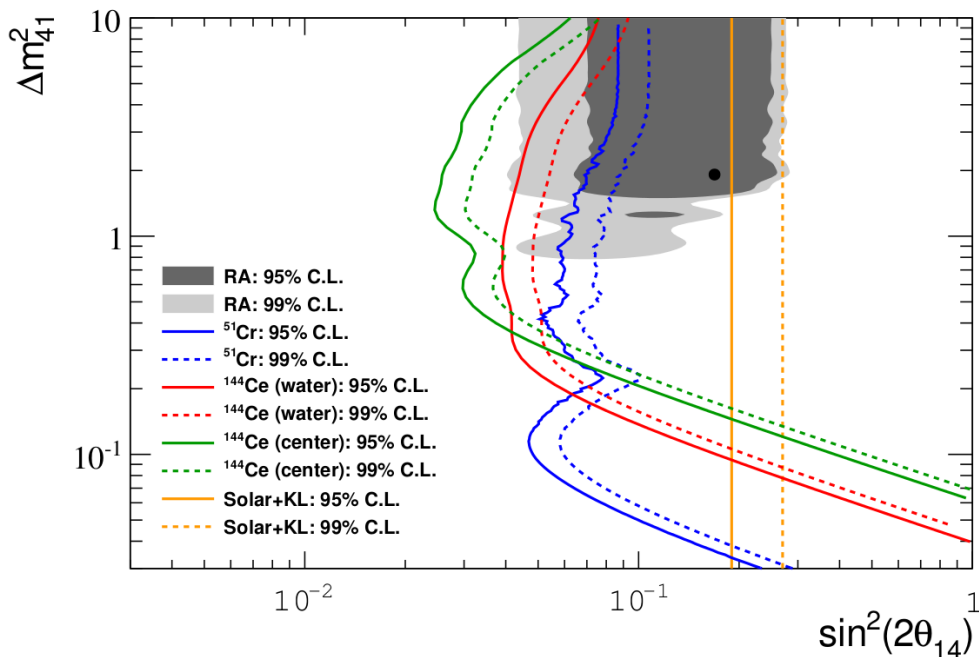
Figure 4: Sensitivity of the Phase A (^{51}Cr external, blue), of Phase B (^{144}Ce–^{144}Pr external, red) and Phase C (^{144}Ce–^{144}Pr center, green). The grey area is the one indicated by the reactor anomaly, if interpreted as oscillations to sterile neutrinos. Both 95% and 99% C.L. are shown for all cases. The yellow line indicates the region already excluded in [23].

have significantly reduced the ^{210}Bi content (by a factor of ~ 3). In October 2011, after the last water extraction cycle was completed, the Phase 2 of Borexino started. The program of this new phase of the experiment is challenging and covers a broad range of fields from stellar and solar physics to particle physics. The first Borexino publications using also the Phase 2 data is the update of geo–neutrino measurement [14] and the search for heavy sterile neutrino mixing in ^{8}B decay [18].

The main goal of Borexino Phase 2 is the detection of neutrinos from the solar CNO fusion cycle. This would be a major breakthrough for stellar evolution theories, since the CNO cycle is believed to be the main mechanism of hydrogen burning in stars more massive than our Sun. Although it should be present in the Sun at a comparatively small level, it has never been observed. Also, the determination of the CNO flux could help disentangling between the so-called low and high metallicity hypothesis for the Sun as the reaction strongly depends on the abundances of carbon, oxygen and nitrogen at the solar center. CNO neutrino detection is very challenging especially because of the degeneracy of their spectral shape with that of the radioactive contaminant ^{210}Bi. The content of ^{210}Bi in the scintillator should be known precisely in order to disentangle its contribution from the CNO rate. A big effort is currently devoted to developing analysis techniques to determine the content of ^{210}Bi by studying the evolution in time of ^{210}Po (which is the ^{210}Bi daughter). This analysis is made difficult by disuniformities of the contaminants in the scintillator volume and variation in time of the content of ^{210}Po and ^{210}Bi due to

operations and convective motions.

An other important goal for the second phase of Borexino is the direct observation of solar neutrinos from the pp reaction. These neutrinos stem from the most basic solar fusion reaction and are responsible for most of the solar luminosity, but have never been observed in real-time because of their low energies (E <420 keV). The main source of background for a measurement in Borexino is the high decay rate of ^{14}C and its pile-up. A knowledge of the ^{14}C rate and of the spectral shape and rate of its pile-up are important to perform a spectral fit to disentangle the pp signal. The already achieved reduction of ^{85}Kr which also affects the low energy portion of the spectrum is an important progress with respect to Phase 1. The pp neutrino analysis has been completed and the respective paper will be submitted shortly to a journal of preference of the collaboration.

Further important results which we expect from the new data of Borexino are the improvement in the precision of the ^{7}Be rate measurement (possibly down to 3%) and of the shape of the electron recoil spectrum. This would be an important achievement "per se" and would also help evidentiating possible effects due to neutrino Non Standard Interactions.

In general, in order to probe possible non-standard effects, it would be important to increase the amount of information in the so-called transition region from vacuum to matter dominated oscillations, by improving the precision on the pep neutrino rate and on the ^{8}B neutrino rate (in the region between 3 and 5 MeV).

5 List of Publications in 2013

1. Borexino collaboration: Measurement of geo–neutrinos from 1353 days of Borexino, Phys. Lett. B 722 (2013) 295-300.

2. Borexino collaboration: Cosmogenic Backgrounds in Borexino at 3800 m water-equivalent depth, JCAP 1308 (2013) 049.

3. Borexino Collaboration: New limits on heavy sterile neutrino mixing in 8B-decay obtained with the Borexino detector, Phys. Rev. D 88 (2013) 072010.

4. Borexino collaboration: Lifetime measurements of 214Po and 212Po with CTF liquid scintillator detector at LNGS, Eur. Phys. J. A49 (2013) 92.

5. Borexino collaboration: SOX: Short distance neutrino Oscillations with BoreXino, JHEP 1308 (2013) 038.

References

[1] Alimonti G *et al.* (Borexino coll.) 2009 *Nucl. Instrum. Methods Phys. Res.* A **600** 568.

[2] Bellini G *et al.* (Borexino coll.) 2011 *JINST* **6** P5005.

[3] Back H.*et al.* (Borexino coll.) 2012 *JINST* **7** P10018.

[4] Arpesella C *et al.* (Borexino coll.) 2008 *Phys.Lett.* B **658** 101.

[5] Arpesella C *et al.* (Borexino coll.) 2008 *Phys.Rev.Lett.* **101** 091302.

[6] Bellini G *et al.* (Borexino coll.) 2011 *Phys.Rev.Lett.* **107** 141302.

[7] Bellini G *et al.* (Borexino coll.) 2012 *Phys.Lett.* B **707** 22.

[8] Bellini G *et al.* (Borexino coll.) *Phys.Rev.Lett.* **108** (2012) 051302.

[9] Bellini G *et al.* (Borexino coll.) 2010 *Phys.Rev.* D **82** 033006.

[10] Bellini G *et al.* (Borexino coll.) 2010 *Phys.Lett.B* **687** 299-304.

[11] Bellini G *et al.* (Borexino coll.) 2010 *Phys.Rev.* C, **81** 034317.

[12] Bellini G *et al.* (Borexino coll.) 2011 *Phys.Lett.* B, **696** 191.

[13] Bellini G *et al.* (Borexino coll.) 2012 *Phys.Rev.* D **85**, 092003.

[14] Bellini G *et al.* (Borexino coll.) 2013 *Phys. Lett.* B **722** 295-300.

[15] Gando A *et al.* (KamLAND coll.) 2013 *Phys. Rev.* D **88** 033001.

[16] Bellini G *et al.* (Borexino coll.) 2013 *JCAP* **1308** 049.

[17] Abe S *et al.* (KamLAND coll.) 2010 *Phys. Rev.* C **81** 025807.

[18] Bellini G *et al.* (Borexino coll.) 2013 *Phys. Rev.* D **88** 072010.

[19] Hagner C *et al.* 1995 *Phys. Rev.* D **52** 1343.

[20] Britton D I *et al.* 1992 *Phys. Rev.* D **46** 885.

[21] Bellini G *et al.* (Borexino coll.) 2013 *Eur. Phys. J.* A **49** 92.

[22] Bellini G *et al.* (Borexino coll.) 2013 *JHEP* **1308** 038.

[23] Palazzo A 2013 *Mod. Phys. Lett.* A **28** No. 7 1330004.

[24] Bellini G *et al.* (Borexino coll.), arXiv:1308.0443.

COBRA Annual Report 2013

A. Bakst[a], J. Durst[a], M. Filipenko[a], T. Gleixner[a], T. Michel[a],

B. Biskup[b], V. Bocarov[b], P. Cermak[b], J. M. Jose[b], I. Stekl[b],

O. Civitarese[c],

C. Disch[d], A. Fauler[d]. M. Fiederle[d],

M. Beilicke[e], F. Kislat[e], H. Krawczynski[e], A. Zajcyk[e],

M. Fritts[f], D. Gehre[f], T. Göpfert[f], O. Reinecke[f], T. Wester[f], S. Zatschler[f], K. Zuber[f,*]

C. Gößling[g], M. Homann[g], R. Klingenberg[g], T. Köttig[g], T. Neddermann[g], S. Rajek[g],

J. Tebrügge[g], T. Quante[g],

V. Braunert[h], J. Ebert[h], C. Hagner[h], N. Heidrich[h], C. Oldorf[h], H. Rebber[h], J. Timm[h],

B. Wonsak[h],

M. Junker[i], F. Simkovic[j], J. Suhonen[k],

[a] *Universität Erlangen–Nürnberg* – Germany
[b] *Technical University of Prague* – Czech Republic
[c] *University of La Plata* – Argentina
[d] *Freiburg Materials Research Center* – Germany
[e] *Washington University in St. Louis* – USA
[f] *Technische Universität Dresden* – Germany
[g] *Technische Universität Dortmund* – Germany
[h] *Universität Hamburg* – Germany
[i] *Laboratori Nazionali del Gran Sasso* – Italy
[j] *University of Bratislava* – Slovakia
[k] *University of Jyvaskyla* – Finnland
(* Spokesperson)

Abstract

The aim of the COBRA-Experiment (**C**admium Zinc Telluride **0**-Neutrino Double-**B**eta **R**esearch **A**pparatus) is to prove the existence of neutrinoless double beta decay ($0\nu\beta\beta$-decay) and to measure its half life.

As a semiconductor, Cadmium-Zinc-Telluride (CdZnTe or simply CZT) offers the low radioactivity levels and good energy resolution required for a rare decay search, with the added advantage of room temperature operation. CZT contains a number of double beta decay candidates. The most promising is ^{116}Cd with a Q-value of 2.8 MeV, which lies above the highest prominent naturally occurring γ-lines from natural radioactivity. Therefore, a detector array made of CZT detectors is operated in the LNGS in Italy. This prototype is used to investigate the experimental issues of operating CZT detectors in low background mode, whilst additional studies are proceeding in surface laboratories. The experiment currently consists of monolithic, calorimetric detectors in a coplanar grid design (CPG detectors). These detectors are 1x1x1 cm^3 and will be operated in a 4x4x4 detector array. In such a configuration it is possible to analyze coincidences between the detectors and make use of the high granularity of such a setup. Furthermore, the installed detector mass can be increased easily.

1   Activities at the LNGS

In 2013 more than fourteen working weeks have been accomplished in 2 shifts at the LNGS. Several upgrades have been done, which are described in the following. Figure 1 shows a total view of the whole experimental setup.

1.1   Experimental Upgrades

1.1.1   Completing the COBRA demonstrator setup

In 2013 the COBRA demonstrator setup has been completed with the installation of the remaining two detector layers. The demonstrator setup consists now of 64 detectors, it collects low background data with a current accumulation rate of approximately 10 kg·days per month. A better procedure to contact the high voltage cables for the bias voltage has been applied at these layers, resulting in much less material in the vicinity of the detectors, which is important, as all material is potentially contaminated. The measurements qualifying the detectors done before installation show that these new detectors are the best used by COBRA so far. So it is a reasonable assumption that these layers will collect data with a better quality than the older ones. Figure 2 shows a detailed view of the inner part of the experimental setup.

1.1.2   Cooling of experimental setup

In order to have all four layers with 64 detectors running, cooling became an issue for the COBRA demonstrator setup for the first time.
The data transmission is very stable and robust due to differential signal transmission used in the electronics read-out system built by the COBRA collaboration. That is why it was decided to move the data acquisition rack, which dissipates ca. 800W, into the server room of the upper hut, which is cooled by an air conditioning system. The cable length of 20m has no impact on the signal quality. Hence the major heat dissipation source in the environment of the experimental
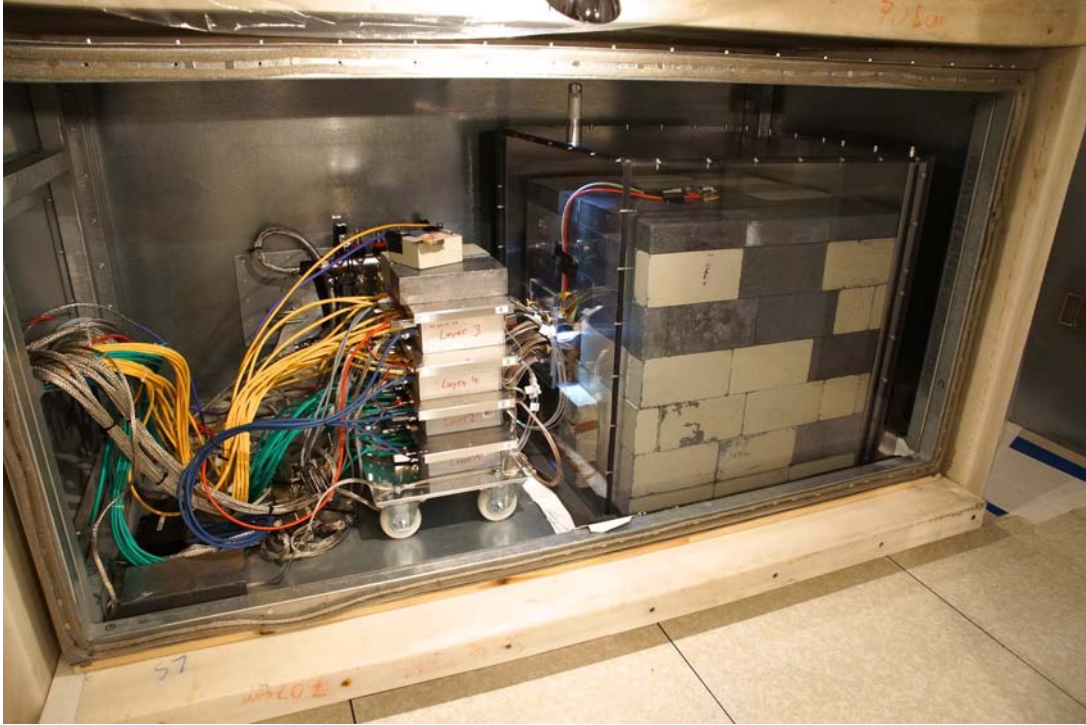
Figure 1: Total view of the experimental setup. Many new things have been installed in 2013, like the new detector layers, the new polycarbonate radon barrier and the preamplifier cooling system. Details to this can be found in section 1.1.

setup was removed.

Nevertheless, the dissipated heat of the preamplifier within the EMI shielding increase the temperature to 25 °C. The overall preamplifier electronics has been doubled due the installation of layer 3 and 4. So the estimated temperature exceeds 35 °C, which is undesirable because the resolution of the of the whole DAQ chain is known to decrease with higher temperatures. To improve the operating temperature a preamplifier cooling system was installed. The temperature inside of the setup was chosen to be constant at 19 °C. Figure 3 shows pictures of the preamplifier cooling system.

1.1.3 Radon barrier

The radon tight foil has been identified as a one of the major EMI problems because of its metalization. It has induced large charge pulses on the capton wires which had to pass through the radon shield. To remove this EMI problem a new radon shield consisting of polycarbonate has been installed (see Fig. 4). This radon barrier is a cube using the two metal plates from the old barrier, and three new polycarbonate plates. All this is carefully commissioned, especially the feedthroughs for the data transmission cables, voltage supply and tubes for nitrogen flushing. Figure 4 shows a picture of the radon barrier cube.

1.1.4 Uninterruptible Power Supply

To improve the overall stability of the experiment, three Uninterruptible Power Supplies (UPS) were installed. One is in the lower hut, securing the bias voltage supply of the detectors and
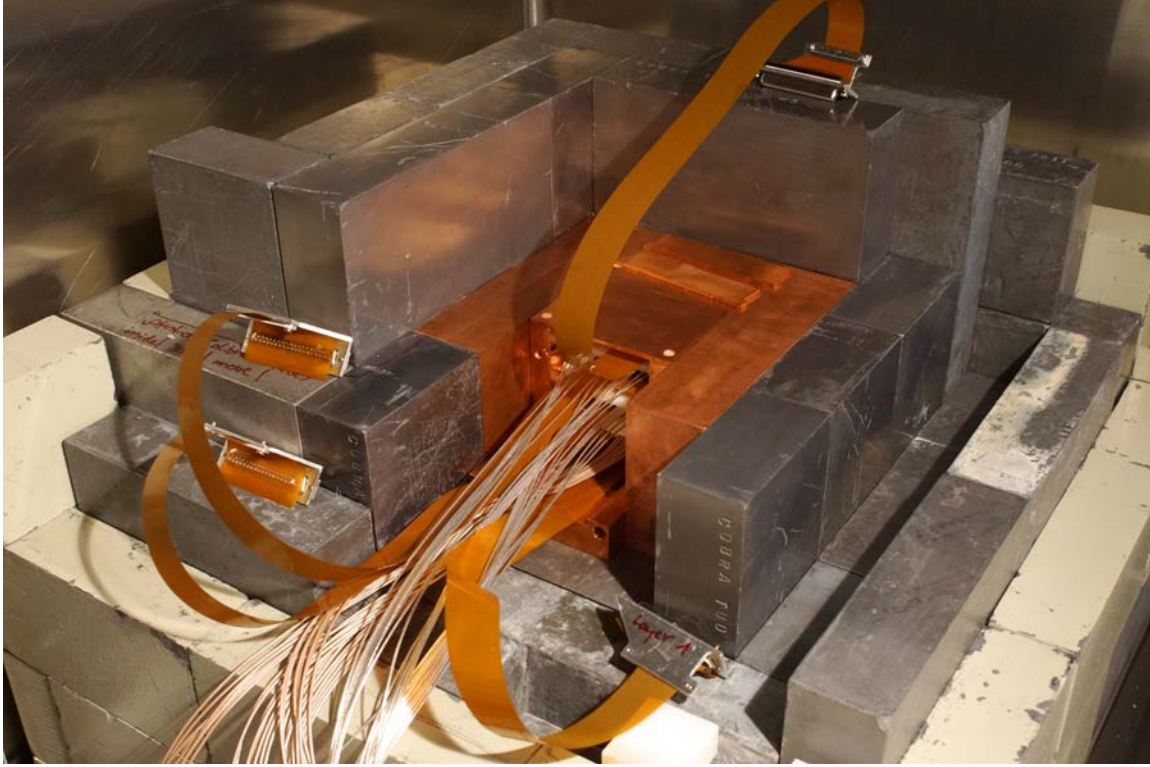
Figure 2: Detailed view of the inner part of the experimental setup. The partly dismantled lead castle can be seen, which surrounds the copper bricks containing the detector layers.

preamplifiers. The other two are in the upper hut, as this part of the DAQ and electronics like Flash-ADCs and server needs much more power.

2 Activities on the COBRA Coplanar Grid Detectors

2.1 Pulse shape analysis of multi-site interactions

The energy deposition of a neutrinoless double beta decay is expected to be a single-site event (SSE) interaction in just one detector of the array. Hence, the differentiation between events with multiple interactions from those with a single-site interaction only is one of the key instruments to further reduce background. A cut criterion based on a pulse shape analysis method has been developed to reject multi-site events (MSE). Such MSEs are typically caused by multiply-scattered highly energetic photons. It is well known that Cadmium, as compound element of the detector material CZT, has a very high cross section for the neutron capture reaction, such as Cd113(n,γ)Cd114 (σ=20 kbarn). The Q value of this reaction is 9.042 MeV. This energy is released in a high energetic photon cascade. Thus, interactions of such photons with the detector material can cause events in the region of interest of COBRA. Since the energy deposition of a $0\nu\beta\beta$ event is expected to be almost always single-site, all events of the same energy clearly identified as MSEs can be rejected in the final analysis.

Figure 5 shows typical examples for single-site and multi-site events taken from an energy calibration of the LNGS setup. To distinguish between SSEs and MSEs the derivative of the difference signal of collecting anode (CA) and non-collecting anode (NCA) is analyzed as shown

15

Figure 3: Left: Picture of the cooling device standing outside of the COBRA hut to dissipate the heat into the tunnel. Right: Picture of the preamplifier cooling system flow distributor supplying the cooling plates above the four preamplifier boxes. The flow in each sub-system can be adjusted individually, so that the uppermost one can be cooled the most, as it heats up most.
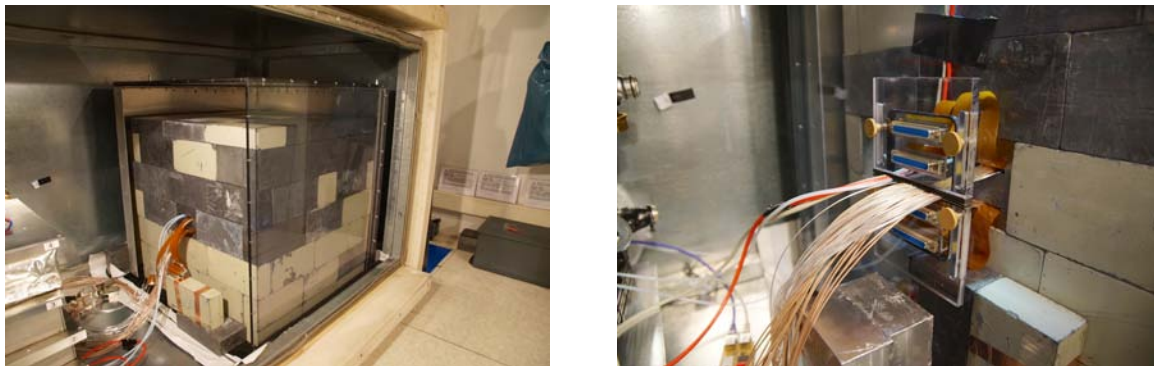

Figure 4: A total view of the radon barrier cube on the left, which shows the metal plates behind the lead castle, and the polycarbonate walls on the other side of the cube. On the right side a detailed view of the feedthrough is shown.

in figure 6. The peaks in the derivative plot get identified by an adapted peak finding algorithm, which is sensitive down to a minimal peak distance of about 10 samples (100 ns). The basic cut method is very robust as the noise level is calculated for each pulse individually. This approach allows for an effective reduction of the influence of electromagnetic noise, especially at low energies.

To improve the cut efficiency and to enhance the understanding of the characteristics of SSE and MSE, lab experiments are ongoing at the TU Dresden. A Compton scattering experiment has been set up to create a library of clear SSEs for different energies and depth regions (see figure 7). The idea is to irradiate one of the $1\,cm^3$ COBRA CPG detectors with a Cs-137 gamma source ($E_\gamma = 661.7\,\mathrm{keV}$) and search for coincidences of scattered photons with a high purity Germanium detector (HPGe). The expected energy deposition E_{CPG} by a primary single scattered photon at the CPG for a fixed scattering angle ϑ is known from the kinematics of Compton scattering.

$$E_{CPG} = \frac{E_\gamma}{\frac{E_\gamma}{m_e}(1 - \cos\vartheta) + 1}$$

Knowing this, the energy deposited by the scattered photon in the HPGe can be calculated as the difference of the initial gamma energy and the energy deposition in the CPG. By adjusting the scattering angle it is possible to investigate different energy regions. If the coincidence condition

$$E_\gamma = E_{CPG} + E_{HPGe}$$

is fulfilled, the energy deposition in the CPG was very likely of single-site character. Using such a library of SSEs would allow to precisely determine the MSE cut efficiency for different energies and to carefully optimize the cut parameters.

First results of an alternative optimization procedure using LNGS calibration data with a Th-228 gamma source are shown in figure 8. At the one hand events in the single escape peak region are expected to be almost always MSE, at the other hand the double escape peak is expected to be almost always single-site. The peak strength of these regions can therefore be maximized respectively minimized using a variation of the cut threshold to find an optimal value.
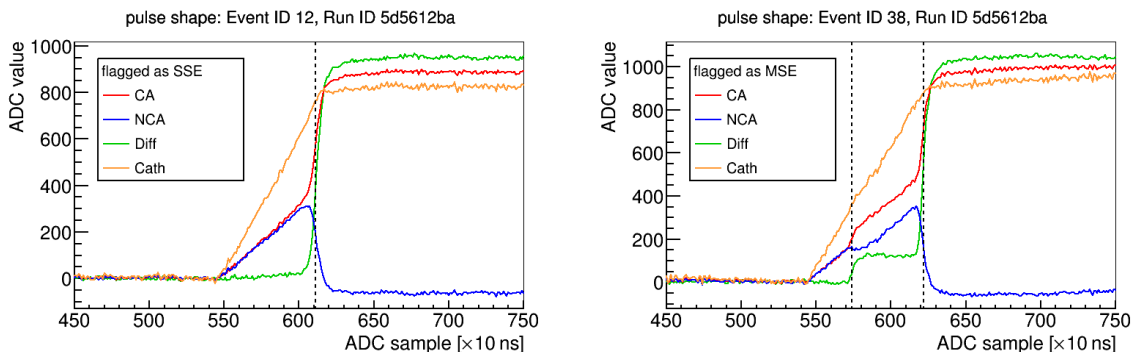

Figure 5: Typical pulse shapes for SSE (left) and MSE (right). The difference signal (green) shows a clear plateau for MSE as result of the multiple energy deposition.
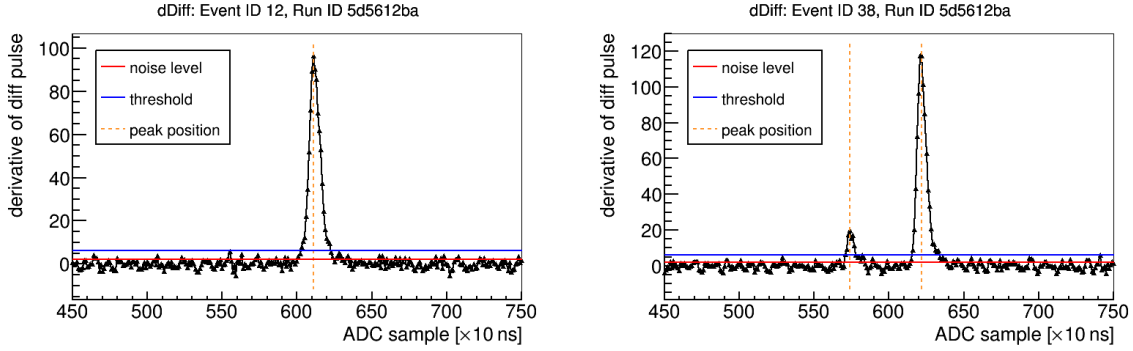
Figure 6: Derivation of difference pulse for the events shown in figure 5. If there are at least two peaks higher than the threshold (blue), the event gets flagged as MSE. The threshold x·noise_level is calculated for each pulse as the product of an optimized constant x and the RMS of the first 200 samples (red).
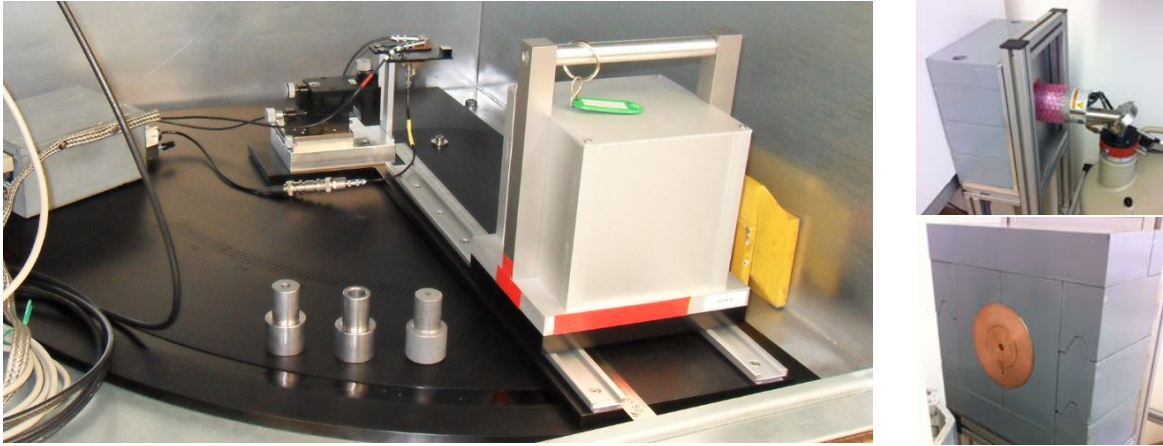

Figure 7: Experimental setup to identify single-site events by the use of Compton Scattering. The CPG detector is mounted at the pivot of a goniometer device and acts as the scatter device. The collimated Cs-137 gamma source is movable on rails to adjust the distance (13.75 - 42.25 cm) and the analyzed scattering angle (0 and 90°) between source, the CPG and the HPGe. Different collimator lead plugs can be used to reach a homogeneous radiation at several positions. The HPGe is collimated towards the pivot of the scattering setup to mainly detect the scattered gammas from the CPG and to suppress the background from the Cs-source (right pictures).

2.2 Lateral Surface Events ("LSE") recognition

Events near the cathode and anode surfaces of a coplanar grid CdZnTe detector are identifiable by means of the interaction depth information encoded in the signal amplitudes. However, the amplitudes cannot be used to identify events near the lateral surfaces. An identification of lateral surface events is possible by means of their pulse shape. Such identification allows for discrimination of surface alpha particle interactions from more penetrating forms of radiation, which is particularly important for rare event searches. The effectiveness in suppressing backgrounds due to alpha contamination in the search for neutrinoless double beta decay is an important
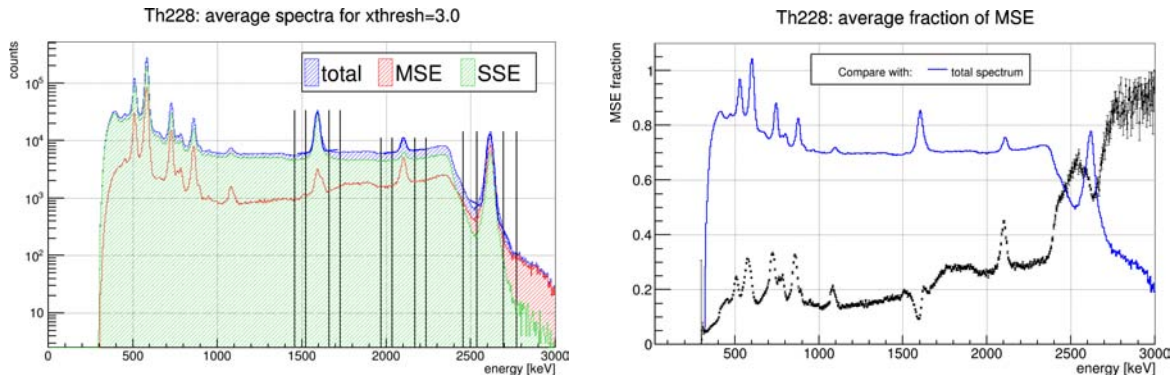
18

Figure 8: First result of MSE cut optimization with LNGS Th-228 calibration data. Left: total energy spectra (blue) compared to the spectra flagged as SSE (green) respectively MSE (red). Right: comparison of total spectra to the fraction of MSE. As expected, there is a dip for the double escape and a peak for the single escape region. Since the Compton valley between Compton edge and full energy peak is expected to be almost always MSE, the fraction of MSE is strongly increasing in this region. The mean fraction for higher energies is with about 90% right at the limit of the applied cut.

improvement in analysis. Much work has been done on this topic in 2013, resulting in a publication in 2014 describing a method to identify lateral surface events by means of their pulse shapes, see "Pulse-shape discrimination of surface events in CdZnTe detectors for the COBRA experiment" in section 6. The LSE cuts are very powerful tools to suppress background, which is shown in figure 9. The count rate could be reduced to less than 1 count / keV / kg / y in the region of interest. On the other hand, the LSE cuts also lower the fiducial volume of each detector. Therefore, it was decided to test $6\,cm^3$ detectors instead of $1\,cm^3$ which decreases the surface to volume ratio by 45 %. This will improve the overall detection efficiency and it will also reduce the efficiency loss induced by the pulse shape analysis cuts.

2.3   Cd-113 spectrum

Furthermore, the beta decay spectrum of ^{113}Cd in the low energy region (50 keV up to 350 keV) was investigated. For the final energy spectrum 24 detectors are used. In figure 10 the preliminary result of the analysis is shown. [1]

For the fit function the theory from Behrens and Janecke is used [2]. There is a good agreement between the fit model and the data ($\chi^2/ndf = 30.69/63$). For the Q_β-value and the half-life the following preliminary results are found: $Q_\beta = (323.6 \pm 0.2(stat) \pm 1.2(sys))\,keV$ and $T_{\frac{1}{2}} = (7.91 \pm 0.09(stat) \pm 0.21(sys)) \times 10^{15}yr$. These values are in good accordance to the results found by other groups. Further investigations are going on to improve the analysis in the region with an energies below $E = 50keV$. For lowering the systematic uncertainties of the half-life, efforts are made to reduce the uncertainty for the content of cadmium within the

---

[1]M. T. Mustonen, M. Aunola, and J. Suhonen, Phys. Rev. C 73, 054301 (2006); 76, 019901(E) (2007) and M. T. Mustonen and J. Suhonen, Phys. Lett. B657, 38 (2007)

[2]H. Behrens and J. Jänecke, Numerical Tables for Beta-Decay and Electron Capture (Springer- Verlag, Berlin, 1969)
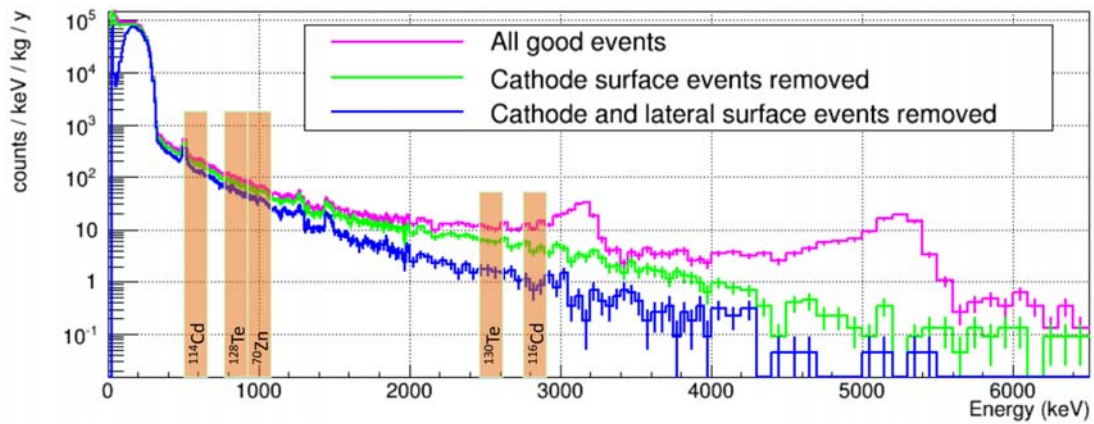
19

Figure 9: Spectrum of the LNGS data. Due to the hardware improvements at the experimental setup and the sophisticated analysis methods, the count rate can be reduced to less than 1 count / keV / kg / y.
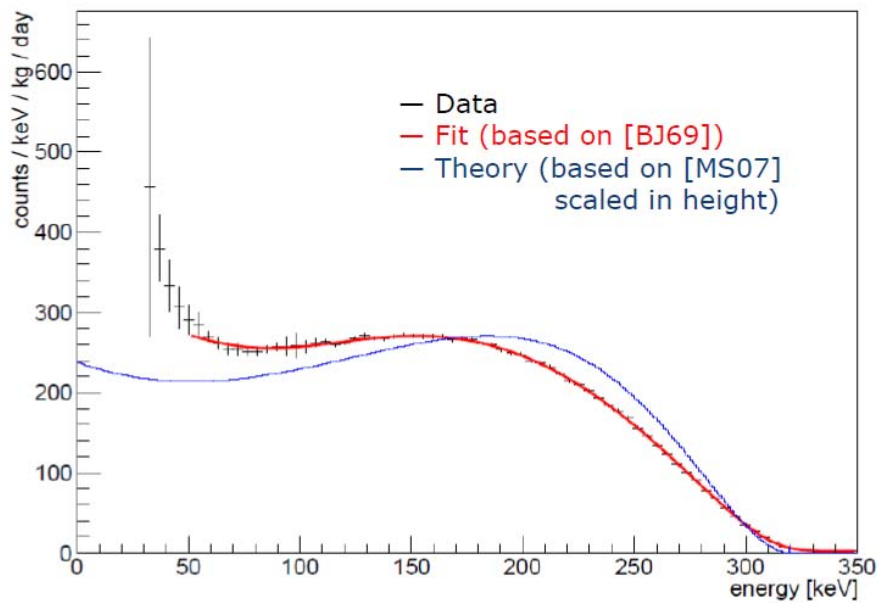

Figure 10: Predicted theoretical shape for ^{116}Cd by Mustonen et. al.[1] (blue); data (black) and fit of the data (red).

detectors.

2.4 Towards a large-scale set-up – Estimation of the total Background Rate

A Monte-Carlo (MC) campaign was initialized to estimate the total background rate, after an efficient radiation shield for a large-scale COBRA experiment was developed based on MC simulations as well. Altogether, 13824 detectors are simulated. The detectors have a size of $2\,\mathrm{cm} \times 2\,\mathrm{cm} \times 1.5\,\mathrm{cm}$ and a weight of $36\,\mathrm{g}$ each. Furthermore, a cathode on one side of the detectors and a lacquer surrounded the detectors are implemented. Nine detectors are arranged in a holder, which is built out of Delrin plates. In addition, the Kapton cable for the anode readout as well as the HV supply are applied. The weight of one holder is $\sim 360\,\mathrm{g}$.

Eight holders are aligned in a row with an ASIC in front of the first holder. Eight rows are lined up in a shelves and finally, 24 shelves are stacked building a cubic arrangement of the detectors. The inner part is surrounded by the developed shield. It consists of $10\,\mathrm{cm}$ copper, followed by $20\,\mathrm{cm}$ of lead. The outer layer is $10\,\mathrm{cm}$ boron loaded polyethylene. The whole set-up has therefore a total volume of $1655 \times 1650 \times 1650\,\mathrm{mm}^3$ and a total mass of $\sim 29200\,\mathrm{kg}$.

In the next step different background radiation sources, e.g. natural, man-made and cosmogenic radioactivity, as well as primary and secondary components of the cosmic radiation were investigated leading to a preliminary upper limit of the total background rate of $< 15.7 \cdot 10^{-3}$ events/kg/keV/year. Altogether, eleven set-up parts, e.g. lacquer, layers of the shield were considered as set-up parts. An important background source are radionuclei emitting alpha particles, which settle down on the set-up parts near the detector, e.g. the cathode, surface of the lacquer and the Delrin structure. This are mainly ^{222}Rn and its progeny, see Figure 11. Since analysis tools, like cuts on lateral surface events and multi-side events, cannot be applied in the simulation, the possibility to further reduce the total background rate is given.
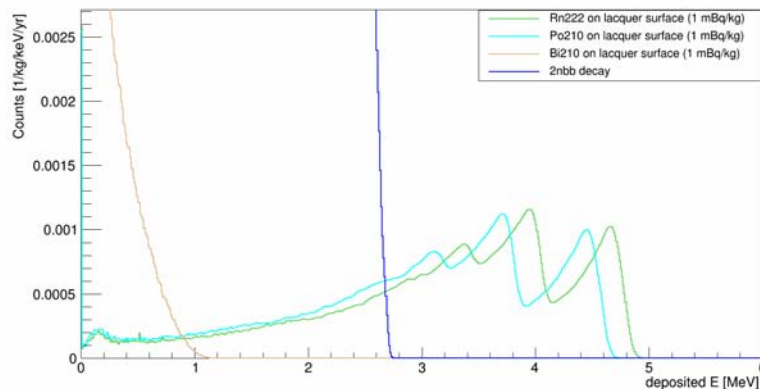

Figure 11: Spectra of ^{222}Rn and its progeny compared to the $2\nu\beta\beta$ decay of ^{116}Cd is depicted with a threshold of $40\,\mathrm{keV}$ and an energy resolution of $2\,\%$ FWHM.
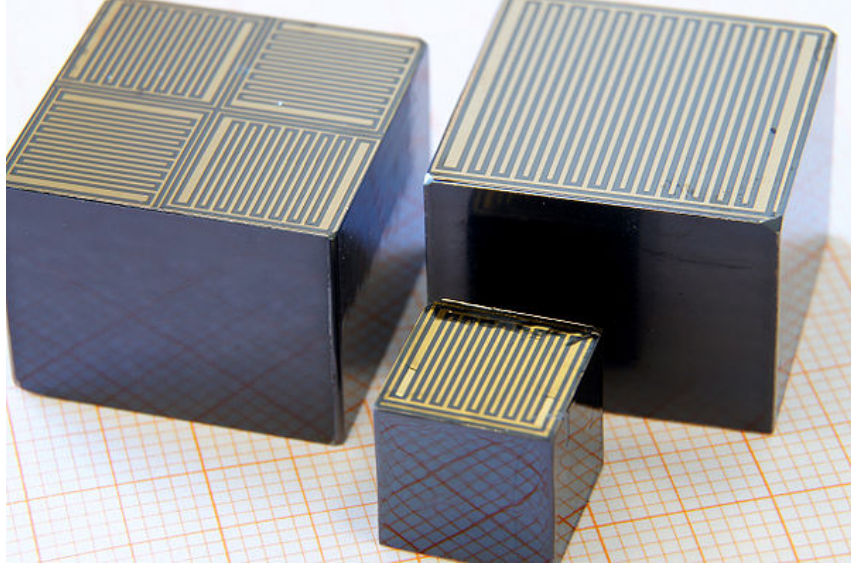
Figure 12: Picture of two of the new 6cm^3 Detectors, compared to the old 1cm^3 one.

3 Large detectors

The new large detectors have two different anode geometries (see fig 12). The first is the scaled anode design of the $1\,\mathrm{cm}^3$ detectors and the second are four standard grids on one detectors. Each grid is rotated by 90° against its neighbors. This ensures that one anode type only covers the sides of the crystal and the other one covers the inter subdetector walls. The behavior of both anode geometries are unknown because they have not been used on such large detectors before. Especially the quad structure will have an influence on the weighting potential of each subdetector. The quad detectors also allows the discrimination of multisite events intrinsically, if they trigger two anode grids, which also increases the signal to background ratio. All knowledge of operating parameters known for the small detectors have to be investigated for the large detectors. Furthermore, all pulse shape analysis cuts have to be validated on the large detectors as well. The first results look very promising that the overall detector performance is not decreased by these anode types.

4 Pixel detectors

The potential of fine pitch pixel hybrid detectors with CdTe sensor was further evaluated in simulations. The optimal pixel with respect to pixel size and sensor thickness has been determined with respect to energy resolution, detection efficiency and discrimination strength for track structures generated by neutrinoless double beta decays against single electron tracks from background processes. The optimal pixel pitch was found to be about 165 micrometers at 3 mm thickness of the CdTe sensor layer with respect to the sensitivity to the effective Majorana neutrino mass. Various topological features for the tracks of decay electrons were defined and used in random decision forests to distinguish between single electron tracks (background) and the tracks of the two electrons after neutrinoless double beta decay. Simulations have shown, that a relative reduction of the single electron background in the region of the Q-value of the double beta decay by about 75% seems possible with fine pitch hybrid pixel detectors.

The energy resolution for the sum energy in electron tracks in hybrid pixel detectors was

investigated in an experiment where pair production photons mimicked track structures of double beta decays. It was demonstrated that measured tracks could be classified as tracks produced by Compton scattering (single electron tracks) or as two tracks generated by pair production (electron, positron) using an artificial neutral network trained with simulated tracks. The results were published in 4.

5   Conclusion

The COBRA demonstrator setup has been completed in 2013. It now consists of all 64 detectors of the size $1 \times 1 \times 1 \times cm^3$. Improved methods contacting the detectors have been applied. Because of the increased heat dissipated with the new detector layers three and four, a cooling system became necessary. That is why the main DAQ rack dissipating the most heat was moved to another room, furthermore a system was installed cooling the preamplifier devices. Additional upgrades to improve the quality of the electronic signal transmission like a new radon barrier including cable feedthroughs were commissioned as well.

In laboratory test measurements new methods to reduce background in the offline analysis were tested. These new methods seem to be a very powerful tool, resulting in a count rate of less than 1 count / keV / kg / y in the region of interest.

More background reduction could be achieved if the detector and other surrounding material is stored, tested and handled in a cleanroom atmosphere.

6   List of Publications

1. Current Status and Future Perspectives of the COBRA Experiment; J. Ebert, M. Fritts, C. Gößling,T. Göpfert, D. Gehre, C. Hagner, N. Heidrich, T. Köttig, T. Neddermann, C. Oldorf, T. Quante, S. Rajek, O. Reinecke, O. Schulz, J. Tebrügge, J. Timm, B. Wonsak, and K. Zuber, published in Advances in High Energy Physics, Volume 2013 (2013), Article ID 703572

2. Pulse-shape discrimination of surface events in CdZnTe detectors for the COBRA experiment, M.Fritts, J. Tebrügge, J. Durst, J. Ebert, C. Gößling, T. Göpfert, D. Gehre, C. Hagner, N. Heidrich, M. Homann, T. Köttig, T. Neddermann, C. Oldorf, T. Quante, S. Rajek, O. Reinecke, O. Schulz, J. Timm, B. Wonsak, K. Zuber, NIMA (2014), DOI. 10.1016/j.nima.2014.02.038; arXiv 1401.5844

3. M. Fritts, J. Durst, T. Göpfert et al. Analytical model for event reconstruction in coplanar grid CdZnTe detectors. Nuclear Instruments and Methods in Physics Research Section A: Accelerators, Spectrometers, Detectors and Associated Equipment 708, 1 – 6 (2013). URL http://www.sciencedirect.com/science/article/pii/S0168900213000454.

4. Characterization of the energy resolution and the tracking capabilities of a hybrid pixel detector with CdTe-sensor layer for a possible use in a neutrinoless double beta decay experiment Mykhaylo Filipenko, Thomas Gleixner, Gisela Anton, Jürgen Durst and Thilo Michel, Eur. Phys. J. C (2013) 73: 2374

5. The potential of CdTe hybrid pixel detectors in the search for the neutrinoless double beta decay of 116Cd, Thilo Michel, Thomas Gleixner, Jürgen Durst, Mykhaylo Filipenko,

and Stefan Geißelsöder, Advances in High Energy Physics Volume 2013 (2013), Article ID 105318

The CRESST Dark Matter Search

G. Angloher [a], M. Bauer [e], A. Bento [f], C. Bucci [d], L. Canonica [d], A. Erb [c],
A. Ertl [c], F. von Feilitzsch [c], P. Gorla [d], A. Guetlein [g], D. Hauff [a], J. Jochum
[e], C. Kister [a], H. Kraus [b], J.C. Lanfranchi [c], J. Loebell [e], A. Mnster [c],
F. Petricca [a], W. Potzel [c], F. Pröbst [a], F. Reindl[a], S. Roth [c], K. Rottler [e],
C. Sailer[e], K. Schäffner[a], S. Schönert [c], J. Schieck [g], W. Seidel [a, +], M. von
Sivers[c], L. Stodolsky [a], C. Strandhagen [e], R. Strauss[c], A. Tanzke[a],
M. Uffinger [e], A. Ulrich [c], I. Usherov[e], S. Wawoczny[c], M. Willers[c],
M. Wüstrich [a], A. Zöller[c]

[a] *MPI für Physik, Föhringer Ring 6, 80805 Munich, Germany*
[b] *University of Oxford, Department of Physics, Oxford OX1 3RH, U.K.*
[c] *Technische Universität München, Physik Department, D-85747 Garching, Germany*
[d] *Laboratori Nazionali del Gran Sasso, I-67010 Assergi, Italy*
[e] *Eberhard-Karls-Universität Tübingen, D-72076 Tübingen, Germany*
[f] *Departamento de Fisica, Universidade de Coimbra, Coimbra, Portugal*
[g] *Institut fr Hochenergiephysik der sterreichischen Akademie der Wissenschaften, Wien, Austria*
[+] *Spokesperson E-mail address: seidel@mppmu.mpg.de*

Abstract

The aim of CRESST (**C**ryogenic **R**are **E**vent **S**earch with **S**uper-
conducting **T**hermometers) is to search for particle Dark Matter and
to contribute to the elucidation of its nature. The experiment is lo-
cated at the 'Laboratori Nazionali del Gran Sasso' (LNGS), Italy,
and it uses low background cryogenic detectors with superconduct-
ing phase transition thermometers for the direct detection of WIMP-
nucleus scattering events.

1 Dark Matter

There is strong evidence for the existence of dark matter on all astronomical scales, ranging from dwarf galaxies, through spiral galaxies like our own, to large-scale structures. The history of the universe is difficult to reconstruct without dark matter, be it Big Bang Nucleosynthesis or structure formation.

Despite this persuasive indirect evidence for its existence, the direct detection of dark matter remains one of the outstanding experimental challenges of present-day physics and cosmology.

A plausible candidate for the dark matter is the Weakly Interacting Massive Particle (WIMP) and it is possible that it can be detected by laboratory experiments, particularly using cryogenic methods, which are well adapted to the small energy deposit anticipated. Supersymmetry provides a well-motivated WIMP candidate in the form of the Lightest Supersymmetric Particle. WIMPs are expected to be gravitationally bound in a roughly isothermal halo around the visible part of our galaxy with a density of about $0.3 \, \mathrm{GeV/cm^3}$ at the position of the Earth.

Interaction with ordinary matter is expected via elastic scattering on nuclei. This elastic scattering can occur via coherent ("spin-independent") and spin-dependent interactions. For the coherent case, a factor A^2 is expected in the cross-section, favouring heavy nuclei.

Conventional methods for direct detection rely on the ionisation or scintillation caused by the recoiling nucleus. This leads to certain limitations connected with the low ionisation or scintillation efficiency of the slow recoil nuclei. The cryogenic detectors developed for CRESST measure the deposited energy calorimetrically, independent of the type of interaction, and allow for the detection of much smaller recoil energies. When such a calorimetric measurement of the deposited energy is combined with a measurement of scintillation light, an extremely efficient discrimination of the nuclear recoil signals from radioactive background signals can be obtained. These type of detectors are being used in the present phase CRESST-II.

2 Detection Principle

The low-temperature calorimeters consist of a target crystal with an extremely sensitive superconducting phase transition thermometer on its surface. A weak thermal coupling to a heat bath restores again the equilibrium temperature after an interaction. The thermometer is made of a tungsten film evaporated onto the target crystal. Its temperature is stabilised within the transition from the superconducting to the normal conducting state, which
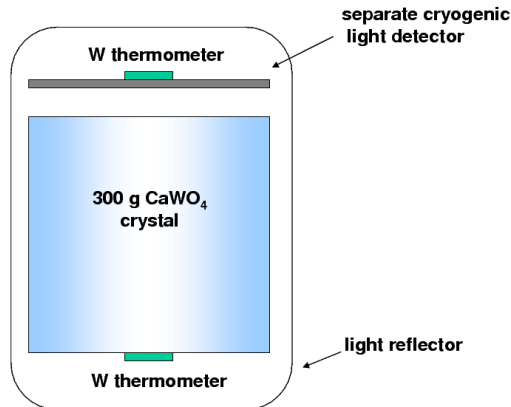
Figure 1: Schematic representation of the detector for simultaneous phonon and light measurement. It consists of two separate cryogenic detectors enclosed in a highly reflective housing, read out by tungsten superconducting phase-transition thermometers. This concept, developed by scientists of the institute, is used in CRESST-II. It allows a very efficient discrimination of the searched nuclear recoil signals from the dominant radioactive β- and γ-backgrounds.

occurs at temperatures of about $10\,\mathrm{mK}$. A typical width of the transition is about $1\,\mathrm{mK}$. A small temperature rise e.g. from a WIMP–nucleus scattering event (typically some $\mu\mathrm{K}$), leads to an increase of resistance, which is measured with a SQUID (**S**uperconducting **Qu**antum **I**nterference **D**evice). For the first phase of CRESST, which ended in 2001, $262\,\mathrm{g}$ sapphire detectors had been developed at MPI. These detectors provided an excellent energy resolution of $133\,\mathrm{eV}$ at $6\,\mathrm{keV}$ and a very low energy threshold of $600\,\mathrm{eV}$.

In the second phase, CRESST-II, we are using $300\,\mathrm{g}$ scintillating $CaWO_4$ target crystals. The scintillating crystal is equipped with a superconducting tungsten phase-transition thermometer for the detection of the phonons created by a particle interaction in the scintillating crystal. A small fraction of $\sim 1\%$ of the deposited energy is emitted as scintillation light, which is measured with a separate cryogenic detector, optimised for light detection. Fig. 1 shows a scheme of this composite detector.

Starting with a proof-of-principle experiment in 1998, the technique of simultaneous measurement of phonons and scintillation light has been developed at the Max-Planck-Institute. The important advantage of this technique is that it offers an extremely efficient suppression of the radioactive background down to very low recoil energies of about $10\,\mathrm{keV}$. While the phonon signal measures the deposited energy, the amplitude of the corresponding light signal depends on the type of interaction. Nuclear recoils,
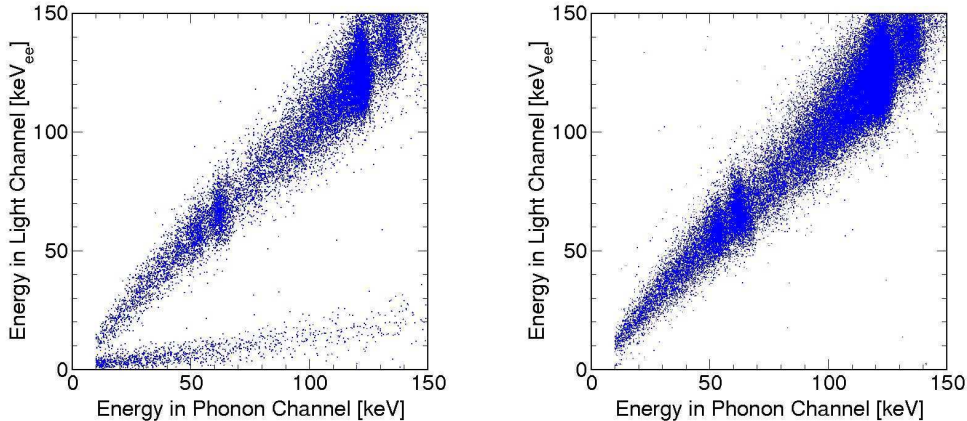
27

Figure 2: Coincident detection of phonons and scintillation light with a $CaWO_4$ detector. Left: The upper band of events is due to irradiation of the $CaWO_4$ crystal with electrons and gammas, whereas the lower band with lower light yield, is from nuclear recoils caused by a neutron source. Right: Removing the neutron source confirms that there is no leakage of ionising events into the nuclear recoil region.

such as WIMP or neutron scattering events, emit substantially less scintillation light than fully ionising interactions, e.g. γ or β interactions, do. As the overwhelming part of the background consists of β and γ interactions, this phonon/light technique provides a very effective method of background suppression. Fig. 2 illustrates this detection method.

Compared with the alternative approach of simultaneous measurement of phonons and charge in a semiconductor crystal, which is applied in the experiments CDMS-II and Edelweiss-II, the method developed for CRESST-II has the important advantage that it does not suffer from dead layers at the surface. A reduced charge collection for ionising events occurring close to the surface in semiconducting crystals may lead to a false identification of low energetic γ's and β's as nuclear recoils. The result in Fig. 2, which was obtained with a gamma and beta source, confirms that the suppression also works for low-energy electrons impinging onto the crystal surface.

3 The CRESST Setup in Gran Sasso

The central part of the CRESST installation at Gran Sasso is the cryostat. The low temperature which is generated in the mixing chamber of the dilution

refrigerator is transferred into the radio-pure cold box, via a 1.5 m long cold finger. The cold finger is protected by thermal radiation shields, all fabricated of low-background copper. The detectors are mounted inside the cold box at the end of the cold finger. Two internal cold shields consisting of low-level lead are attached to the mixing chamber and to a thermal radiation shield at liquid N_2 temperature, respectively, in order to block any line-of-sight from the non-radio-pure parts of the dilution refrigerator to the detectors inside the cold box. The design completely avoids potentially contaminated cryogenic liquids inside the cold box.

An extensive passive shielding of low-background copper and lead surrounds the cold box and serves to shield radioactivity from the surrounding rock. The entire shielding is enclosed inside a gas-tight radon box that is flushed with boil of N_2 gas and maintained at a small overpressure. Special care was taken to minimise above-ground exposure of the construction materials of the cold box and the shielding to cosmic rays, in order to avoid activation.

4 Preparations for the present run

The latest run of CRESST took place between June 2009 and April 2011. It included a neutron test and γ-calibrations with ^{57}Co and ^{232}Th sources. Out of the 18 detector modules installed in the cryostat only 8 were used for the Dark Matter analysis. One was excluded due to its unusually poor energy resolution and an additional one was excluded being equipped with a test $ZnWO_4$ crystal. The remaining ones mainly had difficulties in cooling the light detectors and could therefore not provide the full information needed for Dark Matter analysis, but still were used to tag coincident events with signals in more than one detector module.The validity of events which are considered for analysis is ured with few basic quality cuts applied to the raw data [1]. The data set collected by eight detector modules between July 2009 and March 2011 corresponding to a total net exposure after cuts of 730 kg days showed some hint for the possible existence of a light mass WIMP (see last annual report). To clarify this situation a run with strongly reduced background was prepared. .

In the reporting period a new run has been prepeared with modificatons of detectors and setup aiming at a significant reduction of the overall background level. The most important modification addresses the reduction of the α and ^{206}Pb-recoil backgrounds. Another modification addresses the neutron background. Our main goal for the next run is to either confirm or reject the presence of a low mass WIMP signal with high confidence and
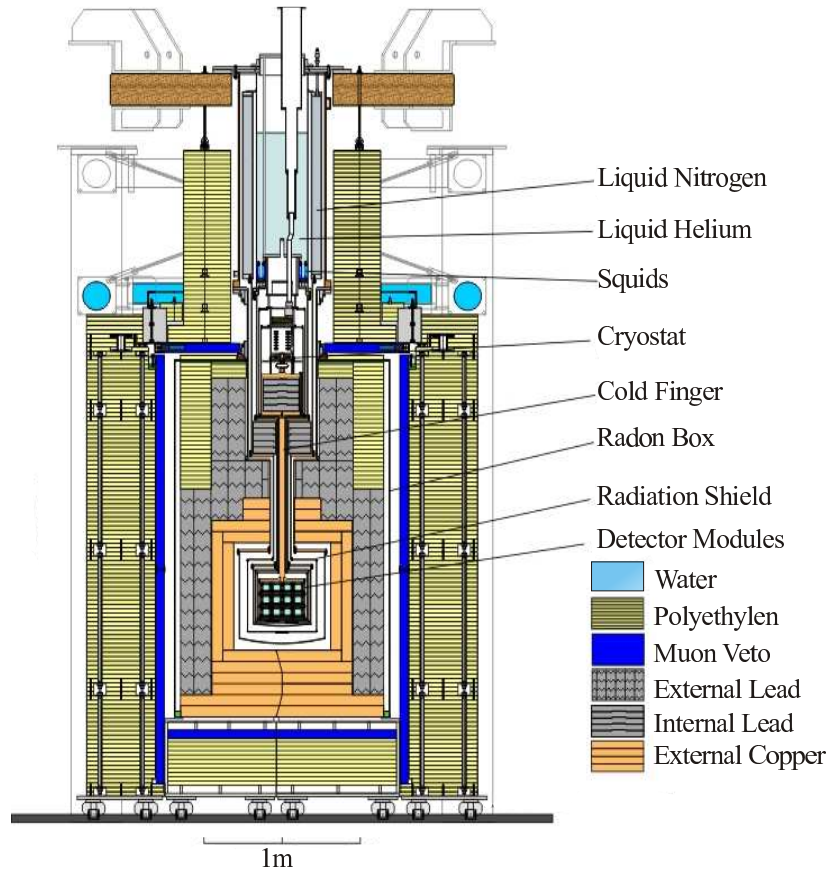
Figure 3: Dilution refrigerator and low-background cold box with its shielding upgraded for CRESST-II. The gas-tight radon box enclosing the Cu (shown in gray) and Pb (blue) shielding is completely covered by a plastic scintillator μ-veto (pink) and 40 cm of polyethylene (red).

negligible systematic uncertainties due to the modeling of backgrounds. In the following sections we will briefly describe the measures for the reduction of background.

4.1 Measures for reduction of background

4.1.1 Neutron background

The neutron shielding in the last run consisted of $\sim$40 cm of polyethylene (PE) surrounding the Pb/Cu shielding. The remaining neutron background in the data was most likely from neutrons in the Pb/Cu shielding, either generated by radioactive processes in the shielding material or by muons

penetrating the Pb/Cu shielding without triggering the muon veto. Such neutrons inside the Pb/Cu shileding have relatively low kinetic energies and can effectively be moderated already by a relatively thin plastic layer placed inside the Pb/Cu shield. Therefore install a 5 cm thick polyethylene layer inside the Pb/Cu shieldwas installed. It is expected to reduce the background from neutrons originating in the Pb/Cu shield by more than an order of magnitude. Part of this shielding is placed in vacuum inside the cold box, and another overlapping part outside. The outside part may be removed to still allow a neutron test with an external neutroun source during the run.

4.2 Degraded α's and ^{206}Pb nuclear recoil background

The silver coated bronze clamps holding the target crystal, which provide the only non scintillationg surface inside the detector housing, were identified as the source of these two types of backgrounds in the last run. The degraded α-particles observed at low energies can be attributed to a significant ^{210}Pb contamination in the bulk material (Cu-Sn bronze) of the clamps, while the ^{206}Pb recoil background was from ^{210}Po or ^{210}Pb atoms deposited at the surface of the silver coated clamps. The range of the 103 keV Pb recoils in silver is just a few tens of atomic layers, and it is only the contamination of the surface which matters here.

The ^{210}Pb atoms may have been deposited during an exposure to radon in air after production of the clamps, e.g. while mounting of detectors in the cold box at Gran Sasso. The cool down of the last run was interrupted by the L'Aquila earthquake and detectors had to be repaired and remounted again underground after the earthquake, before the successful cool down took place. This resulted in a prolonged exposure of about 6 weeks to radon in the air of the underground laboratory.

On the other hand, a very rapid deposition of ^{210}Po may have occurred at the end of the electrolytic silver coating process in the moment, when the voltage was disconnected [2]. Both types of initial deposits, ^{210}Po or ^{210}Pb, can be distinguished via the resulting time dependence of the rate of ejected ^{206}Pb recoils. When ^{210}Pb is deposited, the rate will *increase* with the 138 days half life of ^{210}Po. However, when ^{210}Po is deposited the rate will decrease with the same half life. An analysis of the data of the last run indicates a rise of the rate and and suggests that it is 210Pb freshly deposited just before the start of the run, which is responsible for most of the events in the Pb reference region. This supports the hypothesis that exposure of the clamps to radon in air may have contributed a significant fraction of the low energetic ^{206}Pb recoil background observed in the last run and preventing radon exposure of the clamps may significantly reduce this background.

31

4.2.1 Radon prevention during assembly and mounting of detectors

Originally we planned to assemble detectors for next run in the clean room at MPI and use radon reduced air for mounting of detector modules in the cryostat. The clean room ventilation in Munich was modified to get fresh air with a high flow from about 15 m above ground, where we expected the radon level to be relatively low. First tests in early spring 2012 gave radon levels below $\sim 5\,\mathrm{Bq/m^3}$. However, with rising temperatures outside, the overall level increased and sometimes peaks well above $10\,\mathrm{Bq/m^3}$ were measured. This forced us to give up the plan of conveniently assembling detector modules in the clean room at MPI. An intermediate attempt of mounting in an existing glove box under N_2 atmosphere proved to be too slow and too difficult.

In autumn 2012 we finally decided to build a tight metallic housing around our already existing laminar flow area at the top floor of the CRESST building at Gran Sasso and supply it with deradonized ($¡5[\mathrm{mBq/m^3}]$) air. This setup for assembling detectors has been completed in January 2013.

Additionally, a space around the coldbox of the cryostat was prepared, which can be flushed with deradonized air to avoid radon during the phase of mounting of detectors in the cold box. All detectors were mounted and stored in a Radon free atmosphere.

4.2.2 New clamps

We made a new bronze material from selected Cu and extremely high purity tin and fabricated new clamps from this material. A small tin sample was converted into a cryogenic calorimeter to measure the rate of alpha decyas occurring in the volume. In this measurement no ^{210}Po decay was observed, which translates into an upper limit of the ^{210}Po activity of ¡ 28 mBq/kg. With this type of measurement were able to improve the limit which can be obtained with a conventional low background Ge detector by almost two orders of magnitude. All production steps from the starting material to the final clamps were carefully controlled with mass spectrometry measurements of iostopes in the natural decay chains.

We are very confident that the background of degraded alphas with this new clamps will practically disappear. Instead of using a problematic silver coating, the surface of the clamps is sputter etched and then sputter coated with aluminum. After sputter coating clamps were stored in containers continuously flushed with N^2 gas.

5 Current status of the experiment

The CRESST cryostat was cooled down in May 2013.
All the 18 detector modules mounted became operational within two weeks from the cool down, enhancing the success rate in terms of operational detectors to 100%. The significantly shorter time required with respect to the past can be attributed to an improved thermal coupling of the holding structure of the detectors (carousel) and to the replacement of the full set of detector holders. This last measure was taken to ensure the use of a heat leak free copper for all parts constituting the holders.
The cool down was followed by a gamma calibration and by the optimization of detectors which extended until end of July 2013.
Since July 30th the CRESST experiment is taking Dark Matter data.
One of the 18 light detectors shows an unclear problem with the heater disturbing the stability of the complete carousel. Therefore, the stabilization of it in the operating point had to be avoided.
Our main goal for the current run is to lower neutron, α and ^{206}Po recoil backgrounds by more than an order of magnitude with respect to the achievements of the previous run. This should then allow to either confirm or reject the presence of a low mass WIMP signal with high confidence and negligible systematic uncertainties due to the modeling of these backgrounds.

References

[1] Godehard Angloher et al. Results from 730 kgdays of the CRESST-II dark matter search. *Eur. Phys. J. C*, 72(4), 2012.

[2] F.L.Romines S.C.Ehinger, R.A.Pacer. Separation of the radionuclides ^{210}Pb-^{210}Bi-^{210}Po by spontaneous deposition onto noble metals and verification by cherenkov and liquid scintillation counting. *Journal of Radioanalytical and Nuclear Chemistry*, 98(1):39, 1986.

CUORE
2013 LNGS Report

F. Alessandria,[1] M. Ameri,[2] D. R. Artusa,[3, 4] F. T. Avignone III,[3] O. Azzolini,[5] M. Balata,[4]
T. I. Banks,[4, 6, 7] G. Bari,[8] J. Beeman,[9] F. Bellini,[10, 11] A. Bersani,[2] M. Biassoni,[12, 13]
C. Brofferio,[12, 13] C. Bucci,[4] X. Z. Cai,[14] A. Camacho,[5] L. Canonica,[4] X. Cao,[14] S. Capelli,[12, 13]
M. Capodiferro,[11] L. Carbone,[13] L. Cardani,[10, 11] M. Cariello,[2] M. Carrettoni,[12, 13] N. Casali,[4]
R. Cereseto,[2] G. Ceruti,[13] A. Chiarini,[8] D. Chiesa,[12, 13] N. Chott,[3] M. Clemenza,[12, 13]
C. Cosmelli,[10, 11] O. Cremonesi,[13] C. Crescentini,[8] R. J. Creswick,[3] I. Dafinei,[11] A. Dally,[15]
V. Datskov,[13] A. De Biasi,[5] M. M. Deninno,[8] S. Di Domizio,[2, 16] M. L. di Vacri,[4] L. Ejzak,[15]
D. Q. Fang,[14] H. A. Farach,[3] M. Faverzani,[12, 13] G. Fernandes,[2, 16] E. Ferri,[12, 13] F. Ferroni,[10, 11]
S. Finelli,[8] E. Fiorini,[12, 13] M. A. Franceschi,[17] S. J. Freedman,[6, 7, ‡] B. K. Fujikawa,[7] R. Gaigher,[13]
A. Giachero,[12, 13] L. Gironi,[12, 13] A. Giuliani,[18] J. Goett,[4] P. Gorla,[4] C. Gotti,[12, 13] M. Guerzoni,[8]
T. D. Gutierrez,[19] E. E. Haller,[9, 20] K. Han,[7] K. M. Heeger,[15, 21] R. Hennings-Yeomans,[6]
H. Z. Huang,[22] M. Iannone,[11] R. Kadel,[23] K. Kazkaz,[24] G. Keppel,[5] Yu. G. Kolomensky,[6, 23] Y. L. Li,[14]
C. Ligi,[17] X. Liu,[22] Y. G. Ma,[14] C. Maiano,[12, 13] M. Maino,[12, 13] M. Martinez,[25] R. H. Maruyama,[15, 21]
R. Mazza,[13] Y. Mei,[7] N. Moggi,[8] S. Morganti,[11] T. Napolitano,[17] M. Nastasi,[13] S. Nisi,[4] C. Nones,[26]
E. B. Norman,[24, 27] A. Nucciotti,[12, 13] T. O'Donnell,[6] F. Orio,[11] D. Orlandi,[4] J. L. Ouellet,[6, 7]
M. Pallavicini,[2, 16] V. Palmieri,[5] L. Pattavina,[13] M. Pavan,[12, 13] M. Pedretti,[24] A. Pelosi,[11]
M. Perego,[13] G. Pessina,[13] V. Pettinacci,[11] G. Piperno,[10, 11] C. Pira,[5] S. Pirro,[13] E. Previtali,[13]
V. Rampazzo,[5] C. Rosenfeld,[3] C. Rusconi,[13] E. Sala,[12, 13] S. Sangiorgio,[24] N. D. Scielzo,[24]
M. Sisti,[12, 13] A. R. Smith,[28] F. Stivanello,[5] L. Taffarello,[29] M. Tenconi,[18] F. Terranova,[13]
W. D. Tian,[14] C. Tomei,[11] S. Trentalange,[22] G. Ventura,[30, 31] M. Vignati,[11] B. S. Wang,[24, 27]
H. W. Wang,[14] L. Wielgus,[15] J. Wilson,[3] L. A. Winslow,[22] T. Wise,[15, 21] A. Woodcraft,[32]
L. Zanotti,[12, 13] C. Zarra,[4] B. X. Zhu,[22] S. Zucchelli[8, 33]

(The CUORE Collaboration)

[1]INFN - Sezione di Milano, Milano I-20133 - Italy
[2]INFN - Sezione di Genova, Genova I-16146 - Italy
[3]Department of Physics and Astronomy, University of South Carolina, Columbia, SC 29208 - USA
[4]INFN - Laboratori Nazionali del Gran Sasso, Assergi (L'Aquila) I-67010 - Italy
[5]INFN - Laboratori Nazionali di Legnaro, Legnaro (Padova) I-35020 - Italy
[6]Department of Physics, University of California, Berkeley, CA 94720 - USA
[7]Nuclear Science Division, Lawrence Berkeley National Laboratory, Berkeley, CA 94720 - USA
[8]INFN - Sezione di Bologna, Bologna I-40127 - Italy
[9]Materials Science Division, Lawrence Berkeley National Laboratory, Berkeley, CA 94720 - USA
[10]Dipartimento di Fisica, Sapienza Università di Roma, Roma I-00185 - Italy
[11]INFN - Sezione di Roma, Roma I-00185 - Italy

[12]Dipartimento di Fisica, Università di Milano-Bicocca, Milano I-20126 - Italy

[13]INFN - Sezione di Milano Bicocca, Milano I-20126 - Italy

[14]Shanghai Institute of Applied Physics (Chinese Academy of Sciences), Shanghai 201800 - China

[15]Department of Physics, University of Wisconsin, Madison, WI 53706 - USA

[16]Dipartimento di Fisica, Università di Genova, Genova I-16146 - Italy

[17]INFN - Laboratori Nazionali di Frascati, Frascati (Roma) I-00044 - Italy

[18]Centre de Spectrométrie Nucléaire et de Spectrométrie de Masse, 91405 Orsay Campus - France

[19]Physics Department, California Polytechnic State University, San Luis Obispo, CA 93407 - USA

[20]Department of Materials Science and Engineering, University of California, Berkeley, CA 94720 - USA

[21]Department of Physics, Yale University, New Haven, CT 06520 - USA

[22]Department of Physics and Astronomy, University of California, Los Angeles, CA 90095 - USA

[23]Physics Division, Lawrence Berkeley National Laboratory, Berkeley, CA 94720 - USA

[24]Lawrence Livermore National Laboratory, Livermore, CA 94550 - USA

[25]Laboratorio de Fisica Nuclear y Astroparticulas, Universidad de Zaragoza, Zaragoza 50009 - Spain

[26]Service de Physique des Particules, CEA / Saclay, 91191 Gif-sur-Yvette - France

[27]Department of Nuclear Engineering, University of California, Berkeley, CA 94720 - USA

[28]EH&S Division, Lawrence Berkeley National Laboratory, Berkeley, CA 94720 - USA

[29]INFN - Sezione di Padova, Padova I-35131 - Italy

[30]Dipartimento di Fisica, Università di Firenze, Firenze I-50125 - Italy

[31]INFN - Sezione di Firenze, Firenze I-50125 - Italy

[32]SUPA, Institute for Astronomy, University of Edinburgh, Blackford Hill, Edinburgh EH9 3HJ - UK

[33]Dipartimento di Fisica, Università di Bologna, Bologna I-40127 - Italy

[‡]Deceased

Abstract

CUORE is a challenging experiment designed to exploit the cryogenic bolometer technique to reach a sensitivity of the order 10^{26} years on the $\beta\beta(0\nu)$ half-life of ^{130}Te, thus approaching the inverted hierarchy region of the neutrino masses. The detector will consist of a close-packed array of TeO_2 crystals containing $\sim$ 206 kg of ^{130}Te in total and cooled to an operating temperature of $\sim$ 10 mK inside a large, dedicated cryostat.

CUORE is now in an advanced stage of construction. All construction-related activities are essentially on schedule, and items on the critical path are being followed with particular care. The first phase of the cryogenic commissioning was completed during the summer with the second successful cooldown of the 4 K section. Meanwhile, the detector assembly line has continued to make steady progress in constructing towers and data collection with CUORE-0 has begun. Here we report the most relevant activities carried out for the CUORE experiment in 2013.

1 Detector components

The CUORE detector will consist of 988 TeO_2 crystals arranged into 19 identical towers. Each tower will contain 52 crystals held securely inside a copper structure by specially-designed PTFE brackets (Fig. 1).
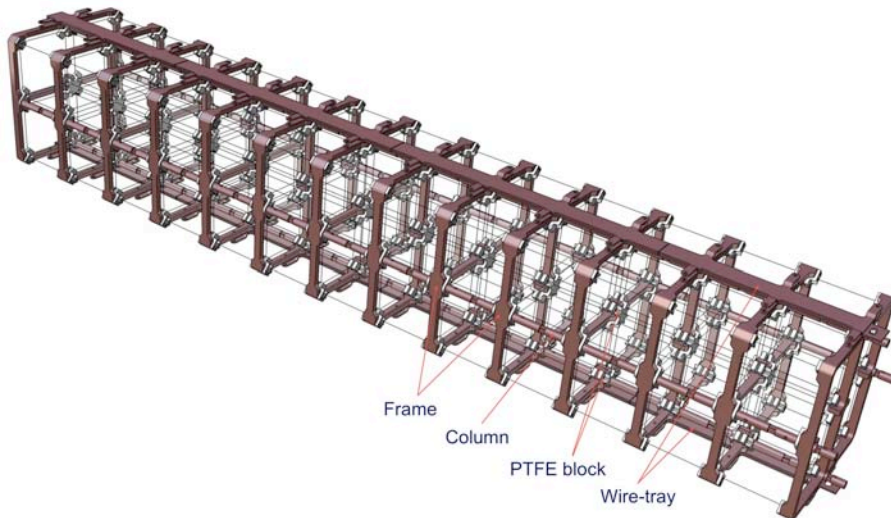
Figure 1: Detailed view of the components of a single CUORE tower.

A temperature sensor (neutron-transmutation doped (NTD) Germanium thermistor) and a Joule heater are glued to one face of each crystal. After a tower is assembled, gold wires are bonded directly from the thermistor and heater to readout ribbons held in specially designed copper trays fixed to the tower structure. A complex procedure for cleaning the tower copper parts—the so-called "TECM" process, based on a sequence of mechanical, electro-chemical, chemical, and magneto-plasma treatments—has been developed in order to guarantee that background contributions from radioactive surface contaminants are reduced to an acceptable level.

A detector-part database has been developed to store relevant information about every component of the CUORE detector, i.e. production time, cleaning history, sea-level exposure time intervals, and so on.

1.1 Crystals

The $5 \times 5 \times 5$ cm^3 TeO$_2$ crystals were grown at the Shanghai Institute of Ceramics, Chinese Academy of Sciences (SICCAS). Crystal production has proceeded steadily since 2009 at a dedicated clean room facility in Jiading, China, and batches of finished crystals were shipped to LNGS every 1–2 months, traveling by sea to limit cosmogenic activation. All 1063 TeO$_2$ absorbers have now been delivered to LNGS. After a visual inspection, the delivered crystals are stored in nitrogen-fluxed cabinets in CUORE's underground Part Storage Area (PSA). Of the 1063 delivered crystals only a fraction (24) were found to have some visible internal flaws, whose origin is unknown. These crystals were returned to SICCAS and replaced with new ones.

Approximately 4% of the delivered crystals are tested as cryogenic bolometers to verify their radio-purity and to check overall performance. In these so-called CUORE Crystal Validation Runs (CCVRs), four crystals are randomly selected from the most recent shipments, assembled into a detector module, and cooled to 10 mK inside the CUORE R&D cryostat in Hall C at LNGS. Each CCVR typically lasts for ~ 1 month, which is

the time needed to acquire sufficient statistics to verify that the crystals meet contract specifications. The last CCVR has been performed in summer 2013. All of the tested crystals have met or exceeded the desired energy resolution and the contract specifications for bulk radioactivity and dimensional tolerances. Based on this, we expect all crystals to meet the requirements for CUORE.

In June 2013, three workers from SICCAS spent two weeks at LNGS to reprocess the surfaces of a total of 44 TeO$_2$ crystals which had been used for CCVRs or which suffered a failure during the gluing procedure. The polishing of the crystal surfaces was accomplished using the same procedures followed at the Chinese plant. Crystals were then vacuum-packed in a double-layered PET bag, before returning to the PSA storage.

1.2 NTD thermistors

Each CUORE crystal is instrumented with a NTD Ge thermistor for signal readout. These devices are produced by irradiating pure Ge wafers at the MIT research reactor for precise lengths of time. This procedure dopes the semiconductor very homogeneously and also very close to the metal-insulator transition, a necessary characteristic of these specialized thermistors. After a nine-month radioactive-decay "cool-off" period, the wafers are further processed into sensors at LBNL. To date, more than 1500 CUORE-specific thermistors have been prepared in this manner. About 1000 are needed to fully instrument CUORE, including 988 used for direct event detection and the remainder used for monitoring temperatures around the cryostat.

In August 2013, the assembly team encountered unusual wire-bonding problems with some of the thermistors in Towers 5 and 6 (Towers 1, 2, 3, and 4 were bonded successfully). Wires were not adhering properly to the gold contact pads on the NTDs during the usual ball-bonding process. Rutherford backscattering (RBS) and Secondary Ion Mass Spectrometry (SIMS) measurements conducted on both bondable and problematic NTDs revealed significant contact metal/Ge alloying within the problematic bonding pads. The measurements are consistent with an overheating of the Ge substrate during the vacuum-deposition plating process. We have subsequently identified two batches of thermistors that show tis phenomenon: those produced in December 2011 and a second set delivered in mid-2013.

In light of this, we have sampled all remaining NTD batches to identify those that are easily bondable prior to gluing the thermistors onto the TeO$_2$ crystals. We have also developed specific techniques that allow us to successfully wire bond to the alloyed-contact devices that are already installed in towers. Concurrent with this work, we designed and fabricated a new mask for producing all remaining thermistors. The new mask incorporates the use of high thermal-conductivity materials, reflective coatings, and a thermal shield to reduce the overall heat load on the NTDs during contact formation. These improvements have shown to be quite effective and the new mask has subsequently been used to fabricate two new batches of devices.

Towers 7, 8, and 9 were assembled with "certified bondable" NTDs and were successfully wire bonded. We are now highly confident about the effectiveness of the NTD selection process and new fabrication procedures. To date, about 300 thermistors have been manufactured with the new process and both SIMS tests and bonding of a small

statistical sample indicate they are easily bondable. A total of 13 towers have been assembled and fully bonded, and the equivalent of over 17 towers worth of thermistors have been glued to the TeO$_2$ crystals. There exist adequate, approved, thermistors to complete all the 19 towers foreseen for CUORE.

1.3 Copper parts

The copper parts that form the scaffolding for the CUORE detector towers are fabricated in the Milano Bicocca and Legnaro workshops, cleaned at LNL (Laboratori Nazionali di Legnaro) according to a special protocol (see Section 1), and then placed in underground storage at LNGS (PSA) until the time comes for assembly. Both the design of the tower structure and the surface cleaning methods are rather different with respect to those used in Cuoricino. A complete test of the copper fabrication, cleaning, and assembly sequence was possible only via the construction and operation of the CUORE-0 tower.

The production of the frames by the Legnaro workshop encountered a major interruption during Spring 2013 due to severe maintenance needs of the Electrical Discharge Machine (EDM) used to process them, which took a few months to be fixed by the CELADA company. The production recovered at the beginning of June 2013. This caused a shift of the completion of CUORE frame production to January 2014, which includes also additional machining requests to replace damaged frames during cleaning and/or assembly steps.

The frame production interruption did not interfere with the cleaning line of the copper parts. Regular TECM cleaning of CUORE copper parts has been steadily going since Easter 2012.Thanks to the new second plasma cleaning machine recently incorporated into the cleaning line, the TECM cleaning throughput is on schedule. Several quality checks are done at various points of the cleaning process, especially for what concerns the radio-purity of the cleaning acids and the alpha-contamination of treated copper test pieces. Copper parts for the first twelve towers were already sent to LNGS and the third batch of six towers was completed and stored inside the PSA.

2 Electronics and data acquisition

Main goal of the CUORE electronics is to provide an effective low-noise system for reading and monitoring CUORE detectors. It is interfaced to the CUORE data acquisition system (DAQ) which records the data and provides a link with the slow-control and data analysis tools.

2.1 Front-end electronics

The pre-production phase of the main board of the front-end electronics has been completed. The corresponding samples are currently under validation at the INFN Milano-Bicocca laboratory. The final production is foreseen to be completed in early 2014. Each board consists of 8 layers of $233\times280\,\mathrm{mm}^2$ PCB that accommodate 6 channels. Each channel is composed of a preamplifier and a second-stage PGA, the load resistors, the

detector biasing system, and a number of other features which allow the thermistor DC characterization and the monitoring of many voltage nodes. The main board contains more than 1000 components and is remotely accessible via CAN serial bus.

The backplane boards for the main board have also been pre-produced. Their final production will follow the prototyping of the pulser boards and power supplies. CAN serial bus is coupled by fibre optic to the electronics and the glue boards for the electrical-light-electrical conversion have been in pre-production since mid September.

UCLA is going to receive the final production of the Bessel filter boards for testing. Their antialising programmable frequencies have been optimized on detectors having characteristics close to those of CUORE-0. USC has produced the boards for the DC/DC conversion system and is assembling the components. As soon as they will be available, they will be tested in CUORE-0. The final phase of the characterization and calibration of the preamplifiers was completed at UCLA. Tests on the connecting link between the mixing chamber and room temperature are ongoing at Milano-Bicocca.

2.2   Faraday cage

The Faraday Cage is mainly needed to shield the high-impedance signal links between the detectors and the front-end electronics from disturbances coming from the main power line (50 Hz), cryogenic pumps and all other EMI interferences which may be injected from the outside. Located on the second floor of the CUORE building, the cage will exploit the existing vertical beams (building steel work) as a mechanical support. The cage volume will be $6.3{\times}6.1{\times}2.9\,\mathrm{m}^3$. The total surface will be close to $150\,\mathrm{m}^2$. The preliminary specification is for a 60 dB attenuation at 50 Hz. Since the disturbances at 50 Hz are mainly induced through the magnetic field, they must be shielded by absorption, which requires a shield made of a high magnetic permeability material. Steel plates of $6\,\mathrm{mm}$ thickness would constitute a good shield, but the overall weight would exceed the maximum load for the hut floor. A lighter solution is to combine a thinner layer of steel with panels of Skudotech, a material specifically designed for low-frequency magnetic shielding. Skudotech comes in panels (Skudal S3022) made of $3\,\mathrm{mm}$ thick aluminum layer, a $0.2\,\mathrm{mm}$ Skudotech layer, and a $2\,\mathrm{mm}$ aluminum layer, which will cover the inner side of the walls of the Faraday cage. The mechanical design of the structure is ongoing. The grounding configuration of the whole experiment is also being studied.

2.3   Slow control

The CUORE Slow Control System (CUORE-SCS) development is carried out by the INFN groups of Bologna, LNGS, and Milano-Bicocca and by a US group at UCLA. The system makes use of the TANGO package and LabVIEW for the high- and low-level systems, respectively. The US group is developing the high-level system (user interfaces, clients, webserver, database, interface with the intermediate level), while the the Italian group is taking care of the low-level (interface with the intermediate level, instrumentation driver), including the interfaces between Tango and LabVIEW.

In Bologna, a dummy connection TANGO/LabVIEW in the same PC has been developed. At UCLA, the first version of the user interface has been completed and doc-

umented. The next step is to install and configure the system in the dedicated machine present in the CUORE control room, joining the two parts and replacing the dummy virtual instrument with a real one.

2.4   Data acquisition system

In 2013 most of the CUORE data acquisition hardware was purchased. All the National Instruments chassis, controllers, and signal cables, and most of the digitizer boards are now in Genova. The remaining digitizer boards and the data acquisition computers will be bought at the beginning of next year. The data acquisition system is now being configured and tested in Genova, and it will be sent to LNGS in 2014. A small DAQ system, based on a single chassis, will be configured and installed at LNGS, where it will be used for the bolometric tests of the CUORE cryostat.

3   Cryogenics

In 2013, the construction and commissioning of the cryostat have achieved several important milestones. The outer cryostat (300 K, 40 K and 4 K vessels) was cooled twice: in April and in June, reaching the temperature of 3.5 K. During the second cool-down, one DCS unit was tested using a dedicated mock-up that simulates the inner cryostat. In parallel, the characterization of the Dilution Unit was completed and the installation of the external lead shield is in progress.

3.1   Installation and test of the cryogenic set-up

The first cool-down of the cryostat was performed using 3 Pulse Tubes; at that time the innermost vessel reached a temperature of 5 K. After warming up, several improvements were implemented in order to reach the nominal temperature (4 K). First, it was realized that two out of six baffles were defective and they detached from the 300 K ports when pumping the IVC - i.e. just before (or during) the cool-down. The design of the baffles was changed and the new baffles were installed before the second cool-down. In addition, the single-layer superinsulation of the 4 K plate was replaced with the same 10 layer MLI used for the 40 K plate. Finally, the thermometers were re-calibrated using their three-point function instead of the standard Lakeshore function and in a few cases, redundancy was assured mounting additional thermometers fixed to the cryostat with an improved thermalization system. The result of the second cool-down was fully satisfactory. A temperature of 7 K was reached in about 7 days and 3 additional days were needed to reach the 3.5 K base temperature: this 3-day tail was due to the presence of the steel mock-up for the DCS inside the 4 K vessel. The mock-up is not simulated in the thermal model but the model reproduces rather well the behavior of the cryostat at thermal equilibrium. Transient phases and cooling times are reproduced within a 30% uncertainty. The IVC-to-OVC leak observed during the first cool-down was visible in the second cooling, too. We hence decided to perform a dedicated test session at room temperature during the startup of the Phase II of the commissioning (see below).

After the warm up, the external vessels were lowered and we installed the missing parts of the outer cryostat. These parts are the fast cooling tubes between the 300 K and 4 K plates, the bars holding the inner plates ("SS bars") and one wiring port (WS3). We also took the opportunity to re-clean the 40 K plate since the cleaning done in Simic in 2012 after the mounting of the steel threads ("helicoil") was significantly worse than the standard one performed for the other plates/vessels at BAMA (Turbigo, Italy). The plate was hence dismounted, sent to BAMA, and mounted back in the cryostat. The remounting procedure was completed at the beginning of October; tests of individual tubes and IVC-to-OVC integral leak tests are in progress.

3.2 Procurement

The inner vessels and the corresponding gilded plates were completed in April. The three inner vessels (600 mK, 50 mK and 10 mK) were cleaned at BAMA and delivered to LNGS at the end of April. The steel rings that are needed to position the vessels were completed in May and delivered to LNGS in June. The titanium bars that hold the inner plates were delivered to LNGS in October. In September, the copper thermalizations for the detector and lead suspensions were characterized and machined while gilding is in progress. The suspensions will be reinstalled with the new thermalizations after the leak tests together with the suspensions for the inner lead (not mounted during the Phase I of the commissioning). In conclusion, all parts needed for the Phase II of the commissioning are ready and delivered.

The 10 mK shield that will be employed in the Phase II is not the one that will host the CUORE detector. The latter is in production at CINEL (Padova, Italy): the tender for the final 10 mK shield is completed and welding tests are in progress. Delivery is expected in early 2014.

3.3 External Shield

The external shield is designed to screen the cryostat from environmental neutrons and γ rays. Neutron thermalization and absorption is achieved by a borated polyethylene terephthalate (PET) floor and by lateral walls of PET followed by boric-acid powders, which are poured in plastic frames. The B-PET shield is followed by lead blocks. To ease its installation on the ground floor of the hut, the steel structure holding the shield was divided into three horizontal rings. The rings were produced by Comasud (Teramo, Italy) and delivered to LNGS in August (Fig. 2). The rings were already equipped with the B-PET floor (lower ring) and with the lateral PET walls at the time of construction in Comasud. Onsite, the rings are filled with lead and the filling proceeds in parallel with the commissioning of the cryostat.

3.4 The Detector Calibration System (DCS)

The CUORE Detector Calibration System (DCS) is designed to introduce a set of radioactive γ-ray sources from outside the CUORE cryostat into the detector region. A total of 12 source strings with ^{232}Th source capsules will be inserted into the cryostat to provide

Figure 2: Delivery of the external shield in Hall A.

an absolute energy calibration of each TeO_2 bolometer at the working temperature of the detector. The DCS consists of a motion system on top of the cryostat operated at 300 K, a thermalization mechanism at the 4 K stage of the cryostat, and a guide tube system that directs the source strings around the structures and internal shields of the cryostat into the detector region. A key technical challenge of the DCS is the insertion of the source string and the cooldown during the deployment process without exceeding the heat-load requirements of the individual cryostat stages. Each individual source capsule has to be thermalized with a custom-design squeezing mechanism. The complete calibration system will consist of 12 guide tubes inside the cryostat and 12 corresponding source strings.

As a technical verification and demonstration of the deployment and cooldown process, the DCS group installed and operated this summer a complete calibration source deployment system for 2 source strings in the cryostat. All elements of the calibration system including the 300 K motion box, electronics and software controls, the thermalization mechanism at 4 K and the guide tube routing were tested at 4 K. A mock-up of the internal cryostat structure was mounted on the 4 K plate to simulate the internal structure of the cryostat as needed for the DCS testing. Specially-instrumented source capsules and thermalization mechanisms were used to collect data on the cooldown rate and thermal behavior of the DCS components. This is the first time that a source string was operated inside the cryostat during a cooldown. The results of the test demonstrated that the thermalization mechanism cools down the source capsules and the source string. The functionality of the detector calibration system was verified. The data from this cooldown is being analyzed and will be used to optimize the deployment parameter such as speed and cooldown time. The remaining hardware parts of the DCS are now in fabrication. Final installation and commissioning of the DCS is scheduled for 2014.

Figure 3: Cooldown test of the Detector Calibration System. Left and middle: Mockup of the internal cryostat structure and guide tube system. Right: Deployment system above 300 K (top) and mechanical source thermalization mechanism below 4 K (bottom).

4 Detector assembly

We began assembling detector towers in late February 2013, and we aim to complete all 19 towers by Summer 2014.

Detector assembly is subdivided into four distinct, sequential operations (Fig. 5):

1. **Cleaning** of assembly tools and equipment, and of tower-readout wire ribbons;

2. **Gluing** of thermistors and heaters to TeO_2 crystals;

3. **Mechanical assembly** of glued crystals, copper, PTFE, and wire ribbons into towers; and

4. **Bonding** of gold wires between crystals' sensors and readout wire ribbons.

Except for cleaning, all of these activities are carried out inside the clean room on the second floor of the CUORE hut. Gluing is performed inside a dedicated glove box which hosts a semi-automated robotic system for attaching sensors to crystals, while mechanical assembly and bonding are carried out using a single workstation with four interchangeable glove boxes. All glove boxes are continuously fluxed with N_2 gas during use to ensure tower components are kept in a Rn-free environment.

Some assembly activities can be carried out in parallel, though there are constraints due to limited availability of personnel and equipment, restrictions on clean-room occupancy, etc. In general we try to glue crystals nearly continuously, while mechanical assembly and bonding take turns using the clean room for 3- or 4-week stretches because they utilize the same workspace and equipment.

43

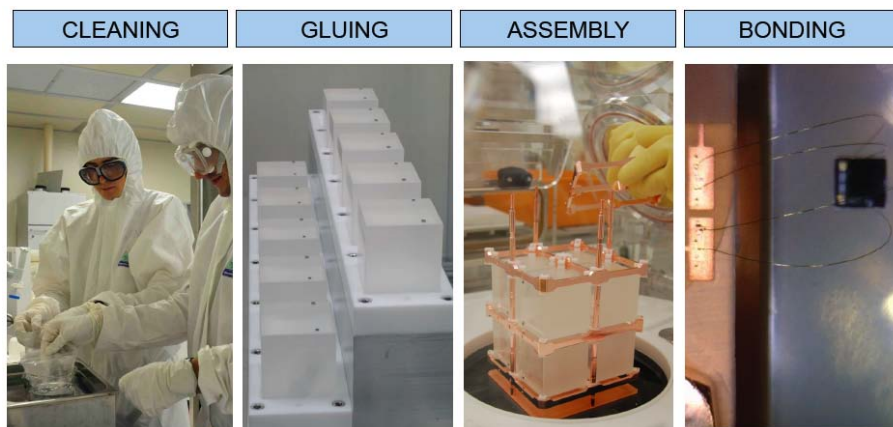Figure 4: The first six detector towers in storage inside the CUORE clean room.

Figure 5: The main steps in the detector assembly process.

4.1 Organization

Most assembly activities are overseen by a "responsible"—i.e., a collaborator in charge of completing that task—and this person works in conjunction with a technical coordinator who maintains the equipment used for that activity. A significant fraction of the gluing and mechanical assembly work is performed by four external-company technicians under the supervision of the responsibles or trained collaborators.

4.2 Cleaning

Cleaning of tools and consumables, now largely a routine activity for the external-company technicians, poses no real problems. The only items that are challenging to clean are the delicate wire-readout ribbons, which must be cleaned and dried carefully to avoid damaging their copper wire traces. In early towers we observed some unexpected darkening of the copper traces after cleaning, but we believe this was due to residual moisture and after making a concerted effort to dry them more thoroughly the problem has largely gone away.

4.3 Crystal gluing

Crystal gluing is a near-continuous activity, interrupted only when the system needs maintenance and on certain days when mechanical assembly is in progress and all of the external-company technicians are needed there. Gluing normally involves two technicians and a collaborator who has volunteered to act in a supervisory role for a two-week shift. The standard rate of gluing production is 12 crystals every two days, resulting in a tower's worth of glued crystals every two weeks.

The gluing system is complicated and consequently it requires near-constant attention and frequent servicings and troubleshooting. Most recently we experienced a serious problem when several of the cartridges used to hold the bicomponent glue epoxy suddenly ruptured inside the glove box during glue-deposition operations. Fortunately, we believe that we have solved the problem by lowering the tools-line pressure by 30%.

As of the end of 2013, fifteen towers worth of crystals have been instrumented by the gluing subgroup. If we maintain the current crystal gluing schedule, gluing operations should finish in April 2014.

4.4 Mechanical assembly

Mechanical assembly found an early rhythm and has run quite smoothly. We generally try to assemble towers in batches of 3–4 for efficiency, and we've been successful in keeping to a schedule of building one tower per week for multiple weeks in a row. The physical assembly of each tower only takes one day, but the preparation, gluing and attachment of the readout ribbons, and the wrap-up work take several days. Assembly work involves the responsible and 3–4 technicians, and we often have to temporarily suspend gluing operations during the two days per tower when all four technicians are needed for assembly. Our rough goal is to assemble three towers every two months. By the end of 2013, eleven towers were mechanically assembled.

4.5 Wire bonding

Like mechanical assembly, wire bonding is performed in batches for efficiency. The bonding subgroup completed 9 towers in 2013. Bonding went smoothly during the first campaign, which saw Towers 1 and 2 successfully bonded. The bonding campaign for Towers 3 through 6 encountered a range of problems: (i) we discovered a technical problem with the bonding machine which required a maintenance visit from the vendor to repair, (ii) we encountered problems with misplaced glue residue on the contacts of previously-glued NTDs re-processed in the gluing glovebox, and (iii) we discovered, as mentioned in Section 1.2, that the gold contacts on the batch of NTDs glued to Towers 5 and 6 did not accept ball bonds carried out using the established protocol. While the first two issues caused some delays, the third was by far the most serious. To avoid this problem in subsequent towers, the gluing and bonding subgroups worked closely together to systematically check a large sample from all thermistor batches delivered to LNGS before gluing them to crystals. In parallel, as detailed in Section 1.2, a more robust contact deposition technique was developed and the bonding subgroup developed a protocol that allowed Towers 5 and 6 to be bonded in December 2013. Towers 7, 8, and 9 which were assembled in the interim with "certified bondable" NTDs were successfully bonded in October 2013.

5 CUORE-0

Main goal of CUORE-0 is a full test and debug of the hardware and procedures specifically developed in recent years for the CUORE detector. CUORE-0 is actually a single CUORE tower, that was built in full accordance with the CUORE recipe and using the CUORE assembly line. After solving a number of serious problems related to the yielding cryogenic setup of Cuoricino, the detector was finally successfully cooled down in March 2013.

Besides being a promising detector that will surpass the limit on the effective neutrino mass set by Cuoricino, CUORE-0 is also an high-statistics check of the improvements implemented to reduce the background sources and to improve the bolometric response of the detectors in view of CUORE. One of the main goals of the CUORE-0 detector is to measure the α background coming from the detector surface (mainly the copper structure surfaces facing the absorber and the crystal surfaces themselves), in order to validate the new cleaning techniques and assembly procedures adopted for CUORE. These surface contaminations are dangerous because they can produce degraded alphas that release only part of their energy in the crystal absorber. These events contribute to a flat background that goes from the full α-particle energy peak to much lower energies, reaching the neutrinoless double beta decay region of interest. The reduction of the flat continuous background in the region of interest would then be a proof of the effectiveness of the new cleaning and assembly procedures.

5.1 Detector operation

After we reached the base temperature of $\sim$10 mK on all the detectors, in April 2013 the detector optimization phase started. A lot of effort was spent in order to understand and reduce all possible sources of noise that worsen the performance of the detectors.
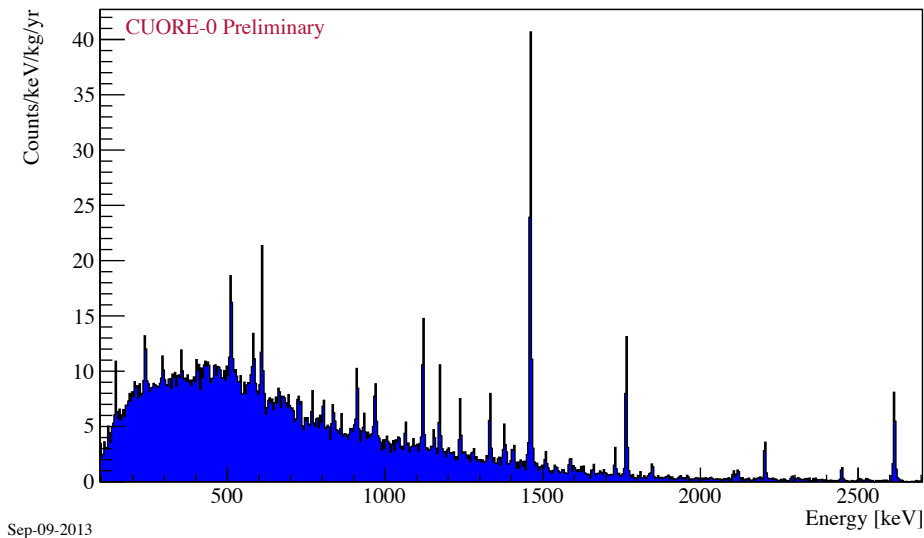
Figure 6: CUORE-0 energy spectrum.

At the end of April the background data taking started. Even though some interruptions occurred due to cryostat maintenance, we run the detector for 4 months, up to the end of August 2013, collecting a total statistics of 6.86 kg·y.

Figure 6 shows the energy spectrum of pulse amplitude recorded by 49 fully active channels during background runs. The energy resolution, evaluated on the ^{208}Tl full-energy peak in the background spectrum of Fig. 6, is 5.6 keV FWHM ($\sigma = 2.1$ keV).

Since the detector is operating in the cryostat used for Cuoricino, the high-energy γ-ray background (coming from ^{232}Th contamination in the cryostat shields) is not expected to change. Having said that, the very preliminary results on the background index in the region of interest are very encouraging. Figure 7 shows the comparison between the background count rate of Cuoricino and CUORE-0 in the region 600-8000 keV.

The γ lines from ^{238}U are now reduced of a factor of 2 with respect to Cuoricino, as an indication of the better Radon control during the assembly of the detector and/or its operation. The α lines from ^{238}U and ^{232}Th are also reduced in CUORE-0, thanks to the new detector surface treatment. The γ lines from ^{232}Th, as expected, are not reduced because they originate from the cryostat shield.

It is interesting to study the energy region between 2.7 and 3.9 MeV that is right above the highest γ-line in the ^{232}Th chain (2.6 MeV), but below the lowest α-line at about 3.9 MeV from ^{232}Th. In this interval it is possible to evaluate the α contribution to the background in the region of interest for the double beta decay of ^{130}Te which lies in a lower energy region.

In the region between 2.7 and 3.9 MeV, excluding the internal α peak from ^{190}Pt, the background from α surface contamination in CUORE-0 (0.019±0.002 counts/keV/kg/y) is $\sim$ 6 times smaller than in Cuoricino (0.110±0.001 counts/keV/kg/y). In the neutrinoless double beta decay region, where the contribution from cryostat γ contamination cannot be reduced, the background index is (0.074±0.012 counts/keV/kg/y). Such a low background
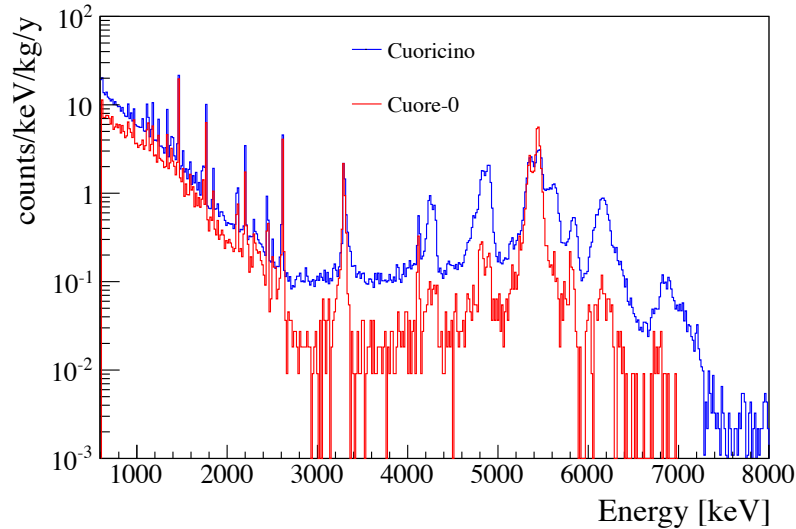
Figure 7: CUORE-0 energy spectrum.

level is the result of a thorough control of all the possible surface recontamination at all assembly line stages. With the current background, CUORE-0 will overcome the Cuoricino sensitivity in about a year of data taking. We look forward to another an exciting and productive year for CUORE-0 and CUORE in 2014.

6 Publications in 2013

1. F. Alessandria *et al.*, "The 4 K outer cryostat for the CUORE experiment: Construction and quality control", Nuclear Instruments and Methods in Physics Research Section A **727**, 65 (2013).

2. F. Alessandria *et al.*, "Validation of techniques to mitigate copper surface contamination in CUORE", Astroparticle Physics **45**, 13 (2013).

3. F. Alessandria *et al.*, "Search for 14.4 keV solar axions from M1 transition of ^{57}Fe with CUORE crystals", Journal of Cosmology and Astroparticle Physics **5**, 007 (2013).

4. L. Pattavina for the CUORE collaboration, "Status of the CUORE experiment", Journal of Physics: Conference Series **447**, 012066 (2013).

5. F. Alessandria *et al.*, "The low energy spectrum of TeO$_2$ bolometers: Results and dark matter perspectives for the CUORE-0 and CUORE experiments", Journal of Cosmology and Astroparticle Physics **1**, 038 (2013).

DAMA

Collaboration:

P. Belli[a], R. Bernabei[a,@], A. Bussolotti[a,*], S. d'Angelo[a], A. Di Marco[a], F. Emiliani[a], F. Montecchia[a], A. d'Angelo[b], F. Cappella[b], A. Incicchitti[b], A. Mattei[b,*], O.G. Polischuk-Shkulkova[b,g], R. Cerulli[c], V. Caracciolo[c], S. Castellano[c], C.J. Dai[d], H.L. He[d], H.H. Kuang[d], X.H. Ma[d], X.D. Sheng[d], R.G. Wang[d], Z.P. Ye[d,e]

in some detector developments, by-product results and small scale experiments: A.S. Barabash[r], R.S. Boiko[g], V.B. Brudanin[h], M. Casalboni[a], D.M. Chernyak[g], F.A. Danevich[g], M.L. di Vacri[c], E. Galenin[n], E.N. Galashov[l], A. Gektin[n], V. Isaienko[i], V.V. Kobychev[g], S.I. Konovalov[r], G.P. Kovtun[m], N.G. Kovtun[m], V.M. Kudovbenko-Mokina[g], M. Laubenstein[c], S.S. Nagorny[g], S. Nisi[c], C. Palazzesi[a], P. Prosposito[a], D.V. Poda[c,g], R. B. Podviyanuk[g], A.P. Shcherban[m], V.N. Shlegel[l], D.A. Solopikhin[m], Yu.G. Stenin[l], J. Suhonen[o], A.V. Tolmachev[q], S. Tkachenko[n], V.I. Tretyak[g], V.I. Umatov[r], Ya.V. Vasiliev[l], I.M. Vyshnevskyi[g], R.P. Yavetskiy[q]

in some studies on $\beta^+\beta^+$, EC/β^+, EC/EC decay modes (under the joint Indo-Italian DST-MAE project and inter-universities agreement): P.K. Raina[p], A.K. Singh[p], P.K. Rath[p], S. Ghorui[p]

[a]Dip. Fisica, Univ. Roma "Tor Vergata" and INFN Tor Vergata, 00133 Roma, Italy.
[b]Dip. Fisica, Univ. Roma "La Sapienza" and INFN-Roma, 00185 Roma, Italy.
[c]Laboratorio Nazionale del Gran Sasso, INFN, 67010 Assergi (Aq), Italy.
[d]IHEP, Chinese Academy, P.O. Box 918/3, Beijing 100039, China.
[e]Physics Dept, Jing Gangshan University 343009, Jiangxi, China.
[g]Institute for Nuclear Research, MSP 03680, Kiev, Ukraine.
[h]Joint Institute for Nuclear Research, 141980 Dubna, Russia.
[i]National University of Kyiv-Mohyla Academy, 04655 Kyiv, Ukraine
[l]Nikolaev Institute of Inorganic Chemistry, 630090 Novosibirsk, Russia.
[m]National Science Center Kharkiv Institute of Physics and Technology, Kharkiv, Ukraine.
[n]Institute for Scintillation Materials, 61001 Kharkiv, Ukraine.
[o]Dep. of Physics, University of Jyvaskyla, P.O. Box 35, FIN-40351, Jyvaskyla, Finland
[p]Indian Institute of Technology, Kharagpur, India.
[q]Institute for Single Crystals, 61001 Kharkiv, Ukraine
[r]Institute of Theoretical and Experimental Physics, 117259 Moscow, Russia
@ Spokesperson; * technical staff.

Abstract

DAMA is as an observatory for rare processes located deep underground at the Gran Sasso National Laboratory of the I.N.F.N. (LNGS) that develops and exploits low background scintillators. In 2013 the main experimental activities have been performed with: i) the second generation DAMA/LIBRA set-up (sensitive mass: $\simeq$ 250 kg highly radiopure NaI(Tl)), upgraded in 2008, 2010 and at the end of 2012; ii) the DAMA/LXe set-up (sensitive mass: $\simeq$ 6.5 kg liquid Kr-free Xenon enriched either in ^{129}Xe or in ^{136}Xe); iii) the DAMA/R&D set-up (a facility dedicated to perform relatively small scale experiments, mainly investigating double beta decay modes in various isotopes); iv) the DAMA/Ge set-up (mainly dedicated to sample measurements and to specific measurements on rare processes); v) a small set-up (named DAMA/CRYS) for prototype tests and detectors' qualification. The main DAMA activities during 2013 are summarised in the following.

1 DAMA/LIBRA

DAMA/LIBRA (Large sodium Iodide Bulk for Rare processes) is an unique apparatus for its sensitive mass, target material, intrinsic radio-purity, methodological approach and all the controls performed on the experimental parameters (c.f.r. [1, 2, 3, 4, 5] and the 2013 publication list). It is the successor of DAMA/NaI[6, 7, 8, 9, 10, 11, 12, 13, 14, 15, 16, 17, 18], with a higher exposed mass, higher duty cycle and increased sensitivity. The main goal of DAMA/LIBRA is the investigation of the DM particles in the galactic halo by exploiting the DM model independent annual modulation signature[19, 20].

The granularity of the apparatus (25 detectors in a matrix 5×5) is an important feature to study Dark Matter and background identification since Dark Matter particles can just contribute to events where only one of the 25 detectors fires (*single-hit* events) and not to whose where more than one detector fire in coincidence (*multiple-hit* events). The apparatus has also the unique feature (as well as DAMA/NaI) that gamma calibrations are regularly performed down to the software energy threshold in the same conditions as the production runs, without any contact with the environment and without switching-off the electronics. The high light yield and other response features have allowed working in a safe and reliable way down to 2 keV (DAMA/LIBRA- phase1). At the end of 2010 new photomultipliers (PMTs) with higher quantum efficiency [21] have been installed, some other optimisations have been done and the data taking of DAMA/LIBRA-phase2 then started. Among the further scientific goals of this set-up we also recall here: i) investigation with high sensitivity of the Dark Matter (DM) particle component in the galactic halo by the model independent approach known as DM annual modulation signature, with highly precise determination of the modulation parameters (which carry crucial information); ii) corollary investigations on the nature of the candidate and on the many possible astrophysical, nuclear and particle physics scenarios; iii) investigations on other possible model dependent and/or model independent approaches to study Dark Matter particles, second order effects and some exotic scenarios; iv) improved search for processes of Pauli exclusion principle violation in ^{23}Na and ^{127}I; v) search for possible electric charge non-conservation (CNC) processes, as the electron decay into invisible channels and in the $e^- \to \nu_e + \gamma$ channel, excitations of nuclear levels of ^{23}Na and ^{127}I after CNC electronic

capture, ..; vi) search for possible nucleon, di-nucleon and tri-nucleon decay into invisible channels in ^{23}Na and ^{127}I; vii) search for solar axions by Primakoff effect in NaI(Tl); viii) search for nuclear rare decays in ^{23}Na, ^{127}I and Tl isotopes (as e.g. superdense states, cluster decay, ...); ix) search for neutral particles (QED new phase) in ^{241}Am decays, etc.

Most of these investigations require further dedicated data taking and high exposure to reach competitive sensitivities. As regards the DM features, which can be suitably exploited further collecting very large exposure, see e.g. the Sect 6 of Ref. [11] and the Appendix of Ref. [2]. In particular, the latter shows how the decreasing of the software energy threshold as in the present DAMA/LIBRA-phase2 offers the unique possibility to investigate the modulation amplitude at the lowest energy, where a discrimination power can disentangle among many of the possible DM scenarios.

1.1 Final model-independent result of DAMA/LIBRA-phase1 on DM annual modulation

The results obtained with the total exposure of 1.04 ton × yr collected by DAMA/LIBRA-phase1 during 7 annual cycles (i.e. adding a further 0.17 ton × yr exposure) have been presented at international conferences and the paper on the final model independent result of DAMA/LIBRA-phase1 was published (see the 2013 publication list).

The same procedures previously adopted (c.f.r. Refs. [1, 2, 3] and the 2013 publication list) were exploited also in the analysis of the data of the seventh annual cycle and several analyses on the model-independent investigation of the DM annual modulation signature have been performed.

Fig. 1 shows the time behaviour of the experimental residual rates of the *single-hit* scintillation events in the (2–4), (2–5) and (2–6) keV energy intervals for the complete DAMA/LIBRA–phase1. The residuals of the DAMA/NaI data (0.29 ton × yr) are given in Refs. [2, 10, 11]. We remind that these residual rates are calculated from the measured rate of the *single-hit* events after subtracting the constant part: $< r_{ijk} - flat_{jk} >_{jk}$. Here r_{ijk} is the rate in the considered i-th time interval for the j-th detector in the k-th energy bin, while $flat_{jk}$ is the rate of the j-th detector in the k-th energy bin averaged over the cycles. The average is made on all the detectors (j index) and on all the energy bins (k index) which constitute the considered energy interval. The weighted mean of the residuals must obviously be zero over one cycle.

In general it is worth noting that rejection strategies cannot safely be applied to the data when a model-independent signature based on the correlation of the measured experimental rate with the Earth galactic motion is pursued; in fact, the effect searched for (which is typically at level of few %) would be largely affected by the uncertainties associated to the rejection procedure. On the other hand, the signature itself acts as an effective background rejection.

The DAMA/LIBRA-phase1 data give evidence for the presence of DM particles in the galactic halo, on the basis of the exploited model independent DM annual modulation signature by using highly radio-pure NaI(Tl) target, at 7.5 σ C.L.. Including also the first generation DAMA/NaI experiment (cumulative exposure 1.33 ton × yr, corresponding to 14 annual cycles), the C.L. is 9.3 σ. At present status of technology the DM annual
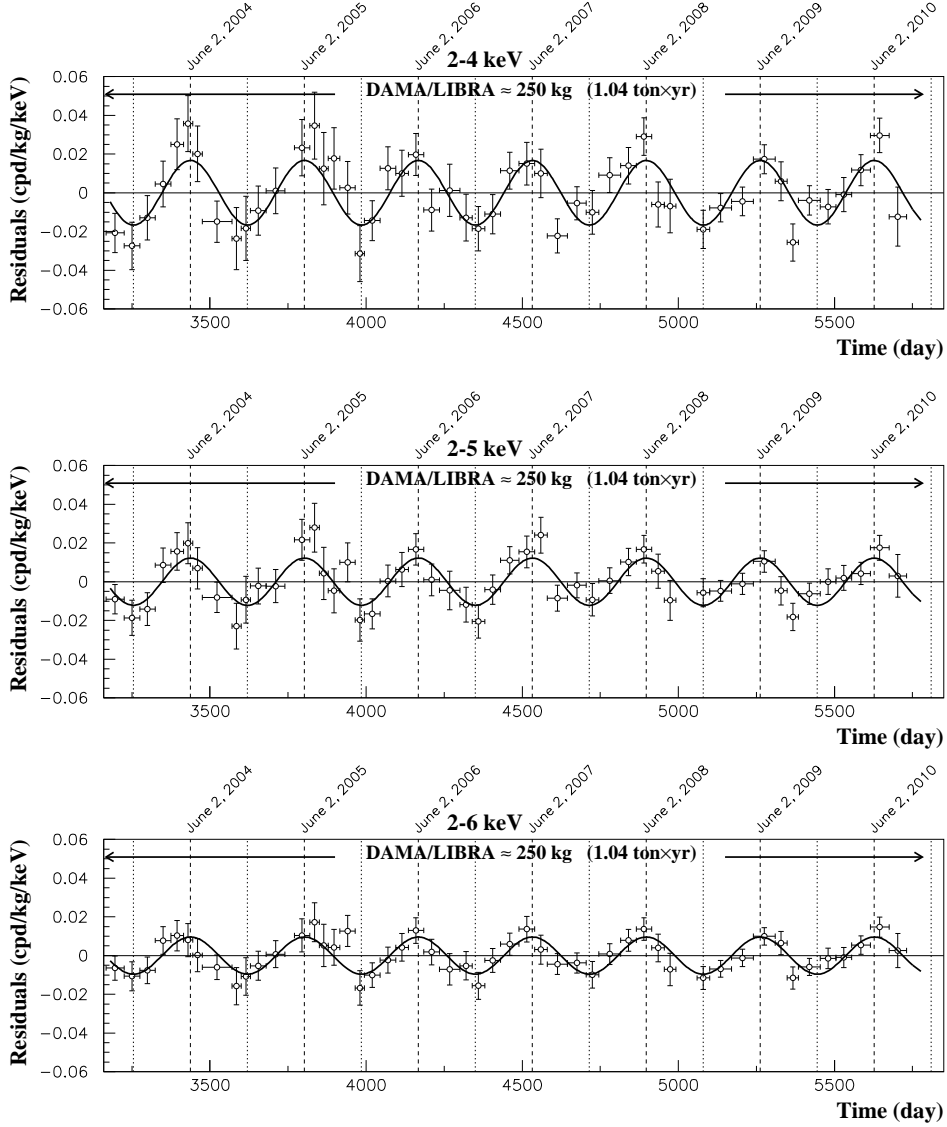
Figure 1: Experimental residual rate of the *single-hit* scintillation events measured by DAMA/LIBRA–phase1 in the (2–4), (2–5) and (2–6) keV energy intervals as a function of the time. The time scale is maintained the same of the previous DAMA papers for coherence. The data points present the experimental errors as vertical bars and the associated time bin width as horizontal bars. The superimposed curves are the cosinusoidal functions behaviours $A \cos \omega(t - t_0)$ with a period $T = \frac{2\pi}{\omega} = 1$ yr, a phase $t_0 = 152.5$ day (June 2nd) and modulation amplitudes, A, equal to the central values obtained by best fit on the data points of the entire DAMA/LIBRA–phase1. The dashed vertical lines correspond to the maximum expected for the DM signal (June 2nd), while the dotted vertical lines correspond to the minimum.

52

modulation is the only model independent signature available in direct dark matter investigation that can be effectively exploited. All the many specific requirements of the signature are fulfilled by the data and no systematic or side reaction able to mimic the exploited DM signature is available (see e.g. Refs.[2, 3, 9, 10, 11, 22, 23, 24, 25, 26, 27, 28] and the 2013 publication list). In particular, only systematic effects or side reactions simultaneously able to fulfil all the specific requirements of the DM annual modulation signature and to account for the whole observed modulation amplitude could mimic this signature; thus, no other effect investigated so far in the field of rare processes offers a so stringent and unambiguous signature.

Studies on other DM features, second order effects, and several other rare processes are in progress with the aim to reach very high sensitivity. Studies for measurements with data taking dedicated to other rare processes are continuing.

It is also worth noting that in the DM field DAMA/LIBRA is the set-up still having the highest intrinsic radio-purity, the largest exposed sensitive mass[1], the largest collected exposure, the deepest controlled running condition and stability, and the only one with highly sensitive ULB (Ultra-Low Background) NaI(Tl) detectors.

The DAMA obtained model independent evidence is compatible with a wide set of scenarios regarding the nature of the DM candidate and related astrophysical, nuclear and particle Physics. For example, some of the scenarios available in literature and the different parameters are discussed in Refs. [10, 11, 7, 12, 13, 14, 15, 16, 17, 5, 29, 30] and in Appendix A of Ref. [2]. A further large literature is available on the topics; many possibilities are open.

No other experiment exists, whose result can be directly compared in a model independent way with those by DAMA/NaI and DAMA/LIBRA. In particular, both the negative results and the possible positive hints (by COGENT, CRESST and CDMS) achieved so-far in the field, are largely compatible with the model independent annual modulation results of DAMA in many scenarios, also considering the large uncertainties in theoretical and experimental aspects, the same holds for indirect approaches; see e.g. some arguments in 2013 publication list and quoted references.

1.2 DAMA/LIBRA-phase2

- During 2013 DAMA/LIBRA has continued to take data in the new phase2 configuration with the PMTs of higher quantum efficiency[21] and new preamplifiers.

- Trigger modules and designs for other developments were realised to further implement the apparatus for low energy studies.

- The results obtained in dedicated measurements for a new search for correlated e^+e^- pairs in the α decay of ^{241}Am were published (see 2013 publication list and Sect.1.2.1).

---

[1]In this case the sensitive mass is the total mass of the NaI(Tl) crystals and not a reduced fiducial mass.

1.2.1 New search for correlated e$^+$e$^-$ pairs in the α decay of ^{241}Am.

A new search for correlated e$^+$e$^-$ pairs in the α decay of ^{241}Am has been carried out deep underground at LNGS by using pairs of NaI(Tl) detectors in the DAMA/LIBRA-phase2.

In the seventies experimental and theoretical investigations of weak interactions in nuclei suggested the presence of various electromagnetic phenomena, which modify the basic decay processes. In the conventional perturbation treatment of the weak interactions these phenomena are attributed to higher-order terms. These higher-order terms, accompanying β decay and shell-electron capture, are [31, 32]: (i) internal bremsstrahlung; (ii) ionisation and excitation of the electron cloud; (iii) internal pair production (IPP). After first estimates [33, 34] and further measurements[35], in 1973 [32] and in the following years the IPP process was also investigated in the α decay, where this effect could give additional information on the higher-order phenomena accompanying nuclear transformations.

Experimental results presently available and theoretical estimates are quoted in Table1.

Table 1: Experimental results and theoretical estimates of $\lambda = \frac{A_{e^+e^-}}{A_\alpha}$ for the IPP process in α decays, where $A_{e^+e^-}$ and A_α are the e^+e^- and α activities, respectively. The superscript ^{a} identifies the λ value derived for IPP from Ref. [36] when adopting the procedure described in the 2013 publication list.

Source	Experiment				Theory		
	λ ($\times 10^{-9}$)	Detectors	Year	Ref.	λ ($\times 10^{-9}$)	Year	Ref.
^{210}Po	5.3 ± 1.7	NaI(Tl)+Ge(Li)	1986	[38]	4.4	1978	[37]
^{239}Pu	7 ± 9	NaI(Tl)+Ge(Li)	1986	[38]	2.2	1978	[37]
^{241}Am	3.1 ± 0.6	NaI(Tl)+Ge(Li)	1973	[32]	1.2	1973	[32]
	2.15 ± 0.25	NaI(Tl)+Ge(Li)	1986	[38]	2.3	1978	[37]
	1.8 ± 0.7^a	Plastics+Ge	1990	[36]			
	4.70 ± 0.63	NaI(Tl) pairs	2013	present work			

In addition, in Ref. [39] a new model where the pair production would be due to a QED strong coupling phase was proposed after some anomalous phenomena were observed in collision of heavy ions at GSI and in collision of heavy ions with e^+ [40]. In Ref. [39] some experimental tests were suggested for this model; one of them is the search for double coincidence events produced by positron annihilation. Thus, in this scenario the production of positronium states in α decay of heavy nuclei may be a concurrent process

with respect to the IPP one. However, since the IPP process is better stated, we have referred the results to it.

The results presented have been obtained through dedicated measurements with some pairs of the NaI(Tl) detectors of the DAMA/LIBRA set-up in the new configuration after the upgrading occurred in fall 2010 when all the PMTs were replaced by new ones with higher quantum efficiency, specially developed by HAMAMATSU; details can be found in Ref. [21]. The light response in this experimental configuration is typically 6–10 ph.e./keV depending on the detector. In the particular measurements dedicated to the present study an ^{241}Am source was placed in the middle of each used NaI(Tl) pair for a total of 6 sources used. The electronic chain was modified with respect to the usual one [1] by excluding the 500 μs blocking time and by using either twelve detectors (six pairs) in the first running period or six detectors (three pairs) in the second one. An improvement of a factor ≈ 2 has been achieved as regards the ratio of the live time over elapsed one in the second dedicated run, where just three pairs have been used (those with the lower number of coincidences in the first run).

In both running periods each pair has the detectors of the other used pairs as anti-coincidences; this implies two different coincidence backgrounds for a same pair in the two different running periods (see 2013 publication list). The excess rates per pair in the region of interest during the two running periods are compatible. Thus, the compatibility and the independence between the first and the second dedicated runs allow us to perform a combined analysis of the two data sets.

The source experimental data show an excess of double coincidences of events with energy around 511 keV in faced pairs of detectors, which are not explained by known side reactions. Moreover, any sizeable contamination of the sources themselves by isotopes β^+ emitters is not present to our knowledge. This measured excess gives a relative activity λ = (4.70±0.63)×10^{-9} for the Internal Pair Production (IPP) with respect to the α decay of ^{241}Am. This value is of the same order of magnitude as the previous determinations [32, 38, 36] obtained by using different set-ups, sources (with different features and producers) and experimental approaches. In a conservative approach the upper limit $\lambda < 5.5 \times 10^{-9}$ (90% C.L.) can be derived. It is worth noting that this is the first result on IPP obtained in an underground experiment, and that the λ value obtained in the present work is independent on the live-time estimate (which is difficult to estimate with very high accuracy in similar experiments because of the relatively high intensities of the ^{241}Am sources).

2   DAMA/LXe

We pointed out since 1990 [41] the possible interest in using the liquid Xenon as target-detector material for particle DM investigations. Since the end of 80's (former Xelidon experiment of the INFN) we have realised several liquid Xenon (LXe) prototype detectors. Since 1996 we pointed out to the INFN-CSN2 the intrinsic problems of this detector medium for large scale experiments dedicated to DM investigation and agreed to pursue the activity by exploiting Kr-free enriched Xenon gases in limited volume.

The presently running set-up (with a Cu inner vessel filled by $\simeq 6.5$ kg – $\simeq 2$ l – of liquid Xenon) can work either with Kr-free Xenon enriched in ^{129}Xe at 99.5% or Kr-free Xenon

enriched in ^{136}Xe at 68.8% [42, 43, 44]. Many competing results were achieved on several rare processes [42, 43, 44, 45, 46, 47]. It is worth noting that e.g. the mass exposed when using the Xenon enriched in ^{129}Xe corresponds for spin-dependent coupled particles to expose 24.5 kg of natural Xenon, while the exposed mass when using the Xenon enriched in ^{136}Xe corresponds for spin-independent coupled particles to an exposed mass of 50.4 kg of natural Xenon.

In the recent period, data are collected by using Kr-free Xenon enriched in ^{136}Xe and focusing the high energy region to study rare processes. Various efforts and data analyses are in progress.

3 DAMA/R&D

The DAMA/R&D installation is a general-purpose low background set-up used for measurements on low background prototypes and for relatively small-scale experiments [48, 49, 50, 51].

The measurements mainly investigate 2β decay modes in various isotopes; both the active and the passive source techniques have been exploited as well as the coincidence technique. Particular attention is dedicated to the isotopes allowing the investigation of the $2\beta^+$ processes and in particular to resonant 2ϵ or $\epsilon\beta^+$ decay channels. In particular, in the first case an enhancement of the rate by some orders of magnitude is predicted for the case of coincidence between the released energy and the energy of an excited state. In the second case the investigation of neutrino-less 2ϵ and $\epsilon\beta^+$ processes can refine the understanding of the contribution of righthanded currents to neutrino-less 2β decay; therefore developments of experimental technique to search for 2ϵ, $\epsilon\beta^+$, and $2\beta^+$ processes are strongly required considering also that in the $2\beta^+$ investigations a gap of several orders of magnitude between theoretical expectations and experimental results is the usual situation and the better achieved sensitivities do not exceed the level of $T_{1/2} \simeq 10^{21}$ yr. Even more important motivation to search for double electron capture appears from a possibility of a resonant process thanks to energy degeneracy between initial and final state of mother and daughter nuclei. Such a resonant process could occur if the energy of transition ($Q_{2\beta}$) minus the energies of two bounded electrons on K or/and L atomic shells of daughter nucleus is near to the energy of an excited level (E_{exc}) of the daughter isotope.

Therefore developments of experimental technique to improve the reachable sensitivity in the searches for 2ε, $\varepsilon\beta^+$, and $2\beta^+$ processes are strongly required.

Finally, investigations on various kinds of new scintillators and preliminary works for the future measurements are also in progress.

Some of the main 2013 results are listed in the following, with more details on the works published in 2013.

- Preliminary results on the application of BaF_2 scintillators have been presented at conference. In particular, the radioactive contamination of a 1.7 kg BaF_2 crystal scintillator was determined to be on the level of few Bq/kg of ^{226}Ra and ^{228}Th. Preliminary pulse-shape analysis of ^{212}Bi -^{212}Po events gives for the half-life of ^{212}Po: $T_{1/2}(^{212}$Po) [299.3±0.9(stat.)±1.2(syst.)] ns, in agreement with the Table value

T$_{1/2}$=299(2) ns, and in a reasonable agreement with the recent Borexino result T$_{1/2}$=294.7(1.0) ns. New measurements are foreseen in near future in DAMA/CRYS (see later) with new crystals to search for double beta decay of barium isotopes and for accurate measurement of the half-lives of some radionuclides of uranium and thorium families.

- Preliminary studies have shown that segregation of thorium and radium is very low in cadmium tungstate (CdWO$_4$) crystals. It gives a hint of possible significant improvement of CdWO$_4$ radio-purity by recrystallisation, which could be an important methodological step to advance sensitivity of double beta decay experiments to search for double beta decay of ^{106}Cd and ^{116}Cd by using CdWO$_4$ crystal scintillators. We are going to measure one of ^{116}CdWO$_4$ crystal scintillators in scintillation mode, recrystallise the sample by the low-thermal-gradient Czochralski technique, and then test radioactive contamination of the crystal obtained by the re-crystallisation. Similar properties are expected also for ZnWO$_4$ and PbWO$_4$ crystal scintillators, which are promising detectors for rare events searches (as we already shown), and in further development.

- Further investigation of beta decay of ^{113m}Cd are in preparation.

- A further paper on the production strategies and achieved performances of enriched CdWO$_4$ detectors as well as some of the future perspectives has been published. Future strategies for developing higher radio-pure detectors are ongoing.

- As regards the search for double beta decay of ^{116}Cd with the help of enriched ^{116}CdWO$_4$ crystal scintillators, the analysis of the data accumulated after the detector upgrade in October 2012 allowed to improve an accuracy of the half-life relatively to the two neutrino mode of decay as T$_{1/2}^{2\nu2\beta}$(^{116}Cd) = [2.6±0.05(stat.)±0.3(syst.)]×10^{19} yr; the previous result was T$_{1/2}$=(2.5±0.5) ×10^{19} yr, while the spread of the half-live values obtained in other experiments are in the range (2.1— 4.0) ×10^{19} yr (taking into account the experimental errors). The improvement was reached thanks to the increased statistic and accurate estimation of the ^{116}CdWO$_4$ crystals radioactive contamination by U/Th daughters (instead of the limit obtained earlier), which allowed the simulation of the energy spectrum with higher accuracy. The detector was upgraded in October 2013 taking into account the data analysis and the Monte Carlo simulation of the experimental data; besides, the previously used liquid scintillator surrounding the ^{116}CdWO$_4$ crystals (contaminated by ^{40}K on the level of ≃2 Bq/kg) was replaced by highly radio-pure liquid scintillator (developed by the Borexino collaboration). A significative background improvement was found (especially in the energy region before 1.4 MeV), which should allow us to improve further the accuracy of the two neutrino mode half-life, and increase the experimental sensitivity to different channels of 2β decay of ^{116}Cd.

- Continuing the previous activity on the subject, new developments on SrI$_2$(Eu) detectors have been under investigation and further measurements are planned firstly in DAMA/CRYS and, then, in DAMA/R&D.

This DAMA/R&D set-up is as a general-purpose set-up and will assure us also in future the possibility to realise many kinds of low background measurements in an efficient way at well reduced cost. In particular the present measurements with the ^{116}CdWO$_4$ crystals are planned with further improvements to continue over about 4 years as needed to reach the proposed goal; then, the other measurements will start in the DAMA/R&D setup after preliminary measurements in DAMA/CRYS (see later).

4 DAMA/CRYS

The installation of this new small set-up, dedicated mainly to test prototypes and to qualify detectors, is almost completed. In particular, in 2013, the automatic opening system has been designed and now is under completing. While the design, the creation and installation of a cryogenic system (to allow the investigation of some scintillator responses as a function of the temperature) is under study. This apparatus will regularly work in the future on several kinds of measurements; at present test measurements at room temperature are carried out.

5 Measurements with DAMA/Ge and LNGS STELLA facility

The measurements on samples and on various R&D developments are performed by means of the DAMA low background Ge detector, specially realised with a low Z window; it is operative deep underground in the STELLA facility of the LNGS. Some selected materials are in addition measured with high sensitivity ICP-MS and mass spectrometers. Also other Ge detectors (in particular, GeMulti) are used for some peculiar measurements.

In particular, the main data takings/results during year 2013 with DAMA/Ge and LNGS STELLA facility are summarised in the following.

- A new stage of the experiment to search for double beta processes in ^{106}Cd by using enriched ^{106}CdWO$_4$ crystal radio-pure scintillator in coincidence with the four low background crystal HPGe gamma spectrometer GeMulti was realised in April 2013. The data acquisition of the experiment was upgraded and additional calibrations with radioactive sources have been done to improve the timing of the detector. New improved limits on double beta processes in ^{106}Cd have been obtained on the level of T$_{1/2}$ >10^{20}-10^{21} yr (only few double β^+ decaying candidate isotopes have been investigated so far at this level of sensitivity) after about 3 thousands hours of data taking; in particular, the half-life limit on decay of ^{106}Cd relatively to the two neutrino electron capture with emission of positron is T$_{1/2}^{2\nu\epsilon\beta^+}$ > 8.4×10^{20} yr at 90% CL. An extended Monte Carlo simulation of the detector background and of the different double beta processes in ^{106}Cd is in progress. We estimate the sensitivity of the experiment after accumulation of a few times larger statistic, in particular to the $2\nu\epsilon\beta^+$ decay of ^{106}Cd, to be on the level of the theoretical predictions T$_{1/2}$

$\simeq 10^{20}$-10^{22} yr. Developments of new enriched detectors with better performances have also been started.

- Search for 2β decays of ^{96}Ru and ^{104}Ru (see Sect. 5.1).

- First experimental investigation for 2β decay of ^{184}Os and ^{192}Os (see Sect. 5.2).

- Radioactive contamination of ^{7}LiI(Eu) crystal scintillators (see Sect.5.3).

- A deep purification of neodymium oxide samples with a total mass about 5 kg was performed to realise an experiment to search for 2β decay of ^{150}Nd to excited levels of ^{150}Sm with the help of low background HPGe detectors. The radioactive contamination of the samples was found to be below the sensitivity of the HPGe gamma and ICP-MS analyses available at the LNGS. The experiment will be realised by using the four crystal HPGe detectors, GeMulti, after the completion of the presently running ^{106}Cd experiment.

- An R&D of low background GSO(Ce) crystal scintillators is in progress to investigate double beta processes in ^{152}Gd and ^{160}Gd. The liquid-liquid extraction method was applied to purify gadolinium and cerium oxides. The main problem is the reduction of the actinium activity in gadolinium compounds, which could be solved by using gadolinium obtained from mineral resources having a low uranium contamination.

- A sample of cerium oxide 0.5 kg of mass was prepared to search for double beta decay of cerium isotopes by using HPGe spectrometry; ^{136}Ce is of especial interest taking into account one of the largest energy of decay and promising theoretical predictions. Preliminary measurements confirmed possibility to improve the experimental sensitivity several times in comparison to the existing results.

- A R&D of methods to purify dysprosium and erbium was started. The materials are of especial interest, taking into account recent theoretical estimations of neutrinoless resonant double electron capture processes in ^{156}Dy and ^{164}Er. New samples will be measured.

- Preparations of other future measurements are in progress.

5.1 Search for 2β decays of ^{96}Ru and ^{104}Ru by ultralow-background HPGe γ spectrometry at LNGS

New measurements with $\simeq$1 kg of purified Ru, in order to investigate the 2β processes of ^{96}Ru and ^{104}Ru isotopes with higher sensitivity, was carried out (see 2013 publication list).

The ^{96}Ru is one of the only six isotopes where the decay with emission of two positrons is allowed [52] thanks to the high energy release: $Q_{2\beta} = (2714.51 \pm 0.13)$ keV [53]. It has also a quite big natural abundance: $\delta = 5.54\%$ [54]. Moreover, in case of capture of two electrons from the K and L shells (the binding energies are $E_K = 20.0$ keV, $E_{L1} = 2.9$ keV [55]) or both from the L shell, the decay energies (2691.61 ± 0.13) keV and (2708.71 ± 0.13)

keV are close to the energy of the excited levels of ^{96}Mo (E_{exc} = 2700.21 and 2712.68 keV [56]). Such a situation could give rise to a resonant enhancement of the neutrinoless KL and $2L$ capture to the corresponding level of the daughter nucleus as a result of the energy degeneracy [57]. In addition, another isotope of ruthenium, ^{104}Ru, is potentially unstable with respect to the $2\beta^-$ decay ($Q_{2\beta}$ = (1301.2 ± 2.7) keV [58], δ = 18.62%).

Despite the high energy release and the high natural abundance, only one search for $2\beta^+/\varepsilon\beta^+$ processes in ^{96}Ru was performed in 1985, giving $T_{1/2}$ limits on the level of 10^{16} yr [59]. The efforts were renewed only in 2009, when a Ru sample with a mass of 473 g was measured for 158 h with an HPGe detector (468 cm^3) underground at LNGS [60] (an updated statistics of 2162 h was then reported in [61]). The achieved sensitivity for the $2\beta^+/\varepsilon\beta^+/2\varepsilon$ decays was $10^{18} - 10^{19}$ yr; for several modes of 2β decay of ^{96}Ru (and ^{104}Ru) $T_{1/2}$ limits were established for the first time. A search for 2β decays of Ru was also performed in the HADES underground laboratory (500 m w.e.) where a sample of Ru with mass of 149 g was measured during 2592 h; $T_{1/2}$ limits were obtained on the level of 10^{19} yr [62].

Our previous measurements [60, 61] showed that the used Ru sample was contaminated by ^{40}K at $\simeq$ 3 Bq/kg, and better results are possible only with purified Ru. In 2013 our final results of the search for $2\beta^+/\varepsilon\beta^+/2\varepsilon$ processes in ^{96}Ru and for $2\beta^-$ decay in ^{104}Ru obtained with a purified sample of Ru (720 g) in measurements during 5479 h were published. Purification of the ruthenium using the electron beam melting method allowed us to reduce the potassium contamination by more than 20 times; activities of ^{226}Ra and ^{106}Ru were decreased as well.

The results of the measurements (before and after the purification) are presented in Fig. 2, where the effect of the purification is clearly visible — the spectra of the GeMulti set-up are the sum of the spectra of the 4 individual HPGe detectors (see also 2013 publication list). With the purified ruthenium samples new improved half life limits on $2\beta^+/\varepsilon\beta^+/2\varepsilon$ processes in ^{96}Ru have been established at the level of 10^{20} yr, in particular for decays to the ground state of ^{96}Mo: $T_{1/2}^{2\nu2\beta^+} \geq 1.4 \times 10^{20}$ yr, $T_{1/2}^{2\nu\varepsilon\beta^+} \geq 8.0 \times 10^{19}$ yr and $T_{1/2}^{0\nu2K} \geq 1.0 \times 10^{21}$ yr (all limits are at 90% C.L.). The resonant neutrinoless double electron captures to the 2700.2 keV and 2712.7 keV excited states of ^{96}Mo are restricted as: $T_{1/2}^{0\nu KL} \geq 2.0 \times 10^{20}$ yr and $T_{1/2}^{0\nu2L} \geq 3.6 \times 10^{20}$ yr, respectively. Various two neutrino and neutrinoless 2β half lives of ^{96}Ru have been estimated in the framework of the QRPA approach. In addition, the $T_{1/2}$ limit for $0\nu2\beta^-$ transitions of ^{104}Ru to the first excited state of ^{104}Pd has been set as $\geq 6.5 \times 10^{20}$ yr.

A new set-up schema is ready for new measurements; all needed materials are at hand. The main aim is to investigate the $\epsilon\beta^+2\nu$ channel whose theoretical T$_{1/2}$ estimate is in the range 10^{21}—10^{22} yr, which is not very far from the presently reached sensitivity.

5.2 First investigation for 2β decay of ^{184}Os and ^{192}Os

Osmium contains two potentially double-β active isotopes: ^{184}Os (decay energy $Q_{2\beta}$ = 1453.7(0.6) keV [63]; isotopic abundance δ = 0.02(1)% [64]; allowed decay channels: 2ε and $\varepsilon\beta^+$) and ^{192}Os ($Q_{2\beta}$ = 412.4(2.9) keV [65]; δ = 40.78(19)% [64]; $2\beta^-$). There is a possibility of a resonant enhancement of the 0ν double-electron capture in ^{184}Os to a few excited levels of ^{184}W. The most promising of them is the level $(0)^+$ 1322.2 keV [66].
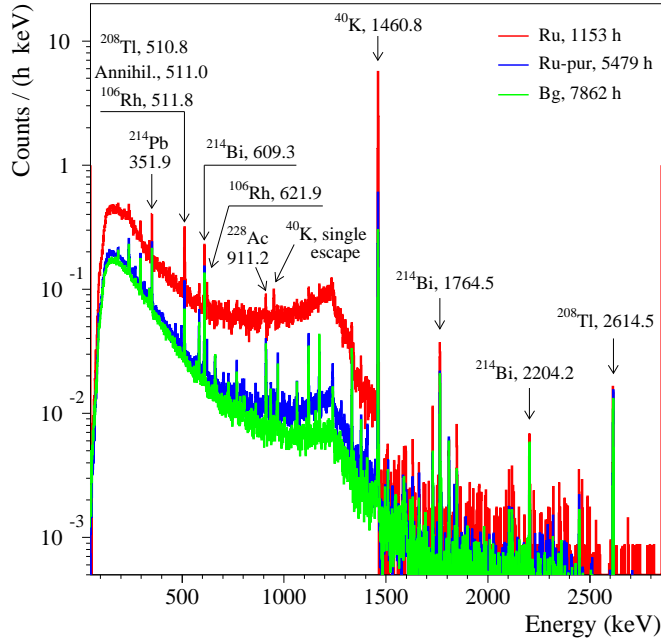
Figure 2: (Color on-line) The energy spectra above 20 keV accumulated with the initial Ru sample over 1153 h (Ru) and with the purified Ru over 5479 h (Ru-pur) in comparison with the background (Bg) of the GeMulti ultra-low background HPGe γ spectrometer measured over 7862 h. The energies of γ lines are in keV.

The investigation of double beta decay of ^{184,192}Os and alpha decay of ^{184}Os to the excited levels of the daughter nuclei, after preliminary results presented in ref.[67] continued by using ultra-pure osmium sample placed in a well-type ultra-low background HPGe detector especially designed for low energy gamma-ray spectrometry. A Monte Carlo simulation of gamma quanta propagation and R&D of methods to cut the osmium sample into thin plates has been performed to estimate the possibility to increase the experimental sensitivity to the alpha decay and to the neutrino accompanied double electron capture in ^{184}Os.

After 2741 h of data taking with a 173 g ultra-pure osmium sample limits on double-β processes in ^{184}Os were established for the first time at the level of $T_{1/2} \sim 10^{14} - 10^{17}$ yr (see Fig. 5.2 and 2013 publication list for the details). Possible resonant double-electron captures in ^{184}Os were searched for with a sensitivity $T_{1/2} \sim 10^{16}$ yr. A half-life limit $T_{1/2} \geq 5.3 \times 10^{19}$ yr was set for the double-β decay of ^{192}Os to the first excited level of ^{192}Pt. The radio-purity of the osmium sample has been investigated and radionuclides ^{137}Cs, ^{185}Os and ^{207}Bi were detected in the sample, while activities of ^{40}K, ^{60}Co, ^{226}Ra and ^{232}Th were limited at the $\approx$ mBq/kg level.

New measurements are foreseen to assess with high C.L. the possible presence of the rare α decay of ^{184}Os to the first excited level 103.5 keV of ^{180}W, for which a possible preliminary indication has been presented at NPAE2012 conference.

The experimental sensitivity to the processes could be improved almost one order of magnitude thanks to cut of the sample in 0.8-1.2 mm plates and to use of a new low

61
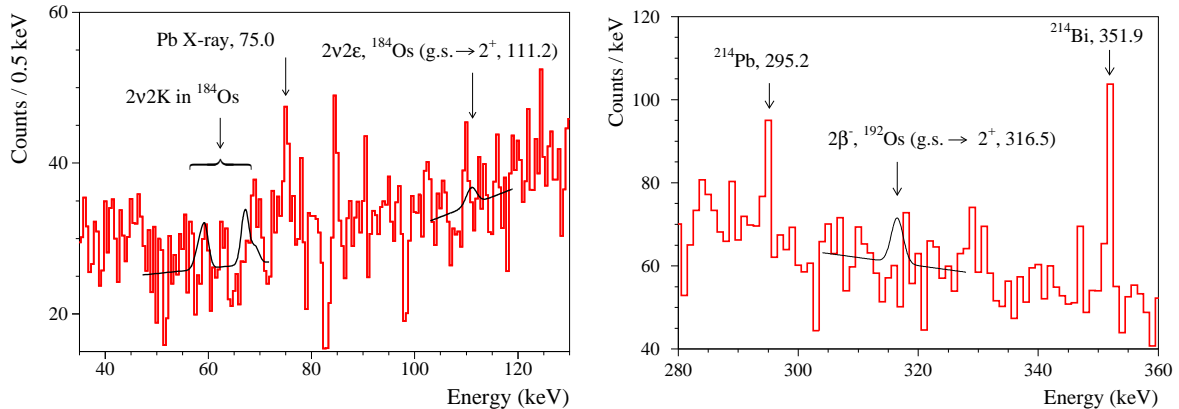
Figure 3: (Color online) Left: low energy part of the energy spectrum accumulated with the osmium sample over 2741 h. Excluded effects of $2\nu2K$ process in ^{184}Os with the half-life $T_{1/2} = 1.9 \times 10^{14}$ yr, and of $2\nu2K$ transition to the excited 2^+ level of ^{184}W with an energy of 111.2 keV with the half-life $T_{1/2} = 3.1 \times 10^{15}$ yr are shown by the solid lines. Right: Part of the energy spectrum where the peak from the 2β decay of ^{192}Os to the first excited level of ^{192}Pt is expected. The excluded – at 90% CL – peak is shown by the solid line.

background broad energy Ge detector. Further progress can be achieved by using osmium enriched in ^{184}Os, although this will require new enrichment techniques to be developed.

5.3 Radioactive contamination of ^{7}LiI(Eu) crystal scintillators

The europium doped lithium iodide (LiI(Eu)) scintillator is known since about 70 years [68]. Single LiI(Eu) crystals, in particular enriched in ^{6}Li, are used for a long time for efficient neutron detection (see e.g. [69, 70, 71, 72]).

Two decades ago the prospects of LiI(Eu) as a solar neutrino detector were considered [73]. Recently, LiI(Eu) scintillators were proposed to search for the resonant capture of axions possibly emitted in the solar pp-cycle by excited ^{7}Li [74]. Taking into account the high natural isotopic abundance of ^{7}Li (92.41% [54]), different Li-containing targets have been already used in several solar axion experiments (see [75] and references therein). In order to search for solar axions, one of the main requirements for the targets is the achievement of a level of radioactive contamination as low as possible. The radio-purity plays an important role also in other applications of scintillation detectors, including neutron detection.

The radioactive contamination of two 26 g samples of low background lithium iodide crystal scintillators doped by europium and enriched in ^{7}Li to 99.9% (^{7}LiI(Eu)) was investigated by scintillation method at the sea level in the Institute for Nuclear Research (Kyiv, Ukraine), and by ultra-low background HPGe γ spectrometry deep underground (see 2013 publication list and Fig.4).

Two ^{7}LiI(Eu) single crystals ($\oslash 20 \times 20$ mm, with masses of ≈ 26 g each one) grown by the Bridgman-Stockbarger method [76] in the Institute of Scintillation Materials (Kharkiv,
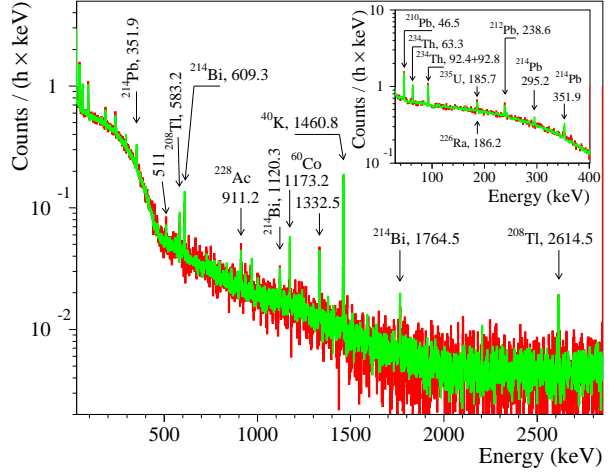
Figure 4: (Color online) Left: the enriched ^{7}LiI(Eu) crystal scintillators. Right: energy spectrum accumulated with the ^{7}LiI(Eu) sample No. 1 (red histogram) over 778 h by ultra-low background HPGe γ spectrometer. The background spectrum measured without sample over 3047 h (green histogram) is also shown. (Insert) Low energy part of the spectra. The energies of γ lines are in keV.

Ukraine) were used in the present study. The enrichment of the lithium used for the crystals growth in ^{7}Li was 99.9%; the concentration of the europium in the initial charge was 8×10^{-3} wt%. Due to the high hygroscopicity of the LiI, the ^{7}LiI(Eu) crystals were housed in oxygen free high conductivity (OFHC) copper containers with an external size of $\oslash 26 \times 32$ mm. The opposite sides of the containers were made of quartz windows $\oslash 24 \times 6$ mm. The lateral surface of the crystals was surrounded by light-reflector made of annealed magnesium oxide to improve the light collection. The total masses of the packed scintillators No. 1 and No. 2 (see Fig. 4 left) are 53.6 and 51.6 g, respectively.

In case of the measurements with ultra-low background HPGe γ spectrometer the samples No. 1 and No. 2 were measured over 788 and 500 h, respectively, whereas the background was accumulated over 3047 h. The energy spectra of the 7LiI(Eu) sample No. 1 and of the background, both normalised to the time of measurements are shown in Fig. 4 right.

No radioactivity was detected in the detectors on the level of sensitivity ~ 1 mBq/kg for ^{226}Ra, ^{228}Th, ^{210}Po, ~ 10 mBq/kg for ^{60}Co, ^{137}Cs and ^{152,154}Eu, $\sim 0.1 - 1$ Bq/kg for ^{40}K, ^{90}Sr and ^{210}Pb.

6   Other activities

In 2013 it continued the investigation on other possible dark matter signatures like the so called diurnal modulation (the daily variation of the interaction rate due to Earth rotational velocity, that is a fully model independent signature) and the so called directionality (the correlation of Dark Matter impinging direction with Earth's galactic motion due to

the distribution of Dark Matter particles velocities) useful to investigate the particular case of those DM candidate particles inducing nuclear recoils.

In particular for directionality in recent years we have made extensive efforts and measurements with $ZnWO_4$ crystal scintillators, already interesting to investigate double beta decay of Zn and W isotopes [49]. These scintillators (see 2013 publication list) have the particular feature to be anisotropic in the light output and in the pulse shape for heavy particles (p, α, nuclear recoils) depending on the direction with respect to the crystal axes. The response to γ/β radiation is isotropic instead. Among the anisotropic scintillators, the $ZnWO_4$ has unique features, which make it an excellent candidate for this type of research, and there is still plenty of room for the improvement of its performances. In 2012 the possibility of a low background pioneer experiment (named ADAMO, Anisotropic detectors for DArk Matter Observation) to exploit deep underground the directionality approach by using anisotropic $ZnWO_4$ scintillators has been explored; for details see in the 2013 publication list.

For completeness, we mention that another interesting idea about a detector with anisotropic response is put forward by us and some external collaborators; it is based on the use of Carbon Nanotubes (CNT).

7 Conclusions

The results, obtained by analysing the data of the last (seventh) annual cycle of DAMA/LI-BRA-phase1, were released, giving the final DM model independent result of DAMA/LI-BRA-phase1. The positive model independent evidence for the presence of DM particles in the galactic halo is now supported at 9.3σ C.L. (on a cumulative exposure of 1.33 ton×yr i.e. 14 annual cycles of DAMA/NaI and DAMA/LIBRA) and is compatible with a wide set of scenarios regarding the nature of the DM candidate and related astrophysical, nuclear and particle Physics.

DAMA/LIBRA-phase2 – started after the replacement of all the PMTs with new ones having higher quantum efficiency– is continuously in data taking. The strictly quality control allows DAMA/LIBRA to be still the highest radio-pure set-up in the field with the largest exposed sensitive mass, the full control of running conditions, the largest duty-cycle and an exposure orders of magnitude larger than any other activity in the field.

Studies are under way towards a possible DAMA/LIBRA-phase3 or a possible DAMA/1 ton experiment (proposed since 1996).

In addition the work for the future (some years from now) installation of the ^{116}Cd detectors in the low-background GeMulti set-up has been progressed as well as the preparations for the future search for super-heavy eca-tungsten with the help of $ZnWO_4$ scintillation and the preparation of the other future measurements (among them: developments on new $SrI_2(Eu)$ crystals, on new enriched $CdWO_4$ depleted in ^{113}Cd, on highly radio-pure $ZnWO_4$, further developing the goals of our project to develop highly radio-pure scintillators for the search of rare processes).

Finally, in 2013 all the DAMA/set-ups have regularly been in data taking and various kinds of measurements are in progress and planned for the future. Several competing results on developments and rare processes have been published.

8   List of Publications during 2013

1. D. Poda, A. Barabash, P. Belli, R. Bernabei, R. Boiko, V. Brudanin, F. Cappella, V. Caracciolo, S. Castellano, R. Cerulli, D. Chernyak, F. Danevich, S. d'Angelo, V. Degoda, M. Di Vacri, A. Dossovitskiy, E. Galashov, A. Incicchitti, V. Kobychev, S. Konovalov, G. Kovtun, M. Laubenstein, A. Mikhlin, V. Mokina, A. Nikolaiko, S. Nisi, R. Podviyanuk, O. Polischuk, A. Shcherban, V. Shlegel, D. Solopikhin, V. Tretyak, V. Umatov, Ya. Vasiliev, V. Virich, $CdWO_4$ crystal scintillators from enriched isotopes for double beta decay experiments, Radiation Measurements 56 (2013) 66.

2. P. Belli, R. Bernabei, S.V. Budakovsky, F. Cappella, R. Cerulli, F.A. Danevich, S. d'Angelo, A. Incicchitti, M. Laubenstein, D.V. Poda, O.G. Polischuk, V.I. Tretyak, Radioactive contamination of ^{7}LiI(Eu) crystal scintillators, Nucl. Instr. & Meth. A 704 (2013) 40.

3. F. Cappella, R. Bernabei, P. Belli, V. Caracciolo, R. Cerulli, F.A. Danevich, A. d'Angelo, A. Di Marco, A. Incicchitti, D.V. Poda, V.I. Tretyak, On the potentiality of the $ZnWO_4$ anisotropic detectors to measure the directionality of Dark Matter, Eur. Phys. J. C 73 (2013) 2276.

4. P. Belli, R. Bernabei, F. Cappella, R. Cerulli, F.A. Danevich, S. d'Angelo, A. Di Marco, A. Incicchitti, G.P. Kovtun, N.G. Kovtun, M. Laubenstein, D.V. Poda, O.G. Polischuk, A.P. Shcherban, V.I. Tretyak, First search for double-β decay of ^{184}Os and ^{192}Os, Eur. Phys. J. A 49 (2013) 24.

5. R. Bernabei, P. Belli, A. Di Marco, F. Montecchia, F. Cappella, A. d'Angelo, A. Incicchitti, V. Caracciolo, R. Cerulli, C. J. Dai, H. L. He, X. H. Ma, X. D. Sheng, R. G.Wang, Z. P. Ye, Particle Dark Matter in the galactic halo: results and perspectives, Int. J. of Mod. Phys. D 22 (2013) 1360001.

6. P. Belli, R. Bernabei, F. Cappella, R. Cerulli, F.A. Danevich, S. d'Angelo, A. Incicchitti, G.P. Kovtun, N.G. Kovtun, M. Laubenstein, D.V. Poda, O.G. Polischuk, A.P. Shcherban, D.A. Solopikhn, J. Suhonen, V.I. Tretyak, Search for 2β decays of ^{96}Ru and ^{104}Ru by ultra-low background HPGe spectrometry at LNGS: final results, Phys. Rev. C 87 (2013) 034607.

7. R. Bernabei, P. Belli, F. Cappella, V. Caracciolo, S. Castellano, R. Cerulli, C.J. Dai, A. d'Angelo, A. Di Marco, H.L. He, A. Incicchitti, M. Laubenstein, X.H. Ma, F. Montecchia, X.D. Sheng, V.I. Tretyak, R.G. Wang, Z.P. Ye, New search for correlated e$^+$e$^-$ pairs in the α decay of ^{241}Am, Eur. Phys. J. A 49 (2013) 64.

8. F.A. Danevich, A.S. Barabash, P. Belli, R. Bernabei, R.S. Boiko, V.B. Brudanin, F. Cappella, V. Caracciolo, R. Cerulli, D.M. Chernyak, S. d'Angelo, V.Ya. Degoda, M.L. Di Vacri, A.E. Dossovitskiy, E.N. Galashov, A. Incicchitti, V.V. Kobychev, S.I. Konovalo, G.P. Kovtun, B.N. Kropivyansky, M. Laubenstein, A.L. Mikhlin, V.M. Mokina, A.S. Nikolaiko, S. Nisi, D.V. Poda, R.B. Podviyanuk, O.G. Polischuk, A.P. Shcherba, V.N. Shlegel, D.A. Solopikhin, V.I. Tretyak, V.I. Umatov, Ya.V. Vasiliev and V.D. Virich, Development of radio-pure cadmium tungstate crystal scintillators from enriched ^{106}Cd and ^{116}Cd to search for double beta decay, AIP Conf. Proc. 1549 (2013) 201.

9. R. Bernabei, P. Belli, F. Cappella, V. Caracciolo, R. Cerulli, C. J. Dai, A. d'Angelo, A. Di Marco, H. L. He, A. Incicchitti, X. H. Ma, F. Montecchia, X. D. Sheng, R. G. Wang, Z. P. Ye, DAMA/LIBRA results and perspectives of the second stage, YADERNA FIZYKA TA ENERHETYKA vol.14 n.2 (2013) 114.

10. O.G. Polischuk, A.S. Barabash, P. Belli, R. Bernabei, R.S. Boiko, F. Cappella, R. Cerulli, F.A. Danevich, A. Incicchitti, M. Laubenstein, V.M. Mokina, S. Nisi, D.V. Poda, V.I. Tretyak, Purification of Lanthanides for Double Beta Decay Experiments, AIP Conf. Proc. 1549 (2013) 124.

11. R. Bernabei, P. Belli,F. Cappella,V. Caracciolo, S. Castellano, R. Cerulli, R.S. Boiko, D.M. Chernyak, F.A. Danevich, C.J. Dai, A. d'Angelo, S. d'Angelo, A. Di Marco, H.L. He, A. Incicchitti, X.H. Ma, V.M. Mokina, F. Montecchia, D.V. Poda, O.G. Polischuk, X.D. Sheng, R.G. Wang, Z.P. Ye, V.I. Tretyak, Crystal scintillators for low background measurements, AIP Conf. Proc. 1549 (2013) 189.

12. R. Bernabei, Direct Dark Matter Investigation, Phys. of Part. and Nuclei Letters 10 (2013) 727.

13. R. Bernabei, P. Belli, S. d'Angelo, A. Di Marco, F. Montecchia, F. Cappella, A. d'Angelo, A. Incicchitti, V. Caracciolo, S. Castellano, R. Cerulli, C.J. Dai, H.L. He, X.H. Ma, X.D. Sheng, R.G. Wang, Z.P. Ye, Dark Matter investigation by DAMA at Gran Sasso, Int. J. of Mod. Phys. A 28 (2013) 1330022 (73 pages).

14. R. Bernabei, P. Belli, F. Cappella, V. Caracciolo, S. Castellano, R. Cerulli, C.J. Dai, A. d'Angelo, S. d'Angelo, A. Di Marco, H.L. He, A. Incicchitti, H.H. Kuang, X.H. Ma, F. Montecchia, D. Prosperi, X.D. Sheng, R.G. Wang, Z.P. Ye, Final model independent result of DAMA/LIBRA-phase1, Eur. Phys. J. C 73 (2013) 2648.

15. A.S. Barabash, P. Belli, R. Bernabei, F. Cappella, V. Caracciolo, S. Castellano, R. Cerulli, D.M. Chernyak, F.A. Danevich, E.N. Galashov, A. Incicchitti, V.V. Kobychev, S.I. Konovalov, M. Laubenstein, D.V. Poda, R.B. Podviyanuk, O.G. Polischuk, V.N. Shlegel, V.I. Tretyak, V. I. Umatov, Ya. V. Vasiliev, First results of the experiment to search for double beta decay of ^{116}Cd with the help of enriched ^{116}CdWO$_4$ cystal scintillators, in the volume of Proceed. of the 4-th Int. Conf. on Current Problems in Nuclear Physics and Atomic Energy (NPAE2012), ed. INR-Kiev (2013) page 353-356 [ISBN 978-966-02-6750-3]

16. P. Belli, R. Bernabei, F. Cappella, R. Cerulli, F.A. Danevich, S. d'Angelo, A. Di Marco, A. Incicchitti, G.P. Kovtun, N.G. Kovtun, M. Laubenstein, D.V. Poda, O.G. Polischuk, A.P. Shcherban, V. I. Tretyak, First search for double beta decay of Osmium by low background HPGe detector (preliminary results), in the volume of Proceed. of the 4-th Int. Conf. on Current Problems in Nuclear Physics and Atomic Energy (NPAE2012), ed. INR-Kiev (2013) page 357-360 [ISBN 978-966-02-6750-3]

17. R. Bernabei, P. Belli, F. Cappella, V. Caracciolo, R. Cerulli, C. J. Dai, A. d'Angelo, A. Di Marco, H. L. He, A. Incicchitti, X. H. Ma, F. Montecchia, X. D. Sheng, R. G. Wang, Z. P. Ye, DAMA/LIBRA results and perspectives of the second stage, in the volume of Proceed. of the 4-th Int. Conf. on Current Problems in Nuclear Physics and Atomic Energy (NPAE2012), ed. INR-Kiev (2013) page 21-27 [ISBN 978-966-02-6750-3]

18. R. Bernabei, P. Belli, A. Di Marco, F. Montecchia, F. Cappella, A. d'Angelo, A. Incicchitti, D. Prosperi, R. Cerulli, C. J. Dai, H.L. He, X.H. Ma, X.D. Sheng, R.G. Wang, Z.P. Ye, Particle Dark Matter: DAMA/LIBRA results and perspectives, in the volume "Particle Physics at the Tercentenary of Mikhail Lomonosov", World Scie. (2013), 219 [ISBN 978-981-4436-82-3]

References

[1] R. Bernabei et al., Nucl. Instr. and Meth. A 592 (2008) 297.

[2] R. Bernabei et al., Eur. Phys. J. C 56 (2008) 333.

[3] R. Bernabei et al., Eur. Phys. J. C 67 (2010) 39.

[4] R. Bernabei et al., Eur. Phys. J. C 62 (2009) 327.

[5] P. Belli et al., Phys. Rev. D 84 (2011) 055014.

[6] P. Belli, R. Bernabei, C. Bacci, A. Incicchitti, R. Marcovaldi, D. Prosperi, DAMA proposal to INFN Scientific Committee II, April 24th 1990.

[7] R. Bernabei et al., Phys. Lett. B 389 (1996) 757; R. Bernabei et al., Phys. Lett. B 424 (1998) 195; R. Bernabei et al., Phys. Lett. B 450 (1999) 448; P. Belli et al., Phys. Rev. D 61 (2000) 023512; R. Bernabei et al., Phys. Lett. B 480 (2000) 23; R. Bernabei et al., Phys. Lett. B 509 (2001) 197; R. Bernabei et al., Eur. Phys. J. C 23 (2002) 61; P. Belli et al., Phys. Rev. D 66 (2002) 043503.

[8] R. Bernabei et al., Il Nuovo Cim. A 112 (1999) 545.

[9] R. Bernabei et al., Eur. Phys. J. C18 (2000) 283.

[10] R. Bernabei el al., La Rivista del Nuovo Cimento 26 n.1 (2003) 1-73.

[11] R. Bernabei et al., Int. J. Mod. Phys. D 13 (2004) 2127.

[12] R. Bernabei et al., Int. J. Mod. Phys. A 21 (2006) 1445.

[13] R. Bernabei et al., Eur. Phys. J. C 47 (2006) 263.

[14] R. Bernabei et al., Int. J. Mod. Phys. A 22 (2007) 3155.

[15] R. Bernabei et al., Eur. Phys. J. C 53 (2008) 205.

[16] R. Bernabei et al., Phys. Rev. D 77 (2008) 023506.

[17] R. Bernabei et al., Mod. Phys. Lett. A 23 (2008) 2125.

[18] R. Bernabei et al., Phys. Lett. B408 (1997) 439; P. Belli et al., Phys. Lett. B460 (1999) 236; R. Bernabei et al., Phys. Rev. Lett. 83 (1999) 4918; P. Belli et al., Phys. Rev. C60 (1999) 065501; R. Bernabei et al., Il Nuovo Cimento A112 (1999) 1541; R. Bernabei et al., Phys. Lett. B 515 (2001) 6; F. Cappella et al., Eur. Phys. J.-direct C14 (2002) 1; R. Bernabei et al., Eur. Phys. J. A 23 (2005) 7; R. Bernabei et al., Eur. Phys. J. A 24 (2005) 51; R. Bernabei et al., Astrop. Phys. 4 (1995) 45.

[19] K.A. Drukier et al., Phys. Rev. D 33 (1986) 3495.

[20] K. Freese et al., Phys. Rev. D 37 (1988) 3388.

[21] R. Bernabei, P. Belli, A. Bussolotti, F. Cappella, V. Caracciolo, M. Casalboni, R. Cerulli, C.J. Dai, A. d'Angelo, A. Di Marco, H.L. He, A. Incicchitti, H.H. Kuang, M. Laubenstein, X.H. Ma, A. Mattei, F. Montecchia, C. Palazzesi, P. Prosposito, X.D. Sheng, R.G. Wang, Z.P. Ye, Performances of the new high quantum efficiency PMTs in DAMA/LIBRA, Journal of Instrumentation 7 (2012) P03009.

[22] R. Bernabei et al., AIP Conf. Proceed. 1223, 50 (2010) (arXiv:0912.0660).

[23] R. Bernabei et al., J. Phys.: Conf. Ser. 203, 012040 (2010) (arXiv:0912.4200); http://taup2009.lngs.infn.it/slides/jul3/nozzoli. pdf, talk given by F. Nozzoli.

[24] R. Bernabei et al., in the volumeFrontier Objects in Astrophysics and Particle Physics (Vulcano 2010), S.I.F. Ed. (2011), 157 (arXiv:1007.0595).

[25] R. Bernabei et al., Can. J. Phys. 89 (2011) 11.

[26] R. Bernabei et al., to appear on Proceed. of the Int. Conf, TIPP 2011.

[27] R. Bernabei et al., arXiv:1210.6199; arXiv:1211.6346.

[28] R. Bernabei, P. Belli, F. Cappella, V. Caracciolo, R. Cerulli, C. J. Dai, A. d'Angelo, A. Di Marco, H. L. He, A. Incicchitti, X. H. Ma, F. Montecchia, X. D. Sheng, R. G. Wang, Z. P. Ye, No role for muons in the DAMA annual modulation results, Eur. Phys. J. C 72 (2012) 2064.

[29] A. Bottino et al., Phys. Rev. D 85 (2012) 095013.

[30] A. Bottino et al., arXiv:1112.5666.

[31] B.G. Pettersson, in Alpha-, Beta-, and Gamma-Ray Spectroscopy, edited by K. Siegbahn (North-Holland, Amsterdam, 1966), p. 1569.

[32] A. Ljubicic and B.A. Logan, Phys. Rev. C 7, 1541 (1973).

[33] N. Arley and C.Møller, Kgl. Danske Videnskab. Selskab, Mat.-Phys. Medd.15, 9 (1938).

[34] L. Tisza, Phys. Z. Sowjetunion 11, 245 (1937).

[35] J.S. Greenberg and M. Deutsch, Phys. Rev. 102, 415 (1956).

[36] T. Asanuma et al., Phys. Lett. B 237, 588 (1990).

[37] K. Pisk et al., Phys. Rev. C 17, 739 (1978).

[38] J. Stanicek et al., Nucl. Instr. Meth. B 17, 462 (1986).

[39] M. Inoue et al., Mod. Phys. Lett. A 5, 309 (1990).

[40] T. Cowan et al., Phys. Rev. Lett. 56, 444 (1986); H. Tsertos et al., Z. Phys. A 326, 235 (1987); W. Koenig et al., Z. Phys. A 328, 129 (1987); E. Berdemann et al., Nucl. Phys. A 488, 683c (1988).

[41] P. Belli et al., Il Nuovo Cim. 103A (1990) 767.

[42] P. Belli et al., Phys. Lett. B 387 (1996) 222 and Phys. Lett. B 389 (1996) 783 (erratum); R. Bernabei et al., New J. Phys. 2 (2000) 15.1; Eur. Phys. J.-direct C11 (2001) 1; Phys. Lett. B 436 (1998) 379; R. Bernabei et al., in the volume "Beyond the Desert 2003", Springer (2003) 365.

[43] R. Bernabei et al., Nucl. Instr. & Meth. A482 (2002) 728.

[44] R. Bernabei et al., Phys. Lett. B 546 (2002) 23; F. Cappella, PhD Thesis, Università di Roma "Tor Vergata", 2005.

[45] P. Belli et al., Il Nuovo Cim. C 19 (1996) 537; Astrop. Phys. 5 (1996) 217.

[46] R. Bernabei et al., Phys. Lett. B 527 (2002) 182.

[47] P. Belli et al., Phys. Rev. D 61 (2000) 117301; Phys. Lett. B 465 (1999) 315; R. Bernabei et al., Phys. Lett. B 493 (2000) 12; Eur. Phys. J. A 27 s01 (2006) 35.

[48] R. Bernabei et al., Astropart. Phys. 7 (1997) 73; R. Bernabei et al., Il Nuovo Cim. A 110 (1997) 189; P. Belli et al., Astropart. Phys. 10 (1999) 115; P. Belli et al., Nucl. Phys. B 563 (1999) 97; R. Bernabei et al., Nucl. Phys. A 705 (2002) 29; P. Belli et al., Nucl. Instr. Meth. A 498 (2003) 352; R. Cerulli et al., Nucl. Instr. Meth. A 525 (2004) 535; R. Bernabei et al., Nucl. Instr. Meth. A 555 (2005) 270; R. Bernabei et al., Ukr. J. Phys. 51 (2006) 1037; P. Belli et al., Nucl. Phys. A 789 (2007) 15; P. Belli et al., Phys. Rev. C 76 (2007) 064603; P. Belli et al., Eur. Phys. J. A 36 (2008) 167; P. Belli et al., J. Phys. G 38 (2011) 015103.

[49] P. Belli et al., Nucl. Phys. A 826 (2009) 256; P. Belli et al., Phys. Lett. B 658 (2008) 193.

[50] P. Belli et al., Nucl. Instrum. Meth. A 626-627 (2011) 31.

[51] P. Belli et al., Nucl. Instr. Meth. A 615 (2010) 301.

[52] V.I. Tretyak, Yu.G. Zdesenko, At. Data Nucl. Data Tables 61, 43 (1995); 80, 83 (2002).

[53] S. Eliseev et al., Phys. Rev. C 83, 038501 (2011).

[54] M. Berglund and M.E. Wieser, Pure Appl. Chem. 83 (2011) 397.

[55] R.B. Firestone et al., Table of Isotopes, 8-th ed. (John Wiley, New York, 1996) and CD update (1998).

[56] D. Abriola, A.A. Sonzogni, Nucl. Data Sheets109, 2501 (2008).

[57] R.G. Winter, Phys. Rev. 100, 142 (1955); M.B. Voloshin et al., JETP Lett. 35, 656 (1982); J. Bernabeu et al., Nucl. Phys. B 223, 15 (1983); Z. Sujkowski, S. Wycech, Phys. Rev. C 70, 052501 (2004); J. Suhonen, Phys. Lett. B 701, 490 (2011).

[58] M. Wang et al., Chin. Phys. C 36, 1603 (2012).

[59] E.B. Norman, Phys. Rev. C 31, 1937 (1985).

[60] P. Belli et al., Eur. Phys. J. A 42, 171 (2009).

[61] P. Belli et al., Nucl. Phys. At. Energy 11, 362 (2010).

[62] E. Andreotti et al., Appl. Radiat. Isot. 70, 1985 (2012).

[63] C. Smorra et al., Phys. Rev. C 86 (2012) 044604.

[64] M. Berglund, M.E. Wieser, Pure Appl. Chem. 83 (2011) 397.

[65] G. Audi, A.H. Wapstra, C. Thibault, Nucl. Phys. A 729 (2003) 337.

[66] M.I. Krivoruchenko et al., Nucl. Phys. A 859 (2011) 140.

[67] P. Belli et al., First search for double beta decay of osmium by low background HPGe detector, to be published in Proc. of 4th Int. Conf. NPAE-Kyiv2012, 3–7 September 2012, Kyiv, Ukraine.

[68] J. Schenck, Nature 171 (1953) 518.

[69] R.B. Murray, Nucl. Instrum. 2 (1958) 237.

[70] D.R. Johnson, J.H. Thorngate, P.T. Perdue, Nucl. Instrum. Meth. 75 (1969) 61.

[71] N.E. Hertel and J.W. Davidson, Nucl. Instrum. Meth. A 238 (1985) 509.

[72] A. Syntfeld et al., IEEE Trans. Nucl. Sci. 52 (2005) 3151.

[73] C.C. Chang, C.Y. Chang and G. Collins, Nucl. Phys. B (Proc. Suppl.) 35 (1994) 464.

[74] P. Belli et al., Nucl. Phys. A 806 (2008) 388.

[75] P. Belli et al., Phys. Lett. B 711 (2012) 41.

[76] D.C. Stockbarger, Rev. Sci. Instrum. 7 (1936) 133.

Spokespeople: C. Galbiati, G. Ranucci

DarkSide
Yearly Report to LNGS
March 2014

C. E. Aalseth,[1] P. Agnes,[2] T. Alexander,[3] D. Alton,[4] K. Arisaka,[5] D. M. Asner,[1]
H. O. Back,[6] B. Baldin,[7] F. Barbato,[8] J. Benziger,[9] K. Biery,[7] G. Bonfini,[10] M. Bossa,[11]
A. Brigatti,[12] J. Brodsky,[6] F. Budano,[13] S. Bussino,[13] L. Cadonati,[3] L. Cadoni,[14]
F. Calaprice,[6] N. Canci,[5] A. Candela,[10] H. Cao,[6] M. Cariello,[15] P. Cavalcante,[10]
A. Chavarria,[16] A. Chepurnov,[17] A. G. Cocco,[8] C. Condon,[6] G. Covone,[8] L. Crippa,[12]
D. D'Angelo,[12] M. D'Incecco,[10] S. Davini,[18] M. De Deo,[10] M. De Vincenzi,[13] A. Derbin,[19]
A. Devoto,[14] F. Di Eusanio,[6] G. Di Pietro,[12] D. Durben,[20] E. Edkins,[21] A. Empl,[18]
A. Fan,[5] G. Fiorillo,[8] K. Fomenko,[10] G. Forster,[3] M. Foxe,[1] D. Franco,[2] F. Gabriele,[10]
C. Galbiati,[6] A. Goretti,[6] L. Grandi,[16] M. Gromov,[17] M. Y. Guan,[22] Y. Guardincerri,[7]
B. Hackett,[21] K. Herner,[7] A. Hime,[23] P. Humble,[1] E. V. Hungerford,[18] Al. Ianni,[10]
An. Ianni,[6] D. E. Jaffe,[24] C. Jollet,[25] A. Kayunov,[19] K. Keeter,[20] C. Kendziora,[7]
S. Kidner,[26] V. Kobychev,[27] G. Koh,[6] D. Korablev,[28] G. Korga,[18] A. Kurlej,[3]
M. Laubenstein,[10] P. X. Li,[22] M. Lissia,[14] P. Lombardi,[12] C. Love,[29] L. Ludhova,[12]
S. Luitz,[30] L. Lukyanchenko,[17] Y. Q. Ma,[22] I. Machulin,[31] A. Mandarano,[13]
S. Mari,[13] J. Maricic,[21] L. Marini,[13] D. Markov,[31] C. J. Martoff,[29] A. Meregaglia,[25]
E. Meroni,[12] P. Meyers,[6] P. Lombardi,[12] T. Miletic,[32, 29] C. Mollo,[8] D. Montanari,[7]
M. Montuschi,[10] M. E. Monzani,[30] P. Mosteiro,[6] B. Mount,[20] V. Muratova,[19] P. Musico,[15]
A. Nelson,[6] S. Odrowski,[10] A. Odrzywolek,[33] M. Okounkova,[6] M. Orsini,[10]
J. L. Orrell,[1] M. Orsini,[10] F. Ortica,[34] L. Pagani,[15] M. Pallavicini,[15] E. Pantic,[5, 35]
L. Papp,[26] S. Parmeggiano,[12] R. Parsells,[6] K. Pelczar,[33] N. Pelliccia,[34] L. Perasso,[15]
S. Perasso,[2] F. Perfetto,[8] A. Pocar,[3] S. Pordes,[7] D. Pugachev,[31] K. Randle,[3] G. Ranucci,[12]
A. Razeto,[10] K. Recine,[29] B. Reinhold,[21] A. Renshaw,[5] A. Romani,[34] B. Rossi,[6, 8]
N. Rossi,[10] S. D. Rountree,[26] D. Sablone,[18] P. Saggese,[10] R. Saldanha,[16] W. Sands,[6]
S. Sangiorgio,[36] E. Segreto,[10] D. Semenov,[19] E. Shields,[6] M. Skorokhvatov,[31]
M. Smallcomb,[4] O. Smirnov,[28] A. Sotnikov,[28] Y. Suvarov,[5] R. Tartaglia,[10] J. Tatarowicz,[29]
G. Testera,[15] J. Thompson,[20] A. Tonazzo,[2] E. Unzhakov,[19] R. B. Vogelaar,[26] M. Wada,[6]
H. Wang,[5] Y. Wang,[22] S. Westerdale,[6] R. Williams,[1] M. Wojcik,[33] A. Wright,[6] J. Xu,[6]
C. G. Yang,[22] J. Yoo,[7] B. Yu,[24] S. Zavatarelli,[15] W. L. Zhong,[22] and G. Zuzel[33]

[1]*Pacific Northwest National Laboratory, Richland, WA 99352, USA*
[2]*APC, Université Paris Diderot, Sorbonne Paris Cité, Paris 75205, France*
[3]*Physics Department, University of Massachusetts, Amherst, MA 01003, USA*

[4]Physics and Astronomy Department, Augustana College, Sioux Falls, SD 57197, USA

[5]Physics and Astronomy Department, University of California, Los Angeles, CA 90095, USA

[6]Physics Department, Princeton University, Princeton, NJ 08544, USA

[7]Fermi National Accelerator Laboratory, Batavia, IL 60510, USA

[8]Physics Department, Università degli Studi Federico II and INFN, Napoli 80126, Italy

[9]Chemical Engineering Department, Princeton University, Princeton, NJ 08544, USA

[10]Laboratori Nazionali del Gran Sasso, Assergi (AQ) 67010, Italy

[11]Gran Sasso Science Institute, L'Aquila 67100, Italy

[12]Physics Department, Università degli Studi and INFN, Milano 20133, Italy

[13]Physics Department, Università degli Studi Roma Tre and INFN, Roma 00146, Italy

[14]Physics Department, Università degli Studi and INFN, Cagliari 09042, Italy

[15]Physics Department, Università degli Studi and INFN, Genova 16146, Italy

[16]Kavli Institute, Enrico Fermi Institute and Dept. of
Physics, University of Chicago, Chicago, IL 60637, USA

[17]Skobeltsyn Institute of Nuclear Physics, Lomonosov Moscow State University, Moscow 119991, Russia

[18]Department of Physics, University of Houston, Houston, TX 77204, USA

[19]Saint Petersburg Nuclear Physics Institute, Gatchina 188350, Russia

[20]School of Natural Sciences, Black Hills State University, Spearfish, SD 57799, USA

[21]Department of Physics and Astronomy, University of Hawai'i, Honolulu, HI 96822, USA

[22]Institute of High Energy Physics, Beijing 100049, China

[23]Los Alamos National Laboratory, Los Alamos, NM 87545, USA

[24]Brookhaven National Laboratory, Upton, NY 11973, USA

[25]IPHC, Université de Strasbourg, CNRS/IN2P3, Strasbourg 67037, France

[26]Physics Department, Virginia Tech, Blacksburg, VA 24061, USA

[27]Institute for Nuclear Research, National Academy of Sciences of Ukraine, Kiev 03680, Ukraine

[28]Joint Institute for Nuclear Research, Dubna 141980, Russia

[29]Physics Department, Temple University, Philadelphia, PA 19122, USA

[30]SLAC National Accelerator Laboratory, Menlo Park, CA 94025, USA

[31]National Research Centre Kurchatov Institute, Moscow 123182, Russia

[32]Chemistry and Physics Department, Arcadia University, Glenside, PA 19038, USA

[33]Smoluchowski Institute of Physics, Jagiellonian University, Krakow 30059, Poland

[34]Chemistry Department, Università degli Studi and INFN, Perugia 06123, Italy

[35]Physics Department, University of California, Davis, CA 95616, USA

[36]Lawrence Livermore National Laboratory, 7000 East Avenue, Livermore, CA 94550
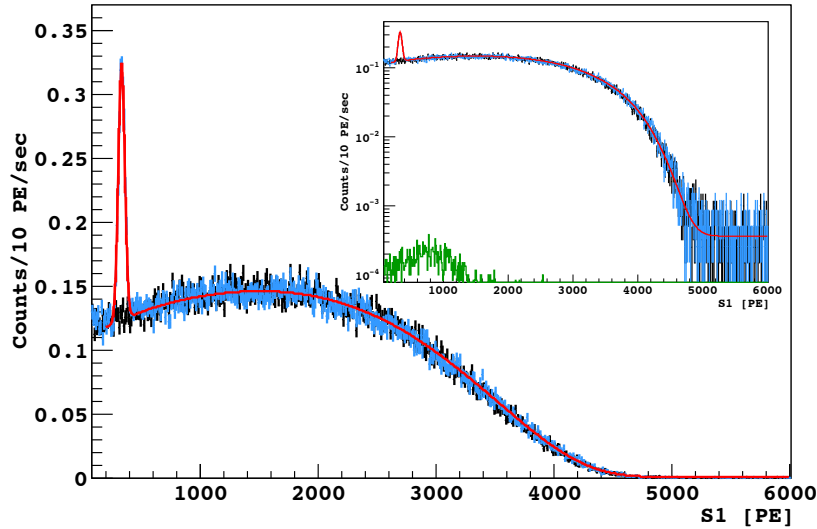
FIG. 1: The primary scintillation (S1) spectrum in a zero-field run in the DarkSide-50 TPC. **Black:** Background only, clearly dominated by the ^{39}Ar beta decay, with a 565 keV endpoint. **Blue:** S1 spectrum obtained during the infusion into the recirculating argon of ^{83m}Kr, which decays with near-coincident conversion electrons summing to 41.5 keV. **Red:** Fit to the ^{83m}Kr+^{39}Ar spectrum, giving a light yield of 8.0 ± 0.5 PE/keV$_{ee}$. **Inset:** Spectra in logarithmic scale. **Green:** S1 spectrum for γ-rays triggering in coincidence with the neutron veto.

I. DARKSIDE-50 COMMISSIONING AND EARLY RUNNING

DarkSide-50 was built and commissioned, and is now operated, with support from NSF (NSF PHY-1004072, NSF PHY-1242585, and associated grants), DOE (DE-FG02-91ER40671 and DE-AC02-07CH11359), and INFN. The DarkSide-50 TPC, as previously reported, is cooled by externally-liquefied argon and will be filled with Underground Argon (UAr) after the current Atmospheric Argon (AAr). The DarkSide-50 TPC has a thick PTFE reflector, fused silica windows with ITO anode and cathode, and Hamamatsu R11065-series low-background, high-QE PMT's submerged in LAr and deployed with cold preamplifiers.

Following a complete test of the TPCfunctionality run in April 2013, the DarkSide-50 TPC was rebuilt with some improvements and with a set of cryogenic PMTs that meet the minimum specs for a background-free run. We are continuing R&D on PMTs to further reduce their background for future expansions of the program. The DarkSide-50 TPC was redeployed into the LSV on September 13, 2013. It was then cooled and filled with AAr. Commissioning proceeded for several weeks, establishing the PMT set points and two-phase TPC operations. The dark matter run started in mid October 2013 and is continuing since. With the neutron veto filled, the trigger rate is very low, ∼50 Hz, consistent with the 1 Bq/kg expected from the ^{39}Ar in AAr. Early tests showed good pressure stability of the cooling system. The electron drift lifetime is very long, >5 ms, demonstrating the ability of the cooling/recirculation system to establish and maintain purity of the argon.

We present here preliminary results from 6.3 day of livetime, running in steady conditions with a drift field of 200 V/cm and an extraction field of 2.8 kV/cm. The data
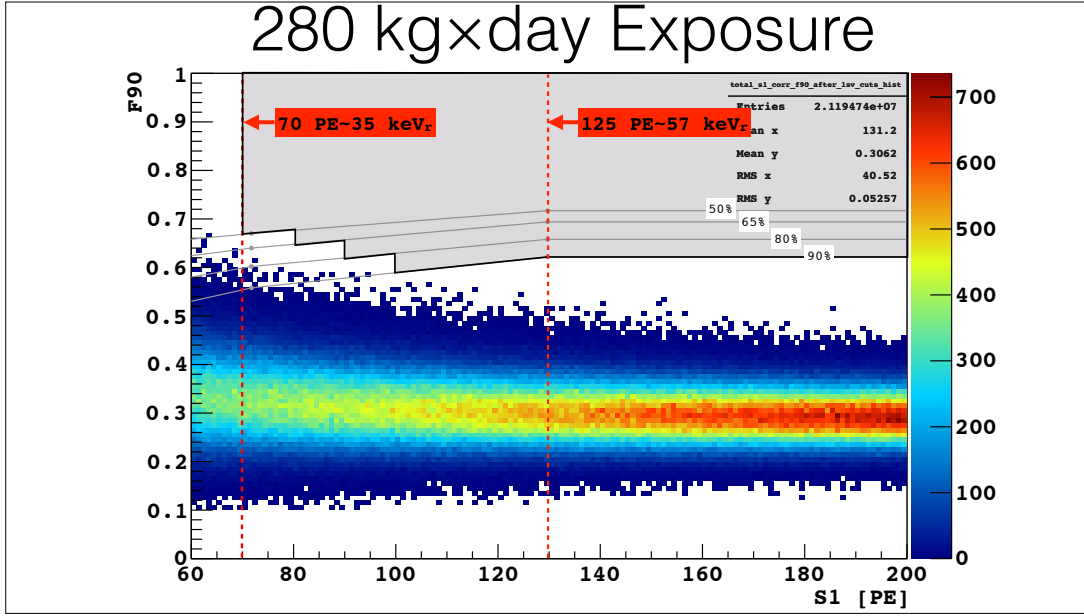
FIG. 2: Results from a run of the three DarkSide-50 detectors with an AAr TPC fill for a 6.3 day livetime, equivalent to >2.6 years of lifetime with UAr in DarkSide-50. We have 2.1×10^7 events above the 55 keV$_r$ DarkSide-G2 threshold, with 3.7×10^6 in the 55–240 keV$_r$ (120–500 PE) dark matter window. The pulse shape discriminant f_{90}, defined as the fraction of primary scintillation pulse observed in its first 90 ns, vs. S1 (total integral of the primary scintillation pulse). The S1 range starts at 60 PE, one half of the conservative, 120 PE or 55 keV$_r$, threshold declared for DarkSide-G2 in this proposal and identified by the red vertical line. The gray, nearly horizontal lines identify the lower boundaries of the nuclear-recoil signal region with the indicated acceptances, as determined using data from the SCENE experiment (see Sec. III and Ref. [2]).

were taken with the Neutron Veto and the Muon Veto full and operational. The TPC trigger required any three PMT's (of the 38 total) to give signals above a threshold of about 0.5 PE in a 100 ns window.

Fig. 1 shows the S1 spectrum recorded in DarkSide-50 in a zero-field run; it is clearly dominated by the ^{39}Ar β decay spectrum. Superimposed on this is a peak at 380 PE due to ^{83m}Kr introduced into the argon recirculation flow as a calibration source. Correcting for the concentration gradient observed for the ^{83m}Kr, we get consistent fits to the light yield of 8.0 ± 0.5 PE/keV$_{ee}$ from both the ^{83m}Kr peak at 41.5 keV and from the ^{39}Ar spectrum. This is well above the 6 PE/keV$_{ee}$ proposed as the DarkSide-50 design goal and the 7.0 PE/keV$_{ee}$ of the DarkSide-10 prototype data used for the most recent sensitivity estimates of DarkSide-50 [1]

6.3 day of running with AAr has as much ^{39}Ar background as 2.6 years of running with UAr. We can thus use this data to measure the expected electromagnetic background in nearly the complete run time of 3 years with UAr. Fig. 2 shows the performance of the main electromagnetic background rejection tool in liquid argon, pulse shape discrimination in the primary scintillation. The pulse shape discriminant f_{90} is defined as the fraction of primary scintillation pulse observed in its first 90 ns. For electron recoils, this is typically about 0.3. For nuclear recoils induced by neutron or WIMP scattering, it is about 0.75. The minimum S1 shown, 60 PE, corresponds to approximately 31 keV$_r$.

Events in Fig. 2 were subjected only to minimal data quality cuts. The ionization signal was used to define a 44 kg out of the 50 kg active mass. We discovered that the

DarkSide-50 Expected Sensitivity
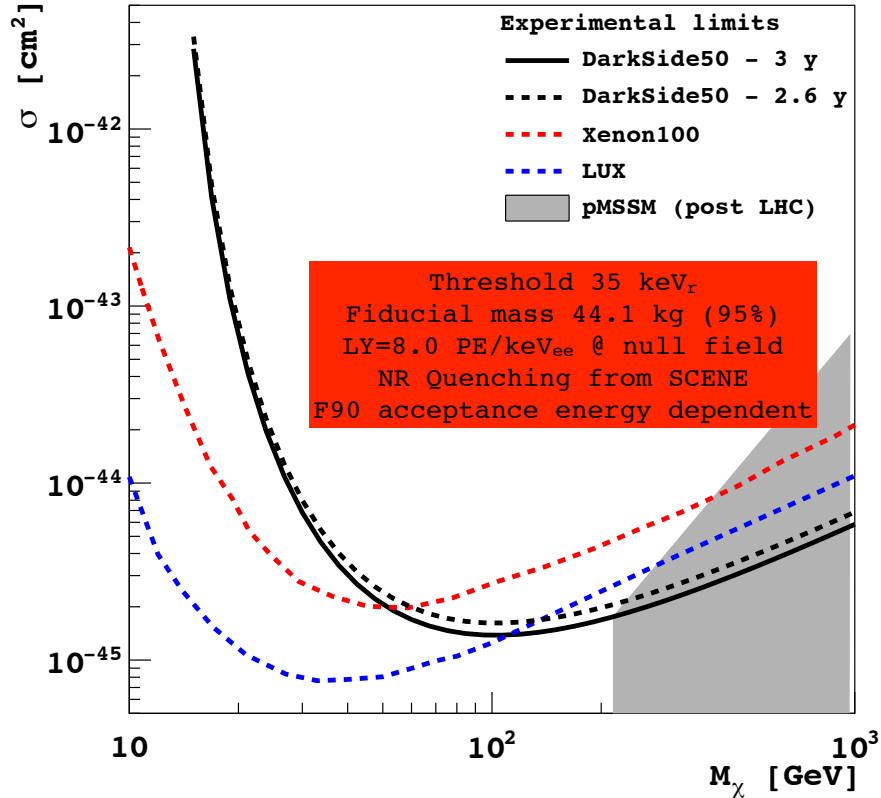
FIG. 3: Projected sensitivity for the DarkSide-50 experiment.

S2/S1 cut and *x-y* reconstruction cut require in-situ calibrations due to S2 disuniformity, and as of today these cuts are not part yet of the standard analysis. In any case, no background is seen in or near the signal region, and we are confident we can reach our PSD performance goals in DarkSide-50.

We use SCENE data and the DarkSide-50 light yield to overlay nuclear recoil acceptance contours of PSD discriminant f_{90} vs. S1 on the DarkSide-50 data. SCENE had a light yield of $4.5\,PE/keV_{ee}$, much lower than that of DarkSide-50, and this difference has a large impact on PSD rejection. This results in a wider spread of the SCENE nuclear recoil band, which is not corrected for, and, in turn, yields conservative values for acceptance contours. Upcoming tests of DarkSide-50 with a neutron source will allow us to redo this study with SCENE calibration of the nuclear-recoil energy scale, but with DarkSide-50-derived parameters for the nuclear recoil response to PSD.

Fig. 3 shows the projected sensitivity for a 3 years run of DarkSide-50.

II. DARKSIDE VETOES COMMISSIONING AND EARLY RUNNING

The Neutron Veto was filled with boron-loaded scintillator during two weeks ending on October 13, 2013. The Muon Veto water fill began October 2 and ended November 15, 2013. Operations with the Neutron Veto began when the water level in the Muon Veto provided sufficient shielding.

The PMTs are operating correctly, with the exception of two PMTs in the neutron veto (out of 110) and four PMTs in the muon veto (out of 80). The muon veto PMTs were recycled from CTF after 15 years of continuous operation; we will probably replace
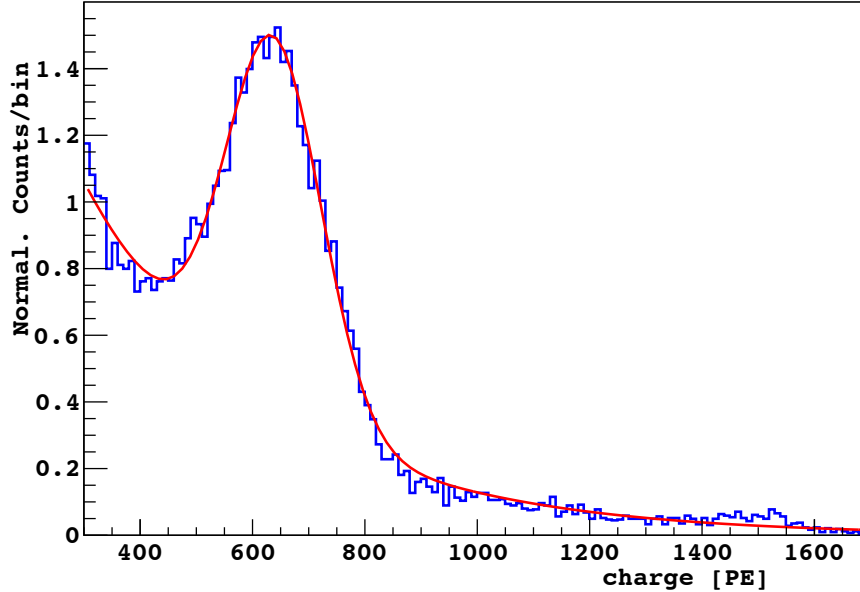
FIG. 4: Blue: portion of the neutron veto spectrum with the combined peak from the 1.17 MeV and 1.33 MeV γ-ray lines from ^{60}Co. **Red:** fit returning a 0.51$\pm$0.07 PE/keV$_{ee}$ light yield.

them for DarkSide-G2. The PMTs in the neutron veto are new: the two failures occurred when the water level reached their submarine cable connectors. The installation and commissioning of the electronics for the Neutron Veto and the Muon Veto, including the HV, the analog front-end modules, the high-speed digitizers, and the data acquisition, are also complete.

With the water shielding in place, the rate of low energy events in the neutron veto was found to be higher than expected, due to unexpectedly high levels of ^{14}C. We have established that the TMB supplier, who had initially provided samples produced from oil-based stock in the US, delivered a batch to LNGS that was produced from biogenic methanol. This higher than expected ^{14}C rate will slightly reduce the anticipated >99.5% efficiency for neutron rejection. This will have to be fixed to reach the design sensitivity of DarkSide-50(see Fig. 3) by replacing the current TMB stock with a suitably low background stock.

The TMB replacement is at this time the greatest operational issue of concern for the collaboration. The local group has been working in collaboration with LNGS staff and management to install the additional equipment required to ensure that this operation can be carried out safely. In the meanwhile, the collaboration has already identified avenues has already identified avenues to remove the present TMB, to obtain and validate TMB with low ^{14}C to LNGS, and to deliver it to LNGS.

We have taken advantage of the ^{60}Co contamination in the stainless steel of the Liquid Scintillator Vessel (LSV) to measure the light yield of the neutron veto. As shown in Fig. 4, a fit of the ^{60}Co spectrum results in an estimate of the light yield of 0.51$\pm$0.07 PE/keV$_{ee}$. This meets the requirement for DarkSide set by the need to measure the low energy α's from neutron capture on ^{10}B.
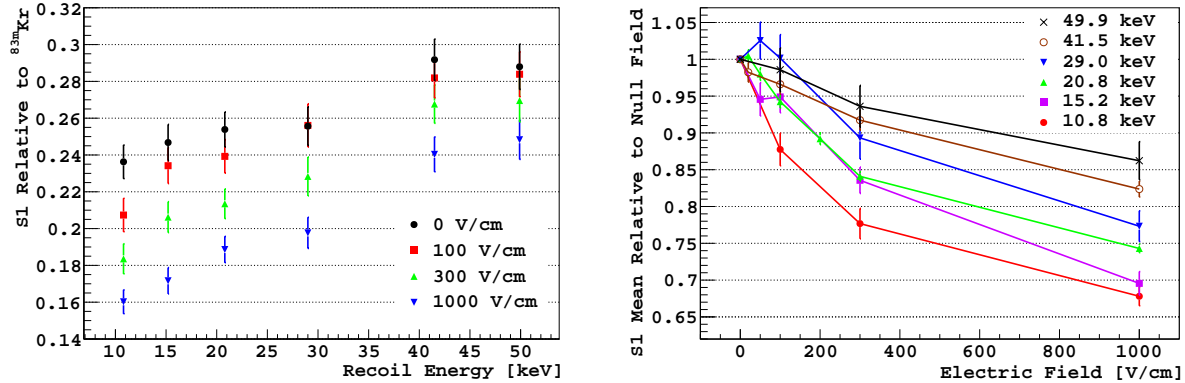
FIG. 5: Results from the SCENE experiment [2]. **Left:** Nuclear recoil light yield, normalized to the light yield at null field of ^{83m}Kr decays (near-coincident conversion electrons summing to 41.5 keV), as a function of drift field and nuclear recoil energy. **Right:** Variation of light yield of nuclear recoils with electric field in LAr. The light yield is normalized to zero field at each recoil energy

III. CALIBRATION OF DARKSIDE-50 WITH SCENE

The SCENE collaboration includes groups from Chicago, Fermilab, LLNL, Naples, Princeton, Temple, UCLA, and UMass, with a large overlap with DarkSide. The collaboration has exposed a two-phase argon TPC to a monochromatic, low energy, pulsed neutron beam at the Notre Dame Institute for Structure and Nuclear Astrophysics to study the scintillation light yield of recoiling nuclei. The neutron beam was produced by the ^{7}Li(p,n)^{7}Be reaction on a lithium fluoride target. The TPC was viewed by two PMT's, one above and one below the LAr. Liquid scintillation counters were arranged to detect and identify coincidences from neutrons scattered in the argon fill of the TPC and thus to select the energy of the recoiling nuclei.

By providing both time-of-flight and pulse-shape discrimination, the SCENE experimental setup enabled the selection of single-scatter nuclear recoils with an excellent signal to background ratio, a large improvement over previous results in the literature. This clean signal has allowed SCENE to perform the first precision measurement of the dependence of the nuclear recoil light yield on applied drift-field in a noble liquid, and to make the first observation of its dependence on electric field. This dependence is as high as 35% at 11 keV$_r$ [2].

The left panel of Fig. 5 shows the energy- and drift-field-dependent light yield of nuclear recoils, normalized to the light yield of ^{83m}Kr decays collected at null field. The right panel of Fig. 5 shows the variation of the nuclear recoils' light yield with drift field, normalized to zero field at each recoil energy. The field-dependent quenching is larger at low recoil energy and becomes significantly smaller for higher energy recoils. In the energy range above 55 keV$_r$, the variation is <25% over the range 0–1.0 kV/cm. This should be compared with a field-dependent quenching of β/γ events of 50% at 1.0 kV/cm. We note also from the figure that the field quenching is quite low at all energies of interest at and below a 0.1 kV/cm drift field.

The SCENE measurement suggests that a lower drift-field is important to retain the best nuclear recoil S1 light yield in a TPC. We are already operating DarkSide-50 at a much lower drift field than our prototype studies, and it is likely that the optimum drift

field for DarkSide-G2 will be in the range 100–200 V/cm.

The SCENE findings have important implications for the DarkSide program. On one hand, operating at lower drift field relaxes the requirements on the high voltage for the TPC. On the other hand, the resulting longer drift times make the requirements on the removal of electronegative contaminants more challenging. At the lowest field we might use, DarkSide-G2 will require an electron drift-lifetime of 5 ms, which we have already achieved in DarkSide-50, as discussed in the next section.

IV.   DARKSIDE-G2 PROPOSAL

The DarkSide collaboration developed a proposal for a second generation dark matter search with a 5.4 tonnes UAr fill and $2\times10^{-47}\,cm^2$ sensitivity. The proposal was submitted to NSF and DOE in November 2013 and to INFN in December 2013. We hereby submit the proposal, as an addendum, to the LNGS Scientific Committee.

[1] T. Alexander et al. (DarkSide Collaboration), Astropart. Phys. **49**, 44 (2013).

[2] T. Alexander et al. (SCENE Collaboration), Phys. Rev. D **88**, 092006 (2013).

GERDA - the search for $0\nu\beta\beta$ decay

M. Agostini [n], M. Allardt [c], E. Andreotti [q], A.M. Bakalyarov [l],
M. Balata [a], I. Barabanov [j], N. Barros [c], L. Baudis [r]C. Bauer [f],
N. Becerici-Schmidt [m], E. Bellotti [g,h], S. Belogurov [k,j], S.T. Belyaev [l],
G. Benato [r], A. Bettini [o,p], L. Bezrukov [j], D. Budjáš [n], A. Caldwell [m],
C. Cattadori [h], A. Chernogorov [k], V. D'Andrea [a], E.V. Demidova [k],
A. Domula [c], V. Egorov [d], R. Falkenstein [q], K. Freund [q], N. Frodyma [b],
A. Gangapshev [j,f], A. Garfagnini [o,p], I. Gooch [m], C. Gotti [g,h],
P. Grabmayr [q], V. Gurentsov [j], K. Gusev [l,d], W. Hampel [f], A. Hegai [q],
M. Heisel [f], S. Hemmer [o,p], G. Heusser [f], W. Hofmann [f], M. Hult [e],
L.V. Inzhechik [j], L. Ioannucci [a], J. Janicskó Csáthy [n], J. Jochum [q],
M. Junker [a], V. Kazalov [j], T. Kihm [f], I.V. Kirpichnikov [k], A. Kirsch [f],
A. Klimenko [f,d], K.T. Knöpfle [f], O. Kochetov [d], V.N. Kornoukhov [k,j],
V.V. Kuzminov [j], M. Laubenstein [a], A. Lazzaro [n], V.I. Lebedev [l],
B. Lehnert [c], H.Y. Liao [m], M. Lindner [f], I. Lippi [p], A. Lubashevskiy [f],
B. Lubsandorzhiev [j], G. Lutter [e], C. Macolino [a], B. Majorovits [m],
W. Maneschg [f], G. Marissens [e], M. Misiaszek [b], I. Nemchenok [d], S. Nisi [a],
D. Palioselitis [m], L. Pandola [a], K. Pelczar [b], G. Pessina [g,h], A. Pullia [i],
M. Reissfelder [f], S. Riboldi [i], N. Rumyantseva [d], C. Sada [o,p],
M. Salathe [f], C. Schmitt [q], B. Schneider [c], J. Schreiner [f], O. Schulz [m],
B. Schwingenheuer [f], S. Schönert [n], H. Seitz [m], E. Shevchik [d],
M. Shirchenko [l,d], H. Simgen [f], A. Smolnikov [f], L. Stanco [p], H. Strecker [f],
C.A. Ur [p], A.A. Vasenko [k], K. von Sturm [o,p], V. Wagner [f], M. Walter [r],
A. Wegmann [f], T. Wester [c], H. Wilsenach [c], M. Wojcik [b], E. Yanovich [j],
P. Zavarise [a], I. Zhitnikov [d], S.V. Zhukov [l], D. Zinatulina [d], K. Zuber [c],
and G. Zuzel [b].

a) INFN Laboratori Nazionali del Gran Sasso, LNGS, Assergi, Italy

b) Institute of Physics, Jagiellonian University, Cracow, Poland

c) Institut für Kern- und Teilchenphysik, Technische Universität Dresden, Dresden, Germany

d) Joint Institute for Nuclear Research, Dubna, Russia

e) Institute for Reference Materials and Measurements, Geel, Belgium

f) Max-Planck-Institut für Kernphysik, Heidelberg, Germany

g) Dipartimento di Fisica, Università Milano Bicocca, Milano, Italy

h) INFN Milano Bicocca, Milano, Italy

i) Dipartimento di Fisica, Università degli Studi di Milano e INFN Milano, Milano, Italy

j) Institute for Nuclear Research of the Russian Academy of Sciences, Moscow, Russia

k) Institute for Theoretical and Experimental Physics, Moscow, Russia

l) National Research Centre "Kurchatov Institute", Moscow, Russia

m) Max-Planck-Institut für Physik, München, Germany

n) Physik Department and Excellence Cluster Universe, Technische Universität München, Germany

o) Dipartimento di Fisica e Astronomia dell'Università di Padova, Padova, Italy

p) INFN Padova, Padova, Italy

q) Physikalisches Institut, Eberhard Karls Universität Tübingen, Tübingen, Germany

r) Physik Institut der Universität Zürich, Zürich, Switzerland

Abstract

The GERmanium Detector Array (GERDA) at the Laboratori Nazionali del Gran Sasso of INFN, Italy searches for neutrinoless double beta ($0\nu\beta\beta$) decay of ^{76}Ge. The GERDA experiment has completed the Phase I in 2013 with a total collected exposure of 21.6 kg·yr. A lower limit on the half-life of the $0\nu\beta\beta$ decay for ^{76}Ge has been estimated: $T^{0\nu}_{1/2} > 2.1 \cdot 10^{25}$ yr at 90% C.L. The major results obtained from GERDA Phase I are here reported, togheter with the activities for the preparation of GERDA Phase II.

1   Introduction

The GERmanium Detector Array, GERDA, searches for neutrinoless double beta decay of ^{76}Ge. The detection principle of GERDA is based on bare high-purity germanium (HPGe) detectors isotopically enriched in ^{76}Ge, immersed in liquid argon (LAr). Neutrinoless double beta decay of atomic nuclei (A, Z) $\rightarrow$ (A, Z+2) + 2e$^-$ is a forbidden process in the Standard Model (SM) of particle physics because it violates lepton number by two units. An observation of such a decay would demonstrate lepton number violation in nature and would prove that neutrinos have a Majorana component.

The aim of GERDA Phase I was to verify the results from previous experiments with a much higher sensitivity. Indeed, an exposure of 21.6 kg·yr and a background index (BI) of the order of BI$\simeq$10^{-2} cts/(keV·kg·yr) have been achieved mainly with the re-processed enriched Heidelberg-Moscow (HdM) and IGEX detectors, having an average energy resolution of 4.8 keV (FWHM) at Q$_{\beta\beta}$. No excess of events from $0\nu\beta\beta$ decay has been detected in the region of interest and a lower limit on the half-life of the decay has been estimated: T$^{0\nu}_{1/2} > 2.1 \cdot 10^{25}$ yr at 90% C.L.

The Phase II of the experiments foresees to add 20 kg of enriched Broad Energy Germanium (BEGe) detectors and to reduce the background contribution by a factor of ten. The goal is to reach the sensitivity on half-life up to 1.4·10^{26} yr, with a background index of 10^{-3} cts/(keV·kg·yr) and after an exposure of 100 kg·yr. Background reduction will be achieved by detecting the liquid argon scintillation as a veto, in combination with pulse-shape discrimination performance showed by the BEGe detectors.

2   The GERDA detector

The GERDA experiment implements germanium diodes enriched to about 86% in ^{76}Ge, placed in strings in a cryostat filled with liquid argon as the cryogenic bath. An artist view of the detector is shown in Fig. 1. The LAr, indeed, acts as both the cooling medium for the semiconductors and as the shield against external background. The internal side of the stainless steel cryostat vessel is covered with a copper lining to reduce gamma radiation from the cryostat walls. The central volume is separated from the rest of the cryostat by a 3 m high and 750 mm diameter cylinder, made of a 30 μm copper foil (called "radon shroud"), with the aim of preventing radon convection close the Ge diodes. The cryostat is surrounded by a large tank (8.5 m high and 10 m of diameter) filled with 590 m^3 of ultra-pure water. The water buffer has various purposes; it is used to: (i) moderate and absorb neutrons, (ii) attenuate the flux of external gamma radiation, (iii) provide the Cherenkov medium for the detection of muons and (iv) provide a backup system for warming up the argon gas in case of emergency. The water tank is instrumented with 66 PMTs, to detect Cherenkov light produced by muons in the water buffer. An array of 36 plastic scintillator panels is placed on the roof of the cleanroom; Cherenkov and scintillation signals are combined (according to a logic OR) as a muon veto for the data acquisition. A clean room and a two-arm lock installed on the top of the GERDA building, to easily insert the detectors into the cryostat. For further details about the GERDA experimental setup see Ref. [1].

The data acquisition of GERDA Phase I started on November, 2011 with nine p-type ^{enr}Ge semi-coaxial (HPGe) detectors, five of them from the previous HdM experiment, one not enriched from the GENIUS-Test-Facility [2] and three from the IGEX experiment, with a total mass of about 20.7 kg (17.7 kg enriched and 3 kg not enriched). On July 2012, other five diodes (Broad Energy Germanium detectors, BEGe [3]), were added, with total mass of about 3.6 kg. These detectors, foreseen for the Phase II of the experiment, were implemented to test them in the

Figure 1: An artist's view of the GERDA detector. The array of Ge detectors is not to scale. (1): the array of germanium detector string; (2): the stainless steel cryostat; (3): the radon shroud; (4): the water tank; (5): the clean room; (6): the insertion lock. Plot from Ref. [1].

GERDA realistic environment. The detectors are placed in individual strings, each of them can contain up to five independent Ge detectors. In the very first phase of GERDA data taking, a very high background was observed ($18 \cdot 10^{-2}$ cts/(keV·kg· yr)) and the line at 1525 keV from ^{42}K, the progeny of ^{42}Ar, shows an intensity much higher than expected [4]. These observations supported the hypothesis that charged ^{42}K ions were drifting in the electric field produced by the 3 to 4 kV bias of the Ge semiconductors. To prevent that, the strings of detectors were enclosed into (60 μm thick) copper cylinders ("mini-shrouds"). Signal read out from the diodes is made by a charge sensitive amplifier located at about 30 cm from the detectors. Signals are digitized by 100 MHz Flash ADCs. Digital filters reconstruct the physical parameters of interest like the energy and the risetime of the event [5].

3 Results

In the following sections the main results obtained from GERDA Phase I are reported. They include the estimation of the $2\nu\beta\beta$ half-life [6], the energy spectrum decomposition [7] and the Pulse Shape Discrimination method for background rejection [8]. In the last section the number of events observed around the Q$_{\beta\beta}$ and the estimation of a limit on the half-life of $0\nu\beta\beta$ for ^{76}Ge are discussed [9].

3.1 Determination of the half-life of $2\nu\beta\beta$ decay in ^{76}Ge

Two-neutrino double beta ($2\nu\beta\beta$) decay of atomic nuclei is a second-order process in which the lepton number is conserved. The estimation of the half-life of this decay is very important because it has been suggested [10, 11] that some constraints on the $0\nu\beta\beta$ nuclear matrix element $\mathcal{M}^{0\nu}$ can be derived from the knowledge of the $2\nu\beta\beta$ nuclear matrix element $\mathcal{M}^{2\nu}$. In addition
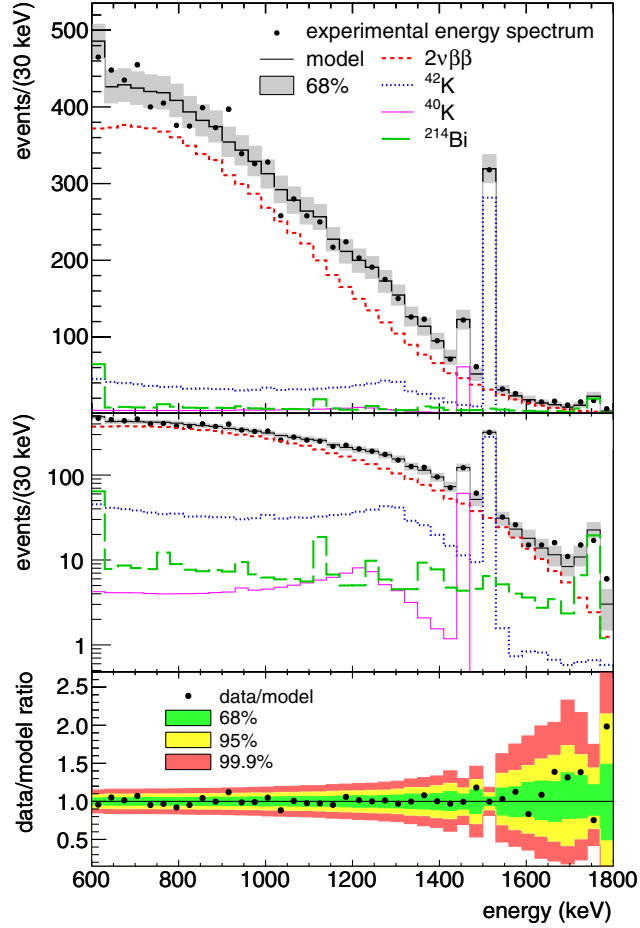
Figure 2: Upper and middle panels: Experimental data (markers) and the best fit model (black histogram) for the sum of the six detectors (linear and logarithmic scale). Individual contributions from the decay (red), ^{42}K (blue), ^{40}K (purple) and ^{214}Bi (green) are shown separately. The shaded band indicates the 68% probability range for the data calculated from the expected event counts of the best fit model. Lower panel: ratio between experimental data and the prediction of the best fit model.

to that, the estimated value of $\mathcal{M}^{2\nu}$ can be directly compared to the predictions based on charge exchange experiments [12, 13] and the comprehension of the nuclear aspects of $2\nu\beta\beta$ decay can be verified. The events considered have been detected by GERDA between 9 November 2011 and 21 March 2012, for a total of 125.9 days and corresponding to an exposure of 5.04 kg yr [6]. The $2\nu\beta\beta$ decay is the dominant contribution in the energy spectrum above the endpoint of the ^{39}Ar decay; the analysis for $2\nu\beta\beta$ decay is performed between 600 and 1800 keV, on a total number of 8796 events. The analysis, based on Bayesian approach via a maximum likelihood fit [14], has been applied on the energy spectra from six enriched coaxial diodes (two detectors exhibited a leakage current of tens of pA), fitting the spectra with a global model (Monte Carlo simulated spectrum), containing the $2\nu\beta\beta$ decay of ^{76}Ge and three independent background contributions, ^{42}K, ^{214}Bi and ^{40}K, whose gamma lines are clearly seen from the observed spectra at 1525 keV for ^{42}K (progeny of ^{42}Ar), 1460 keV for ^{40}K, 1764 keV for ^{214}Bi.

The half-life of the $2\nu\beta\beta$ decay is a common parameter in the fit to the six spectra, while the intensities of the background components are considered for each detector independently. Nuisance parameters, given by the active mass and the ^{76}Ge abundance of each detector, are integrated at the end of the analysis. The considered prior probability density function (PDF) for $T_{1/2}^{2\nu}$ is a flat function between 0 and 10^{22} yr, while the prior PDFs for the active mass fraction and the ^{76}Ge isotopic abundance of each detector are modeled according to a Gaussian distribution. In Fig. 2 the experimental data for the sum of the six detectors is shown together with the best fit model and the individual components obtained from the fit. The expected number of events predicted by the best fit model is 8797.0 divided as following: 7030.1 (79.9%) from the $2\nu\beta\beta$ decay of ^{76}Ge; 1244.6 (14.1%) from ^{42}K; 335.5 (3.8%) from ^{214}Bi and 186.8 (2.1%) from ^{40}K. The average signal to background ratio is 4:1 and the model reproduces very well the experimental data, with a p-value of the fit equal to p=0.77.

The best estimate of the half-life is $T_{1/2}^{2\nu} = (1.84^{+0.09}_{-0.08}(\text{fit})^{+0.11}_{-0.06}(\text{syst}))\cdot 10^{21}$ yr. The systematic uncertainties on $T_{1/2}^{2\nu}$ (evaluated separately from the fit) include uncertainties related to the fit model, uncertainties due to the Monte Carlo simulation details and uncertainties due to the data acquisition and data handling. The combination in quadrature of all these contributions gives a systematic uncertainty of $^{+6.2}_{-3.3}\%$, which corresponds to $^{+0.11}_{-0.06}\times 10^{21}$ yr.

From the estimated half-life one can derive the experimental nuclear matrix element for the $2\nu\beta\beta$ decay of ^{76}Ge. Using the phase space factors from the improved electron wave functions reported in [15], the nuclear matrix element is $\mathcal{M}^{2\nu} = 0.133^{+0.004}_{-0.005}$ MeV^{-1}, 11% smaller than that used in [10]. According to the relation between $\mathcal{M}^{2\nu}$ and $\mathcal{M}^{0\nu}$, described in [10], the new value for $\mathcal{M}^{2\nu}$ corresponds to an increase of about 15% in the predicted half-life for $0\nu\beta\beta$, well within the uncertainty of the model calculation. The nuclear matrix elements for $2\nu\beta\beta$ decay of ^{76}Ge estimated from charge exchange reactions[12, 13] (d,^{2}He) and (^{3}He,t) have larger values but still consistent with the one derived by GERDA.

3.2   Background decomposition of the energy spectrum

The experimental energy spectra measured by GERDA with the enriched and natural detectors are shown in Fig. 4. The green boxes indicate the energy interval $Q_{\beta\beta}\pm 20$ keV where the events were "blinded", *i.e.* they were not processed until the calibration was finalized and all the selection cuts and analyses were fixed. The energy spectra show gamma peaks from ^{40}K and ^{42}K decays and from the decay chains of ^{226}Ra and ^{232}Th. At the lowest energies the spectrum is dominated by the β decay of ^{39}Ar which has an endpoint of 565 keV. In the region between 600 and 1400 keV the contribution to the spectrum from $2\nu\beta\beta$ decay in ^{76}Ge is clearly visible. Above 4000 keV a background contribution from α decay of ^{210}Po and ^{226}Ra decay chain dominates in the spectrum from the semi-coaxial detectors. The energy scale is determined by calibrating the detectors with ^{228}Th sources once per week. The exposure-weighted average energy resolution (FWHM), extrapolated at $Q_{\beta\beta}$, is (4.8±0.2) keV for semi-coaxial detectors and (3.2±0.2) keV for BEGes. The estimated resolution was stable during the entire data acquisition period. Indeed, the differences between the reconstructed peaks of the ^{228}Th spectrum and the ones from the calibration curves are smaller than 0.3 keV.

The energy spectrum from semi-coaxial detectors and BEGe detectors is fitted to a background model in the energy range between 570 and 7500 keV (for further details see Ref. [7]). The data are split into three sets; one containing the BEGe data (labelled "BEGe"), a second one (labelled "Silver" set) for the period of semi-coaxial data with higher background index (at the time when the BEGe detectors were deployed) and the third containing the rest of the data from semi-coaxial detectors (labelled "golden"). Different possible contributions were considered and
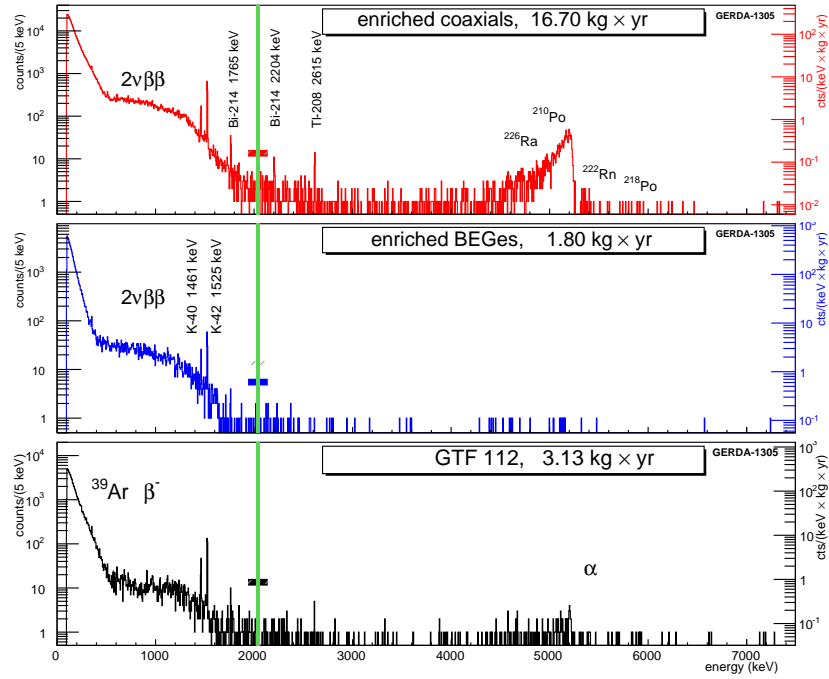
Figure 3: Spectra from enriched semi-coaxial (top), enriched BEGe (middle) and non-enriched (bottom) detectors of GERDA Phase I. The green line indicates the $Q_{\beta\beta} \pm 20$ keV region of blinded data. The bar on the right side of the y-axis indicates the corresponding background index. Plots from Ref. [7].

the background components were simulated to be located into different hardware components of the detector setup. Two global models were considered for the "golden" data set, a "minimum model" fit, were only a minimum amount of background components were considered, and a "maximum model" fit, containing all the possible contributions. In the "minimum model" only background sources located close to the detectors (up to 2 cm), were considered. In the "maximum model" further medium and large distance background components were considered, as well as additional surface background sources. A Bayesian fit of the simulated energy spectrum to the measured one was performed and from the fit the activities of the different background contributions were derived. Both models fit well the experimental spectrum and there is is no unique determination of the count rates of the different background components. However, the dominant background contribution comes from sources located close to the detectors or on the detector surfaces and no peak is expected to appear in a ± 20 keV window around $Q_{\beta\beta}$. The background can be approximated by a constant in the energy window from 1930 to 2190 keV, with the exclusion of the ± 5 keV regions around the position of gamma lines, (single escape peak from ^{208}Tl at 2104 keV and gamma line at 2119 keV from ^{214}Bi). The experimental spectrum and the "minimum model" fit are shown in Fig. 4, together with the background components of the model. The models are in good agreement with the observed spectrum around $Q_{\beta\beta}$. The blinded region was partially unblinded (30 out of the 40 keV) after the background decomposition analysis was finalized. The number of events predicted by the model was 8.6 for the "minimum model" fit and 10.3 for the "maximum" one, while 13 events were observed. The value predicted by the models for the BI is BI=$1.75^{+0.26}_{-0.24} \times 10^{-2}$ cts/(keV·kg·yr) for semi-coaxial detectors and
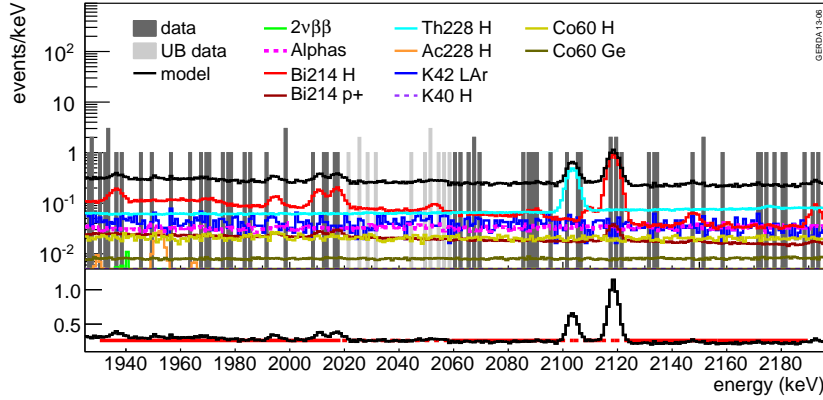
Figure 4: Experimental energy spectrum from semi-coaxial enriched detectors around $Q_{\beta\beta}$ and the background decomposition with different possible contributions. The labels for the location mean "p$^+$" on p$^+$ detector surface, "H" close to the detector, e.g. on the holder, "LAr" homogeneous in the argon, "Ge" inside the Ge detectors. The interval of 20 keV around $Q_{\beta\beta}$ was blinded and not used for the fit. The light grey histogram shows a partially unblinded interval. Plot from Ref. [7].

BI$=3.6^{+1.3}_{-1.0}\times10^{-2}$ for BEGes.

3.3 Pulse Shape Discrimination Analysis

$0\nu\beta\beta$ events exhibit a specific energy deposition and thus the pulse shape observed in the GERDA detectors can be used to discriminate them from background. Indeed, the two electrons from $0\nu\beta\beta$ decay deposit their energy mainly by ionization in a single location (these events are called Single Site Events, SSE). Conversely, the background for GERDA is mainly due to gammas which deposit their energy at different locations in the detector, via multiple Compton scatterings; the gamma can, indeed, travel several centimeters (these events are called Multi Site Events, MSE). The discrimination of $0\nu\beta\beta$ events, based on the shape of the recorded pulses, is called Pulse Shape Discrimination (PSD). In GERDA Phase I two different methods for PSD were used, according to the different characteristics of the pulses and of the electric field distribution in semi-coaxial and BEGe detectors [8].

For what concerns the BEGe detectors, the ratio between the maximum A of the current pulse (obtained by numerical differentiation of the charge pulse) and the energy E of the event (corresponding to the maximum of the charge pulse) is the discrimination parameter for Single Site Events with respect to Multi Site Events. This is due to the specific electric field profile and to the fact that in BEGes only holes contribute to the signal; thus holes migrate towards the p$^+$ electrode with very similar paths, independently from where the energy deposition occurred. As a consequence, for a localized deposition, the maximum of the current pulse and the energy are proportional. In Fig. 5, different examples of pulse traces and the derived current pulses are shown. SSE data (top left) are expected to have a nearly Gaussian distribution of A/E; the mean of the A/E values is set to one for the distribution of SSE data. MSE events (top right) have time-separated pulses; in this case the value of A/E is below 1. In general, for surface events near the p$^+$ electrode, A/E is larger than 1 because both electrons and holes contribute;

87
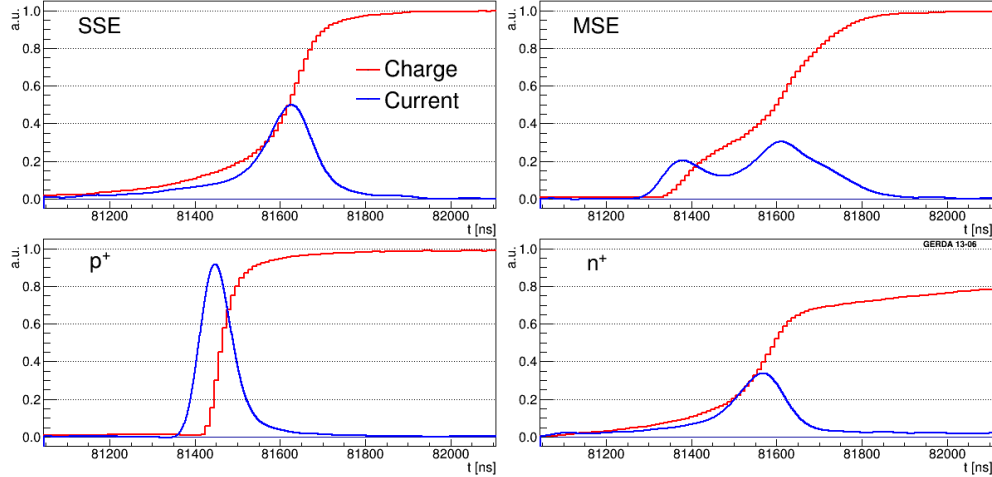
Figure 5: Pulse traces from the BEGe detectors. The maximum of the charge pulse amplitude is set to 1 and current pulses have equal integrals.

while for n^+ surface events A/E is less than unity, since the current reaches its maximum at the end of the pulse, due to the slow process of charge diffusion from the dead layer to the active volume. The A/E based method has been tested with calibration data, considering the double escape peak (DEP) at 1592.5 keV of the 2614.5 keV line, appearing in the ^{228}Th spectrum (from the ^{208}Tl decay), as a proxy for SSE. The single escape peak (SEP) at 2103.5 keV or full energy peaks (FEP) (like e.g. at 1620.7 keV) represent are considering as representing MSE data. Accepted events have A/E between 0.965 (low A/E cut) and 1.07 (high A/E cut). Events below the low A/E cut are identified as MSE and n^+ events, while events above the high A/E cut are discriminated as p^+ electrode events.

In Fig. 6 the energy spectrum of BEGe data is shown before and after the PSD cut. Seven out of 40 events survive the cut in the 400 keV region around $Q_{\beta\beta}$ (excluding the 8 keV blinded window) and the observed BI is reduced from 0.042±0.007 to $0.007^{+0.004}_{-0.002}$ cts/(keV·kg·yr). The acceptance efficiency for signal-like events (i.e. the survival fraction of $0\nu\beta\beta$ events) is 0.92±0.02 and it is derived from the survival fraction of DEP events and from Monte Carlo simulations of the $0\nu\beta\beta$ signal. This value has also been cross-checked with $2\nu\beta\beta$ events. The fraction of rejected events from background, at $Q_{\beta\beta}$, is about 80%. The method shows a very good performance, with both high background reduction and high acceptance efficiency.

The current pulses in semi-coaxial detectors have different shapes, due to the contribution of both electrons and holes to the pulse. For this reason the A/E parameter does not represent a useful variable for pulse shape discrimination for semi-coaxial detectors. Instead, a method based on the artificial neural network for the rising part of the charge pulses was applied. The method is based on the TMlpANN[16] algorithm (implemented in the TMVA[17] toolkit of ROOT) based on multilayer perceptrons and on the so called "supervised learning" algorithm. Two hidden layers with 50 and 51 neurons were used. The times $t_1\, t_2\, , \cdots, t_n$, at which the 1,3,5,...,99% of the full height of the pulse is reached, were used as input parameters. Being the sampling frequency in GERDA 100 MHz, two consecutive time bins were interpolated.

Calibration data were used for the network's training; data at the DEP peak were considered as SSE and those at the full line of ^{212}Bi (1621 keV) were considered as MSE. The cut value on the ANN response was set to yield 90% efficiency (survival fraction) on DEP events from the
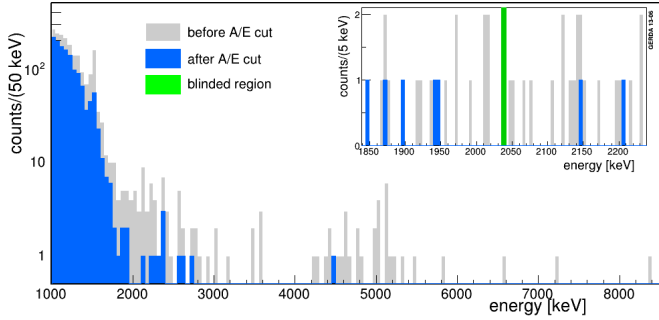
Figure 6: Energy spectrum for the *BEGe* data set before (grey) and after (blue) the PSD cut. A zoom in the ±100 keV window around Q$_{\beta\beta}$ is shown in the inset.
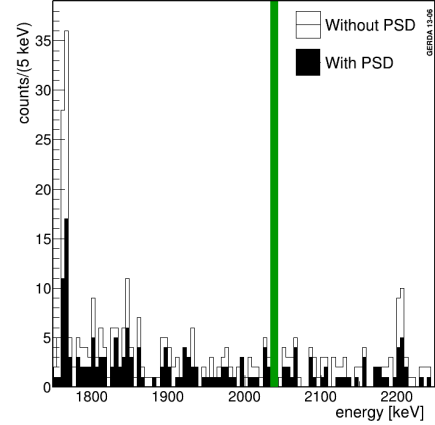

Figure 7: Energy spectrum from semi-coaxial detectors before (open) and after (filled) the PSD selection with TMlpANN.

gamma line of ^{208}Tl decays at 2.6 MeV. The output of the neural network is a number between ~0 (corresponding to background like events) and ~1 (for signal like events).Considering the possible influence of an energy dependence or of a volume effect, associated to different contributions from DEP and $0\nu\beta\beta$ events, the final value for the $0\nu\beta\beta$ efficiency is $0.90^{+0.05}_{-0.09}$, where the error contributions are quadratically summed. The systematic uncertainties have been addressed by the cross-check of the efficiency with $2\nu\beta\beta$ events and events at the Compton edge of the 2614.5 keV gamma line. The method rejects about 45% of the events in the 230 keV window around Q$_{\beta\beta}$. The energy spectrum before and after the PSD cut is shown in Fig. 7. Other two methods were considered to cross check the results from neural network analysis, the first based on a likelihood method and the second on the correlation between the A/E parameter and the pulse asymmetry. In the 230 keV window around Q$_{\beta\beta}$, about 90% of the events rejected by the neural network method were also rejected by the two other analyses.

3.4   Limit on the half-life of the $0\nu\beta\beta$ decay in ^{76}Ge

With a total collected exposure of GERDA Phase I, corresponding to 21.6 kg·yr, a limit on the half-life of $0\nu\beta\beta$ decay in ^{76}Ge was derived (see refs. [9] and [18]). After the analysis cuts and methods were fixed, the region around Q$_{\beta\beta}$±5 keV was unblinded. In this energy region seven events are observed while 5.1±0.5 are expected from background counts. The PSD cut rejects three of the six events from the semi-coaxial detectors and the one from the BEGe detector. The BI after Pulse Shape Discrimation on "golden" data is $0.01\cdot10^{-2}$ cts/(keV·kg·yr).

To derive the signal strength $N^{0\nu}$ and a frequentist coverage interval, a profile likelihood fit of the three data sets is performed. The fitted function consists of a constant term for the background and a Gaussian peak for the signal with mean at Q$_{\beta\beta}$ and standard deviation σ_E. The fit has four free parameters: the backgrounds of the three data sets and $1/T^{0\nu}_{1/2}$, which relates to the peak integral. The likelihood ratio is only evaluated for the physically allowed region $T^{0\nu}_{1/2} \geq 0$ and after Pulse Shape Discrimination is applied to the data. The systematic uncertainties due to the detector parameters, selection efficiency, energy resolution and energy scale are folded
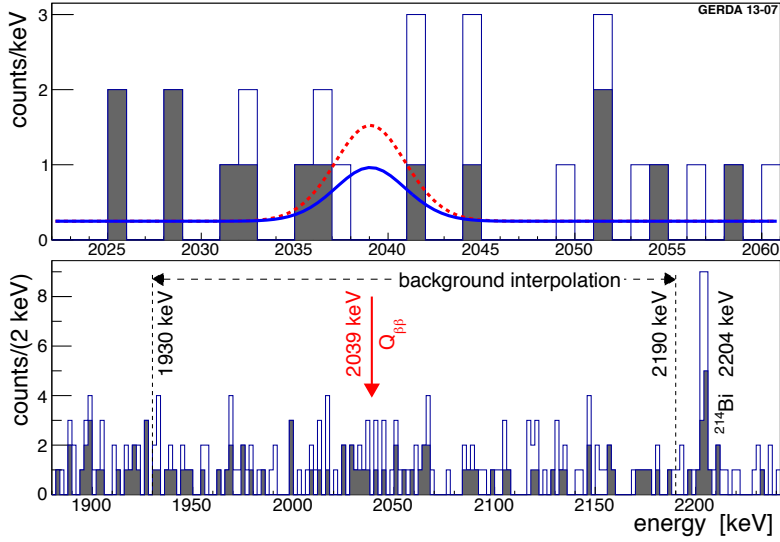
Figure 8: Energy spectrum from all ^{enr}Ge detectors with (filled) and without (open) the PSD selection. In the upper panel the expectation based on the central value of the half-life predicted by ref. [19] is also shown (red), together with the 90% C.L. limit predicted by GERDA Phase I (blue). In the lower panel the energy window used for the backgrund interpolation is indicated. Plot from ref. [9].

in with a Monte Carlo approach which takes correlations into account. The best fit value is $N^{0\nu}$=0, namely no excess of signal events above the background. The limit on the half-life is

$$T_{1/2}^{0\nu} > 2.1 \cdot 10^{25} \text{ yr (90\% C.L.),}$$

including the systematic uncertainty.

The limit on the half-life corresponds to $N^{0\nu}$ <3.5 counts, displayed as solid blue curve in Fig. 8. Given the background levels and the efficiencies, the median sensitivity for the 90 % C.L. limit is $2.4 \cdot 10^{25}$ yr. In Fig. 8 the spectrum before and after PSD is shown, together with the likelihood fit and the expectation based on the claim from Ref. [19]. Taking $T_{1/2}^{0\nu}$ from Ref. [19] at its face value, 5.9±1.4 decays are expected in $\Delta E = \pm 2\sigma_E$ and 2.0 ± 0.3 background events after the PSD cuts (red dotted curve in Fig. 8). This can be compared with three events detected after PSD cuts, none of them within $Q_{\beta\beta} \pm \sigma_E$. The model ($H_1$), which includes the $0\nu\beta\beta$ signal calculated above, gives in fact a worse fit to the data than the background-only model (H_0): the Bayes factor, namely the ratio of the probabilities of the two models, is $P(H_1)/P(H_0)$ =0.024. Assuming the model H_1, the probability to obtain $N^{0\nu}$ =0 as the best fit from the profile likelihood analysis is $P(N^{0\nu} = 0|H_1)$=0.01. The GERDA result is consistent, though stronger, with the limits by the previous HdM [21] and IGEX [22] experiments. The profile likelihood fit is extended to include the energy spectra from HdM and IGEX. Constant backgrounds for each of the five data sets and Gaussian peaks for the signal with common $1/T_{1/2}^{0\nu}$ are assumed. Experimental parameters (exposure, energy resolution, efficiency factors) are obtained from the original references or, when not available, extrapolated from the values used in GERDA. The best fit yields $N^{0\nu} = 0$ and a limit of

$$T_{1/2}^{0\nu} > 3.0 \cdot 10^{25} \text{ yr (90\% C.L.).}$$
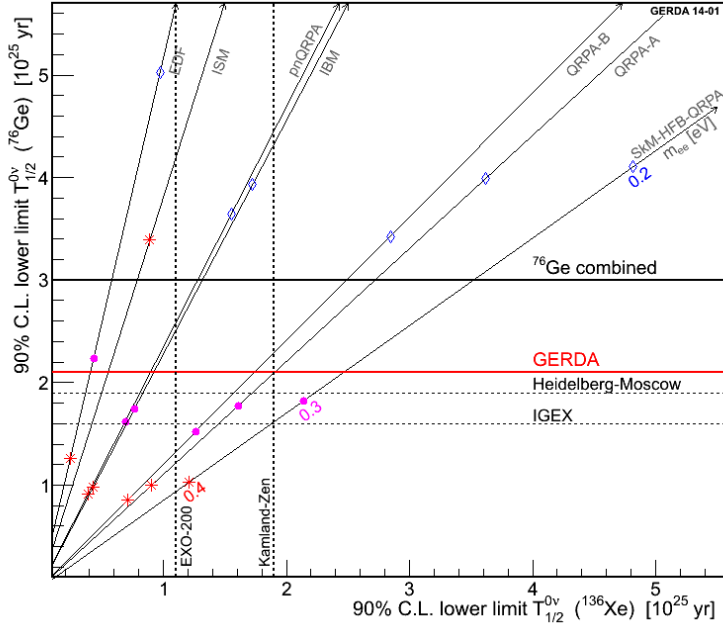
Figure 9: Comparison of recent 90% C.L. limits on $T_{1/2}^{0\nu}$ for ^{76}Ge and ^{136}Xe and correlations of the two half-lives for different matrix element calculations (assuming light neutrino exchange). No axial vector quenching is assumed, i.e. $g_A = 1.25$. Corresponding values of the effective neutrino mass 0.2 eV (diamonds), 0.3 eV (dots) and 0.4 eV (stars) are marked on all axes. Plot from ref. [20].

The Bayes factor is $P(H_1)/P(H_0) = 2 \cdot 10^{-4}$; the claim is hence strongly disfavored. Results from ^{76}Ge experiments are also compared to the recent 90% C.L. limits from KamLAND-Zen [23] and EXO-200 [24] on ^{136}Xe half-life, by rescaling the value of the half-life by the square of the ratio between the nuclear matrix elements $\mathcal{M}_{0\nu}(^{76}\text{Ge})/\mathcal{M}_{0\nu}(^{136}\text{Xe})$. Fig. 9 In Fig. 9 the limits on $T_{1/2}^{0\nu}$ for ^{76}Ge and ^{136}Xe by the different experiments and by combining Ge results, are shown, togheter with a selection of different nuclear matrix element calculations for the case of light neutrino exchange.

Considering the most recent value for the ^{76}Ge phase-space factor [15] and the NME calculations reported in refs. from [25] to [31] (scaling the different g_A and R_A parameters according to ref. [33]), the upper limit on the half-life estimated from GERDA corresponds to upper limits on the effective electron neutrino mass between 0.2 and 0.4 eV.

4   Phase II preparation

The preparation of GERDA Phase II has been ongoing in parallel to the Phase I activities during 2013. The main goal of GERDA in its second phase is to get a larger exposure and a background level reduced of one order of magnitude with respect to Phase I. This will be achieved mainly by increase the total mass of the enriched material and by detecting the liquid argon scintillation light as a veto signal, in combination with the powerful pulse shape discrimination performance of the novel BEGe detectors.
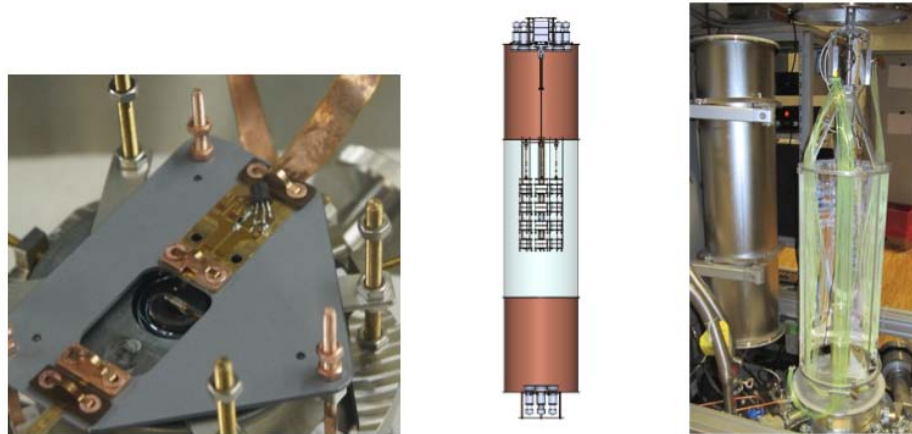
Figure 10: *left*: BEGe detector contacted by bonding to prototype front end electronics on a silicon holder board. *center*: Schematic sketch of detector string surrounded by the PMT LAr instrumentation setup. *right*: Picture of a SiPM fiber test setup.

In the second phase of GERDA 30 BEGe detectors and the 8 Phase I semi-coaxial detectors will be implemented in 7 strings. The Phase II detectors will be mounted back-to-back in strings through a single-arm lock system, which has been already constructed. This consists of a single holder system made of low background copper and silicon plates. Enriched germanium procurement and BEGe detectors production has been made under the organization of the GERDA collaboration. The germanium was enriched in the Electrochemical Plant Zelenogorsk (Russia) and zone-refined by PPM Pure Metals GmbH Langelsheim (Germany). The crystals where pulled at Canberra Oak Ridge (USA) and the production of the diodes was made at Canberra Olen (Belgium). All the 30 novel BEGe detectors have been characterized by GERDA collaborators in the HADES underground facility of SCK·CEN in Mol, Belgium [34] with calibration measurements. During the production chain and during transportation exposure to cosmic rays was minimized to few days per detector. All the detectors have been stored in the LNGS underground laboratory. The total mass of the 30 novel BEGe detectors is 20 kg, corresponding to 53.4% of the total mass of Ge detectors available (37 kg). Low background aluminum (Al) has been evaporated for detector contacting on p^+ and n^+ surfaces. Signal and HV contacts will be made by bonding Al wires between the evaporated spots on the detector and cuflon cables. The latter are fixed to a Si support plate with CuSn6 clamps. A new preamplifier, called CC3, has been produced, having the JFET and the feedback resistor placed in the very vicinity of the detectors. The new setup has already been tested and shows an energy resolution of 2.7 keV at 2.6 MeV.

LAr scintillation light is generated in liquid argon (at 128 nm wavelenght) by radioactive background decays or cosmic muons; the decays can occur either in liquid argon or in the detectors, with the emission of gamma particles which eventually excite the argon. The LAr veto of GERDA is based on a hybrid design, made of a cylindrical shroud which is composed of three parts, being the uppermost and lowermost made of copper, while the central one lines with wavelenght shifting fibers readout by SiPMs. The copper surfaces are also lined with a wavelenght shifter (Tetra Phenyl Butadiene) and a VM2000 reflector foil. The light produced in this volume is shifted in the coated copper surfaces and in the fiber surface and then guided towards PMTs located at the top and bottom, or guided in the fiber towards the SiPMs. In Fig. 10 a schematic
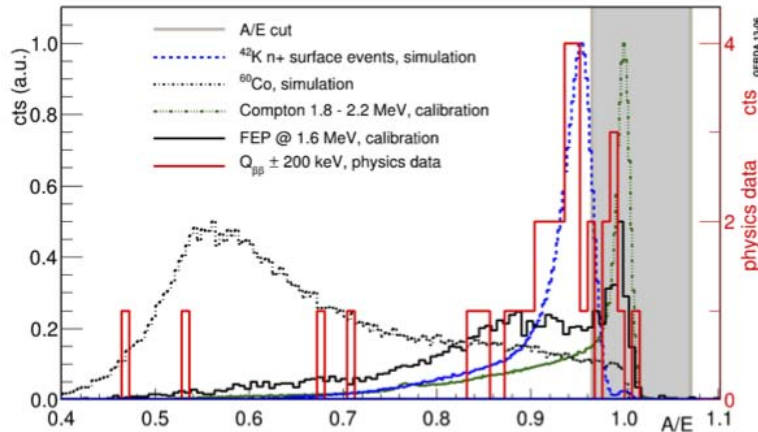
Figure 11: PSD qualifier (A/E) histogram of experimental data from BEGe detectors within 200 keV around $Q_{\beta\beta}$. Result from data is compared to Compton continuum events (green dot-dot dashed), 1621 FEP events (black) from calibration data, simulations of ^{42}K decays at the n$^+$ electrode surface (blue dashed) and ^{60}Co decay (black dot-dashed). The accepted interval is show in grey. Plot from ref. [8].

view of the Phase II hybrid design is shown. The capability to reduce the background by the LAr veto was already demonstrated in the GERDA R&D facility LArGe, where the suppression factors for internal sources of ^{228}Th and ^{214}Bi in around the $Q_{\beta\beta}$ were up to 1180 and 4.6, respectively [35]. Simulations of the new setup for GERDA Phase II (including the LAr veto) have shown that high suppression factors can be reached for most of background events external to the detector assembly. The suppression factors for different backround sources are reported in Table 1. One of the challenges for GERDA Phase II are the background signals created by ^{42}K β decays ($T_{1/2}$=12.3 h, Q-value=3.525 MeV) on the detectors surfaces. In Phase I the individual detector strings were enclosed into copper cylinders, minimizing the drift of ^{42}K ions on the detector surfaces. In Phase II, since the LAr scintillation light near the detectors has to be detected, a transparent TPB coated shroud will be used instead of the copper one. Measurements in the LArGe facility show that the nylon shroud suppresses ^{42}K by a factor of 17 with respect to the case where no shroud is considered. Simulated suppression factors in GERDA Phase II, obtained from the combination of LAr veto togheter with the implementation of copper shrouds, nylon shrouds or no shrouds respectively, are shown in Table 1. In addition, residual background contamination will be rejected by the Pulse Shape Discrimination, as described in ref. [8]. Indeed, it has been already shown from GERDA Phase I data that ^{42}K contamination is well rejected by the cut based on the PSD qualifier (A/E value) for BEGes. This is shown in Fig. 11, where physics data within 200 keV of $Q_{\beta\beta}$ are compared to simulations of ^{42}K decays at the n$^+$ electrode surface. An even better rejection of such contamination is still possible, tuning the best value for both ^{42}K rejection and selection efficiency for single site events. The estimation of the expected background index for GERDA Phase II, based on suppression factor measurements from LArGe and MC simulations, is of the order of 10^{-3} cts/(keV·kg·yr) when the combination of LAr veto and Pulse Shape Discrimination is used; the major background suppression is obtained by the Pulse Shape Discrimation method.

The commissioning of the Phase II upgrade is currently ongoing and the starting of data taking

Table 1: Simulated suppression factors of the LAr instrumentation setup with a copper mini shroud as used in Phase I, a TPB coated transparent mini shroud and without any mini shroud.

Background component	Suppression Factor		
	copper shroud	nylon shroud	no mini shroud
^{214}Bi on holders	2.4±0.1	9.9±0.4	9.1±0.2
^{214}Bi on surface	1.80±0.01	3.4±0.2	3.5±0.1
^{214}Bi homogeneous in LAr	5.3±0.3	38.2±2.7	54.8±7.9
^{42}K homogeneous in LAr	1.2±0.1	9.6±4.2	5.3±0.6
^{42}K on surface	1.06±0.01		
^{218}Th on holders			320±34

is foreseen in 2014.

5 Conclusions

The GERDA experiment has completed the Phase I during 2013 with a total collected exposure of 21.6 kg·yr and a background level of BI≃10^{-2} cts/(keV·kg·yr) after Pulse Shape Discrimination. A limit on the half-life of $0\nu\beta\beta$ decay of ^{76}Ge was derived: $T_{1/2}^{0\nu} > 2.1 \cdot 10^{25}$yr, corresponding to an upper limit on the effective neutrino mass between 0.2 and 0.4 eV.

The background level in GERDA Phase II will be a factor about ten times lower than in Phase I, *i.e.* BI≃10^{-3} cts/(keV·kg·yr). Thanks to the increased mass of enriched germanium an exposure of 100 kg·yr will be reached in about 3 years. The corresponding sensitivity on the half-life of $0\nu\beta\beta$ decay is about $T_{1/2}^{0\nu} \simeq 1.4 \cdot 10^{26}$ yr.

6 List of Publications

1. *The GERDA experiment for the search of $0\nu\beta\beta$ decay in ^{76}Ge.*
   The GERDA collaboration, K.-H. Ackermann *et al.*.
   Eur. Phys. J. **C73** (2013) 2330.

2. *HEROICA: an underground facility for the fast screening of germanium detectors.*
   E. Andreotti, A. Garfagnini, W. Maneschg, N. Barros, G. Benato, R. Brugnera, F. Costa, R. Falkenstein, K.K. Guthikonda, A. Hegai, S. Hemmer, M. Hult, K. Jaenner, T. Kihm, B. Lehnert, H. Liao, A. Lubashevskiy, G. Lutter, G. Marissens, L. Modenese, L. Pandola, M. Reissfelder, C. Sada, M. Salathe, C. Schmitt, O. Schulz, B. Schwingenheuer, M. Turcato, C. Ur, K. von Sturm, V. Wagner, and J. Westermann.
   J. of Instrumentation **8** (2013) P06012.

3. *High voltage capacitors for low background experiments.*
   C. O'Shaughnessy, E. Andreotti, D. Budjas, A. Caldwell, A. Gangapshev, K. Gusev, M. Hult, A. Lubashevskiy, B. Majorovits, S. Schönert, and A. Smolnikov.
   Eur. Phys. J. **C73** (2013) 2445.

4. *Isotopically modified Ge detectors for* GERDA: *from production to operation.*
   D. Budjas, M. Agostini, L. Baudis, E. Bellotti, L. Bezrukov, R. Brugnera, C. Cattadori, A. di Vacri, R. Falkenstein, A. Garfagnini, S. Georgi, P. Grabmayr, A. Hegai, S. Hemmer, M. Hult, J. Janicsko Csathy, V. Kornoukhov, B. Lehnert, A. Lubashevskiy, S. Nisi, G. Pivato, S. Schönert, M. Tarka, and K. von Sturm.
   J. of Instrumentation **8** (2013) P104018.

5. *Measurement of the half-life of the two-neutrino double β decay of Ge-76 with the* GERDA *experiment.*
   The GERDA collaboration, M. Agostini *et al.*.
   J. Phys. G: Nucl. Part. Phys. **40** (2013) 035110.

6. *Status and prospects of searches for neutrinoless double beta decay.*
   B. Schwingenheuer.
   Ann. Phys. (Berlin) **525** (2013) 269.

7. *Status of the* GERDA *Experiment at the Laboratori Nazionali del Gran Sasso.*
   R. Brugnera and A. Garfagnini.
   Adv. High Energy Phys. **2013** (2013) 506186.

8. *Results on neutrinoless double beta decay from* GERDA *Phase I.*
   C. Macolino on behalf of the GERDA collaboration.
   Mod. Phys. Lett. A 29 (2014) 1430001.

9. *The background in the neutrinoless double beta decay experiment* GERDA.
   The GERDA collaboration, M. Agostini *et al.*.
   Accepted by Eur. Phys. J. C (2013) in press.

10. *Pulse shape discrimination for* GERDA *Phase I data.*
    The GERDA collaboration, M. Agostini *et al.*.
    Eur. Phys. J. C **73** (2013) 2583.

11. *Results on neutrinoless double beta decay of* ^{76}Ge *from* GERDA *Phase I .*
    The GERDA collaboration, M. Agostini *et al.*.
    Phys. Rev. Lett. **111** (2013) 122503.

References

[1] The GERDA collaboration, *Eur. Phys. J. C* **73**, 2330 (2013).

[2] H.V. Klapdor-Kleingrothaus et al., *Nucl. Instr. Methods A* **481**, 149 (2002).

[3] D. Budjáš et al., *J. Instrum.* **8**, P04018 (2013).

[4] V.D. Ashitkov et al., *Instr. and Exp. Techn.* **46**, 153 (2003).

[5] M. Agostini et al., *J. Instrum.* **6**, P08013 (2011).

[6] The GERDA collaboration, *J. Phys. G: Nucl. Part. Phys.* **40**, 035110 (2013).

[7] The GERDA collaboration, *submitted to Eur. Phys. J. C*, arXiv:1306.5084.

[8] The GERDA collaboration, *Eur. Phys. J. C* **73**, 2583 (2013).

[9] The GERDA collaboration, *Phys. Rev. Lett.* **111**, 122503 (2013).

[10] V. A. Rodin, A. Fässler, F. Šimkovic and P. Vogel, *Nucl. Phys. A* **766**, 107 (2006).

[11] F. Simkovic, R. Hodak, A. Fässler and P. Vogel, *Phys. Rev. C* **83**, 015502 (2011).

[12] E.-W. Grewe et al., *Phys.Rev.C* **78**, 044301 (2008).

[13] J. H. Ties et al., *Phys. Rev. C* **86**, 014304 (2012).

[14] A. Caldwell and K. Kröninger, *Phys.Rev. D* **74**, 092003 (2006).

[15] J. Kotila and F. Iachello, *Phys. Rev. C* **85**, 034316 (2012).

[16] for documentation see http://root.cern.ch/root/html/TMultiLayerPerceptron.html

[17] for documentation see http://tmva.sourceforge.net

[18] C. Macolino on behalf of the GERDA collaboration, *Mod. Phys. Lett. A* **29**, 1430001 (2014).

[19] H.V. Klapdor-Kleingrothaus et al., *Phys. Lett. B* **586**, 198 (2004).

[20] B. Schwingenheuer, *To appear in the Proceedings of the TAUP 2013 Conference*, Asilomar 2013.

[21] H.V. Klapdor-Kleingrothaus et al., *Eur. Phys. J. A* **12**, 147 (2001).

[22] C.E. Alseth et al., *Phys. Rev. D* **65**, 092007 (2002).

[23] A. Gando et al., *Phys. Rev. Lett.* **110**, 062502 (2013).

[24] J.B. Albert et al., arXiv:1402.6956v1.

[25] T. R. Rodriguez and G. Martinez-Pinedo, *Phys. Rev. Lett.* **105**, 252503 (2010).

[26] J. Menendez et al., *Nucl. Phys. A* **818**, 139 (2009).

[27] J. Barea, J. Kotila, and F. Iachello, *Phys. Rev. C* **87**, 014315 (2013).

[28] J. Suhonen and O. Civitarese, *Nucl. Phys. A* **847**, 207 (2010).

[29] A. Meroni, S. T. Petcov, and F. Simkovic, *JHEP* **1302**, 25 (2013).

[30] F. Simkovic, V. Rodin, A. Faessler, and P. Vogel, *Phys. Rev. C* **87**, 045501 (2013).

[31] M. T. Mustonen and J. Engel, *Phys. Rev. C* **87**, 064302 (2013).

[32] P.S. Bhupal Dev et al., *Phys. Rev. D* **88** 091301 (2013).

[33] A. Smolnikov and P. Grabmayr, *Phys. Rev. C* **81**, 028502 (2010).

[34] E. Andreotti et al., *J. Instrum.* **8**, P06012 (2013).

[35] M. Heisel, PhD thesis, U. Heidelberg, April 2011.

GINGER/G-GranSasso-RD - Annual Report 2013

J. Belfi[1], N. Beverini[2], F. Bosi[1], B. Bouhadef[1], M. Calamai[2], G. Carelli[2], G. Cella[1], D. Cuccato[3] , A. Di Virgilio[1], E. Maccioni[2], A. Ortolan[4], A. Porzio[5], M.L. Ruggiero[6], S. Solimeno[5], R. Santagata[7], F. Sorrentino[8], and A. Tartaglia[6]

[1]*INFN Sezione di Pisa, Pisa Italy,* [2] *Department of Physics, University of Pisa,* [3] *DEI, University of Padua,* [4] *INFN, Legnaro National Laboratory,* [5] *CNISM and INFN-Naples,* [6] *Polythecnic of Turin,* [7] *Department of Physic, University of Siena,* [8] *Department of Physics, University of Florence*

GINGER (Gyroscopes IN GEneral Relativity) is an INFN proposal to measure the gravito-magnetic (Lense-Thirring) effect of the rotating Earth by means of an array of ring lasers. An underground location is essential for this challenging experiment, and LNGS may be a suitable location. G-GranSasso-RD is the experiment financed by the INFN Commission II, which is aiming at the planning, installation and operation of GINGER. Moreover, the GINGER project is carried out in collaboration with a group in Germany (TUM, U. Schreiber) and in NewZealand (U.C., J.P. Wells). The Italian group has developed two ring laser prototypes: GP2 and G-Pisa. GP2 is the new prototype [1] installed in S. Piero a Grado, and expressly designed to study the control of the geometry of the ring. G-Pisa is our first prototype, a square ring with side length of 1.35m. It is a transportable device, which so far has been installed in different locations, with different orientation (horizontal, vertical, and aligned with the North Pole direction in order to maximize the Sagnac frequency). Before it was moved to LNGS, it has taken data in different experimental sites: the INFN-Pisa section, the central area of Virgo (during its last scientific run), and the CMS clean room of S. Piero a Grado. Last spring, the prototype G-Pisa was installed at LNGS inside hall B with horizontal orientation, and the data taking lasted for several weeks. At the end of May it was disassembled since it interfered with the installation of Xenon1T. This first test showed several advantages of an underground location, as a good thermal stability. Some auxiliary instruments have been installed in the same experimental set-up, in particular two seismometers and a nano-tiltmeter. The seismometer data showed that the site is close to the Low Noise Model (LNM) of the Earth, but further investigations are required to characterize the lower part of the spectrum (frequencies below 1 mHz). Following this first experiment, a suitable location inside the LNGS has been selected, and an improved experimental set-up has been defined for the new installation that we named GINGERino. The improved GINGERino experiment will consist of a 3.6 m side length square ring laser, in this way the sensitivity will be increased by a factor of 7, and all the laser systematic effects (backscat-

tering and frequency pulling) will be highly depressed. The new installation of GINGERino is expected to start in spring 2014, and at the time of summer 2014 the experiment should be in data taking.

1. INTRODUCTION

One of the pillars of contemporary understanding of matter, energy and space-time is general relativity (GR). Its successes in explaining the behaviour of the world around us and of the whole universe are well known, as well as its so far unresolved conflicts with quantum mechanics in the high energy domain. It is however true that also in the very low energy sector of the gravitational interaction there are predictions of GR which have not been fully explored up to nowadays. A typical example is the so called gravito-magnetic component of the gravitational field, whose direct verification relies for the moment on three experiments in space: i) Gravity Probe B (GP-B)[2] ; ii) the two LAGEOS satellites orbital nodes analysis [3, 4] ; and iii) the LARES mission, under way and gathering data, launched in February 2012 [5] . GP-B verified the geodetic effect in the gravitational field of the Earth with an accuracy of 28% and the Lense-Thirring (LT) drag with an accuracy of 19%; the analysis of the precession of the nodes of the LAGEOS satellites verified the LT effect with the accuracy of 10%; finally, LARES is working to determine the LT drag with an accuracy of a few % (possibly 2%). Other evidence of gravito-magnetic effects may be found in the laser ranging of the orbit of the moon and in the study of the dynamics of binary systems composed of at least one compact massive object (neutron star).

Besides pure GR effects, the observation of the universe on the widest scale provides also facts which can be consistent with GR assuming that otherwise unseen entities exist, such as dark matter, producing the additional gravity required to explain the rotation curves of galaxies and the speeds of the components of star or galaxy clusters, or the dark energy necessary to generate the push required by the accelerated expansion of the universe. These facts have stimulated ideas implying that GR might need some extension. What matters here is that the phenomenology to look for and to analyse in search for differences from GR is in the domain of low and ultra-low energies. All above said gives motivations for working experimentally on the gravitational interaction in the weak domain looking for post-Newtonian effects and Parametrized Post Newtonian (PPN) descriptions which could evidence deviations from classical GR. Among various possible experimental approaches, a perfect tool is represented by light. Light is indeed intrinsically relativistic and is affected in various ways by the gravitational field. In the classical domain and, as far as a theory is considered treating space-time as a continuous four- dimensional Riemannian manifold, light completely covers the manifold with a network of null geodesics. If we find the way of reading the local and global configuration of the null geodesics tissue we can reconstruct the "shape" of space-time i.e. the gravitational field and see whether it fully corresponds to the GR description or maybe there is

something missing. In our devices the measured quantity is the beat note $\delta\nu$ between the two laser modes, and it can be shown that for a ring laser fixed on the Earth[6]

$$\delta\nu = 4\frac{A}{\lambda P}[\Omega - 2\frac{\mu}{R}\Omega\sin\theta\widehat{u_\theta} + \frac{GJ_\oplus}{c^2R^3}(2\cos\theta\widehat{u_r} + \sin\theta\widehat{u_\theta})] \cdot \widehat{n} \ , \tag{1}$$

where $A\widehat{n}$ is the vector area of the ring and P is its perimeter, λ is the wavelength of the light, Ω is angular velocity of the Earth, θ is the colatitude of the laboratory, $\widehat{u_r}$ and $\widehat{u_\theta}$ are unit vectors that represent the azimuthal and north-south directions, $M_\oplus$, $J_\oplus$ and R are the mass, the angular momentum and the radius of the Earth, respectively. Here $\mu = G\frac{M_\oplus}{c^2} \approx 4.4 \times 10^{-3}$ m is half of the Schwarzschild radius of the Earth.

In summary, the ring laser beat note has 3 terms, i.e. Sagnac, de Sitter (Geodetic term) and gravito-magnetic (Lense-Thirring) which are proportional to Ω, μ and $J_\oplus$, respectively. The Earth angular velocity Ω is independently measured with very high accuracy by VLBI, which measure the Earth rotation with respect to the fixed stars. Thus the relativistic terms can be obtained by subtracting from the ring laser data the Sagnac term measured by VLBI. The de Sitter term has been studied with very high accuracy, so the proposed apparatus can improve the accuracy of the Lense-Thirring effect [7].

The ring laser appears today as a most interesting apparatus to probe the structure of space-time at the laboratory scale. At his early stage, the expected sensitivity of GINGER will not be competitive with space measurements to test PPN theories, but being the apparatus on Earth, improvements of the ring laser technology will be feasible with time.

Our final goal is a very accurate local measurement of the frame dragging effect, and so GINGER must be underground located in order to reduce, as much as possible, very low frequency top soil disturbances due to wind load, atmospheric pressure changes, etc.. Accordingly, the aim of GINGERino is to measure the level of disturbances present inside the underground laboratory of LNGS.

2. G-PISA AND ITS EXPERIMENTAL SET UP

The ring laser G-PISA consists in a square optical cavity with a side length of 1.350 m. The four cavity mirrors are contained in a steel vacuum chamber entirely filled with a He-Ne gas mixture. This design allows to change the perimeter of the ring simply by changing the length of the tubes connecting the four cavity mirrors. In the middle of one of the tubes there is a pyrex capillary, and this is the position where the capacitive discharge is located. Two optically transparent windows
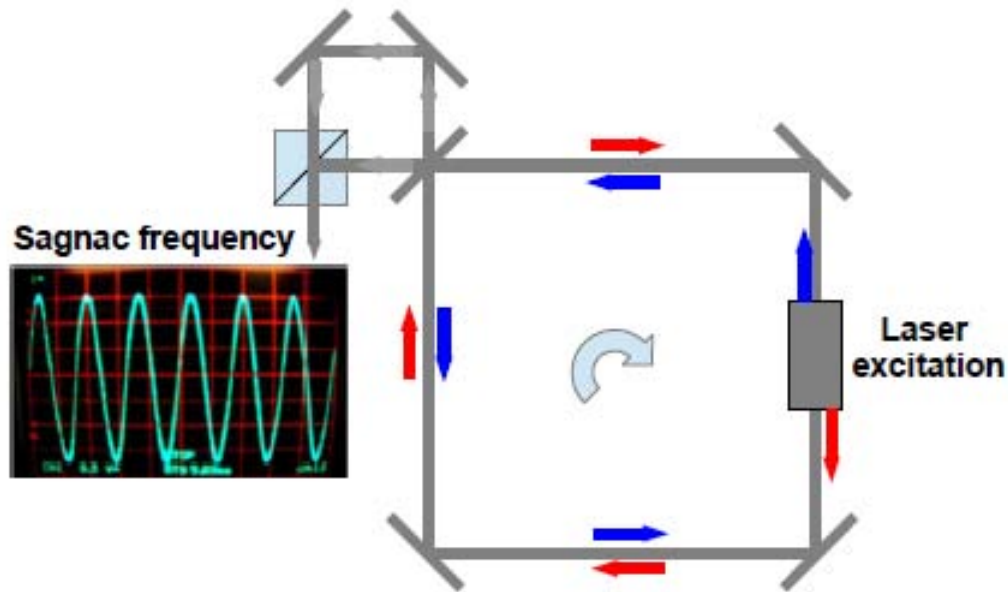
FIG. 1. A schematic picture of the ring lasers: the 4 mirrors delimiting the ring square cavity, the two laser modes conter-rotating, in one of the corners the two output beams are interfering and the beat note Sagnac frequency is shown. The beat note, or Sagnac frequency, at LNGS was 104Hz

FIG. 2. G-Pisa on top of its granite table, moved from its installation in S. Piero Lab (Pisa)

are mounted on each corner of the cavity and allow to monitor the 8 beams exiting the cavity. Two of the four mirrors are equipped with a piezo-transducer, which moves the mirror along a diagonal of the square. They are used to keep constant the perimeter of the ring allowing a continuous measurement of the angular velocity of the ring. Fig. 1 shows a schematic of the ring laser.

For this installation, the experimental set up already existing has been used. G-PISA [8],[9],[10]

has been fixed to a granite table that, in its turn, is firmly attached to a special monument, the one developed for the installation inside the Virgo central area. The monument is made of reinforced concrete, which can support the ring laser and its granite table in two different position: horizontal and vertical. We decided to keep the ring in horizontal configuration. Two broad-band seismometer and a tilt-meter, with nrad resolution in frequency below a mHz, have been installed on top of the granite table. The monument was not fixed to the ground, it was simply laying against the floor. However, care was used for positioning G-Pisa horizontally and in order to make its position stable. In this configuration, the Sagnac frequency due to the Earth rotation is about $104Hz$. Our system can operate free running or enabling the control loop of the perimeter. In the free running mode, any time that the perimeter of the laser changes more than one wavelength of the laser (λ) a mode jump occurs, and the number of wavelengths inside the perimeter changes. After few seconds the normal operation of the ring restarts. Split mode operation may take place; in such a case the beat frequency is the standard Sagnac frequency plus one free spectral range of the laser cavity (53 MHz). The perimeter is controlled by keeping the wavelength of one of the two modes of the ring laser constant, using a stabilized laser source as an external reference. For this purpose we have used a Doppler-stabilized, single-frequency He-Ne laser associated with a Lambda Meter LM-10. A simple acoustic and thermal shielding was constructed around the ring laser, the acquisition of the Sagnac interferogram was continuous, and some additional environmental monitoring channels were acquired at the same time, i.e. one tilt-meter, 2 different seismometers (provided by TUM and by INGV-Pisa), temperature and humidity probes etc. The data were sent to our storage area in Pisa. Unfortunately, it was not possible to synchronize the DAQ clock to the GPS. Fig. 3 shows the experimental set-up of G-Pisa, attached to the granite table, horizontally oriented. A simple box has been mounted around the apparatus, and the structure to hold the "stiferite" panels used for the acoustic shielding is also visible. The data acquisition is based on a NI PXI system,the signals from the ring laser are acquired at 5 kHz, while the auxiliary channels (temperature, humidity etc.) are acquired at 1 Hz. Each hour a file is created, and copied in a PC, which takes care of copying the data directly to our storage area in Pisa. The DAQ reconstructs the angular rotation with and AR2 filter, while Kalman filters to subtract the backscatter noise [11, 12], and most of the analysis are done off-line using Matlab.

G-Pisa was moved to LNGS in March. The whole apparatus was mounted in two weeks, and easily removed, at the end of May, in order to clear the space for the installation of XENON1t. From April to May 2013 G-Pisa was taken data, the first two weeks it was free running, then the perimeter control has been activated.

FIG. 3. First installation of G-Pisa inside LNGS, Hall B.

3.   FIRST MEASUREMENTS AT LNGS

Inside the Hall B the fan coils, regularly located on the two sides of the hall, were continuously running at full speed. It was immediately clear that they were causing problems to the ring laser; we noticed in the data a very strong signal around 1 Hz, probably due to a resonance of the mechanical structure of the ring, excited by the air flow. Fortunately, after few tests it was clear that it was possible to run properly the ring switching off half of the fan coils.

Fig. 4 shows the full set of data with the ring laser operating in closed loop under the action of perimeter control. After approximately 20 days of data taking, the ring laser had a failure (see the final part of time series reported in Fig. 4). There was a lack of pressure in the capillary (where the gas discharge happens) so that the gas mixture was contaminated by air. After a while the capillary was completely broken and the laser suddenly stopped. Fig. 5 shows the power spectrum of the raw data relative to the interferogram of clockwise and counter-clockwise beams. Data taken at LNGS exhibit lower noise compared to S. Piero data, that was taken with the same instrument, in similar conditions (Sunday in both cases when the human activity is minimal). The response of G-Pisa at LNGS is a bit worse in the mHz region, this is probably due to the reference laser used at LNGS which was not so good as the one in S. Piero Lab (Iodine stabilised laser). Another advantage of the S. Piero installation was a higher rotational bias because the

103
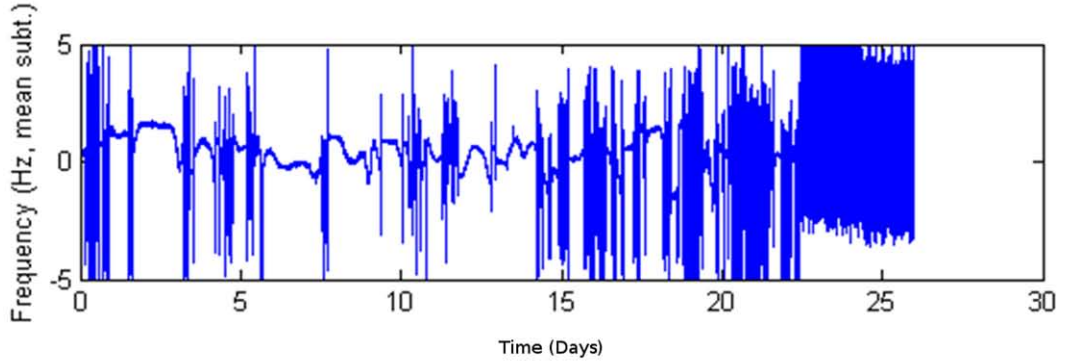
FIG. 4. The whole raw data of our ring laser collected at LNGS.

ring was at maximum of the Sagnac frequency, which implies a reduction of the systematics of the Laser. LNGS has a very good thermal stability, in fact, free running G-Pisa was running for 2 days continuously. This first set of measurements shows that most of the disturbances of the ring laser result from human activity. Despite the perimeter control loop, from time to time the perimeter control was not tight enough to keep the apparatus operating properly; this is a problem which has not been fixed for lack of time. Luckily, there are several time intervals which are good. To evaluate the Allan deviation a not working day has been selected, a day in which the instrument was well behaving. This has been compared with the data taken in S. Piero in February, in similar conditions. The kalman filter has been used, in order to reduce the low frequency disturbances due to the systematics of the laser. The Allan deviation for the two different locations are reported in Fig. 6, and it is worth noticing that the long term stability (i.e. the time at which the Allan deviation has its minimum) at LNGS is higher than in S. Piero lab.

A two channel tilt-meter with nano-radiant precision has been installed on top of the granite table. It shows that a large motion is present during working days when people work inside the hall, while the situation during weekend and vacation is completely different. Fig. 7 below shows the full set of the tilt-meter data. The two channels show several large changes, probably due to inadequate anchorage of the apparatus to the floor, and the position of the tilt-meter was not stable enough. Despite the large noise in the data, the very tiny periodic signals coming from the diurnal and semi-diurnal polar motion are visible. This tilt is due to the deformation of the Earth crust, due to the tidal effect of the moon, as one can see in Fig. 8. Fig. 9 shows one of the two channels of the tilt-meter. The full set of data is split in two pieces, which correspond to: working time and rest of the day. The figure shows that most disturbances occur during human activities. Moreover,
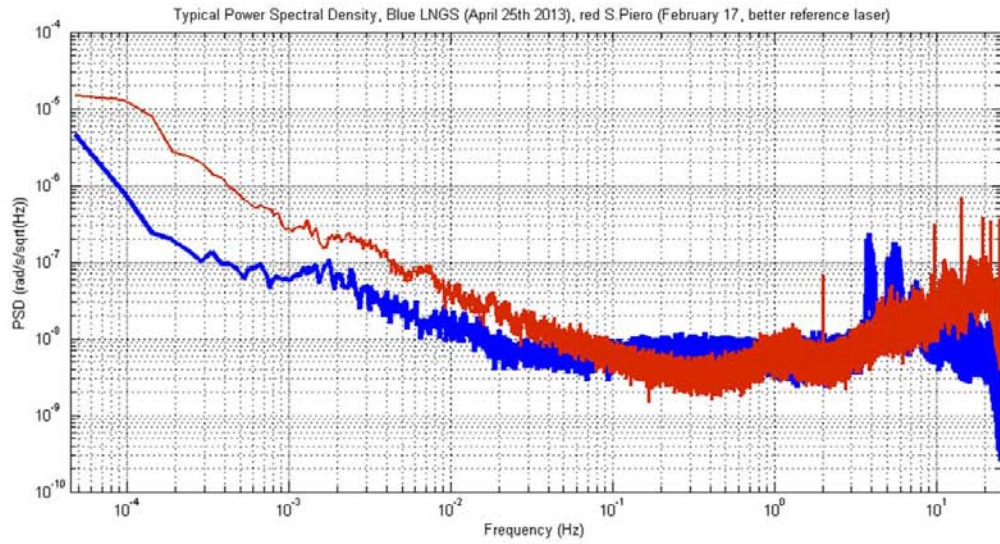
FIG. 5. Power Spectrum of the Sagnac frequency. The data were taken at S. Piero (red, Febrary 2013) and at LNGS (blue); we used the data collected in a Sunday, when there are no people working around
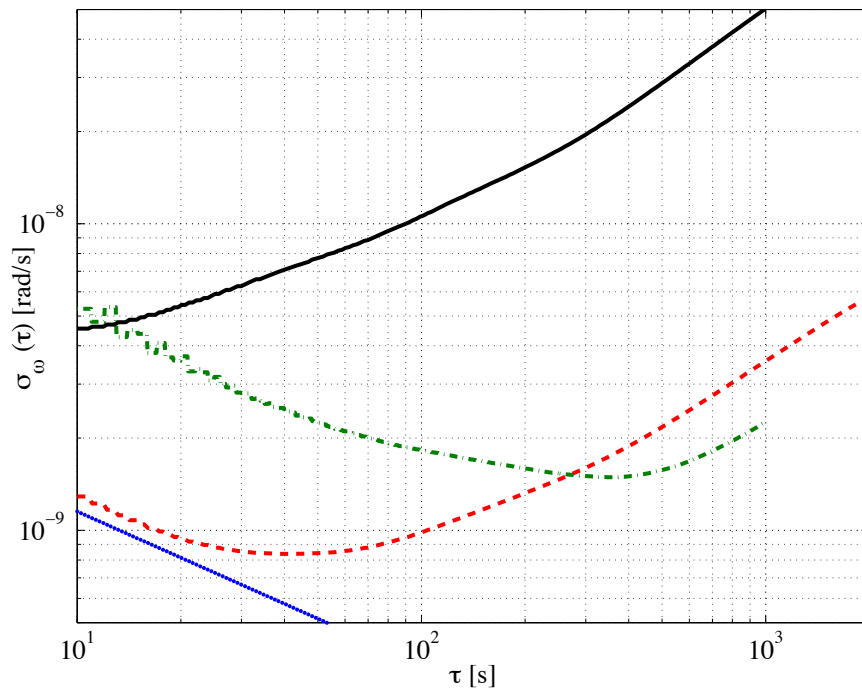
FIG. 6. Allan deviation of the Sagnac frequency as a function of time. The data were collected at S. Piero (red dashed line, Febrary 2013) and at LNGS (green dot-dashed line) after the removal of laser systematics by Kalman filtering. The Allan deviation was calculated using data collected in a Sunday, when there are no people working around.

105
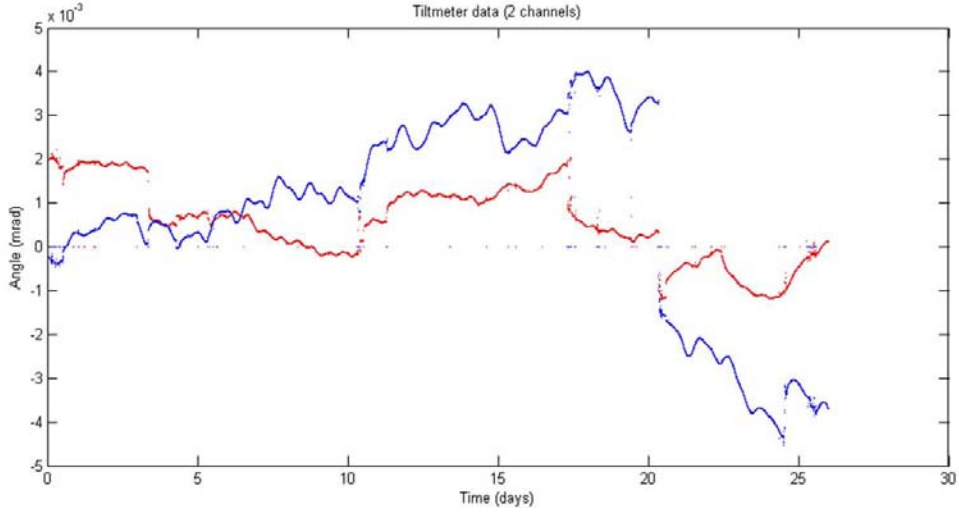
FIG. 7. The full set of data of the two channels of the tilt-meter.
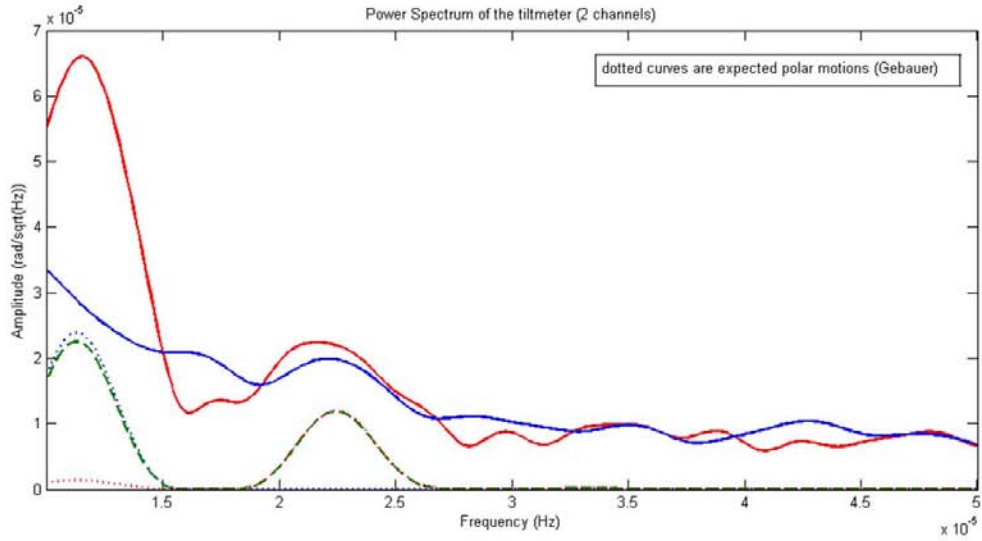
FIG. 8. Detail of the power spectrum of the tilt-meter data. The two typical frequencies of the diurnal $(1.15 \times 10^{-5}\ Hz)$ and semi-diurnal $(2.31 \times 10^{-5}\ Hz)$ polar motion are visible; in the same figure the expected polar motion. These two frequencies are not coming from night/day temperature changes, and can be induced only by the tidal effect of the moon.

we verified that large transient signals in the nights come from far away strong earthquakes.

The level of seismic background noise depends on the location of the site on Earth; however, a low noise background is described by the Low Noise Model (LNM), which has a typical structure induced by the oceans motion below 1Hz. Fig. 10 compares the measurements at LNGS with the

106
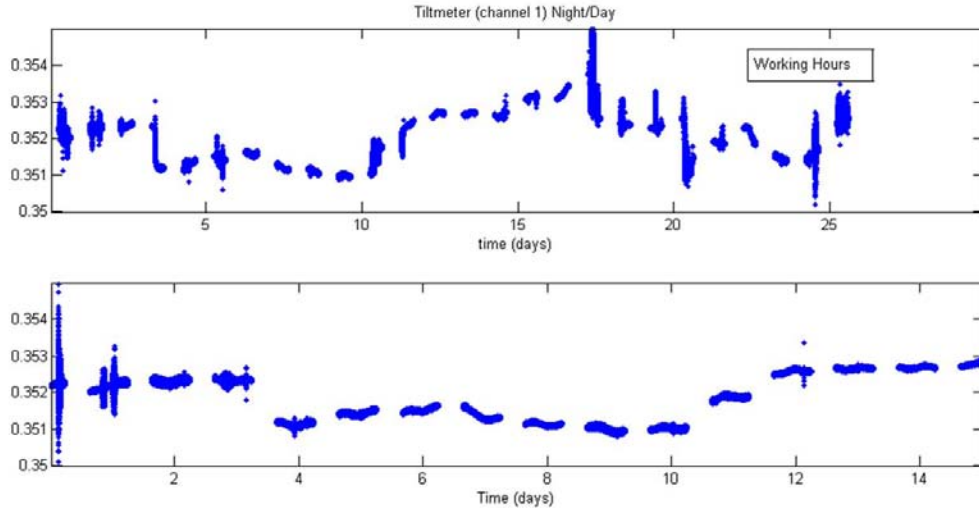
FIG. 9. Top: one of the two channels of the tilt-meter during working time. Bottom: the same channel during the rest of the time; in this case some teleseismic events are clearly visible

LNM (the three translational displacements). The noise level at low frequency is higher especially for the two horizontal translations. At the moment it is not possible to say whether this behaviour depends on air flows and external disturbances or if it is a characteristic of the GranSasso site. Kalman filters have been applied to a selected bunch of data, in order to see the microseismicity in the milli-Hz region, Fig. 11 shows the comparison between the microseismicity detected by the seismometer and by the ring laser. Teleseismic events was observed in the seismometers and tilt-meters, but not in the ring laser data.

4. CONCLUSIONS AND FUTURE PLAN

The first set of data are showing a longer integration time compared with the installation in S. Piero a Grado, but several improvements are needed to better understand the low frequency part of the spectrum due to LNGS environment conditions, namely:

i) The monument must be well connected to the floor;

ii) A good acoustic isolation is required, and the instrument should be possibly far from human activities;

iii) It is important to enlarge the ring, our plan is to go up to 3.6 m, which represents an improvement of a factor of 7 in sensitivity;
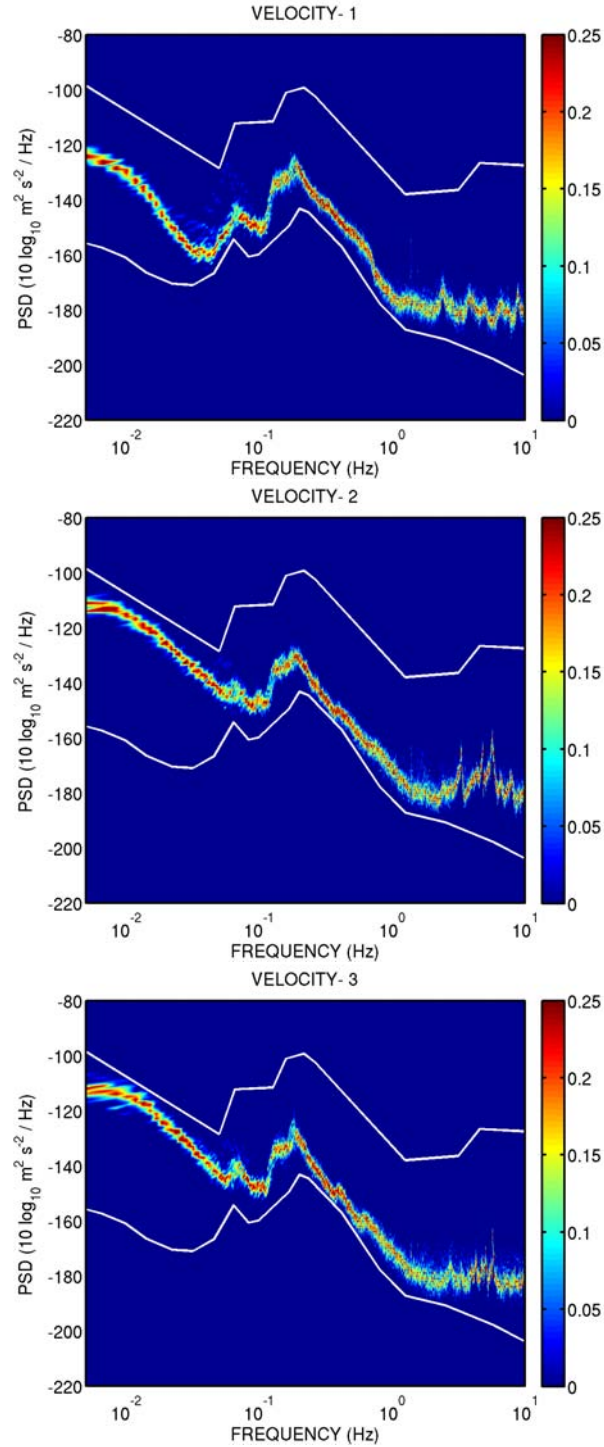
FIG. 10. Power spectra evaluated with the seismometer data compared with the Low Noise Model (LNM) of the seismic background. The top one is the vertical direction

iv) The iodine stabilized laser, which is an absolute frequency stabilized source, should be used for the perimeter control;

108
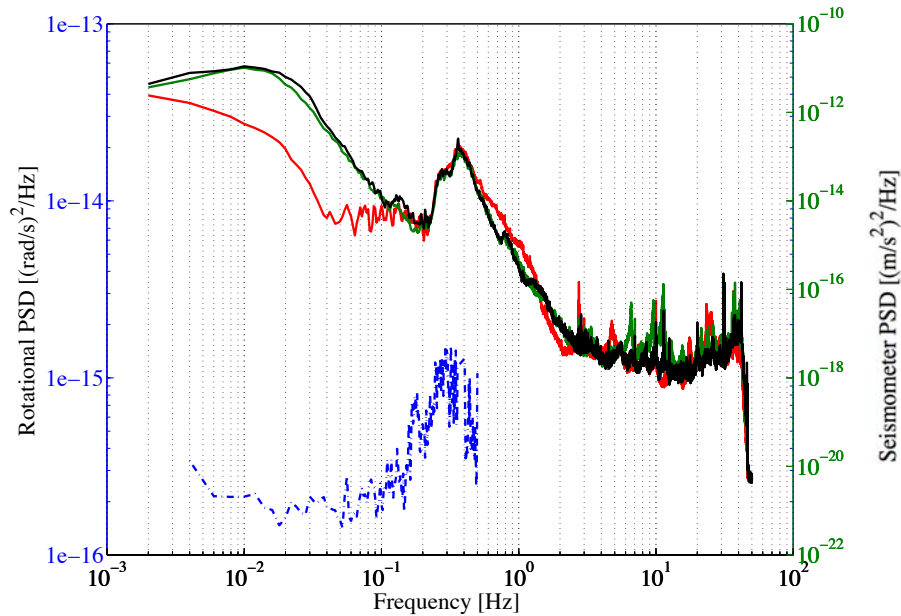
FIG. 11. Microsismicity shown by the three channels of the seismometer (continuos red, green and black lines) and by the ring laser data (dotted blu line), the structure in the ring laser data is visible only after the use of the Kalman filter used to remove the systematic effects of the laser.

v) The clock of the acquisition must be synchronized with the GPS signal and, for geophysical studies, the UTC time stamp is also required.

The new installation of the ring laser, that we have named GINGERino, will be in the corridor between Node A and Node B, construction is expected to start in spring 2014, and likely we expect to have the device operating at the time of summer 2014.

5. AKNOWLEDGMENT

109

REFERENCES

---

[1] N Beverini et al."Measuring general relativity effects in a terrestrial lab by means of laser gyroscopes". In: *Modern Problems of Laser Physics* (2014).

[2] C.W. Everitt and et al. In: *Phys. Rev. Lett.*(106) (2011), p. 221101.

[3] I. Ciufolini and C. Pavlis. "Controlling the non-linear intracavity dynamics of large He-Ne laser gyroscopes". In: *Nature* 958 (2004), pp.1-19.

[4] I. Ciufolini and et al. In: *The European Physical Journal Plus* 126 (2011), pp.1-19.

[5] I. Ciufolini and et al. In: *The European Physical Journal Plus* 127 (2012), pp.127-133.

[6] K.U. Schreibel and J.-P. Wells In: *Invited Review Article, Review of Scientific Instrument* 84 (2013), pp.041101-26.

[7] F Bosi et al. "Measuring gravitomagnetic effects by a multi-ring-laser gyroscope" In: *PHYSICAL RE-VIEW D, PARTICLES, FIELDS, GRAVITATION, AND COSMOLOGY* 84 (2011). PACS numbers: 42.15.Dp, 42.30.Sy, 42.55.Lt, 91.10.Nj pp.122002–1–122002–23. ISSN: 1550-7998. DOI: 10.1103/Phys-RevD.84.122002. URL: http://dx.medra.org/10.1103/PhysRevD.84.122002.

[8] J Belfi et al. "A 1.82 m2 ring laser gyroscope for nano-rotational motion sensing" In: *APPLIED PHYSICS. B, LASERS AND OPTICS* 106 (2012), pp. 271-281. ISSN: 0946-2171. DOI: 10.1007/s00340-011-4721-y. URL: http://dx.medra.org/10.1007/s00340-011-4721-y.

[9] J Belfi et al. "High sensitivity rotation measurements with a mid-size laser gyroscope" In: *ICONO 2010: International Conference on Coherent and Nonlinear Optics (Proceedings Volume)* Vol. 7993H Kazan (Russian Federation): Society of Photo-Optical instrumentation Engineers, 2011, 79931H-79931H-7. DOI: 10.1117/12.880971. URL: http://dx.medra.org/10.1117/12.880971.

[10] A Di Virgilio et al. "Performances of G-Pisa: a middle size gyrolaser" In: *CLASSICAL AND QUAN-TUM GRAVITY* 27 (2010), pp. 084033. ISSN: 0264-9381. DOI: 10.1088/0264-9381/27/8/084033. URL: http://dx.medra.org/10.1088/0264-9381/27/8/084033.

[11] D Cuccato et al. "Controlling the non-linear intracavity dynamics of large He?Ne laser gyroscopes" In: *METROLOGIA* 51 (2014), pp. 97-107. ISSN: 0026-1394. DOI: 10.1088/0026-1394/51/1/97. URL: http://dx.medra.org/10.1088/0026-1394/51/1/97.

[12] A Beghi et al. "Compensation of the laser parameters fluctuations in large ring laser gyros: a Kalman filter approach" In: *APPLIED OPTICS* 51 (2012), pp. 7518–7528. ISSN: 0003-6935. DOI: 10.1364/AO.51.007518. URL: http://dx.medra.org/10.1364/AO.51.007518.

The ICARUS Experiment

The ICARUS Collaboration

M. Antonello[a], B. Baiboussinov[b], P. Benetti[c], F. Boffelli[c], A. Bubak[m], E. Calligarich[c], S. Centro[b], A. Cesana[e], K. Cieślik[f], D.B. Cline[g], A.G. Cocco[d], A. Dabrowska[f], D. Dequal[b], A. Dermenev[h], R. Dolfini[c], A. Falcone[c], C. Farnese[b], A. Fava[b], A. Ferrari[i], G. Fiorillo[d], D. Gibin[b], S. Gninenko[h], A. Guglielmi[b], M. Haranczyk[f], J. Holeczek[m], M. Kirsanow[h], J. Kisiel[m], I. Kochanek[m], J. Lagoda[l], S. Mania[m], A. Menegolli[c], G. Meng[b], C. Montanari[c], S. Otwinowski[g], P. Picchi[n], F. Pietropaolo[b], P. Plonski[o], A. Rappoldi[c], G.L. Raselli[c], M. Rossella[c], C. Rubbia[1,a,i], P. Sala[e], A. Scaramelli[e], E. Segreto[a], F. Sergiampietri[p], D. Stefan[a], R. Sulej[a,l], M. Szarska[f], M. Terrani[e], M. Torti[c], F. Varanini[b], S. Ventura[b], C. Vignoli[a], H.G. Wang[g], X. Yang[g], A. Zalewska[f], A. Zani[c] K. Zaremba[o],

[a]INFN - Laboratori Nazionali del Gran Sasso, Assergi, Italy
[b]Università di Padova e INFN, Padova, Italy
[c]Università di Pavia e INFN, Pavia, Italy
[d]Università Federico II di Napoli e INFN, Napoli, Italy
[e]Politecnico di Milano e INFN, Milano, Italy
[f]H.Niewodniczański Institute of Nuclear Physics, Kraków, Poland
[g]Department of Physics, UCLA, Los Angeles, USA
[h]Institute for Nuclear Research of the Russian Academy of Sciences, Moscow, Russia
[i]CERN, Geneva, Switzerland
[l]Nuclear Center for Nuclear Research, Warszawa, Poland
[m]Institute of Physics, University of Silesia, Katowice, Poland
[n]INFN Laboratori Nazionali di Frascati, Frascati, Italy
[o]Institute for Radioelectronics, Warsaw Univ. of Technology, Warsaw, Poland
[p]Università di Pisa e INFN, Pisa, Italy

Abstract

In 1977 C.Rubbia [1] conceived the idea of a LAr-TPC (Liquid Argon Time Projection Chamber). The ICARUS T600 cryogenic detector is the largest LAr-TPC ever built and operated. Installed in the Gran Sasso underground laboratory and exposed to the CNGS neutrino beam, on June 26th 2013 ICARUS has completed 3 years of data taking collecting about 3000 CNGS neutrino events but also cosmic rays, and showing optimal performances. The cosmic ray data taking after CNGS beam stop (December 3rd, 2012), including a summary of the T600 detector operation, will be here reported along with the detector decommissioning. The updated results from the search for the $\nu_\mu \to \nu_e$ anomalies with the CNGS beam and future perspectives for the ICARUS T600 detector will be also presented.

---

[1]Spokesman of the ICARUS Collaboration

1 ICARUS T600 Detector

The ICARUS T600 detector is the largest Liquid Argon Time Projection Chamber (LAr-TPC) ever built and operated. The detector consists of a large cryostat split into two identical, adjacent half-modules with internal dimensions $3.6 \times 3.9 \times 19.6$ m^3 and filled with a total of 760 tons of ultra-pure LAr. Each half-module houses two TPCs separated by a common cathode, with a drift length of 1.5 m. Ionization electrons, produced by charged particles along their path, are drifted under uniform electric field ($E_D = 500$ V/cm) towards the TPC anode made of three parallel wire planes, facing the drift volume. A total of 54000 wires are deployed, with a 3 mm pitch, oriented on each plane at different angles (0^0, $+ 60^0$, $- 60^0$) with respect to the horizontal direction. The drift time of each ionization charge signal, combined with the electron drift velocity information ($v_D = 1.55$ mm/s), provides the position of the track along the drift coordinate. Combining the wire coordinate on each plane at a given drift time, a three-dimensional image of the ionizing event can be reconstructed. The absolute time of the ionizing event is provided by the prompt ultra-violet scintillation light emitted in LAr and detected through an array of 74 Photo Multiplier Tubes (PMTs), installed in LAr behind the wire planes, which are also used for triggering purposes. The detector is completed by a cryogenic plant made of a liquid Nitrogen cooling circuit which keeps Argon in liquid phase and guarantees high LAr thermal stability (within 1K). The LAr purity is a key issue for the detector imaging capability and for a correct estimation of the ionization charge of events at any depth along the drift path. A system of LAr purifiers, operating both in gas and in liquid phase, keep the LAr purity under control.

The ICARUS T600 detector performances can be summarized as follows: 1 mm^3 precision in event topology, e/γ separation with 2% X$_0$ sampling, electromagnetic showers energy resolution $\sigma(E)/E = 0.03/\sqrt{E(GeV)} \oplus 0.01$, low energy electrons resolution $\sigma(E)/E = 0.11/\sqrt{E(GeV)} \oplus 0.02$ and hadronic showers resolution $\sigma(E)/E = 0.30/\sqrt{E(GeV)}$.

During 2013, after the definitive CNGS beam stop on December 3rd 2012, the ICARUS T600 detector continued its data taking with cosmic rays untill June 26th, when the detector decommissioning started. These three years of continuous underground operation (June 2010 - June 2013) have proven that the LAr-TPC detection technique, developed by the ICARUS Collaboration, is well understood and can be adapted for the next-generation experiments. In three years of continuative data taking, ICARUS collected $\sim$3000 events of CNGS-beam neutrino interaction and cosmic ray events with energy spanning from tens of MeV to tens of GeV.

The analysis of the collected data sample is progressing along several paths. The present effort is mainly devoted to: (1) the search for anomalous $\nu_\mu \to \nu_e$ transitions; (2) the search for the disappearance anomaly from initial muons from the CERN beam; (3) the finalization and validation of the multiple scattering algorithm for the measurement of muon momentum in the few GeV energy range. The more complete study of the actual nature of the CNGS events and the study of cosmic ray and other data is continuing on a longer time schedule. On the technical side, the development of automatic reconstruction tools is progressing, as well as a detailed investigation of the detector uniformity using long muon tracks from external neutrino interactions.

This report will focus on the following items: (1) the updated search for the $\nu_\mu \rightarrow \nu_e$ anomalies with the CNGS beam[P3], confirming with an almost doubled statistics the early ICARUS result[P1]; (2) final operation of the cryogenic plant; (3) cosmic ray data taking after CNGS beam stop (December 3rd, 2012) including summary of the T600 detector operation; (4) phases of the detector decommissioning which started just after the run was stopped.

2 Search for anomalies in the ν_e appearance from the CNGS ν_μ beam

ICARUS has performed an updated search for anomalies with the CNGS beam. This analysis extends with an almost doubled event statistics our previously published result [P1] showing that there was a possible agreement of all published experimental results only for a narrow surviving region centered around $(\Delta m^2, sin^2(2\theta))_{new} = (0.5eV^2, 0.005)$.

Following the previous analysis [P1], the events with a clear electron neutrino signature have been efficiently visually identified by requiring the presence of a primary charged track initially consistent with a minimum ionizing relativistic particle and subsequently building up into a shower. The track has to be spatially separated from other ionizing tracks from the primary vertex.

In the newly added sample we have found two additional electron events that bring to four the total observed number of events. This is compatible with the visible background expectation of 6.4 ± 0.9 due to conventional sources: the probability to observe a statistical under-fluctuation resulting in four or less ν_e events is 25%.

The first new event, shown in Figure 1, has a total energy of $\sim$27 GeV and an electron of 6.3 ± 1.5 GeV, taking into account the partially escaping fraction of the e.m. showers. The electron is clearly separated from the other tracks after 1 cm from the main vertex. The progressive evolution of the electron from the single ionizing particle to an electromagnetic shower is clearly visible in the plot of dE/dx along the individual wires in Figure 1.

The second new event, shown in Figure 2, has a total energy of $\sim$14 GeV and an electron of 6.4 ± 0.3 GeV. The corresponding three-dimensional reconstruction of the event is also shown. In both events the single electron shower in the transverse plane is opposite to the remaining of the event, with the electron transverse momentum of 3.5 ± 0.9 GeV/c and 1.2 ± 0.2 GeV/c respectively. At statistical confidence levels of 90% and 99% the limits are respectively 3.7 and 8.3 events. The corresponding new limits on the oscillation probability are $\langle P(\nu_\mu \rightarrow \nu_e) \rangle \le 3.4 \times 10^{-3}$ and $\langle P(\nu_\mu \rightarrow \nu_e) \rangle \le 7.6 \times 10^{-3}$ respectively, see the exclusion plot in Figure 3 left. This result is in published in [P3].

The LSND result [2] was based on anti-neutrino events. A small $\sim$2% antineutrino event contamination is also present in the CNGS beam as experimentally observed [4]. In the limiting case in which the whole effect is due to $\overline{\nu_\mu} \rightarrow \overline{\nu_e}$, the absence of an anomalous signal gives a limit of 4.2 events at 90% CL. The corresponding limit on the oscillation probability is $\langle P(\overline{\nu_\mu} \rightarrow \overline{\nu_e}) \rangle \le 0.32$. The resulting (small) exclusion area is shown in Figure 3 right. As shown in Figure 3, a major fraction of the initial two dimensional plot $[\Delta m^2, sin^2(2\theta)]_{new}$ of the main published experiments sensitive to the
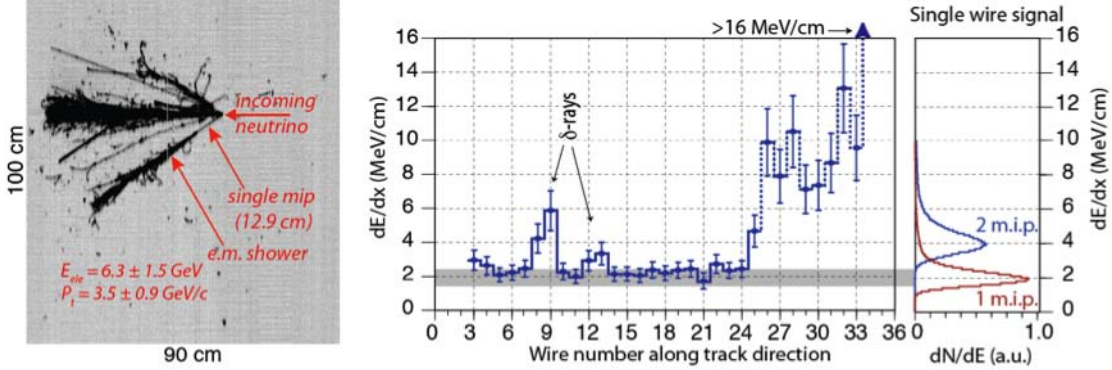
Figure 1: *Experimental pictures of the first of the two new events with a clear electron signature found in the additional sample of 904 neutrino interactions. The evolution of the actual dE/dx from a single track to an e.m. shower for the electron shower is shown along the individual wires. The event has a total energy of ~27 GeV and an electron of 6.3 ± 1.5 GeV with a transverse momentum of 3.5 ± 0.9 GeV/c.*

$\nu_\mu \to \nu_e$ anomaly [2, 3, 5, 6, 7] is now excluded by the present result. There is tension between the limit $sin^2(2\theta_{new}) < 6.8 \times 10^{-3}$ at 90% CL and $< 1.52 \times 10^{-2}$ at 99% CL of ICARUS and the neutrino lowest energy points of MiniBooNE with $200 < E_\nu^{QE} < 475$ MeV, suggesting an instrumental or otherwise unexplained nature of the low energy signal reported by Ref. [3]. Recently a similar search performed at the same CNGS beam by the OPERA experiment has confirmed our finding and the absence of anomalous oscillations with an independent limit $sin^2(2\theta_{new}) < 7.2 \times 10^{-3}$ [8]. As a conclusion, the LSND anomaly appears to be still alive and further experimental efforts are required to prove the possible existence of sterile neutrinos.

3   Detector operation

The T600 cryogenic plant worked efficiently, safely and reliably all over the 3-year run without causing any detector dead time. A paper is in preparation on successful commissioning and underground operation of the cryogenic plant. The Nitrogen cooling plant and Nitrogen re-liquefaction system have been highly reliable thus avoiding any safety problem of interference with the detector data taking. The Argon purification system has guaranteed the continuous maintaining of the LAr purity much above the foreseen target value. The evolution of LAr purity all over the T600 run is represented in Figure 4. As one can see, the several LAr recirculation stops due to pumps maintenance haven't affected detector performance: electron lifetime has been maintained most of the time above 5 ms in both cryostats when recirculation system was active, corresponding to 60 ppt O_2 equivalent impurity concentration.

The installed pumps required more frequent stops than planned. Hence, the 2013 period of T600 operation has been dedicated to the installation, test and run of the new Barber Nichols LAr recirculation pump with not-immersed motor. This is characterized by a higher reliability and an increased recirculation speed. The new pump (BNHEP-23-000 model) is similar to the T600 LN_2 cooling pumps that worked more than 10000 hours
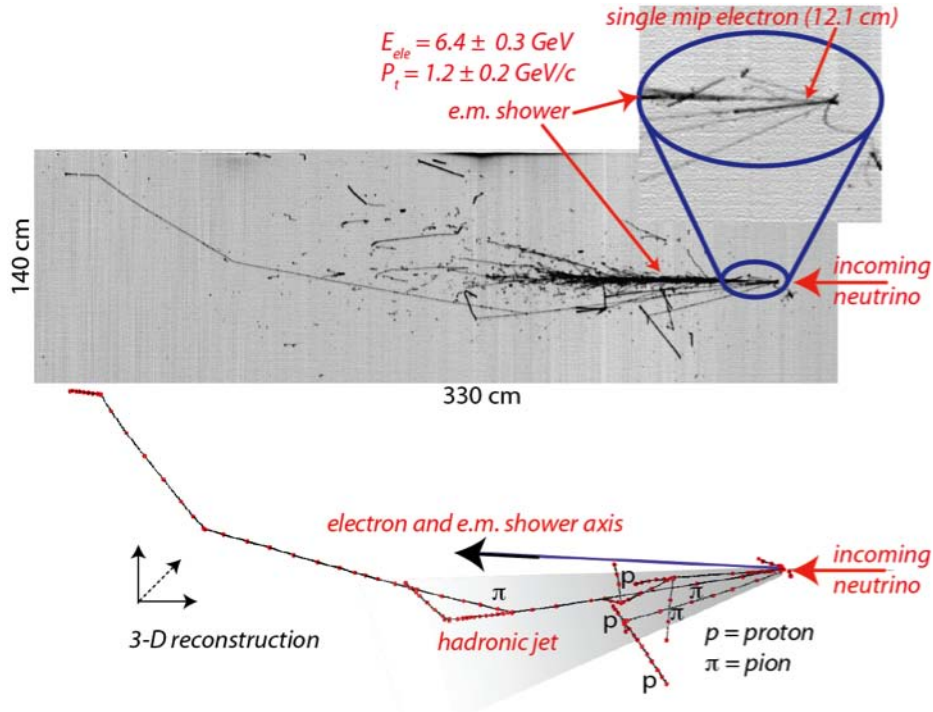
Figure 2: *Second ν_e event. It has a total energy of $\sim$14 GeV and an electron of 6.4 ± 0.3 GeV with transverse momentum of 1.2 ± 0.2 GeV/c. The 3D reconstruction of primary particles in the event is also shown (red dots correspond to vertices of polygonal fit [P2]).*

without requiring any maintenance. A picture of the new pump is shown in Figure 5.

The Barber-Nichols pump was delivered at the beginning of March 2013. Two weeks of major works to upgrade the LAr recirculation system on East cryostat were carried out stopping the LN_2 cooling and the T600 data taking. Then the pump was installed and put in operation at the beginning of April 2013. The last part of the run was dedicated to the test of the new pump and to monitor the trend of purity in the new configuration. With few weeks of operation after the long stop for major installation works it was possible to exceed 7 ms electron lifetime. A zoom of the electron lifetime trend is shown in Figure 6. As one can see the increase of pump recirculation speed is clearly visible. The last purity drop was caused by the interruption of the LN_2 cooling, which is needed for the LAr recirculation, while the new Barber Nichols pump did not report any damage. Before the definitive run stop, the new pump operated for a period equivalent to the mean working-period of the old ACD pumps ($\sim$ 2000 hours), but performing at a purification rate 1.5 times higher.

4   Data taking after CNGS beam stop

The ICARUS-T600 data taking continued after CNGS beam stop (December 3rd, 2012) to collect cosmic ray data until June 26th, 2013, when the run was stopped to allow the decommissioning procedures to start. The exposure to cosmic rays in this period corresponded to 0.203 kton year, providing an overall ICARUS T600 exposure to cosmic
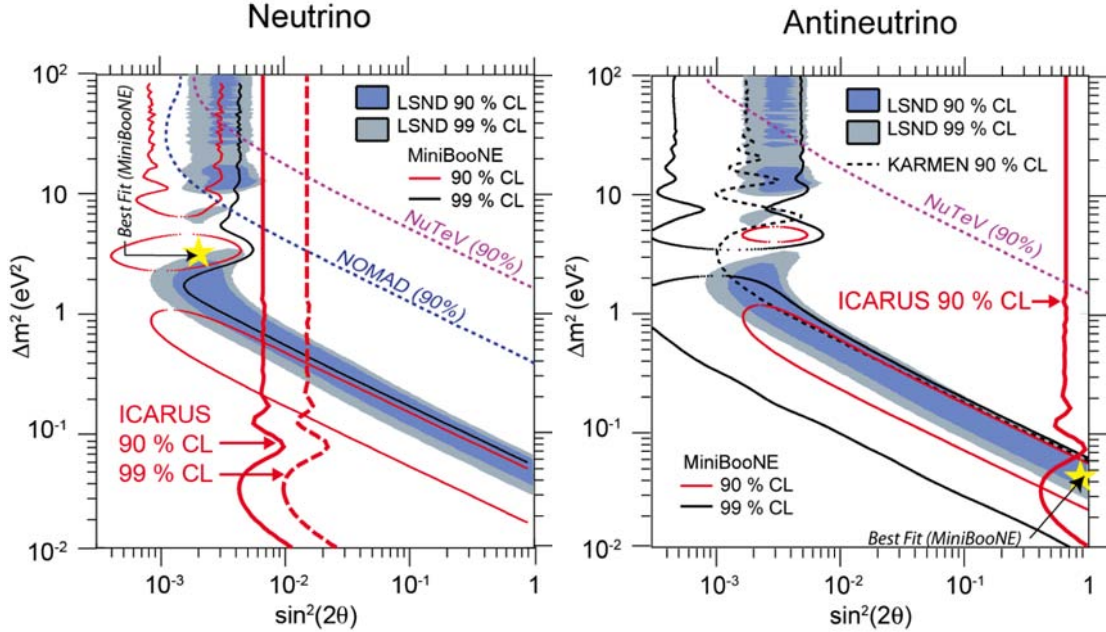
Figure 3: *Neutrino (left) and antineutrino (right) with Δm^2 as a function of $\sin^2(2\theta_{new})$ for the main experiments sensitive to the $\nu_\mu \to \nu_e$ and $\overline{\nu_\mu} \to \overline{\nu_e}$ anomalies [2, 3, 5, 6, 7] and for the present result (continuous red lines). The yellow stars mark the best fit points of MiniBooNE [3]. The ICARUS limits on the oscillation probability for $\nu_\mu \to \nu_e$ are $\leq 3.4 \times 10^{-3}$ and $\leq 7.6 \times 10^{-3}$ at 90% and 99% CL, corresponding to $\sin^2(2\theta_{new}) \leq 6.8 \times 10^{-3}$ and $\sin^2(2\theta_{new}) \leq 1.5 \times 10^{-2}$ respectively. The ICARUS limit on the $\nu_\mu \to \nu_e$ oscillation probability is ≤ 0.32 at 90% CL, corresponding to $\sin^2(2\theta_{new}) \leq 0.64$.*

rays equal to 0.733 kton year, corresponding to 615 days of ICARUS T600 data taking. The upgraded ICARUS T600 PMTs trigger system, based on the coincidence of the PMT sum signals of the two adjacent chambers in the same module, worked properly with a steady trigger rate of about 35 mHz, leading to about 130 cosmic events per hour collected on the full T600. Moreover, the SuperDaedalus set-up, introduced in the data taking for cosmic rays since September 2012 with the aim of recovering the lowest energy part of the cosmic ray spectrum, continued operating smoothly with a ∼120 mHz raw trigger rate including both Collection and Induction 2 views. A dedicated paper is currently under preparation to provide all the details concerning the main features and efficiencies of the ICARUS T600 different trigger sources, both for CNGS run and for cosmic rays. The last part of the 2013 cosmic ray run was dedicated to a few special data taking, whose results are currently under analysis:

1. set-up with a stochastic trigger to study the low energy background sources in ICARUS T600: about 50,000 events were collected, corresponding to about 50 seconds of exposure of the whole detector;

2. set-up with different values of the drift electric field, from 270 V/cm up to 900 V/cm, to study the ionization electron diffusion and to verify the methodology used to measure the liquid Argon purity with cosmic muons;

3. test of long lasting high values of the HV applied to the cathode (nominal 75 kV, tested up to 150 kV for 2 days, which corresponds to a drift electric field of about
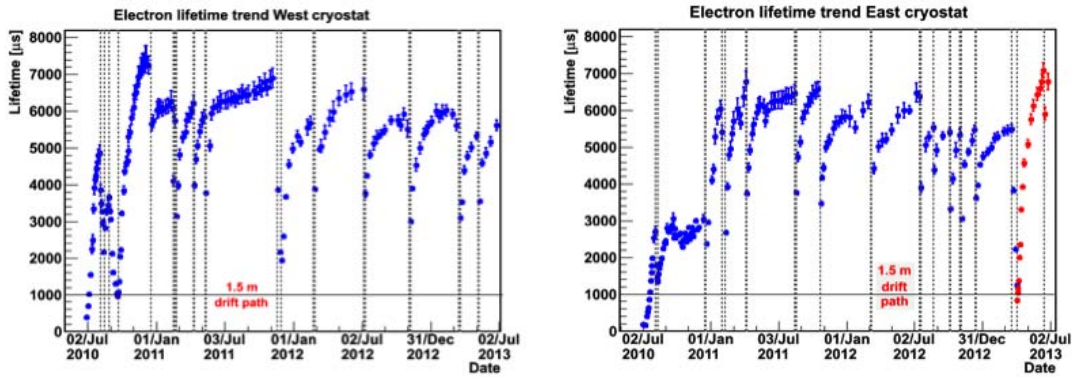
Figure 4: *Electron lifetime evolution in West and East modules from the full T600 live-time. LAr recirculation stops for pumps maintenance are marked by the dotted lines.*
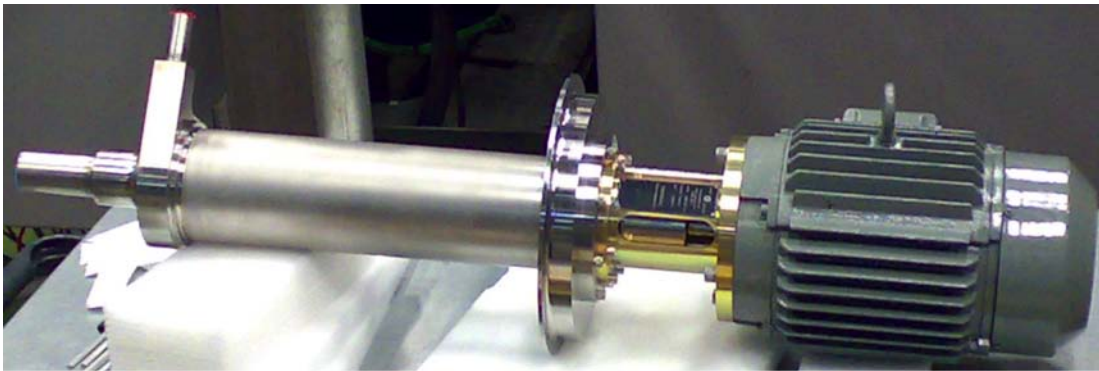

Figure 5: *The new LAr recirculation pump: Barber Nichols pump (BNCP-32C-000 model).*

1000 V/cm).

5   T600 decommissioning

The last part of the T600 run was dedicated also to the T600 decommissioning preparation. In particular an emptying skid to host an immersed LAr pump was installed together with an intermediate buffer to speed up the emptying process.

An administrative procedure to sell the 530,000 l of LAr back to ALIS Company was done. A detailed safety and technical procedure together with a precise schedule and logistic plan were defined with LNGS management in order to maximise safety and minimize interference with other underground activities.

The decommissioning phase started on June 27th 2013 proceeding with the following phases:

1. Cryostat emptying phase.

   This phase started on June 27th 2013 and ended on July 25th 2013, lasting less than one month (only working days) and was operated in safe and smooth way. The emptying phase was carried out in parallel on the two modules transferring the liquid Argon inside an intermediate vessel (20000 *l*) with a high transfer speed (7000
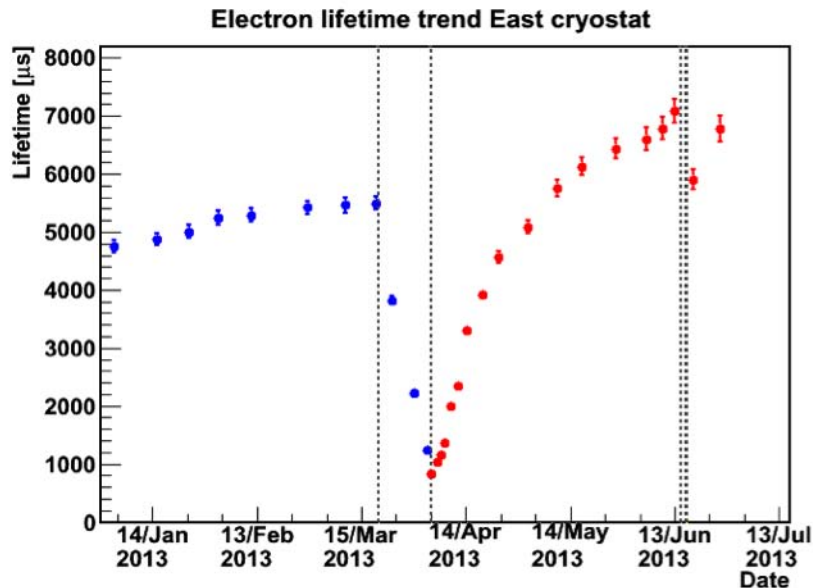
Figure 6: *Electron lifetime evolution in the East module in the last months of T600 run at LNGS (the red dots are relative to the new pump).*

l/h). This allowed to speed up the process and to decouple the emptying procedure from the truck uploading (Figure 7). 740 over a total of 760 LAr tons were recovered and sold to the ALIS company with a total number of 33 trucks (1-2 truck/day).

2. Cryostat warming-up phase.

   This phase started on July 25th and took about one month proceeding with the help of a heating system to speed-up the process circulating warm GN_2 inside T600 cooling screens while keeping the thermal gradients within the $\Delta T_{max} < 50\ K$ specification, to prevent thermal shocks on wire chambers (Figure 8).

3. T600 dismantling phase.

   This phase was started in September 2013 and will globally last about 10 months. It can be divided into two sub-phases: the first one is finalized to the cryostat opening (in order to recovery the internal detectors and possibly the cold vessels) and to the recovery of the cryogenic plant and electronics to be reused in the future projects (see section n. 6); the second phase is aiming at the final emptying of the ICARUS Area in Hall B.

6   Future perspectives

The successful operation of the ICARUS experiment has conclusively demonstrated that the LAr-TPC is the leading technology for the future short and long baseline accelerator driven neutrino physics.

   The INFN has concluded an important cooperation agreement towards a joint experiment with the US-LBNE collaboration, involving the long term realization of a truly large

Figure 7: *Tracks upload with liquid Argon during the emptying phase in Hall B.*

mass underground LAr-TPC detector for a search of CP violation in the lepton sector, proton decay and other topics.

For the next years, the ICARUS collaboration is proposing a new experiment with an intense low energy neutrino beam with the aim of definitely clarify the possible existence of additional neutrino states, as hinted by calibration-source neutrino experiments, reactor and accelerator experiments, and eventually measure the corresponding oscillation parameters. The experiment is based on two identical LAr-TPCs, detecting electron and muon neutrino events at a Far and Near location. The ICARUS T600 detector, which was operated underground in the LNGS underground laboratory, will be the Far detector while an additional 1/4 of the T600 detector (T150) will be constructed and used as the Near detector.

The proposal SPC-P-247 (ICARUS-NESSIE) has been conditionally approved by the August 2013 CERN Research Board with CERN code WA104. Conditionality implies that, at the moment in time, the construction of a short-baseline neutrino beam is not granted and the focus is mainly on detector technology development and qualification with test beams. Within WA104 the T600 will be overhauled and a smaller T150 detector "clone" will be constructed. The existing internal detector together with many ancillary equipments of the LNGS set-up will be recovered.

Vigorous technology developments, while maintaining the already achieved basic features of T600, will introduce important new features addressing in particular: 1) the magnetization of LAr; 2) the LAr purification; 3) new thermal insulation; 4) new cold bodies design; 5) compensation of recombination effects to improve the calorimetric energy measurement; 6) modification on T600 and new electronics for T150; 7) new light detection system.

ICARUS will then be operated either at CERN [P4], [P5], if a neutrino beam will be made available in a reasonable time schedule, or else at FNAL [P6], provided it will be approved. This experiment will offer remarkable discovery potentialities, collecting a large statistics of ν events in both neutrino and antineutrino channels, largely adequate to settle the origin of the observed neutrino related anomalies. This large neutrino event sample ($> 10^6$) with the appropriate energy will be also permit to maintain the appropriate levels in RD/participation in physics developments within a "learning" process based on real ν events in the preparatory phase of LBNE experiment.

On a longer time scale the overhauled ICARUS T600 detector could also provide a convenient near detector in LBNE.

List of Publications Year 2013

[**P1**] M.Antonello e al. [ICARUS Coll.], Experimental search for the LSND anomaly with the ICARUS LAr TPC detector in the CNGS beam, Eur. Phys. J. C, 73:2345 (2013).

[**P2**] M. Antonello et al. (ICARUS Collaboration), Precise 3D track reconstruction algorithm for the ICARUS T600 liquid argon time projection chamber detector, Adv.High Energy Phys. 2013 (2013) 260820.

[**P3**] M. Antonello et al. [ICARUS Coll.], Search for anomalies in the ν_e appearance from a ν_μ beam , Eur.Phys.J. C73 (2013) 2599.

[**P4**] M. Antonello et al. [ICARUS - NESSiE Coll.], Search for anomalies in the neutrino sector with muon spectrometers and large LArTPC imaging detectors at CERN, e-Print: arXiv:1208.0862 [physics.ins-det].

[**P5**] M. Antonello et al. [ICARUS - NESSiE Coll.], Search for anomalies from neutrino and anti-neutrino oscillations at $\Delta m^2 \sim 1 eV^2$ with muon spectrometers and large LArTPC imaging detectors. Technical proposal. CERN-SPSC-2012-010 and SPSC-P-347.

[**P6**] M. Antonello et al. [ICARUS Coll.], ICARUS at FNAL, e-Print: arXiv:1312.7252 [physics.ins-det].

References

[1] C.Rubbia, CERN-EP/77-08 (1977).

[2] A. Aguilar et al. [LSND Collaboration], Phys. Rev. D 64, 112007 (2001).

[3] A. A. Aguilar-Arevalo et al. [MiniBooNE Collaboration], arXiv:1207.4809v1 [hep-ex] 19 Jul 2012 and references therein.

[4] N. Agafonova et al. [OPERA Coll.], New J. Phys. 13 (2011), 053051.

[5] B. Armbruster et al., [KARMEN Collaboration] Phys. Rev. D 65, 112001 (2002).

[6] P. Astier et al., [Nomad Collaboration] Phys. Lett. B 570 19 (2003).

[7] S. Avvakumov et al., [NuTeV Collaboration] Phys. Rev. Lett. 89 (2002) 011804.

[8] N. Agafonova et al. [OPERA Coll.], JHEP 1307 (2013) 004.

LUNA: Laboratory for Underground Nuclear Astrophysics

M. Aliotta[a], M. Anders[b], D. Bemmerer[b], A. Best[c], C. Broggini[d], C. Bruno[a],
A. Caciolli[e], F. Cavanna[f], P. Corvisiero[f], T. Davinson[a], R. Depalo[e], A. Di Leva[g],
Z. Elekes[b], F. Ferraro[f], A. Formicola[c], Zs. Fülöp[h], G. Gervino[i], A. Guglielmetti[j],
C. Gustavino[k], Gy. Gyürky[h], G. Imbriani[g], M. Junker[c], R. Menegazzo[d], P. Prati[f],
D. Scott[a], E. Somorjai[h], O. Straniero[l], F. Strieder[m], T. Szucs[h], D. Trezzi[j]

SPOKESPERSON: A. GUGLIELMETTI

[a]University of Edinburgh, Edinburgh, United Kingdom
[b]Helmholtz-Zentrum Dresden-Rossendorf, Dresden, Germany
[c]INFN, Laboratori Nazionali del Gran Sasso (LNGS), Assergi (AQ), Italy
[d]INFN, Padova, Italy
[e]Università degli Studi di Padova and INFN, Padova, Italy
[f]Università degli Studi di Genova and INFN, Genova, Italy
[g]Università degli Studi di Napoli "Federico II", and INFN, Napoli, Italy
[h]Institute for Nuclear Research (MTA ATOMKI), Debrecen, Hungary
[i]Università degli Studi di Torino and INFN, Torino, Italy
[j]Università degli Studi di Milano and INFN, Milano, Italy
[k]INFN, Roma, Italy
[l]Osservatorio Astronomico di Collurania, Teramo, and INFN Napoli, Italy
[m]Institut für Experimentalphysik III, Ruhr-Universität Bochum, Bochum, Germany

Abstract

Aim of the LUNA experiment is the direct measurement of the cross section for nuclear reactions relevant for stellar nucleosynthesis. The year 2013 was dedicated to the study of the $^{17}O(p,\alpha)^{14}N$ and $^{22}Ne(p,\gamma)^{23}Na$ reactions. The former was measured using a solid target and an array of silicon detectors while the latter required a differentially pumped gas target and two HPGe detectors. After the optimization and calibration of the two setups, new data were obtained for both reactions. The data taking and analysis is still on going. Moreover, new developments occurred for the LUNA-MV project.

1 The ^{17}O(p,α)^{14}N reaction

1.1 Introduction

The rare isotopes ^{17}O and ^{18}F play an important role in a number of astrophysical scenarios, including classical novae and massive stars. Their abundances are influenced by the two competing reactions ^{17}O(p,α)^{14}N and ^{17}O(p,γ)^{18}F, both part of the CNO cycle. The CNO cycle takes place in the inner part of massive stars, depleting the ^{17}O abundance. Surprisingly, observed surface abundances of these RGB or AGB stars also show a depletion of ^{17}O with respect to solar values indicating a connection between the envelope and the energy generating region of these stars. A few attempts have been made to explain the observation [1, 2] and a better understanding of the ^{17}O destruction rate may shed some light on the issue, improving our understanding of the evolution of many types of stars, including our Sun.

Classical novae are frequent phenomena in our galaxy, taking place in binary systems consisting of a white dwarf and a main-sequence or red giant star. Mass from the latter accretes on the white dwarf up to unstable conditions. Every 10^3-10^4 years this process leads to a thermonuclear runaway, triggering Hot-CNO reactions [3, 4]. In particular ^{18}F is produced, a rare isotope unstable to β^+ decay. The gamma rays from the annihilation of the positrons emitted during its decay may, in principle, be detected by space telescopes, but have not been observed to date. A better understanding of the production rate of ^{18}F at the relevant astrophysical energies would help constrain theoretical models and predictions. The ^{17}O(p,γ)^{18}F reaction has been studied at LUNA and results have already been published [5, 6]. The complementary investigation of the ^{17}O(p,α)^{14}N (Q = 1.2 MeV) reaction started recently and focus on two narrow resonances at E_p = 70 and 193 keV, which dominate the reaction rate at energies of astrophysical interest (0.03-0.4 GK). The 193 keV resonance is already relatively well known [7, 8] and was measured chiefly to commission the setup. The main objective of the campaign is the precise direct measurement of the 70 keV resonance, very challenging because of its extreme weak resonance strength. A few direct [9] and indirect [10] attempts had been made in the past, but they painted an incomplete picture which motivated our campaign.

1.2 Experimental approach and preliminary results

The thick target yield technique was employed to investigate the two resonances. Protons from the 400 kV LUNA-II accelerator with typical beam currents of 150 μA, impinged on a solid Ta$_2^{17}$O$_5$ target. These targets were produced by anodization using water enriched in ^{17}O: the same technique employed for the ^{17}O(p,γ)^{18}F campaign [11]. Alpha particles produced by the reaction were detected using an array of eight silicon detectors arranged in two rows at 135° and 102.5° with respect to the beam axis, as shown in fig.1. A standard electronic chain was used to process the signal which was acquired in list mode using MIDAS [12]. To improve the reduction in background, the setup was surrounded by 5cm lead bricks.

The fragile silicon detectors are continuously hit by elastically scattered protons, causing damages to the detectors and increasing the background. To prevent this, protective

Figure 1: (Left) the scattering chamber with the silicon detector mounted. The proton beam enters from the copper tube on the top. (Right) the inside of the aluminium dome on which the detectors are mounted, showing 1 cm diameter collimators.

aluminized Mylar foils ($\sim 2\mu$m thick) were mounted in front of each detector. The thickness was chosen so as to stop the protons while still letting the reaction alpha particles pass through. Finding a compromise between these two requirements was very challenging, since alpha particles are produced with an energy of around 1 MeV only. The setup efficiency was determined using two independent GEANT4-based simulations. The very intense and well-known [13] resonance at 151 keV in ^{18}O(p,α)^{15}N was used to validate the simulations and to provide a cross-check for the efficiency values found. The agreement obtained was satisfactory, giving a final total efficiency value of around 11%. The second step in the setup commissioning was the measurement of the 193 keV resonance in ^{17}O(p,α)^{14}N. Unfortunately, the aluminized Mylar foils proved insufficient to completely suppress the beam-induced background from elastically scattered protons and additional precautions had to be taken. Thin steel collimators, with small apertures of 0.5 cm in radius, were mounted in front of all detectors as shown in fig.1. They suppressed the beam-induced background and allowed the measurement. The resonance strength value found was in very good agreement with previous investigations (see fig.2 for a sample spectrum). Employing the peak from the 151 keV resonance in ^{18}O(p,α)^{15}N and that from the 193 keV resonance in ^{17}O(p,α)^{14}N, we were able to calibrate the detectors and to provide a precise (± 0.1 μm) value for the thickness of the aluminized Mylar foils used. Identifying the region of interest where the alpha particles from the 70 keV resonance are located (typical energy approx. 200 keV) is especially crucial in light of the very low rates expected (few counts per Coulomb of charge on target). It provides both a way to precisely estimate an upper limit if no signal can be seen and a reliable sanity check in case a counting excess or an actual peak are observed.
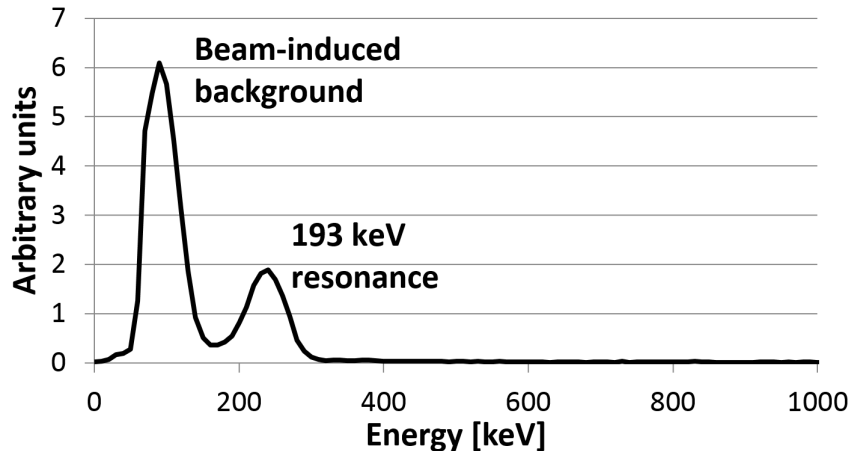
Figure 2: A typical spectrum for the 193 keV resonance. The resonance peak is well separated from the beam-induced background due to backscattering protons.

Data taking for the 70 keV resonance has already started and we have collected several days of data on-resonance, off-resonance and without beam. Collecting data off-resonance is mandatory to understand any possible beam-induced background which could affect our measurement. Data analysis is still on-going and more data are required before conclusions can be drawn. However, preliminary results are very encouraging and indicate a value for the resonance strength parameter of the 70 keV resonance can be obtained in the following months.

2 Study of the ^{22}Ne(p,γ)^{23}Na reaction

2.1 Motivation and previous work

The ^{22}Ne(p,γ)^{23}Na reaction is included in the hydrogen burning neon-sodium (NeNa) cycle. This cycle affects the nucleosynthesis of neon and sodium isotopes, and it plays a key role in the study of the surface composition of Red Giant Branch stars (Gamow peak 30-100 keV), the composition of the ejecta from Asymptotic Giant Branch Stars and classical novae (Gamow peak 100-600 keV) [14] and possibly in the simmering phase prior to the explosion of a type Ia supernova [15].

The ^{22}Ne(p,γ)^{23}Na is the NeNa cycle reaction with the most uncertain cross section. In the energy range relevant for astrophysics, the ^{22}Ne(p,γ)^{23}Na reaction rate is poorly known because of the contribution of a large number of resonances (fig. 3), many of which have never been observed directly [9, 16]. The mere existence of several of these energy levels, e.g. the ones corresponding to the Ep = 215 and 104 keV resonances, is even doubted [17].

The lowest-energy resonance with a directly measured strength is the one at E_p = 479 keV [18]. For the resonances below that energy, only upper limits are reported in the literature [19, 20]. For the Ep = 215 and 104 keV resonances, indirect resonance strength data have been reported [21] but later not confirmed in a more recent experiment [22].
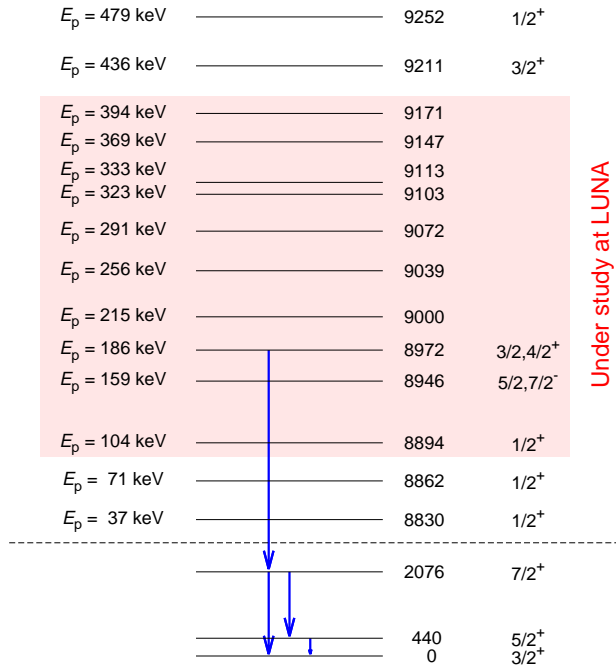
Therefore, a new study is highly desirable.

Figure 3: List of resonances in the ^{22}Ne(p,γ)^{23}Na reaction that have been discussed in the literature. The corresponding states in the ^{23}Na compound nucleus and their spin-parities, where known [17], are also shown. The γ rays detected in the $E_p = 186$ keV resonance (figs. 4 and 5) are marked with blue arrows.

2.2 Experimental setup for the HPGe-based measurement

The experimental setup for the measurement of the ^{22}Ne(p,γ)^{23}Na consists of a windowless gas target with three differential pumping stages and a gas recirculation system [23].

In summer 2013 the preparatory phase of the experiment has been completed with the study of the gas target properties. In particular, the gas density profile along the target chamber and the beam heating effect have been measured using natural neon gas. The gas density without beam has been deduced from pressure and temperature measurements at different positions inside the target chamber. The thinning of the target gas through the energy deposited by the ion beam, i.e. the so-called beam heating effect, has been studied with the resonance scan technique, using an intense ^{21}Ne(p,γ)^{22}Na resonance at 271 keV proton energy.

Subsequently, the final setup for the ^{22}Ne(p,γ)^{23}Na HPGe phase has been constructed. It consists of two HPGe detectors, one at 90° with respect to the beam direction, and the other one at 55° effective angle. The use of two high resolution detectors with well defined solid angles will allow a measurement not only of the total resonance strength, but also of the different branching ratios of the resonance decay. The two detectors are shielded by about 20 cm of lead in order to suppress the environmental background.
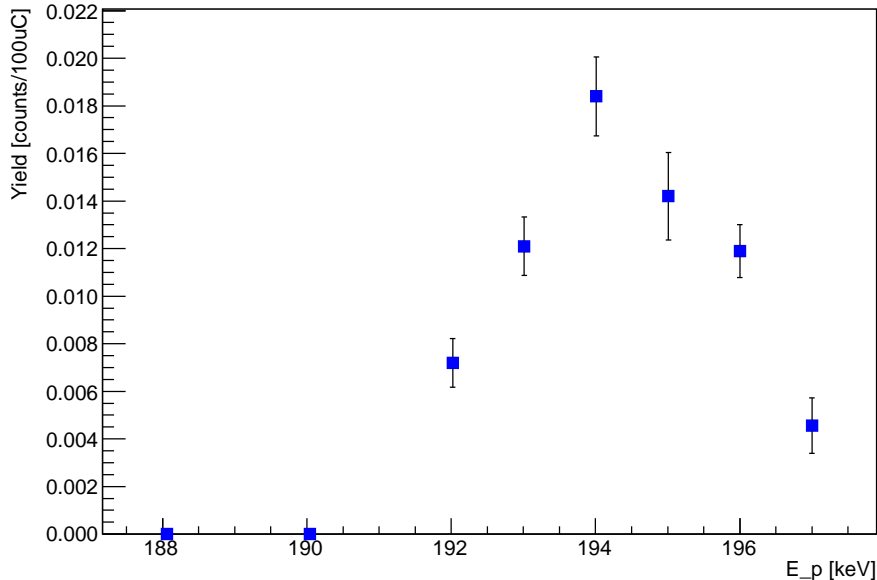
Figure 4: Scan of the ^{22}Ne(p,γ)^{23}Na resonance at $E_\mathrm{p} = 186\,\mathrm{keV}$: Yield in the $440\,\mathrm{keV}$ γ ray as a function of proton beam energy.

2.3 Data taking and preliminary results

The ^{22}Ne(p,γ)^{23}Na data taking with enriched neon-22 gas has started in late 2013. So far, the resonances at $E_\mathrm{p} = 159$, 186 keV, 256, and 323/333 keV proton energy have been detected, all of them for the first time. Previous experiments at the surface of the Earth had only resulted in upper limits [19, 20]. This clearly shows the power of the LUNA technique for measuring nuclear reaction cross sections underground.

As an example of the newly discovered resonances, fig. 4 shows the energetic resonance profile, and fig. 5 the in-beam γ-ray spectrum. The signature of the resonance is clearly seen, and the decay scheme can be deduced.

2.4 Outlook

The HPGe-detector based phase of the experiment is expected to conclude in spring 2014. This phase will establish the strengths and the decay schemes of the newly discovered resonances, and place improved limits on the other reported resonances.

As a next phase, a much higher-luminosity measurement is planned. The two shielded HPGe detectors will be replaced by a 4π summing borehole bismuth germanate (BGO) scintillator. This detector will enable γ calorimetry with its typical γ-detection efficiency of 70% [23]. The enhanced efficiency will come at the expense of resolution, however.

In the BGO-based phase of the ^{22}Ne(p,γ)^{23}Na experiment, the upper limits for un-detected resonances will be pushed to even lower levels, and it will be attempted to measure the direct-capture part of the cross section. The necessary changes in the setup are planned to be done in summer 2014, and the BGO-based measurement should start
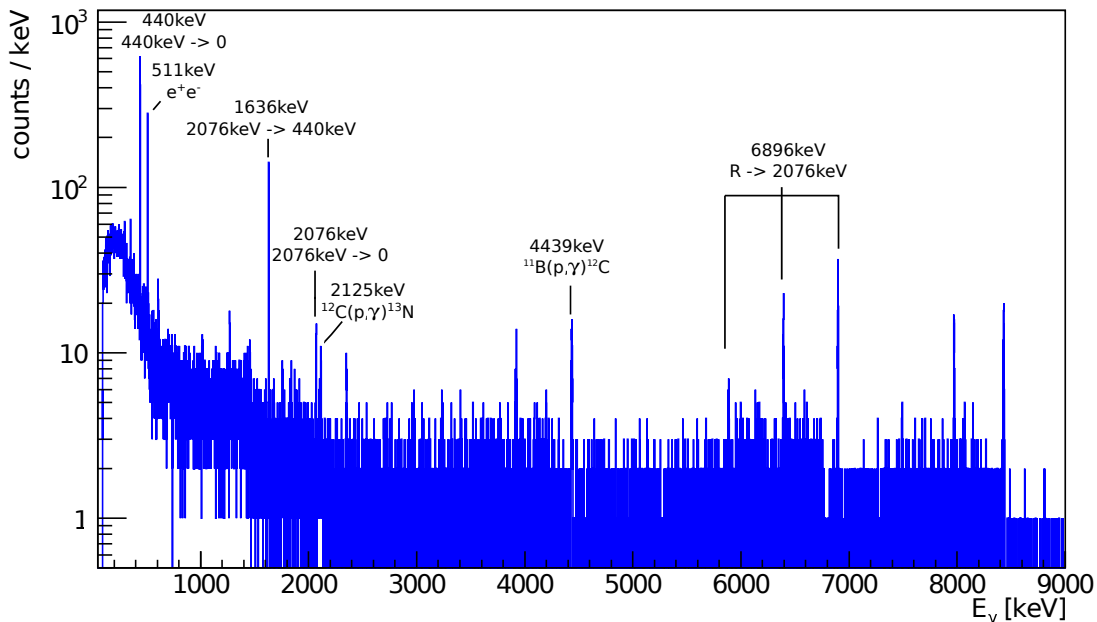
in late 2014.

Figure 5: In-beam γ-ray spectrum obtained in the 55° detector in an overnight run on top of the $E_\mathrm{p} = 186\,\mathrm{keV}$ resonance in the $^{22}\mathrm{Ne(p,\gamma)}^{23}\mathrm{Na}$ reaction.

3 The LUNA-MV project

The LUNA-MV project foresees the realization of a worldwide unique facility inside the underground Gran Sasso Laboratory centered on a 3.5 MV single-ended accelerator able to provide intense proton and alpha beams. Two different beam lines are foreseen devoted to solid and gas target experiments, respectively. This will allow us to study key reactions of the Hydrogen and Helium burning and the so-called neutron source reactions, which provide the neutron flux necessary for the slow neutron capture process. Originally, the B node site was identified as the best place inside LNGS to build such a facility, due to its position far away from the main experimental halls and to its dimensions. However, given the presence of water utilities of the Teramo aqueduct in the B node site, an official question was put to the "Istituto Superiore di Sanità" (main Health Institute) on the possible impact of the LUNA MV project and site preparation on the water quality. The official response arrived to the LNGS Director at the end of July 2013. The Director analyzed deeply the document during the summer break, together with the LNGS technical division and INFN management. At the beginning of September he communicated to the LUNA collaboration the decision of not proceeding with the installation of the LUNA-MV accelerator in the B node site since the time required for facing the legal implications of an installation in that location are considered to be unpredictable and too long thus incompatible with the timeline of the project. The Director is in contact

with the INFN management in order to find as soon as possible an alternative location inside the LNGS. Different hypothesis have already been analyzed and discussed with the collaboration but a final decision has not yet arrived. A location inside one of the main halls would have the advantage of requiring less preparation work with respect to the B node site. The LUNA collaboration and LNGS technical division have already elaborated a project of installation of the 3.5 MV accelerator with two beam lines in the Hall C (see fig.6). Shielding calculations and Montecarlo simulations of the expected neutron flux just outside the experimental area have been performed for the new configuration and demonstrate that the envisioned shielding concept based on water and boron loaded concrete allows to mantain the neutron flux produced by LUNA MV at a level of 1% with respect to the LNGS natural neutron flux. The request of almost 3 Meuros for the LUNA MV project in the framework of the "Progetti Premiali" call (year 2013) has been considered eligible for funding by the Italian Research Ministry. The total allocated budget is about 2.5 Meuros which sums to the 2.8 Meuros obtained in the previous call of the year 2012. This money will allow us to prepare the site, setup the shielding of the accelerator room and buy a commercial machine including one target beam line. Explorative efforts have been devoted to define the characteristics of the neutron detector for measuring the neutron source reactions and to study the behavior under beam of carbon targets which will be used for the $^{12}C(\alpha, \gamma)^{16}O$ reaction measurement. The collaboration is eager to start the engineering of the shielding and the technical infrastructures as well as the tendering of the accelerator itself but is still awaiting the final decision on the location of LUNA MV.
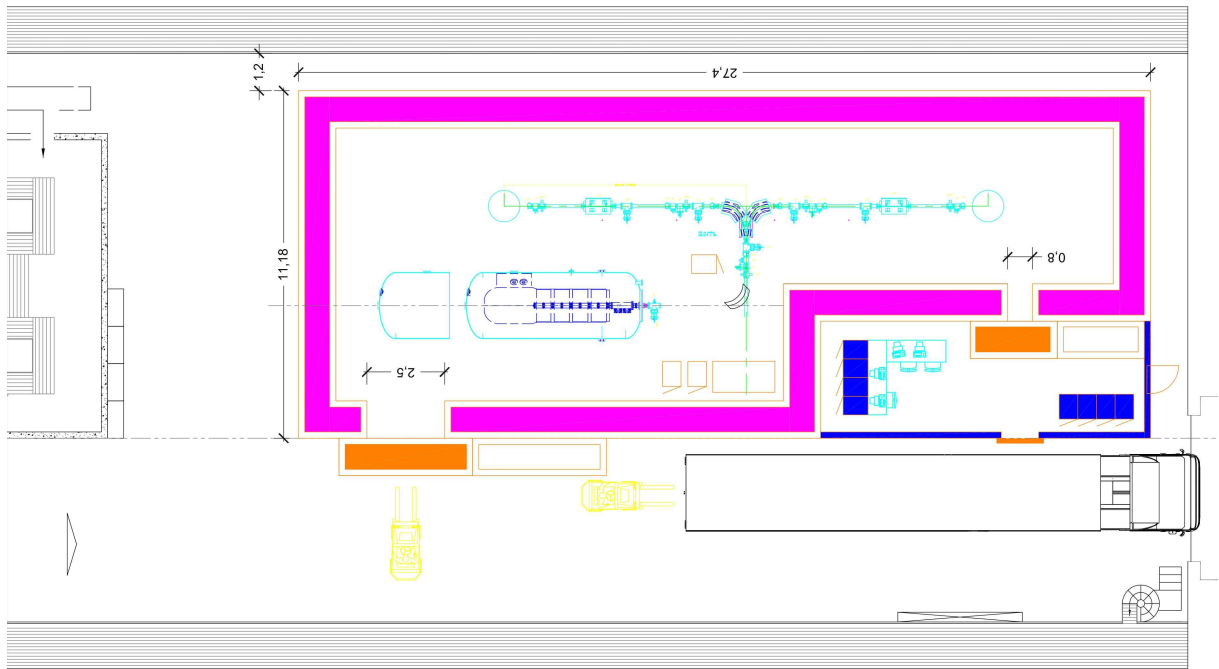

Figure 6: Preliminary sketch of the installation of the LUNA MV accelerator in the Hall C. The tank and two beam lines are indicated. A shielding composed of a sandwich of water and concrete is foreseen (pink region).

References

[1] K.M. Nollet *et al.*, The Astr. J. **582**, 1036 (2003).

[2] S. Palmerini et al., The Astr. J. **764**, 128 (2013).

[3] M. Hernanz *et al.*, The Astr. J. **526**, L97 (1999).

[4] J. José and M. Hernanz, J. of Physics G **34**, 431 (2007).

[5] D.A. Scott et al., Phys. Rev. Lett. **109**, 208001 (2012).

[6] A. Di Leva *et al.*, Phys. Rev. C **89**, 015803 (2014).

[7] A. Chafa *et al.*, Phys. Rev. Lett. **75**, 035810 (2007).

[8] J. Newton *et al.*, Phys. Rev. C **75**, 055808 (2007).

[9] C. Angulo *et al.*, Nucl. Phys. A **656**, 3 (1999).

[10] M.L. Sergi *et al.*, Phys. Rev. C **82**, 032881 (2010).

[11] A. Caciolli *et al.*, Eur. Phys. J. A **48**, 144 (2012).

[12] See URL *http://npg.dl.ac.uk/MIDAS/*

[13] H.W. Becker *et al.*, Z. Phys. A **351**, 453 (1995).

[14] C. Iliadis, *et al.*, Astrophys. J. Suppl. Ser. **142**, 105 (2002).

[15] D. A. Chamulak *et al.*, Astrophys. J. **677**, 160 (2008), 0801.1643.

[16] C. Iliadis *et al.*, Nucl. Phys. A **841**, 251 (2010).

[17] R. B. Firestone, Nucl. Data Sheets **108**, 1 (2007).

[18] R. Longland *et al.*, Phys. Rev. C **81**, 055804 (2010).

[19] J. Görres *et al.*, Nucl. Phys. A **385**, 57 (1982).

[20] J. Görres *et al.*, Nucl. Phys. A **408**, 372 (1983).

[21] J. R. Powers *et al.*, Phys. Rev. C **4**, 2030 (1971).

[22] S. E. Hale *et al.*, Phys. Rev. C **65**, 015801 (2002).

[23] C. Casella *et al.*, Nucl. Inst. Meth. A **489**, 160 (2002).

4 List of Publications

- *"Impact of a Revised $^{25}Mg(p,\gamma)^{26}Al$ Reaction Rate on the Operation of the Mg-Al Cycle"*,
O. Straniero, G. Imbriani, F. Strieder, D. Bemmerer, C. Broggini, A. Caciolli, P. Corvisiero, H. Costantini, S. Cristallo, A. DiLeva, A. Formicola, Z. Elekes, Zs. Fulop, G. Gervino, A. Guglielmetti, C. Gustavino, Gy. Gyürky, M. Junker, A. Lemut, B. Limata, M. Marta, C. Mazzocchi, R. Menegazzo, L. Piersanti, P. Prati, V. Roca, C. Rolfs, C. Alvarez, E. Somorjai, F. Terrasi, and H.-P. Trautvetter
ApJ 763 (2013) 100

- *"Neutron-induced background by an α-beam incident on a deuterium gas target and its implications for the study of the $^2H(\alpha,\gamma)^6Li$ reaction at LUNA"*,
M. Anders, D. Trezzi, A. Bellini, M. Aliotta, D. Bemmerer, C. Broggini, A. Caciolli, H. Costantini, P. Corvisiero, T. Davinson, Z. Elekes, M. Erhard, A. Formicola, Zs. Fulop, G. Gervino, A. Guglielmetti, C. Gustavinoc, Gy. Gyürky, M. Junker, A. Lemut, M. Marta, C. Mazzocchi , R. Menegazzo, P. Prati, C. Rossi Alvarez, D. Scott, E. Somorjai, O. Straniero, and T. Szucs
Eur. Phys. J A 49 (2013) 28

- *"Underground study of the $^{17}O(p,\gamma)^{18}F$ reaction relevant for explosive hydrogen burning"*,
A. Di Leva, D. A. Scott, A. Caciolli, A. Formicola, F. Strieder, M. Aliotta, M. Anders, D. Bemmerer, C. Broggini, P. Corvisiero, Z. Elekes, Zs. Fulop, G. Gervino, C. Gustavino, A. Guglielmetti, Gy. Gyürki, G. Imbriani, J. Jos, M. Junker, M. Laubenstein, R. Menegazzo, E. Napolitani, P. Prati, V. Rigato, V. Roca, E. Somorjai, C. Salvo, O. Straniero, T. Szucs, F. Terrasi, D. Trezzi
Phys. Rev. C 89 (2014) 015803

- *"Cross-section measurements at astrophysically relevant energies: The LUNA experiment"*,
A. Formicola, C.G. Bruno, A. Caciolli, F. Cavanna, R. Depalo, A. Di Leva, D.A. Scott, D. Trezzi, M. Aliotta, M. Anders, D. Bemmerer, C. Broggini, P. Corvisiero, Z. Elekes, Zs. Flp, G. Gervino, A. Guglielmetti, C. Gustavino, Gy. Gyürky, G. Imbriani, M. Junker, R. Menegazzo, P. Prati, E. Somorjai, O. Straniero, F. Strieder, T. Szuecs
Nucl. Instr. Meth. Phys. Res. A (in press)

- *"S-factor measurement of the the $^2H(\alpha,\gamma)^6Li$ reaction at energies relevant for Big-Bang nucleosynthesis"*,
M. Anders
PhD thesis Technische Universität Dresden, Dresden (Germany) 2013

- *"Direct measurement in nuclear astrophysics: ERNA and LUNA"*,
L. Gialanella and A. Guglielmetti
Scholarpedia 8(5) (2013) 11959

5 Conference and seminar contributions

- M. Anders, "Big Bang nucleosynthesis and the results of the $^2H(\alpha,\gamma)^6Li$ experiment at LUNA", talk at the DPG-Frühjahrstagung, Dresden (Germany) 04-08.03.2013

- M. Anders, "Results of the first direct measurement of the $^2H(\alpha,\gamma)^6Li$ S-factor at Big Bang energies", talk at "Nuclear Physics in Astrophysics VI", Lisbon (Portugal) 19-24.05.2013

- C. Broggini, "Hydrogen and Helium burning studied at Gran Sasso" invited seminar at "The international school on nuclear physics, 35th course, neutrino physics: present and future", Erice (Italy) 16-25.09.2013

- C. Broggini, "Luna and the Sun" invited seminar at "The seventh european summer school on experimental nuclear astrophysics", Santa Tecla (Italy) 15-27.09.2013

- C. Broggini, "L'esperimento Luna" invited lesson at "XXIII giornate di studio sui rivelatori, scuola INFN F. Bonaudi", Torino (Italy) 22-25.10.2013

- A. Caciolli, "Studying stars by going underground: the LUNA experiment at Gran Sasso Laboratory", invited talk at "XXXIII Mazurian Lakes Conference on Physics", Piaski (Poland) 01-07.09.2013

- F. Cavanna, "Exploring the ^{22}Ne(p,γ)^{23}Na reaction at LUNA and at HZDR", talk at "Seventh European summer school on experimental nuclear astrophysics", Santa Tecla (Italy) 14-27.09.2013

- F. Cavanna, "Exploring the ^{22}Ne(p,γ)^{23}Na reaction at LUNA", poster at "INPC: International Nuclear Physics Conference 2013", Firenze (Italy) 02-07.06.2013

- F. Cavanna, "The LUNA-MV project", talk at the workshop "Open problems and future directions in heavy element nucleosynthesis", ATOMKI Debrecen (Hungary) 10-12.04.2013

- R. Depalo, "Towards the study of ^{22}Ne(p,γ)^{23}Na at LUNA in Gran Sasso", poster at "XV International Workshop on Neutrino Telescopes" Venezia (Italy) 11-15.03.2013

- R. Depalo, "Towards the study of ^{22}Ne(p,γ)^{23}Na at LUNA" poster at "Nuclear Physics in Astrophysics VI", Lisbon (Portugal) 19-24.05.2013

- R. Depalo, "Underground study of the ^{22}Ne(p,γ)^{23}Na reaction and its role in stellar nucleosynthesis" talk at "International School of Subnuclear Physics", Erice (Italy) 24.06-03.07.2013

- R. Depalo, "Esperimento LUNA: Studiare le stelle sotto il Gran Sasso", invited talk at "Incontri di Fisica 2013", INFN - Laboratori Nazionali di Frascati (Italy) 08-10.10.2013

- A. Formicola, "Cross section measurements of fusion reactions at astrophysically relevant energies: the LUNA experiment" invited talk at "RICAP-13 Roma International Conference on AstroParticle Physics", Rome (Italy) 22-24.05.2013

- A. Guglielmetti, "The LUNA-MV project at Gran Sasso laboratory", invited talk at "Second NEDENSAA NuPNET project meeting", Acireale (Italy) 20-22.02.2013

- A. Guglielmetti, "Studying stars by going underground: the LUNA experiment at Gran Sasso Laboratory", invited talk at "INPC: International Nuclear Physics Conference 2013", Firenze (Italy) 02-07.06.2013

- A. Guglielmetti, "Nuclear astrophysics and underground accelerators", invited plenary review talk at "TAUP: Topics in Astroparticle and Underground Physics 2013", Asilomar (United States) 08-13.09.2013

- A. Guglielmetti, "The LUNA experiment at Gran Sasso Laboratory: studying stars by going underground", invited talk at "Direct Measurements in Nuclear Astrophysics with Recoil Mass Separators", Caserta (Italy) 04-05.10.2013

- A. Guglielmetti, "The LUNA experiment at Gran Sasso Laboratory", invited talk at "Wigner 111 - Colourful & Deep", Budapest (Hungary) 11-14.11.2013

- A. Guglielmetti, "Measuring stars by going underground: the LUNA experiment at Gran Sasso Laboratory", invited seminar at Notre Dame University (United States) 26.09.2013

- C. Gustavino, "The Underground Nuclear Astrophysics in the Precision Era of BBN: Present Results and Future Perspectives", poster at "Nuclear Physics in Astrophysics VI", Lisbon (Portugal) 19-24.05.2013

- C. Gustavino, "The ^{2}H$(\alpha,\gamma)^6$Li experiment at LUNA" poster at "INPC: International Nuclear Physics Conference 2013", Firenze (Italy) 02-07.06.2013

- G. Imbriani, "Underground experiments and their impact on stellar modeling", invited talk at "The origin of cosmic elements: past and present achievements, future challenges", Barcelona (Spain) 12-15.06.2013

- G. Imbriani, "Nuclear reactions of interest in astrophysics", invited talk at "XXXVI Brazilian Meeting on Nuclear Physics Maresias Beach", São Sebastião (Brazil) 01-05.09.2013

- M. Junker, "Stellar cross section measurements in Gran Sasso", invited talk at "Second workshop on Stellar Opacities", Bordeaux (France) 27-28.02.2013

- M. Junker, "Experiences and Prospects of Nuclear Astrophysics in Underground Laboratories", keynote talk at "Nuclear Physics in Astrophysics VI", Lisbon (Portugal) 19-24.05.2013

- M. Junker, "Low Energy Measurements at Gran Sasso", invited lecture at "Seventh European summer school on experimental nuclear astrophysics", Santa Tecla (Italy) 15-27.09.2013

- M. Junker, "The LUNA Experiment at LNGS", talk at Gentner Colloquium, Max-Planck Institut fuer Kernphysik, Heidelberg (Germany) 16.12.2013

- R. Menegazzo, "Astrophysical S-factor for the $^1 7O(p,\gamma)^1 8F$ reaction at Novae energy", invited talk at "INPC: International Nuclear Physics Conference 2013", Firenze (Italy) 02-07.06.2013

- R. Menegazzo, "The LUNA experiment at the Gran Sasso Laboratory", invited talk at "XCIX Congresso Nazionale Società Italiana di Fisica", Trieste (Italy) 23-27.09.2013

- D. Scott, "Underground Measurement of the $^1 7O(p,\gamma)^1 8F$ Reaction", poster at "Nuclear Physics in Astrophysics VI", Lisbon (Portugal) 19-24.05.2013

- F. Strieder, "LUNA-MV-The next Underground Accelerator Facility", talk at "EuroGENESIS Workshop-Origin of the Elements", Barcelona (Spain) 10-15.06.2013

- D. Trezzi, "Physics cases of LUNA MV", seminar at INFN - Laboratori Nazionali del Gran Sasso (Italy) 19.03.2013

2013 LVD STATUS REPORT

The LVD Collaboration

N.Yu.Agafonova[7], M.Aglietta[8], P.Antonioli[1], V.V.Ashikhmin[7], G.Bari[1], R.Bertoni[8],
V.V.Boyarkin[7], E.Bressan[1], G.Bruno[5], V.L.Dadykin[7], W.Fulgione[8], P.Galeotti[8],
M.Garbini[1], P.L.Ghia[2], P.Giusti[1], F.Gomez[8], E.Kemp[3], V.B.Korchaguin[7], A.S.Mal'gin[7],
B.Miguez[3], A.Molinario[8], R.Persiani[1], I.A.Pless[6], A.Romero[8], V.G.Ryasny[7],
O.G.Ryazhskaya[7], O.Saavedra[8], G.Sartorelli[1], M.Selvi[1], I.R.Shakiryanova[7],
G.C.Trinchero[8], M.Ventura[4], C.Vigorito[8], V.F.Yakushev[7], A.Zichichi[1]

[1] *University of Bologna and INFN-Bologna, Italy*
[2] *CNRS-IN2P3, Paris, France*
[3] *University of Campinas, Campinas, Brazil*
[4] *INFN-LNF, Frascati, Italy*
[5] *INFN-LNGS, Assergi, Italy*
[6] *Massachusetts Institute of Technology, Cambridge, USA*
[7] *Institute for Nuclear Research, Russian Academy of Sciences, Moscow, Russia*
[8] *INFN-Torino, INAF-OATO, Torino and University of Torino, Italy*

Abstract

The Large Volume Detector (LVD) in the INFN Gran Sasso National Laboratory, Italy, is a neutrino observatory mainly designed to study low energy neutrinos from core collapse supernovae. The experiment has been monitoring the Galaxy since June 1992, under increasing larger configurations, in January 2001 it has reached its present active mass $M = 1$ kt. No neutrino burst candidate has been found over 7212 days of live-time, the resulting 90% C.L. upper limit to the rate of gravitational stellar collapses in the Galaxy ($D \leq 25$ kpc) is 0.116 yr^{-1}.

Since July 2005 has been member of the Supernovae Early Warning System (SNEWS) project, the network of neutrino observatories whose aim is to provide the astronomical community with a prompt ad confident alert of the occurrence of a galactic supernova event.

Since 2006 LVD has been acting as a far-monitor of the CNGS project, the high energy, wide band ν_μ beam, set up at Cern and sent towards the INFN Gran Sasso National Laboratory, for the observation of the ν_τ appearance, through neutrino flavor oscillation. In 2012 LVD gave a primary contribution to establish the inconsistency of the OPERA result of a superluminal neutrino velocity and furthermore confirmed that the neutrino speed is compatible with c, its deviation being $< 3.8 \cdot 10^{-6}$ at 99% C.L.. The sensitivity of this measurement was by one order of magnitude better than that of previous ones in a similar energy range.

1   Introduction

The detection of neutrinos from SN1987A, first observation of neutrinos from extrasolar origin, marked the beginning of the experimental phase of neutrino astrophysics [Hirata et al.(1987), Bionta et al.(1987), Alekseev et al.(1987)] and [Aglietta et al.(1987)]. Core collapse supernovae are the known most powerful neutrino emitters. While the observation of neutrinos from SN1987A was guided by the optical observation, currently running ν detectors must be able to identify a neutrino burst even in the absence of an electromagnetic counterpart. Neutrinos can actually travel across our Galaxy and reach the Earth were they can be identified, while light gets partially or totally absorbed by dust in the Galactic plane. As the great part (~ 80 %) of core collapse supernovae in our Galaxy are not visible through their light emission, neutrino detection is in many cases the only possibility to detect and study these events. In the presence of an electromagnetic counterpart, on the other hand, the prompt identification of the neutrino signal could alert the worldwide network of observatories [Antonioli et al.(2004)] allowing to study many aspects of the rare event from its onset.

Previous direct searches of supernova neutrino bursts from our Galaxy have given null results [Dye et al.(1989)]; [Ahrens et al.(2002)]; [Alekseev & Alexeyeva (2002)]; [Ambrosio et al.(2004)]; [Novoseltseva et al.(2011)]. The Super-Kamiokande Collaboration set an upper limit at 90% c.l. for the supernova explosion rate out to 100 kpc of 0.32 per year [Ikeda et al.(2007)].

The Large Volume Detector (LVD), in the INFN Gran Sasso National Laboratory (Italy), at the depth of 3600 m of water equivalent, is a one kiloton liquid scintillator

detector [Aglietta et al.(1992)]. It consists of an array of 840 scintillator counters, 1.5 m^3 each, viewed from the top by three photomultipliers (PMTs), 2520 in total, arranged in 105 modules hosting clusters of 8 counters. The whole array is divided in three identical towers with independent power supplies, trigger, absolute clock and data acquisition, DAQ.

LVD started the commissioning phase in February 1992 for five months till June 1992, mainly dedicated to stabilize the DAQ system. Since June 6th 1992, with the first tower completely built, the detector started the first science run. The experiment has been running under increasing larger configurations since then and in January 2001, with the completion of the last tower, it reached its final layout: the scintillator mass of one kton. Thanks to its modularity and dedicated DAQ system LVD allows a very high duty cycle. It can be serviced during data taking and in case of failures, the neutrino observatory automatically remove the not properly working region and reconfigures itself at lower mass. The effect is to adjust dynamically the LVD active mass, M_{act}.

Neutrinos can be detected in LVD through charged current (CC) and neutral current (NC) interactions on proton, Carbon nuclei and electrons of the liquid scintillator. The iron support structure of the detector, whose total mass is about 0.85 kt can also act as a target for neutrinos and antineutrinos, with a certain probability that the product of the interaction may reach the liquid scintillator and be detected [Agafonova et al.(2007-a)]. The total LVD target consists of:

free protons - 8.313 x 10^{31}

C nuclei - 4.267 x 10^{31}

Fe nuclei - 9.7 x 10^{30}

electrons - 3.393 x 10^{32}

Neutrino interaction channels, relevant to the detector, are reported here:

$$\bar{\nu}_e + p \rightarrow e^+ + n \qquad \text{(1.8 MeV)} \quad \text{(88\%)} \tag{1}$$

$$\nu_e + {}^{12}C \rightarrow {}^{12}N + e^- \qquad \text{(17.3 MeV)} \quad \text{(1.5\%)} \tag{2}$$

$$\bar{\nu}_e + {}^{12}C \rightarrow {}^{12}B + e^+ \qquad \text{(14.4 MeV)} \quad \text{(1.0\%)} \tag{3}$$

$$\nu_i + {}^{12}C \rightarrow \nu_i + {}^{12}C^* + \gamma \qquad \text{(15.1 MeV)} \quad \text{(2.0\%)} \tag{4}$$

$$\nu_i + e^- \rightarrow \nu_i + e^- \qquad \text{(--)} \quad \text{(3.0\%)} \tag{5}$$

$$\nu_e + {}^{56}Fe \rightarrow {}^{56}Co^* + e^- \qquad \text{(10. MeV)} \quad \text{(3.0\%)} \tag{6}$$

$$\bar{\nu}_e + {}^{56}Fe \rightarrow {}^{56}Mn + e^+ \qquad \text{(12.5 MeV)} \quad \text{(0.5\%)} \tag{7}$$

$$\nu_i + {}^{56}Fe \rightarrow \nu_i + {}^{56}Fe^* + \gamma \qquad \text{(15. MeV)} \quad \text{(2.0\%)} \tag{8}$$

Cross sections of different interactions are obtained referring to [Strumia & Vissani(2010)] for interaction 1, [Fukugita et al.(1988)] for interactions 2 and 4, [Bahcall et al.(1995)] for interaction 5 and [Kolbe & Langanke(2001)] and [Toivanen et al.(2001)] for interactions 6 and 8.

The main neutrino reaction in hydrogenate targets, at the typical energy of neutrino from gravitational stellar collapses (GSC), is the inverse beta decay, IBD, (1) which gives two detectable signals: the prompt one due to the e$^+$ (visible energy $E_{vis} \simeq E_{\bar{\nu}_e} - 1.8$ MeV

+ 2 $m_e c^2$) followed by the signal from the np $\rightarrow$ dγ capture ($E_\gamma = 2.2$ MeV, mean capture time $\simeq 185$ μs).

At present a universally accepted model of neutrino emission associated with GSC does not exist. This is due to the great complexity of the problem, in which all known forces interplay with each other in extreme physical conditions. The critical role of neutrinos for the energy transport, as first suggested in [Colgate & White(1966)], is however generally accepted. A few other points are nowadays well established. The total energy of the collapse, the binding energy of the future neutron star, is between 2 and 3 $\cdot 10^{53}$ erg, and 99% of this is delivered by neutrino emission. The formation of a region where neutrinos are trapped determines the time scale of this emission, as confirmed by the observation of neutrino from SN1987A, of the order of ten seconds.

There has been a wide discussion whether SN1987A data show an hint of the presence of an accretion phase, which would occur in the first stage of neutrino emission. Important reference in this discussion is the paper by Loredo and Lamb [Loredo & Lamb(2002)] where it is argued that the SN1987A observations can be used to claim for an evidence of the accretion phase.

The neutrino-driven mechanism [Bethe & Wilson(1985)], or delayed scenario for the explosion, has been the most studied so far. In this scenario the explosion of the massive star receives crucial assistance from the energy deposition due to an initial, intense neutrino luminosity. Simulations based on this model have given different estimations of mean energies and luminosity of neutrino emission. In particular early one-dimensional simulations gave quite different results for the mean energies of various neutrino flavors (10-12 MeV for ν_e, 11-17 MeV for $\bar{\nu}_e$, 15-24 MeV for $\nu_\mu, \bar{\nu}_\mu$, $\nu_\tau, \bar{\nu}_\tau$, hereafter ν_x) [Totani et al.(1998)]. However, recent studies [Tamborra et al.(2012)], [Janka(2012)] show a tendency towards lower values for the mean energies as well as a smaller spread among them. It should be noted though that models, assuming a quite different scenario, have been proposed enlarging the theoretical panorama [Imshennik & Ryazhskaya(2004)].

A parallel approach to this problem is the attempt to parameterize the neutrino emission, of which a remarkable example can be found in [Keil et al.(2003)]. Another work [Pagliaroli et al.(2009)] considers the microscopic processes of the collapse to build a parameterization of the neutrino emission, which comprehends both an accretion and a cooling phase. The free parameters are then determined with a maximum likelihood procedure on the data from SN1987A.

We refer to this study for an estimation of the neutrino signal from a GSC in LVD. MSW effect while crossing the matter of the collapsing star [Wolfenstein(1978)], [Mikheev & Smirnov(1985)] is taken into account, while ν-ν interactions are neglected. The normal mass hierarchy scenario has been assumed together with the most recent values of θ_{12} and mass squared differences Δm_{12}^2 and Δm_{23}^2. In this scenario the recent discovery of a non null value for θ_{13} mixing angle [An et al.(2012)] has no significant impact on the expected neutrino signal. We find that a total of about 300 events would be detected in LVD (1kt) for a GSC at 10 kpc from the Earth. They would be shared among the possible interaction channels as shown in the previous table. Focusing on the Inverse Beta Decay (IBD) interaction (1), it results that 250 of these signals would be recorded (and recognized) in LVD, which is quite on the conservative side. The neutrino signal is expected to develop on a time scale of 20 s, being 90% (50%) the fraction of

detected events in the first 10s (1s).

The LVD neutrino burst sensitivity for different selection algorithms and energy cuts, E_{cut}, has been exhaustively discussed in [Agafonova et al.(2008)] for real background conditions. The highest sensitivity can be achieved, in LVD, for $E_{cut} = 10$MeV, $\Delta t = 10$ seconds and without any additional selection criterium based on the expected neutrino flavor content. Different choices on the duration of the time interval Δt, based on model predictions, and supported by the SN1987A data, increase the model dependence of the search without introducing an important improvement in sensitivity.

LVD working stand alone, with an imitation frequency threshold, F_{im}, of one fake event every 100 years, reaches the sensitivity shown in figure 1, calculated for $E_{cut} = 10$ MeV and for $300 \leq M_{act} \leq 1000$ ton. Even in this very conservative panorama, LVD results to be observing, with full efficiency, a region of space centered in the Earth with radius 25 kpc as long as its active mass remains greater than 300 tons.
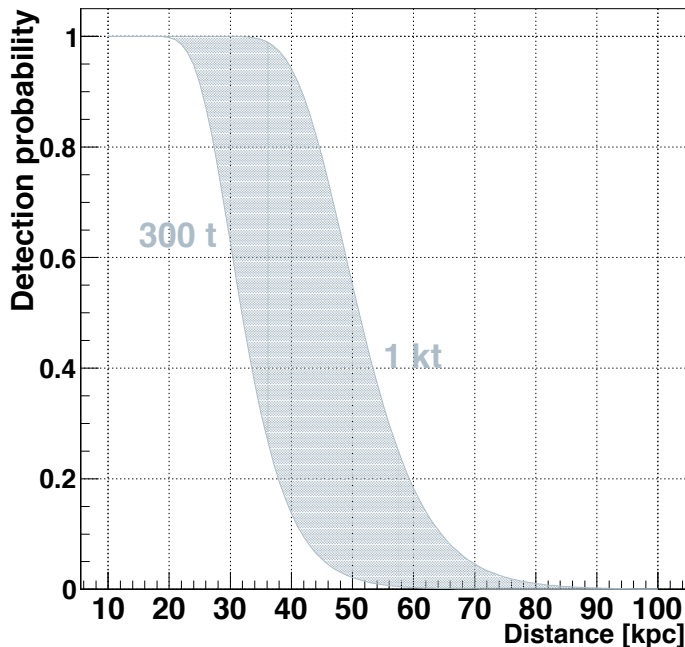
Figure 1: *LVD efficiency versus distance for E_{cut}=10MeV and active mass, M_{act}, between 300 and 1000 ton.*

2 Core Collapse SN Monitor

2.1 Data set

The whole LVD data taking can be devided in 2 periods according to slightly different values of the trigger threshold. In the first period, from June 6th, 1992, to December, 31st, 2003, the hardware trigger energy threshold was set to $\mathcal{E}_H \simeq 5$ MeV, for the core counters, i.e., counters not directly exposed to the rock radioactivity which represent 47%
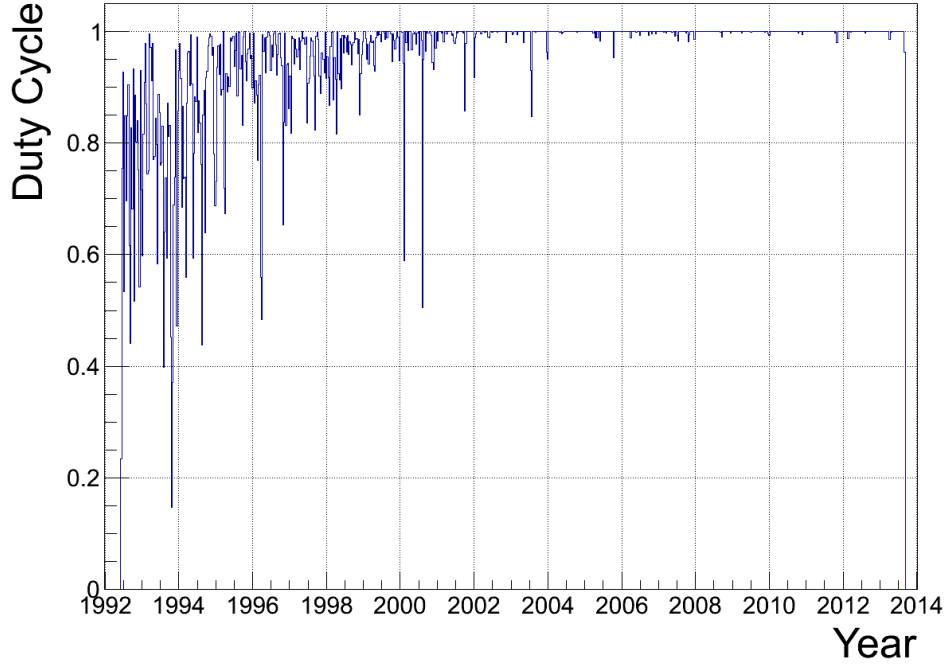
Figure 2: *LVD duty Cycle as a function of time.*

of the total, and $\mathcal{E}_H \simeq 7$ MeV, for external ones. In the second period, from January 1st, 2004 up to now, the trigger energy threshold of the array was set uniformly to $\mathcal{E}_H \simeq 4$ MeV. A secondary energy threshold, $\mathcal{E}_L \simeq 0.5$ MeV, to detect gammas from n-captures, is enabled during 1 ms after the occurrence of each trigger and remained unchanged during both periods. Duty cycle of the detector, averaged over 10 days windows, is shown in figure 2. Fluctuations on the duty cycle, after the construction period, are mainly due to maintenance activity. The duty cycle of the whole data set achieves 95.8% (99.6% since 2001 and 99.8% since 2008).

The detector active mass, M_{act}, is dynamically adjusted. M_{act} is continuously monitored through the atmospheric muon flux. The muon rate observed by the whole LVD array is 0.097 ± 0.01 muons per second, while each counter detects, on average, 1.8 muons per hour. The detector active mass is updated every 8 hours by considering the counters that detected at least one muon in this period. Quality cuts on single counters are applied at this level to determine the reliable active mass of the detector:

- The response to atmospheric muons is used to identify and discard bad working counters, problems that are mainly due to electronic failures.

- Counters with a background rate $R(E \geq 7MeV) \geq 3 \cdot 10^{-3} s^{-1}$ [Agafonova et al.(2008)] are rejected as noisy. On average this problem regards less than 2% of the counters.

LVD active mass, M_{act}, as a function of time is shown in figure 3. From June 9th 1992 to August 31st 2013 M_{act} remained greater than 300 t during 7212 days.
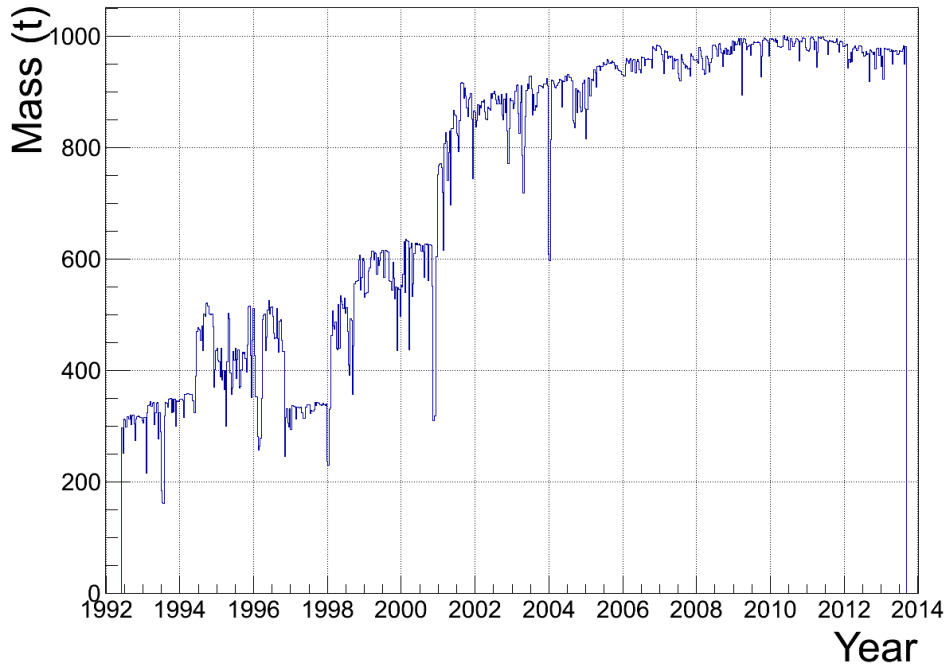
Figure 3: *LVD active mass as a function of time. M_{act} remained greater than the 300 t limit during 7212 days, from June 9th 1992 to August 31st 2013.*

2.2 Selection criteria

Most accredited model and numerical experiments predict that in core collapse supernovae neutrinos emission occur in three main phases:

- ν_e are emitted in shock breakout, when ν_e produced in electron captures (neutronization) are freed by the passage of the shock wave trough the neutrino sphere, duration few milliseconds;

- ν_e and $\bar{\nu}_e$ are emitted during the accretion phase, whose duration, around 500 ms, will determine the future evolution of the collapse;

- neutrinos and antineutrinos, ν_i and $\bar{\nu}_i$, of all flavors are emitted during the thermal cooling, duration few tents of seconds.

Average energy of emitted neutrinos ranges between 10 and 25 MeV, energy spectra are approximately thermal. On the bases of these expectations the data set dedicated to the search for neutrino burst must be free from the atmospheric muon component and limited to a convenient energy window to cut most of the background due to radioactivity. For these reasons the following cuts on single events are applied:

- coincident events in 2 or more counters within 200 ns, are rejected as muon candidates. To avoid the contamination of any signal associated with muon interactions inside the detector or in the surrounding rock, a dead time of 1 ms is applied after each muon event. This cut introduces a dead time, $t_{dead} \leq 0.01\%$, corresponding to less than 1 hour per year. The possibility that the product of a neutrino interaction involves more than one counter (and for this reason is rejected) has been evaluated in [Antonioli et al.(1991)]. Convolving this probability with the expected energy

140

spectra we obtain that about 3% of neutrino interactions will be excluded from the following burst candidate selection process because of this cut. In case of a positive detection, i.e., the burst identification, these events will be recovered.

- According to the expected signal, the energy of the trigger events are selected in the range $E_{cut} \leq E_{trigger} \leq 100 \ MeV$. Two energy ranges are considered with $E_{cut} = 7 \ MeV$ and $10 \ MeV$. Radioactivity background is highly suppressed at these energies, while the impact on the expected signal is negligible because of the energy dependence of the cross sections.

Moreover applying these two filters, in particular the second one, the rate becomes almost independent from the local hardware configuration and the effect due to the threshold change is negligible.

The core of the algorithm for the neutrino bursts candidate selection consists in the search for a cluster of signals within a fixed time window, Δt. The burst candidate is simply characterized by its multiplicity m, i.e., the number of events detected during Δt and Δt itself. All the other characteristics of the cluster, as its topological distribution inside the detector, the detailed time structure, energy spectrum and ν flavor content, are left to a subsequent independent analysis (consistency check). A set of dedicated cuts are introduced in the process of burst candidate selection. They are occasionally applied to disentangle and reject local fluctuations of the trigger rate due to temporary failures, electric noise or human activities in the experiment. They can involve single counters (S-Cut) or sets of counters which are in some way connected as modules (M-Cut) or groups (G-Cut).

All these cuts are based on the simple requirement that events belonging to the cluster are due to low energy neutrinos that, because of their huge mean free path, are expected to interact uniformly inside an array made by elements with same detection efficiency. After applying the cut, the cluster is reanalyzed with the new multiplicity $m' = m - m_i$ and new background rate, f'_{bk}. We refer to these cuts as *topological cuts*. Their effects are carefully monitored along data taking and processing. For clusters that, before applying topological cuts, had an imitation frequency lower than 1 per month, an individual inspection is performed. The majority of these downgraded clusters are due to electronics failures, in particular TDC failures impacting muon rejection. It is not rare to see that the increasing of the number of downgraded clusters is correlated with a decreased number of recognized muons.

2.3 Results

At the end of the data selection and after applying topological cuts, the LVD background data should behaves as a stochastic series well described by the Poisson statistic independently from the local hardware configuration.

In the search for a cluster of events within a fixed time window, Δt, each data period, T, is scanned through a "sliding window" with duration Δt=20s, that is, it is divided into N=$\frac{T}{\Delta t}$ intervals. This process has been repeated twice, where the Δt windows are

relatively shifted of $\Delta t/2$. In this way the unbiased time window is 10s. The expected frequency of clusters of duration 20s and multiplicity $\geq m$, due to background, is:

$$F_{im}(m, f_{\text{bk}}) = C \cdot \sum_{k \geq m} P(k; 20 \cdot f_{\text{bk}}) \; ev \cdot day^{-1} \qquad (9)$$

where f_{bk} is the background counting rate of the detector for visible energy, $E_{\text{vis}} \geq E_{\text{cut}}$ ($E_{cut} = 10\text{MeV}$ in this analysis), $P(k; f_{\text{bk}}\Delta t)$ is the Poisson probability to have clusters of multiplicity k if $f_{\text{bk}}\Delta t$ is the average background multiplicity, and $C = 86400/(2 \cdot \Delta t)$ is the number of trials per day.

Indeed, a candidate burst is defined by its multiplicity to which, for a known background rate, an imitation frequency is associated (through eq.9). F_{im}^{-1} thus represents the significance of the detected cluster defined as the average time you have to wait for a fake event originated by the Poissonian background [Agafonova et al.(2008)].

To check the performance of the selection procedure and to validate the reliability of the algorithm to reproduce background fluctuations, a number of test had been performed in the past and are periodically repeated. We simulate clusters of events in a subset of counters equipped with a LED system. We test, and online continuously monitor, the cluster selection criteria at low thresholds, i.e., with $F_{im} \leq 1 \cdot \text{day}^{-1}$, $1 \cdot \text{week}^{-1}$, $1 \cdot \text{month}^{-1}$. While for LVD working standalone a detected cluster is considered a candidate neutrino burst only if its significance is higher than 100 years. This request is relaxed to 1 month when working in coincidence with other detectors in the SNEWS project [Antonioli et al.(2004)].

The comparison between expected and detected clusters in the whole period and for different imitation frequencies, F_{im}, is summarized in table 1.

Table 1: *Comparison between expected and detected clusters in the period from 6-9-1992 to 8-31-2013.*

	$F_{im} \leq 1/\text{day}$	$F_{im} \leq 1/\text{week}$	$F_{im} \leq 1/\text{month}$
expected	2224	416	74
detected	2261	418	97

On the bases of these results, we conclude that:
- the detector behavior has been under control during the whole period of data taking;
- the method used in the search for neutrino burst candidates is reliable and
- the threshold of the F_{im} set at 1 every 100 year, in the standalone search, is a reasonable choice.

All the clusters of Table 1 are shown in figure 4. Among them, 97 with significance $F_{im}^{-1} > 1$ month (74 were expected) have been individually inspected and resulted fully compatible with chance coincidences among background signals. Ten have a significance better than 1 year (against 5 expected). The maximum detected significance was $F_{im}^{-1} = 5$

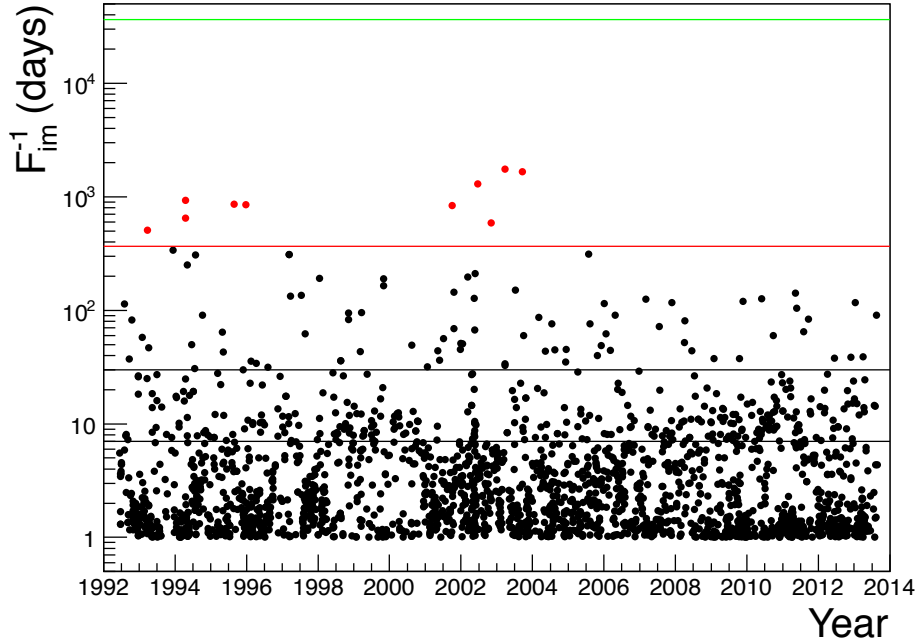years, in two clusters, being 100 years the significance necessary to have a neutrino burst

Figure 4: *Detected clusters: in red clusters whose significance is better than $F_{im}^{-1} \geq 1$ year.*

candidate. Furthermore, in case of detection, the neutrino burst candidate will be sent to a second level analysis, which aims at studying the consistency of these clusters with the features of a real neutrino burst. This second level analysis is called consistency check[1].

LVD has been observing the Galaxy searching for neutrino bursts from core collapse SN since June 1992. The detector is considered active only if its active mass, M_{act}, was at least 300 t, being, in this way, fully sensitive to core collapse SN occurring at a distance $D \leq 25$ kpc from the Earth. No neutrino burst candidate has been detected during 7212 days, from June 9th 1992 to August 31st 2013. The corresponding upper limit on the rate of gravitational stellar collapse at 90% C.L. is: 0.116 year^{-1}. This is the most stringent limit to date achieved by the direct observation of the entire Galaxy searching for neutrino bursts.

3 CNGS beam monitor and the neutrino speed

Since 2006 LVD has been acting as a far-monitor of the CNGS beam [Aglietta et al.(2004)] [Agafonova et al.(2007-b)]. Muons, produced by charged current interactions of muon neutrinos in the rock, are responsible for the bulk ($\sim 80\%$) of CNGS events in LVD. At the nominal intensity 4.510^{19} p.o.t./y the LVD event rate corresponds to more than 100 CNGS events per day, against a practically negligible background.

In 2012, as a consequence of the neutrino time of flight measurement performed by OPERA experiment, unexpectedly showing evidence for superluminal propagation of ν_μ

---

[1]In the SNEWS project, the required coincidence with other detectors is considered, by LVD, the main instrument to confirm the reliability of the alarm. No additional test on the detected cluster is performed in this case before sending the alarm to the central server if the cluster has $F_{im} \leq 1/month$.
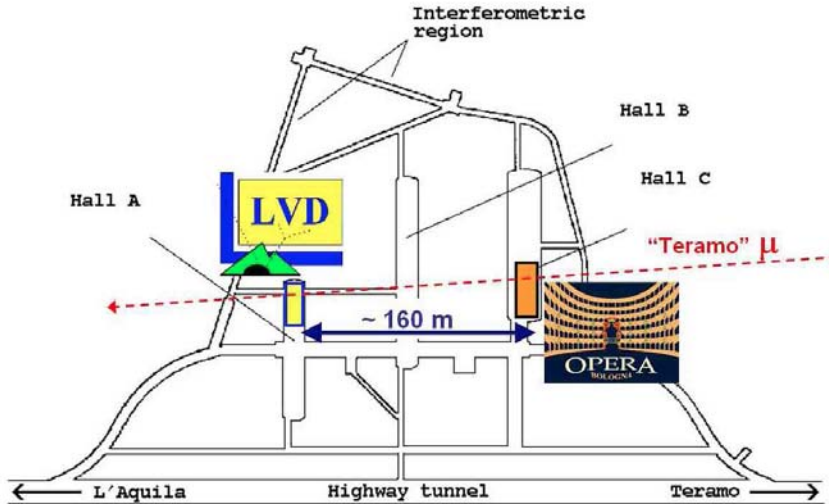
Figure 5: *Sketch of the LNGS map with the position of the LVD and OPERA experiments.*

neutrinos, we studied the sample of cosmic muon events in time coincidence between the LVD and OPERA detectors, during a calendar time period from mid 2007 until 2012, for a total live time of about 1200 days. In a time-window of $1\mu s$, and excluding events in time with the CNGS beam spill, we found 306 events due to single muons entering horizontally from the OPERA side and going through the LVD detector. Indeed, the OPERA-LVD direction lies along the so-called Teramo valley, where the Gran Sasso mountain profile exhibits small depths even in the horizontal direction. Visual inspection confirms this pattern. See in fig. 5 a sketch of the LNGS with the position of the two detectors and the direction of those muons.
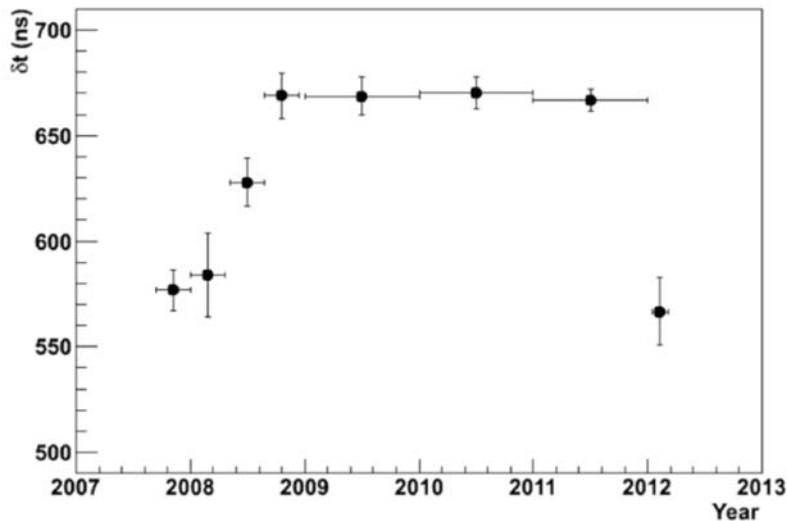
Figure 6: *Distribution of $\delta t = t_{LVD} - t_{OPERA}$ for the 306 events inside 1 μs time coincidence.*

The calendar time evolution of the time difference $\delta t = t_{LVD} - t_{OPERA}$ for various periods of data-taking shows a variation of the average value in each period larger than

144

statistical uncertainties. This behavior, shown in fig.6, corresponds to a negative time shift for OPERA of the same order of the excess leading to a neutrino velocity higher than the speed of light.

Further checks of the OPERA experimental apparatus showed evidence for equipment malfunctioning. The result of this joint analysis provided a check that was totally independent from the TOF measurements of CNGS neutrino events, pointing to the existence of a possible systematic effect in the OPERA neutrino velocity analysis [Agafonova et al.(2012-a)].

Furthermore, to allow a more accurate neutrino time of flight measurement, from May 10th to May 24th, 2012, the CERN-SPS accelerator was operated with a new beam structure. This structure was made of four batches separated by about 300 ns, with 16 bunches per batch, with a narrow width of ~3 ns each, separated by 100 ns. For this occasion, a new High Precision Time Facility (HPTF), designed by the Borexino collaboration, was installed in the external buildings of the LNGS. In view of the new neutrino beam, LVD modified a subset of counters, with the aim of improving their timing performances. We have chosen 58 of them (Super-Set, see fig. 7) to maximize the acceptance with respect to CNGS neutrinos while minimizing the number of detectors to be modified. From data taken since 2006 from the CNGS beam we have learnt that the Super-Set counters were involved in 40% of the CNGS events detected by LVD, while
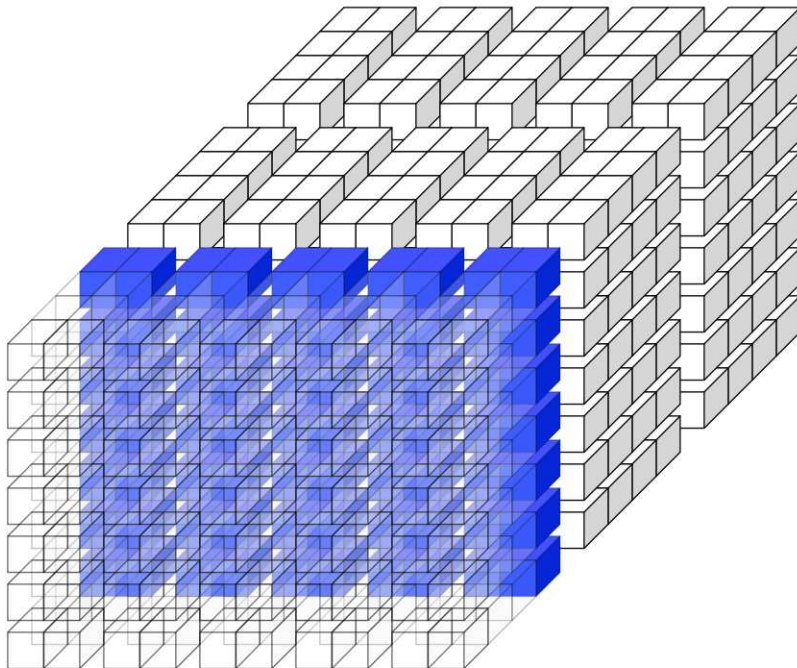
Figure 7: *Schema of LVD counters. The blue ones represent the Super-Set, see text.*

On the one hand, to avoid time fluctuations in the trigger formation at the single-

counter level, we have modified the cabling of the PMTs, by delaying only one of them. The change guarantees that the 3-fold coincidence among the PMTs in every counter is always formed due to the same tube. On the other hand, to perform a measurement of the transit time in each counter, we have equipped them with a LED system. The transit time, is the time between the light generation inside a counter and the formation of the trigger. By means of the LED system, we have measured the behavior of the transit time versus energy for each counter.

The trigger of the array has been upgraded too. An independent fast trigger logic has been implemented in the counters of the Super Set. The trigger has been connected to one of the Time Interval Counters of the HPTF, which provides a high precision time difference between the LVD trigger and the absolute GPS time. Thanks to this improvement, the absolute time accuracy of LVD is of the order of few nanoseconds. Finally a new, independent, high precision geodesy measurement was performed. The CNGS-LVD baseline, namely the distance between the center of the BFCTI.400344 intensity monitor at CERN and the LVD Super-Set upstream entry wall (taken as the LVD reference), was found to be 731291.87±0.04 m.

During the bunched-beam run we found 190 events in total, consistent with the $1.89 \cdot 10^{17}$ protons on target (p.o.t.) delivered. For the measurement of the neutrino velocity, we have used only events involving at least one of the Super-Set counters. We have found 79 of them out of 190, i.e., 40% as expected from the Super-Set geometry. To limit the sources of systematic uncertainties, we have applied quality cuts to them. First we have required the non-saturation of ADC of the triggering counter, as the saturation would not allow a precise measurement of the transit time. Second, because the number of photoelectrons for energy releases E<30 MeV is too low to guarantee that the counter is triggered by direct (i.e., fast) light, we have selected only events where the energy release associated to the triggering counter was above a certain value. We have tested different cuts, between 30 and 100 MeV. The r.m.s. of the distribution becomes stable for E>50 MeV, this value being our final choice. The described quality cuts reduce the sample to 48 events, that have been used for the final analysis.

The systematic uncertainties associated to the measurement of the difference between the neutrino time-of-flight tof_ν and the expected one at speed of light tof_c:

$$\delta t = tof_\nu - tof_c \tag{10}$$

are summarized in Table 2. The baseline between LVD and CERN is known with an uncertainty lower than 0.3 ns. In fact, neutrino-induced muons responsible for events in the Super-Set can be generated as far as several hundreds of meters from LVD. This makes shorter the actual neutrinos baseline, while part of the distance is travelled by the produced muons of different energy. This effect has been investigated through a Monte Carlo simulation and has a negligible impact on the measurement. Constant delays at CERN give an additional uncertainty of 1.5 ns. The uncertainty due to the system time inter-calibration has been measured and it is 1.1 ns. Also, the delay between the proton extraction time and the recording of the BCT waveforms by a digitizer has been measured, with an uncertainty of 1.0 ns. The variable correction δ_{LVD} (energy and counter dependent) introduces a further systematic uncertainty, 0.4 ns, evaluated through the propagation of the one associated to the energy measurement. Finally, the last three

146

Systematic uncertainties	ns	Error dist.
Baseline (< 10 cm)	< 0.3	Gauss.
Const. corr. at CERN	2.0	Gauss.
BCT calibration	1.0	Gauss.
Time link calibration	1.1	Gauss.
GPS syncronization accuracy	1.0	Gauss.
PMT transit time correction	0.4	Gauss.
Absolute transit time cal.	1.5	Flat
Optical fiber length	0.5	Gauss.
Fluorescence lifetime	0.6	Exp.
Total systematic	$\pm$ 3.2	

Table 2: *Sources of systematic uncertainty in the measurement.*

terms in Table 2 are related to the constant corrections in the absolute time calibration of the Super-Set counters. They account for the unknown time delay between trigger and LED light generation, 2.6 ± 1.5 ns; the uncertainty associated to the optical fiber length, 0.5 ns, and the difference between the detector response to LED light and to particle ionization, 1.1 ± 0.6 ns (the scintillator decay time is $\tau = 3.3$ ns.

By quadratically summing up all these contributions, we obtain a total systematic uncertainty of 3.2 ns. The distribution of δt for the 48 events is shown in figure 8 compared with the superposition of all the peaks of the waveforms correlated to detected events. The mean value of the measured distribution is:

$$\delta t = -0.3 \pm 0.6_{stat} \pm 3.2_{sys} \text{ ns} \tag{11}$$

The neutrino speed is compatible with c, its deviation being, at 99% C.L.:

$$-3.3 \cdot 10^{-6} < (v_\nu - c)/c < 3.5 \times 10^{-6} \tag{12}$$

These values are an order of magnitude lower than previous direct measurements [Agafonova et al.(2012-b)].
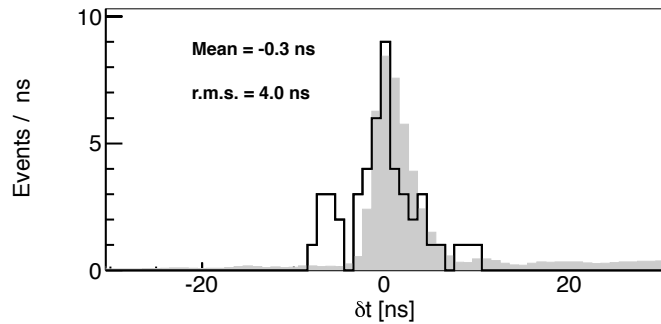
Figure 8: *Distribution of $\delta t = tof_\nu - tof_c$, for each of the 48 selected events, compared with the superposition of all the peaks of the waveforms correlated to detected events (grey).*

References

[Agafonova et al.(2007-a)] Agafonova N.Yu. et al., 2007, Astroparticle Physics, 27, 254-270; [hep-ph/069305].

[Agafonova et al.(2007-b)] Agafonova N.Yu. et al., 2007, Eur. Phys. J. C 52, 849-855 (2007).

[Agafonova et al.(2008)] Agafonova N.Yu. et al., 2008, Astroparticle Physics, 28, 516

[Agafonova et al.(2012-a)] Agafonova N.Yu. et al., 2012, Eur. Phys. J. Plus, 127-6, 71 (2012)

[Agafonova et al.(2012-b)] Agafonova N.Yu. et al., 2012, Phys. Rev. Lett., 109-7, 070801 (2012). [arXiv:1208.1392v2]

[Aglietta et al.(1987)] Aglietta, M. et al., 1987, Europhys. Letters, 3, 1315

[Aglietta et al.(1992)] Aglietta, M. et al., 1992, Il Nuovo Cimento A, 105, 1793

[Aglietta et al.(2004)] Aglietta M. et al., Nuclear Instruments and Methods in Physics Research A 516, 96 (2004).

[Ahrens et al.(2002)] Ahrens, J., et al. 2002, Astropart. Phys., 16, 345

[Alekseev et al.(1987)] Alekseev, E. N., et al., 1987, J. Exp. Theor. Phys. Lett., 45, 589

[Alekseev & Alexeyeva (2002)] Alekseev, E. N., & Alexeyeva, L. N. 2002, J. Exp. Theor. Phys, 95, 10

[Ambrosio et al.(2004)] Ambrosio, M., et al. 2004, Eur. Phys. J. C, 37, 265

[An et al.(2012)] An, F. P., et al., 2012, Phys. Rev. Lett., 108, 171803

[Antonioli et al.(2004)] Antonioli, P., et al., 2004, New J.Phys., 6, 114

[Antonioli et al.(1991)] P. Antonioli, W. Fulgione, P. Galeotti and L. Panaro, NIM A **309** (1991) 569.

[Bahcall et al.(1995)] Bahcall, J.N., Kamionkowski, M., Sirlin, A., 1995, Phys. Rev. D 51, 6146

[Bethe & Wilson(1985)] Bethe H.A., Wilson J.R., 1985, Astrophys.J.,295, 14

[Bionta et al.(1987)] Bionta, R. M., et al. (IMB collaboration). 1987, Phys. Rev. Lett., 58, 1494

[Colgate & White(1966)] S.A. Colgate, R.H. White, Astrophys. J. 143 (1966) 626

[Dye et al.(1989)] Dye, S. T., et al., 1989, Phys. Rev. Lett., 62, 2069

[Fukugita et al.(1988)] Fukugita M., Kohyama Y., Kubodera K., 1988, Physics Letters B, 212, 139

[Hirata et al.(1987)] Hirata, K., et al., 1987, Phys. Rev. Lett., 58, 1490

[Ikeda et al.(2007)] Ikeda, M., et al., 2007, The Astrophysical Journal, 669,519

[Imshennik & Ryazhskaya(2004)] Imshennik, V.S. & Ryazhskaya, O., 2004, Astronomy Letters, 30, 14

[Janka(2012)] H. T. Janka, Annual Review of Nuclear and Particle Science, 62, (2012), 407-451 arXiv:1206.2503v1

[Loredo & Lamb(2002)] T.J. Loredo, D.Q. Lamb, Phys. Rev. D 65 (2002) 063002

[Keil et al.(2003)] M. T. Keil, G. G. Raffelt, and H.-T. Janka, Astrophys. J. 590, 971 (2003)

[Kolbe & Langanke(2001)] Kolbe E., Langanke K., 2001, Phys. Rev. C, 63, 025802

[Mikheev & Smirnov(1985)] Mikheev, S.P. & Smirnov, A.Yu., 1985, Sov.J.Nucl.Phys., 42

[Novoseltseva et al.(2011)] Novoseltseva et. al., Bulletin of the Russian Academy of Sciences: Physics, vol 75, issue 3, (2011) pp. 419 - 422

[Pagliaroli et al.(2009)] Pagliaroli G., Vissani F., Costantini M.L., Ianni A., 2009, Astroparticle Physics 31, 163

[Strumia & Vissani(2003)] Strumia A., Vissani F., 2003, Physics Letters B, 564

[Strumia & Vissani(2010)] Strumia, A. & Vissani, F., arXiv:hep-ph/0606054v3

[Tamborra et al.(2012)] [4] I. Tamborra, B. Muller, L. Hudepohl, H. T. Janka, G.Raffelt, Phys. Rev. D 86, 125031 (2012)

[Toivanen et al.(2001)] Toivanen J., Kolbe E., Langanke K., Martinez-Pinedo G., Vogel P., 2001, Nuclear Physics A, 694, 395

[Totani et al.(1998)] Totani, T. et al., 1998, Astrophys. J., 496, 216

[Wilson(1985)] Wilson, J.R., 1985, Numerical Astrophysics, ed. J. M. Centrella, J. M. LeBlanc and R. L. Bowers, Jones and Bartlett Boston, 422

[Wolfenstein(1978)] Wolfenstein, L., 1978, Phys.Rev. D, 17

OPERA

May 29, 2014

N. Agafonova[1], A. Aleksandrov[2], O. Altinok[3], A. Anokhina[4], S. Aoki[5], A. Ariga[6], T. Ariga[6], D. Autiero[7], A. Badertscher[8], A. Bagulya[9], A. Bendhabi[10], A. Bertolin[11,*], C. Bozza[12], T. Brugière[7], R. Brugnera[13,11], F. Brunet[14], G. Brunetti[15,16,7], S. Buontempo[2], A. Cazes[7], L. Chaussard[7], M. Chernyavskiy[9], V. Chiarella[17], A. Chukanov[18], N. D'Ambrosio[19], F. Dal Corso[11], G. De Lellis[20,2], P. del Amo Sanchez[14], Y. Déclais[7], M. De Serio[21], F. Di Capua[2], A. Di Crescenzo[20,2], D. Di Ferdinando[16], N. Di Marco[22,a], S. Dmitrievski[18], M. Dracos[23], D. Duchesneau[14], S. Dusini[11], T. Dzhatdoev[4], J. Ebert[24], O. Egorov[25], R. Enikeev[1], A. Ereditato[6], L. S. Esposito[8], J. Favier[14], T. Ferber[24], R. A. Fini[21], D. Frekers[26], T. Fukuda[27], A. Garfagnini[13,11], G. Giacomelli[15,16], M. Giorgini[15,16,b], C. Göllnitz[24], J. Goldberg[28], D. Golubkov[25], L. Goncharova[9], Y. Gornushkin[18], G. Grella[12], F. Grianti[29,17], A. M. Guler[3], C. Gustavino[19,c], C. Hagner[24], K. Hamada[27], T. Hara[5], M. Hierholzer[24], A. Hollnagel[24], K. Hoshino[27], M. Ieva[21], H. Ishida[30], K. Jakovcic[31], C. Jollet[23,*], F. Juget[6], M. Kamiscioglu[3], K. Kazuyama[27], S. H. Kim[32,d], M. Kimura[30], N. Kitagawa[27], B. Klicek[31], J. Knuesel[6], K. Kodama[33], M. Komatsu[27], U. Kose[13,11], I. Kreslo[6], H. Kubota[27], C. Lazzaro[8], J. Lenkeit[24], I. Lippi[11], A. Ljubicic[31], A. Longhin[13,11,e], P. Loverre[34], G. Lutter[6], A. Malgin[1], G. Mandrioli[16], K. Mannai[10], J. Marteau[7], T. Matsuo[30], V. Matveev[1], N. Mauri[15,16,e], E. Medinaceli[16], F. Meisel[6], A. Meregaglia[23,*], P. Migliozzi[2], S. Mikado[30], S. Miyamoto[27], P. Monacelli[22], K. Morishima[27], U. Moser[6], M. T. Muciaccia[35,21], N. Naganawa[27], T. Naka[27], M. Nakamura[27], T. Nakano[27], D. Naumov[18], V. Nikitina[4], K. Niwa[27], Y. Nonoyama[27], S. Ogawa[30], N. Okateva[9], A. Olchevski[18], M. Paniccia[17], A. Paoloni[17], B. D. Park[32,f], I. G. Park[32], A. Pastore[35,21], L. Patrizi[16], E. Pennacchio[7], H. Pessard[14], K. Pretzl[6], V. Pilipenko[26], C. Pistillo[6], N. Polukhina[9], M. Pozzato[15,16], F. Pupilli[22], R. Rescigno[12], T. Roganova[4], H. Rokujo[5], G. Romano[12], G. Rosa[34], I. Rostovtseva[25], A. Rubbia[8], A. Russo[20,2], V. Ryasny[1], O. Ryazhskaya[1], O. Sato[27], Y. Sato[36], A. Schembri[19], W. Schmidt-Parzefall[24], H. Schroeder[37], L. Scotto Lavina[20,2,g], A. Sheshukov[18], H. Shibuya[30], G. Shoziyeov[4], S. Simone[35,21], M. Sioli[15.16], C. Sirignano[13,11], G. Sirri[16], J. S. Song[32], M. Spinetti[17], L. Stanco[11], N. Starkov[9], M. Stipcevic[31], T. Strauss[8,h], P. Strolin[20,2], S. Takahashi[27], M. Tenti[15,16], F. Terranova[17], I. Tezuka[36], V. Tioukov[2], P. Tolun[3], A. Trabelsi[10], T. Tran[7], S. Tufanli[3,h], P. Vilain[38], M. Vladimirov[9], L. Votano[17], J. L. Vuilleumier[6], G. Wilquet[38], B. Wonsak[24] V. Yakushev[1], C. S. Yoon[32], T. Yoshioka[27], J. Yoshida[27], Y. Zaitsev[25], S. Zemskova[18], A. Zghiche[14] and R. Zimmermann[24].

1. INR-Institute for Nuclear Research of the Russian Academy of Sciences, RUS-117312 Moscow, Russia
2. INFN Sezione di Napoli, I-80125 Napoli, Italy
3. METU-Middle East Technical University, TR-06531 Ankara, Turkey
4. SINP MSU-Skobeltsyn Institute of Nuclear Physics of Moscow State University, RUS-119992 Moscow, Russia
5. Kobe University, J-657-8501 Kobe, Japan
6. Albert Einstein Center for Fundamental Physics, Laboratory for High Energy Physics (LHEP), University of Bern, CH-3012 Bern, Switzerland
7. IPNL, Université Claude Bernard Lyon 1, CNRS/IN2P3, F-69622 Villeurbanne, France
8. ETH Zurich, Institute for Particle Physics, CH-8093 Zurich, Switzerland
9. LPI-Lebedev Physical Institute of the Russian Academy of Sciences, RUS-117924 Moscow, Russia
10. Unité de Physique Nucléaire et des Hautes Energies (UPNHE), Tunis, Tunisia
11. INFN Sezione di Padova, I-35131 Padova, Italy
12. Dipartimento di Fisica dell'Università di Salerno and INFN, I-84084 Fisciano, Salerno, Italy
13. Dipartimento di Fisica dell'Università di Padova, I-35131 Padova, Italy
14. LAPP, Université de Savoie, CNRS/IN2P3, F-74941 Annecy-le-Vieux, France
15. Dipartimento di Fisica dell'Università di Bologna, I-40127 Bologna, Italy
16. INFN Sezione di Bologna, I-40127 Bologna, Italy

17. INFN - Laboratori Nazionali di Frascati dell'INFN, I-00044 Frascati (Roma), Italy
18. JINR-Joint Institute for Nuclear Research, RUS-141980 Dubna, Russia
19. INFN - Laboratori Nazionali del Gran Sasso, I-67010 Assergi (L'Aquila), Italy
20. Dipartimento di Scienze Fisiche dell'Università Federico II di Napoli, I-80125 Napoli, Italy
21. INFN Sezione di Bari, I-70126 Bari, Italy
22. Dipartimento di Fisica dell'Università dell'Aquila and INFN, I-67100 L'Aquila, Italy
23. IPHC, Université de Strasbourg, CNRS/IN2P3, F-67037 Strasbourg, France
24. Hamburg University, D-22761 Hamburg, Germany
25. ITEP-Institute for Theoretical and Experimental Physics, RUS-117259 Moscow, Russia
26. University of Münster, D-48149 Münster, Germany
27. Nagoya University, J-464-8602 Nagoya, Japan
28. Department of Physics, Technion, IL-32000 Haifa, Israel
29. Università degli Studi di Urbino "Carlo Bo", I-61029 Urbino, Italy
30. Toho University, J-274-8510 Funabashi, Japan
31. IRB-Rudjer Boskovic Institute, HR-10002 Zagreb, Croatia
32. Gyeongsang National University, ROK-900 Gazwa-dong, Jinju 660-300, Korea
33. Aichi University of Education, J-448-8542 Kariya (Aichi-Ken), Japan
34. Dipartimento di Fisica dell'Università di Roma "La Sapienza" and INFN, I-00185 Roma, Italy
35. Dipartimento di Fisica dell'Università di Bari, I-70126 Bari, Italy
36. Utsunomiya University, J-321-8505 Tochigi-Ken, Utsunomiya, Japan
37. Fachbereich Physik der Universität Rostock, D-18051 Rostock, Germany
38. IIHE, Université Libre de Bruxelles, B-1050 Brussels, Belgium
a. Now at INFN - Laboratori Nazionali del Gran Sasso, I-67010 Assergi (L'Aquila), Italy
b. Now at INAF/IASF, Sezione di Milano, I-20133 Milano, Italy
c. Now at Dipartimento di Fisica dell'Università di Roma "La Sapienza" and INFN, I-00185 Roma, Italy
d. Now at Pusan National University, Geumjeong-Gu Busan 609-735, Korea
e. Now at INFN - Laboratori Nazionali di Frascati dell'INFN, I-00044 Frascati (Roma), Italy
f. Now at Asan Medical Center, 388-1 Pungnap-2 Dong, Songpa-Gu, Seoul 138-736, Korea
g. Now at SUBATECH, CNRS/IN2P3, F-44307 Nantes, France
h. Now at Albert Einstein Center for Fundamental Physics, Laboratory for High Energy Physics (LHEP), University of Bern, CH-3012 Bern, Switzerland

Abstract

The OPERA neutrino detector at the underground Gran Sasso Laboratory (LNGS) was designed to perform the first detection of neutrino oscillations in appearance mode through the study of $\nu_\mu \to \nu_\tau$ oscillations. The apparatus consists of a lead/emulsion-film target complemented by electronic detectors. It is placed in the high-energy long-baseline CERN to LNGS beam (CNGS) 730 km away from the neutrino source. Runs with CNGS neutrinos were successfully conducted in 2008, 2009, 2010, 2011 and 2012 for a total luminosity of 18×10^{19} p.o.t. (*proton on target*). In November 2012 the CNGS run has been stopped and subsequently the beam line has been dismounted. The emulsion analysis has continued during last year and will presumably continue for the whole 2014. After a brief description of the beam and of the experimental apparatus we report on the data and related analysis results.

1   Introduction

The solution of the long-standing solar and atmospheric neutrino puzzles has come from the hypothesis of neutrino oscillations. This implies that neutrinos have non vanishing and non-degenerate mass eigenstates, and that their flavor eigenstates involved in weak interaction processes are a superposition of the mass eigenstates. Several experiments carried on in the last decades with solar and reactor neutrinos, as well as with atmospheric and accelerator neutrinos, contributed to build-up our present understanding of neutrino mixing. Atmospheric neutrino oscillations have been studied mainly by the Kamiokande, MACRO, Super-Kamiokande and SOUDAN2 experiments. Long baseline experiments with accelerator neutrinos (K2K and MINOS) confirmed the oscillation scenario first pointed out by the Super-Kamiokande experiment supporting the $\nu_\mu \to \nu_\tau$ oscillation channel for atmospheric neutrinos, while the CHOOZ and Palo Verde reactor experiments excluded the $\nu_\mu \to \nu_e$ channel as the dominant one. However, the direct appearance of a different neutrino flavor is still an important open issue. This is the main goal of the OPERA experiment [1] that uses the long baseline (L=730 km) CNGS neutrino beam from CERN to LNGS. The challenge of the experiment is to measure the appearance of ν_τ from ν_μ oscillations in an almost pure muon-neutrino beam. This requires the detection of the short-lived τ lepton ($c\tau = 87.11$ μm)
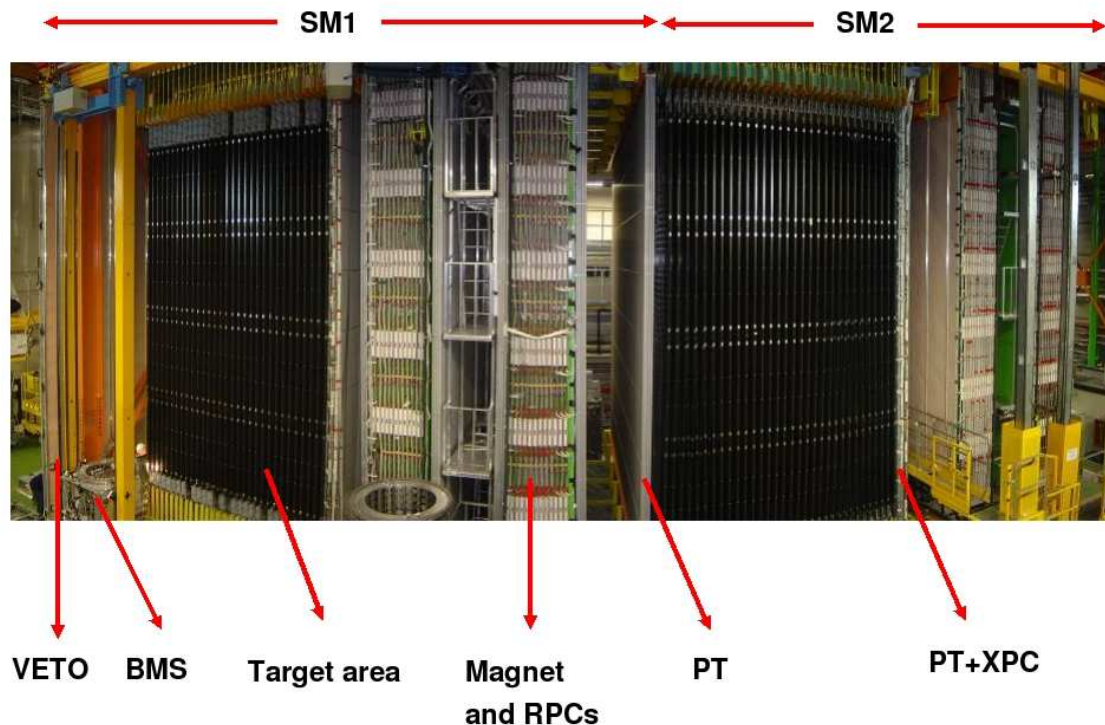
Figure 1: Fish-eye view of the OPERA detector. The upper horizontal lines indicate the position of the two identical supermodules (SM1 and SM2). The "target area" is made of walls filled with ECC bricks interleaved with planes of plastic scintillators (TT). Arrows also show the position of the VETO planes, the drift tubes (PT), the RPC with diagonal strips (XPC), the magnets and the RPC installed between the magnet iron slabs. The Brick Manipulator System (BMS) is also visible. See [2] for more details.

produced in the charged-current interaction of a ν_τ. This sets two conflicting requirements: a large target mass needed to have sufficient statistics and an extremely high accuracy detector technique to observe the short-lived τ lepton. The τ is identified by the detection of its characteristic decay topologies either in one prong (electron, muon or hadron) or in three prongs. The τ track is measured with a large-mass active target made of 1 mm thick lead plates (target mass and absorber material) inter-spaced with thin nuclear emulsion films (high-accuracy tracking devices). This detector is historically called Emulsion Cloud Chamber (ECC). Among past applications it was successfully used in the DONUT experiment for the first direct observation of the ν_τ.

The OPERA detector [2] is made of two identical Super Modules (SM) each consisting of a target section of about 625 tons made of lead/emulsion-film ECC modules (hereafter called "bricks"), of a scintillator tracker detector (TT) needed to trigger the read-out and pre-localize neutrino interactions within the target, and of a muon spectrometer (Figure 1). A single SM has longitudinal dimensions of about 10 m. The detector is equipped with an automatic machine (the Brick Manipulator System, BMS) that allows the on-line removal of bricks from the detector. Ancillary facilities exist for the handling, the development and the scanning of the emulsion films. The film scanning is performed with two independent types of scanning microscopes: the European Scanning Sytem (ESS) in Europe and the S-UTS in Japan.

A target brick consists of 56 lead plates of 1 mm thickness interleaved with 57 emulsion films [3]. The plate material is a lead alloy with a small calcium content to improve its mechanical properties [4]. The transverse dimensions of a brick are 12.8×10.2 cm^2 and the thickness along the beam direction is 7.9 cm
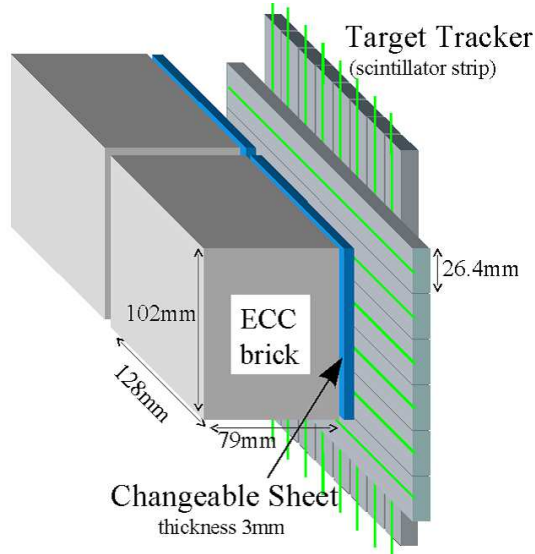
Figure 2: Schematic view of two bricks with their Changeable Sheet and target tracker planes.

(about 10 radiation lengths). The construction of more than 150,000 bricks for the neutrino target has been accomplished by an automatic machine, the Brick Assembly Machine (BAM) operating underground in order to minimize the number of background tracks from cosmic-rays and environmental radiation. The bricks have been inserted in the detector target by the BMS and housed in a light support structure placed between consecutive TT walls. The support structure has been designed with the requirement of minimizing the material along the neutrino beam direction in order to reduce to the 0.1% level the number of interactions in regions not instrumented with emulsion films or scintillators. In order to reduce the emulsion scanning load the use of Changeable Sheets (CS) [5], successfully applied in the CHORUS experiment, was extended to OPERA. Tightly packed doublets of emulsion films are attached to the downstream face of each brick and can be removed without opening the brick. Charged particles from a neutrino interaction in the brick cross the CS and produce signals in the TT scintillators. Following these signals the brick is extracted and the CS developed underground and analyzed in the scanning facilities at LNGS and in Nagoya. The information of the CS is used for a precise prediction of the position of the tracks in the most downstream films of the brick, hence guiding the so-called *scan-back* vertex finding procedure. The brick, CS and TT layout [5] is schematically shown in Figure 2.

2 Evidence of $\nu_\mu \to \nu_\tau$ appearance in the CNGS beam with direct τ detection

The CNGS neutrino beam was designed and optimized for the study of $\nu_\mu \to \nu_\tau$ oscillations in appearance mode, by maximizing the number of charged current (CC) ν_τ interactions at the LNGS site. For a detailed description of the CNGS beam we refer to [2].

After the beam commissioning run in 2006, the CNGS run started on September 2007 at rather low intensity. The first event inside the OPERA target was observed on October 3rd. Longer runs took place in 2008, 2009, 2010, 2011 and 2012. On December 2012 the last CNGS neutrinos were delivered to LNGS. A long shutdown is foreseen at CERN for 2013 and 2014 for the upgrade of LHC and the CNGS beam has been decommissioned. The global CNGS performance during the 2008 to 2012 runs is summarized in table 1.

A first ν_τ interaction candidate was found in 2010 [6].

A second ν_τ interaction candidate was found in 2011 and presented in 2012 [9] (Fig.4).

A third ν_τ interaction candidate was found in 2012 and officially presented in a seminar at LNGS on
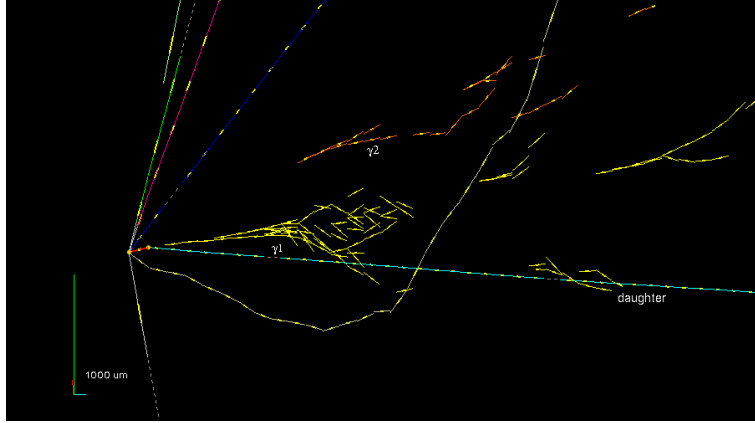
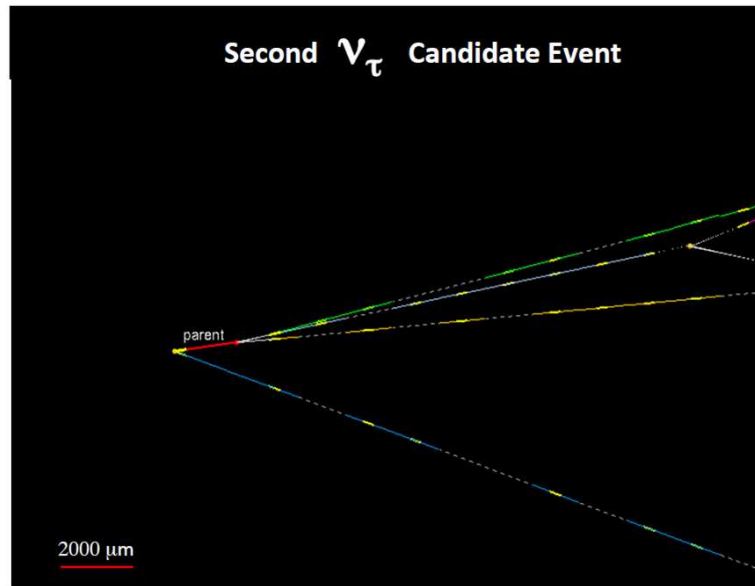Figure 3: The first OPERA tau candidate (see [6] for details).

Figure 4: The second OPERA tau candidate (see [9] for details).

March the 26th 2013 [10] (Fig.5). The sample of events analyzed up to now consisted of:

- all the 0μ events collected and searched for in the two most probable bricks for the 2008-2009 runs and in the most probable one for the 2010-2011 runs,

- all the 1μ events with $p_\mu < 15$ GeV/c collected and searched for in the two most probable bricks for the 2008-2009 runs and in the most probable one for the 2010 run.

Two ν_τ candidate events in the hadronic decay channels were observed: the first in the 2009 run data with a one-prong topology [6], the second in the 2011 run data with a three-prong topology [9]. The analysis was then performed on the most probable bricks of 1μ events with $p_\mu < 15$ GeV/c collected during the 2011 and 2012 runs. A ν_τ candidate event in the muonic decay channel was observed in this data sample. The three candidate events found, together with a conservative background estimation, mostly due to charm candidates with undetected muon, give a significance of 3.4 sigma for the direct detection of $\nu_\mu \to \nu_\tau$ oscillations
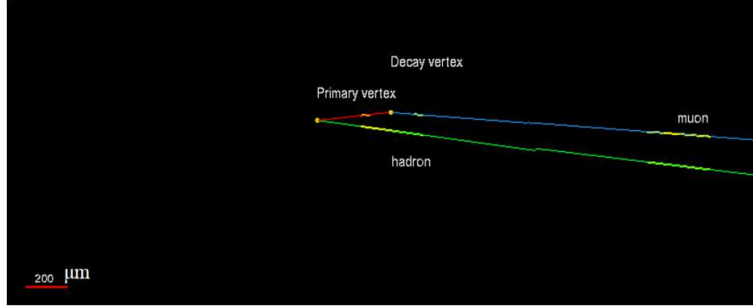
Figure 5: The third OPERA tau candidate; in this candidate event the short track is seen to decay leptonically into one muon which stops in the spectrometer.

The kinematical quantities of the tracks measured in the emulsion films for the third candidate event are given in the following:

- track p_0 has a momentum $p_{p_0} = (0.90^{+0.18}_{-0.13})$ GeV/c, measured by MCS. It was found in the CS films. It was followed into the downstream brick where it disappears after having crossed 18 lead plates. No charged particle track could be detected at the interaction point. It is classified as a hadron by its momentum-range correlation [10];

- track d_1 is the τ decay daughter. Its angle with the τ lepton track (θ_{kink}) is (245 ± 5) mrad. The impact parameter with respect to the primary vertex is (93.7 ± 1.1) μm. The track, found also on the CS films, agrees with the muon track reconstructed in the electronic detectors in both momentum $(\Delta p = 0.3^{+0.9}_{-0.5}$ GeV/$c)$ and angle $(\Delta\theta = 18 \pm 25$ mrad);

- the shower originating from a γ-ray conversion has an energy of $(3.1^{+0.9}_{-0.6})$ GeV. The conversion to an e^+e^- pair is observed 2.1 mm $(0.36\ X_0)$ downstream of the primary vertex to which it points with an impact parameter of (18 ± 13) μm. It is incompatible with originating from the secondary vertex, the impact parameter being (96 ± 12) μm.

In the plane transverse to the beam direction, the angle between the τ candidate direction and the sum of the transverse momenta of the other primary particles $(p_0$ and $\gamma)$ is $\Delta\phi_{\tau H} = (155 \pm 15)°$. The transverse momentum at the secondary vertex (p_T^{2ry}) amounts to (690 ± 50) MeV/c. The scalar sum of the momenta of all the particles is $p_{sum} = (6.8^{+0.9}_{-0.6})$ GeV/c.

With the present statistics and the observation of three ν_τ candidates, the absence of a signal from $\nu_\mu \to \nu_\tau$ oscillations is excluded at 3.4 σ [10].

3 Measurement of TeV atmospheric muon charge ratio

The muon charge ratio $R_\mu \equiv N_{\mu^+}/N_{\mu^-}$, defined as the number of positive over negative charged muons, is studied since many decades. It provides an understanding of the mechanism of multiparticle production in the atmosphere in kinematic regions not accessible to accelerators, as well as information on the primary cosmic ray composition. A charge ratio larger than unity reflects the abundance of protons over heavier nuclei in the primary cosmic radiation. The charge asymmetry is preserved in the secondary hadron production, and consequently in the muon fluxes, due to the steepness of the primary spectrum which enhances the forward fragmentation region. The kaon contribution to the muon flux increases with the muon energy. Since the production of positive kaons is favored by the associated production ΛK^+, the muon charge ratio is expected to rise with energy. Assuming the hypothesis of complete scaling we expect an energy independent charge ratio above the TeV energy region at sea level once the kaon contribution to the muon flux reached its asymptotic value. At higher energies, around $O(100)$ TeV, the heavy flavor contribution, as well as changes in the primary composition, may become significant. The momentum and charge reconstruction was obtained via the Precision Trackers (PT) of the OPERA spectrometers.

Layers of vertical drift tubes are arranged in PT stations instrumenting the two identical dipole magnets. The momentum and charge information is given by the angle $\Delta\phi$ in the bending plane, i.e. the difference between the track directions reconstructed by the two PT stations before and after each magnet arm. For nearly horizontal muons up to four bending angles can be measured in the two dipole magnets.

OPERA collected charge-separated cosmic ray data between 2008 and 2012. More than 3 million atmospheric muon events were detected and reconstructed, among which about 110000 multiple muon bundles. The charge ratio $R_\mu \equiv N_{\mu^+}/N_{\mu^-}$ was measured separately for single and for multiple muon events. The analysis exploited the inversion of the magnet polarity which was performed on purpose during the 2012 Run. The combination of the two data sets with opposite magnet polarities allowed minimizing systematic uncertainties and reaching an accurate determination of the muon charge ratio. Data were fitted to obtain relevant parameters on the composition of primary cosmic rays and the associated kaon production in the forward fragmentation region. The charge ratio of single muons impinging on the apparatus was computed combining the two polarity data sets [11]. After the correction for charge misidentification and detector misalignment, the final measurement with the complete 5-year statistics yields the result:

$$R_\mu(n_\mu = 1) = 1.377 \pm 0.006(stat.)^{+0.007}_{-0.001}(syst.) \tag{1}$$

The charge ratio of multiple muon events was computed using all the muon charges reconstructed in events with $n_\mu > 1$. It is not computed within the bundle itself, but summing up all the positive and the negative charges belonging to the bundle subsample. The result after polarity combination and correction for misidentification is significantly lower than the single muon value:

$$R_\mu(n_\mu > 1) = 1.098 \pm 0.023(stat.)^{+0.015}_{-0.013}(syst.) \tag{2}$$

In the surface energy range 1-20 TeV investigated by OPERA, R_μ is well described by a parametric model including only pion and kaon contributions to the muon flux, showing no significant contribution of the prompt component. The energy independence supports the validity of Feynman scaling in the fragmentation region up to 200 TeV/nucleon primary energy.

4   Conclusions and plans for 2014

The extraction of bricks from the Opera apparatus, and the scanning and analysis of the remaining events in the emulsions, will continue during 2014 in order to complete the search for ν_τ events collected in the last years and not yet found. All the most probable event bricks and most of the second probable bricks have been measured and analised. During the year 2014 the remaining third and fourth most probable bricks (for those events which have not been confirmed in the first and second brick) will be extracted and analyzed. The extraction will continue till the end of 2014 while the scanning and analysis will last also in the year 2015. In 2015 the apparatus is foreseen to be decommissioned.

References and list of publications

[1] M. Guler *et al.*, OPERA proposal, CERN/SPSC 2000-028, SPSC/P318, LNGS P25/2000.

[2] R. Acquafredda *et al.* [OPERA Collaboration] "The OPERA experiment in the CERN to Gran Sasso neutrino beam", JINST 4:P04018,2009.

[3] T. Nakamura *et al.*, "The Opera Film: New Nuclear Emulsion For Large-Scale, High-Precision Experiments," Nucl. Instrum. Meth. A **556** (2006) 80.

[4] A. Anokhina *et al.* [OPERA Collaboration], "Study of the effects induced by lead on the emulsion films of the OPERA experiment," JINST **3** P07002 (2008).

[5] A. Anokhina *et al.* [OPERA Collaboration], "Emulsion sheet doublets as interface trackers for the OPERA experiment," JINST **3** (2008) P07005

[6] N. Agafonova *et al.* [OPERA Collaboration], "Observation of a first ν_τ candidate in the OPERA experiment in the CNGS beam," Phys. Lett. *B691* , 138 (2010).

[7] N. Agafonova *et al.* [OPERA Collaboration], "Search for ν_μ -ν_e oscillation with the OPERA experiment in the CNGS beam." JHEP *1301* 1307 (2013) 004, Addendum-ibid 1307 (2013) 085

[8] T. Adam *et al.* [OPERA Collaboration], "Measurement of the neutrino velocity with the OPERA detector in the CNGS beam using the 2012 dedicated data." JHEP *1301* , 153 (2013)

[9] N. Agafonova *et al.* [OPERA Collaboration], New result on $\nu_\mu \rightarrow \nu_\tau$ appearance with the OPERA Experiment in the CNGS beam." JHEP11 *1301* , 036 (2013)

[10] N. Agafonova *et al.*[OPERA Collaboration],"Evidence for $\nu_\mu \rightarrow \nu_\tau$ appearance in the CNGS neutrino beam with the OPERA experiment." Phys.Rew. D 89 051102(R),(2014)

[11] N. Agafonova *et al.* [OPERA Collaboration]"Measurement of TeV atmospheric muon charge ratio with the full OPERA data.arXiv:1403.0244(2014)sbm.to EPJC

THEORY GROUP

The LNGS theory group is organized in the following five working subgroups (or IS, from *Iniziative Specifiche*): PI12, PI21, CT51, FA51, PD51. The coordinators are indicated in bold face in the members list. The research topics concern five main areas: astroparticle physics (mainly FA51); compact stellar objects and dense hadronic matter (CT51); cosmology, large scale structures and dark matter (PD51); computer simulations of gauge theories (PI12); particle physics phenomenology (mainly PI21). There is a tradition of collaboration between the LNGS theory group and several experimental groups. In this report, we briefly describe the activities of the theory group in 2013.

Members of the group: R. Aloisio, Z. Berezhiani, V. Berezinsky, R. Biondi, P. Blasi, D. Boncioli, M. Crisostomi, G. Di Carlo, G. Di Panfilo A. Maiezza, **M. Mannarelli**, M. Mitra, G. Pagliaroli, A. Parisi, L. Pilo, N. Rossi, F.L. Villante, F. Vissani.

Updated information can be found at: `http://theory.lngs.infn.it/index.html`

———————— Lattice QCD (PI12) ————————

Member: **G. Di Carlo**.

In collaboration with V. Azcoiti, E. Follana, M. Giordano (Universidad de Zaragoza, Spain) and A. Vaquero (The Cyprus Institute, Cyprus).

Scientific work

The research activity has been focused on the study of the sign problem and topology in lattice field theories: non-zero baryonic density QCD, so-called Aoki phase and models with θ-term.

We have continued a long standing study on the structure of the vacuum in QCD into the Aoki phase; in a paper, published on Nucl Phys. B [1], we provide numerical evidence, coming from HMC simulations, supporting a vacuum structure for this model more complex than the one assumed in the standard picture, in contradiction with the χ PT predictions for the Aoki phase. In another paper, also published in Nucl. Phys. B [2], we substantiate this evidence with an analysis of the corrisponding Aoki phase structure in the Nambu-Jona Lasinio model sharing the same low energy symmetries of 2 flavours Wilson fermions lattice QCD. Next we tried to extend these results by adding a chemical potential term, looking for possible hints of new parity-broken phases, but we failed in finding different behaviour with respect to the zero chemical potential case.

Fundamental Interactions and Gauge Theories (PI21)

Members: **Z. Berezhiani**, R. Biondi, A. Maiezza, G. Di Panfilo, N. Rossi, F. Villante.
IA. Dolgov (University of Ferrara), I. Tkachev (INR, Moscow),
P. Geltenbort, V. Nesvizhevsky (ILL, Grenoble), A. P. Serebrov (PNPI, St. Petersburg),
Yu. Kamyshkov (Univ. Tennessee, USA) .

Scientific work

The research activity has been focused on the following topics:

(i) Millicharged dark matter: generation of galactic magnetic fields and the BBN limits.
A new scenario for creation of galactic magnetic fields has been proposed which is operative at the cosmological epoch of the galaxy formation, and which relies on unconventional properties of dark matter. Namely, it requires existence of feeble but long range interaction between the dark matter particles and electrons. In particular, millicharged dark matter particles or mirror particles with the photon kinetic mixing to the usual photon can be considered. We show that in rotating protogalaxies circular electric currents can be generated by the interactions of free electrons with dark matter particles in the halo, while the impact of such interactions on galactic protons is considerably weaker. The induced currents may be strong enough to create the observed magnetic fields on the galaxy scales with the help of moderate dynamo amplification. In addition, the angular momentum transfer from the rotating gas to dark matter component could change the dark matter profile and formation of cusps at galactic centers would be inhibited. The global motion of the ionized gas could produce sufficiently large magnetic fields also in filaments and galaxy clusters [3]. In addition, effects of light millicharged dark matter particles on primordial nucleosynthesis were studied. It is shown that if the mass of such particles is much smaller than the electron mass, they lead to strong overproduction of Helium-4. An agreement with observations can be achieved by non-vanishing lepton asymmetry. Baryon-to-photon ratio at BBN and neutrino- to-photon ratio both at BBN and at recombination are noticeably different as compared to the standard cosmological model. For higher mass of new particles the effect is much weaker and may even have opposite sign [4].

(ii) Sterile Neutrinos and Leptogenesis. Sterile neutrinos can naturally emerge as neutrinos from a shadow or mirror gauge sector. Among other interesting phenomenological and astrophysical implications, this picture suggests the possibility of natural co-leptogenesis of the ordinary and dark matter fractions. The mechanism is based on the $B - L$ violating scattering processes like $l\phi \to l'\phi'$ that transform ordinary leptons and Higgs into the shadow ones which are out of equilibrium in the early universe [5].

(iii) Baryon number violation. Several reviews and reports were prepared for the Community Planning Study - Snowmass 2013 - and "Project X: Accelerator Reference Design, Physics Opportunities, Broader Impacts", which summarize the theoretical motivations and the experimental efforts to search for baryon number violation, focussing on nucleon

decay and neutron-antineutron oscillations. Present and future nucleon decay search experiments using large underground detectors, as well as planned neutron-antineutron oscillation search experiments with free neutron beams were highlighted [6, 7, 12]. In addition, members of our group (Z. Berezhiani, R. Biondi, N. Rossi) participated in the experiment on the search of neutron–mirror neutron oscillation at the Institute Laue-Langevin (ILL), Grenoble, together with the colleagues from the ILL and St. Petersburg Nuclear Physics Institute. The experiment was preformed on the pf2 facility, EDM beamline, using the ultra-cold neutron chamber with the 200 l volume. The results of the experiment are under elaboration and will be published.

——— Cosmology and Dark Matter (PD51) ———

Members: Z. Berezhiani, M. Crisostomi, **L. Pilo** and F.L. Villante.

In collaboration with E. Babichev (LPT-Orsay) L. Canton and C. Broggini (INFN-Padova), A. Serenelli (UAM-Barcellona), D. Comelli (INFN-Ferrara), A. Dolgov and A. Drago (University of Ferrara).

Scientific work

The research activity has been focused on the following topics:

i) Modifications of gravity. We have studied modification of gravity at large distances. We focused our activity on both the internal consistency of such models and on their phenomenological implications. All the theories with five degrees of freedom has been classified and constructed. The physically important cases of spherically symmetric solutions and cosmological FRW solutions were analysed in detail.

ii) Big Bang Nucleosynthesis. Effects of light millicharged dark matter particles on primordial nucleosynthesis were studied. It is shown that if the mass of such particles is much smaller than the electron mass, they lead to strong overproduction of Helium-4. An agreement with observations can be achieved by non-vanishing lepton asymmetry. Baryon-to-photon ratio at BBN and neutrino- to-photon ratio both at BBN and at recombination are noticeably different as compared to the standard cosmological model. For higher mass of new particles the effect is much less pronounced and may even have opposite sign.

iii) Neutrino astronomy. The study of the distintive signatures of ultra high energy events recently seen by IceCube can allow to single the neutrino origin out. We have discussed the possibility to discriminate the neutrino origin by measuring the fraction of the muon tracks. For any initial composition, because of the occurrence of flavor oscillations and despite their uncertainties, the fraction of muon tracks in the cosmic neutrinos is smaller than the one of atmospheric neutrinos, even hypothesizing an arbitrarily large

contribution from charmed mesons. A good understanding of the detection efficiencies and the optimization of the analysis cuts, along with a reasonable increase in the statistics, should provide us with a significant test of the cosmic origin of these events.

—— Theoretical Astroparticle Physics (FA51) ——

Members: R. Aloisio, **V. Berezinsky**, P. Blasi, D. Boncioli, M. Mitra, F.L. Villante, F. Vissani

In collaboration with V. Dokuchaev (INR, Moscow), Yu. Eroshenko (INR, Moscow), A. Gazizov (DESY Zeuthen), S. Grigorieva (INR, Moscow), M. Kachelriess (Trondheim Univ. Norway) and A. Vilenkin (Tufts University, USA).

Scientific work

The group worked in the following fields: ultra-high energy cosmic rays (UHECR), UHE neutrinos, neutrinos and gamma-rays from SN and SNRs, neutrino properties, and cosmology of the dark matter (clumps). From this list two works may be mentioned,

In the first one the propagation of UHE nuclei in CMB and EBL radiations has been studied in analytical approach. The work is published in the form of two papers [41, 42]. Early such calculations have been performed as Monte-Carlo simulations, in which the role of physical processes in formation of spectral features is lost. In these two papers three different analytical methods are developed on the basis of analytic solutions to kinetic (transport) equations. The trajectory method in backward time gives clear picture of nuclei propagation in the background radiation with explosive behavior of trajectories in the end of backward time, which affects the shape of the spectra. The most precise calculations of spectra are obtained in the method of coupled kinetic-equations. The spectra of primary and secondary nuclei, and spectra of secondary protons are calculated by this method and obtained results agree with Monte Carlo simulations reasonably well. A new approach for the observational discrimination of the neutrino mass hierarchy has been proposed by C. Lujan-Peschard, G. Pagliaroli and F. Vissani in [10]. An ordinary muon neutrino beam from pion decay of 6-8 GeV, observed at a distance 6000-8000 km in a Mton detector, results in 1000 muon events with a 30% difference for the cases of normal and inverted mass hierarchy, caused by the matter oscillation effect. The pairs of accelerator-detector CERN-Baikal lake or Fermilab-Mediterranean Sea are at the ideal distance for such an experiment.

—— Astrophysics and high energy physics (CT51) ——

Members: **M. Mannarelli**, A. Parisi, G. Pagliaroli, and F. Vissani.
In collaboration with F. Nesti (GSSI), G. Senjanovic (GSSI), F.L. Villante (University

of L'Aquila and INFN), A. Ianni (LNGS), F. Lombardi (LNGS), L. Tolos (ICE-UAB), C. Manuel (ICE-UAB), J. Soto (UB), M. Escobedo (Munich, Tech. U.), F. Giannuzzi (INFN-Bari), R. Anglani (CNR-Bari), M. Ruggieri (University of Catania), G. Colucci (Frankfurt University), R. Casalbuoni (University of Florence and INFN), R. Gatto (University of Geneve).

Scientific work

The scientific achievements concern several aspects of neutrino physics [10] and of matter in extreme conditions. The properties of r-modes in compact been studied in [43, 44], in which it was shown that the so-called rocket effect might lead to a damping of these oscillations for a certain range of temperature and frequencies. The propagation in the quark gluon plasma of heavy quarkonia has been studied in [45], with particular emphasis on the medium induced modification of the the energy levels and widths. A review on crystalline color superconductors has been completed [46], which should soon appear on Reviews of Modern Physics. The properties of phonons in the superfluids have been discussed in [47, 48].

Publications in journals, proceedings and preprints

[1] V. Azcoiti, G. Di Carlo, E. Follana and A. Vaquero, "Elucidating the Vacuum Structure of the Aoki Phase," Nucl. Phys. B **870**, 138 (2013) [arXiv:1208.0761 [hep-lat]].

[2] V. Azcoiti, G. Di Carlo, E. Follana, M. Giordano and A. Vaquero, "Phase structure of a generalized Nambu-Jona Lasinio model with Wilson fermions in the mean-field or large-N expansion" Nucl. Phys. B **875**, 45 (2013) [arXiv:1305.1765 [hep-lat]].

[3] Z. Berezhiani, A. D. Dolgov and I. I. Tkachev, "Dark matter and generation of galactic magnetic fields," Eur. Phys. J. C **73**, 2620 (2013).

[4] Z. Berezhiani, A. D. Dolgov and I. I. Tkachev, JCAP **1302**, 010 (2013) [arXiv:1211.4937 [astro-ph.CO]].

[5] Z. Berezhiani, "Sterile Neutrinos and Leptogenesis of Matter and Dark Matter," Nucl. Phys. Proc. Suppl. **237-238**, 263 (2013).

[6] K. S. Babu, E. Kearns, U. Al-Binni, S. Banerjee, D. V. Baxter, Z. Berezhiani, M. Bergevin, S. Bhattacharya *et al.*, "Baryon Number Violation," arXiv:1311.5285 [hep-ph].

[7] K. Babu, S. Banerjee, D. V. Baxter, Z. Berezhiani, M. Bergevin, S. Bhattacharya, S. Brice, T. W. Burgess *et al.*, arXiv:1310.8593 [hep-ex].

[?] A. S. Kronfeld, R. S. Tschirhart, U. Al-Binni, W. Altmannshofer, C. Ankenbrandt, K. Babu, S. Banerjee, M. Bass, Z. Berezhiani *et al.*, "Project X: Physics Opportunities," arXiv:1306.5009 [hep-ex].

[8] G. Bellini, L. Ludhova, G. Ranucci, F.L. Villante, "Neutrino oscillations", Advances in High Energy Physics, 2013 (191960).

[9] F. Vissani, G. Pagliaroli, F. L. Villante, "The fraction of muon tracks in cosmic neutrinos" JCAP **1309**, 017 (2013).

[10] K. Scholberg, F.L. Villante, "Oscillations at low energies" Nucl.Phys.Proc.Suppl. **237-238**, 352 (2013).

[11] S. Bertolini, A. Maiezza and F. Nesti, "$K \to \pi\pi$ hadronic matrix elements of left-right current-current operators," Phys. Rev. D **88**, no. 3, 034014 (2013)

[12] D. Comelli, F. Nesti, L. Pilo, "Massive gravity: a General Analysis" JHEP **1206**, 07 (2013) 161.

[13] D. Comelli, F. Nesti, L. Pilo "Weak Massive Gravity" Phys.Rev.**D87** (2013) 124021

[14] E. Babichev, M. Crisostomi "Restoring General Relativity in massive bi-gravity theory" Phys.Rev. **D88** (2013) 084002.

[15] G. Bellini, L. Ludhova, G. Ranucci, F.L. Villante, "Neutrino oscillations", Advances in High Energy Physics (191960) 2013

[16] F.L. Villante, A.M. Serenelli, F. Delahaye, M.H. Pinsonneault, "The chemical composition of the Sun from helioseismic and solar neutrino data", accepted for publication by Astrophys. Journal

[17] Z. Berezhiani, "Sterile Neutrinos and Leptogenesis of Matter and Dark Matter," Nucl. Phys. Proc. Suppl. **237-238**, 263 (2013).

[18] Z. Berezhiani, A. D. Dolgov and I. I. Tkachev, "BBN with light dark matter," JCAP **1302**, 010 (2013)

[19] Z. Berezhiani, A. D. Dolgov and I. I. Tkachev, "Dark matter and generation of galactic magnetic fields," Eur. Phys. J. C **73**, 2620 (2013).

[20] P. Blasi, Astron. Astrophys. Rev. **21**, 70 (2013).

[21] R. Aloisio, V. Berezinsky and P. Blasi, arXiv:1312.7459 [astro-ph.HE].

[22] P. Blasi, arXiv:1312.1590 [astro-ph.HE].

[23] P. Blasi, arXiv:1311.7346 [astro-ph.HE].

[24] G. Morlino, P. Blasi, R. Bandiera and E. Amato, arXiv:1311.1300 [astro-ph.HE].

[25] P. Soffitta, X. Barcons, R. Bellazzini, J. oBraga, E. Costa, G. W. Fraser, S. Gburek and J. Huovelin *et al.*, Exper. Astron. **36**, 523 (2013) [arXiv:1309.6995 [astro-ph.HE]].

[26] V. S. Berezinsky, V. I. Dokuchaev and Y. .N. Eroshenko, JCAP **1311**, 059 (2013) [arXiv:1308.6742 [astro-ph.CO]].

[27] R. Aloisio and P. Blasi, arXiv:1307.5045 [astro-ph.HE].

[28] R. Aloisio, Nucl. Phys. Proc. Suppl. **239-240**, 169 (2013).

[29] V. Berezinsky, EPJ Web Conf. **53**, 01003 (2013) [arXiv:1307.4043 [astro-ph.HE]].

[30] R. Aloisio, D. Boncioli, A. Di Matteo, A. F. Grillo, S. Petrera and F. Salamida, arXiv:1307.3895 [astro-ph.HE].

[31] :, O. Abril, B. S. Acharya, M. Actis, G. Agnetta, J. A. Aguilar, F. Aharonian and M. Ajello *et al.*, arXiv:1307.2232 [astro-ph.HE].

[32] G. Morlino, P. Blasi, R. Bandiera and E. Amato, arXiv:1306.6762 [astro-ph.HE].

[33] G. Morlino, P. Blasi, R. Bandiera and E. Amato, arXiv:1306.6454 [astro-ph.HE].

[34] R. Aloisio and P. Blasi, JCAP **1307**, 001 (2013) [arXiv:1306.2018 [astro-ph.HE]].

[35] B. S. Acharya, M. Actis, T. Aghajani, G. Agnetta, J. Aguilar, F. Aharonian, M. Ajello and A. Akhperjanian *et al.*, Astropart. Phys. **43**, 3 (2013).

[36] V. Berezinsky, Astropart. Phys. **53**, 120 (2014) [arXiv:1301.0914 [astro-ph.HE]].

[37] G. Morlino, P. Blasi, R. Bandiera, E. Amato and D. Caprioli, Astrophys. J. **768**, 148 (2013) [arXiv:1211.6148 [astro-ph.HE]].

[38] P. Blasi, Nucl. Phys. Proc. Suppl. **239-240**, 140 (2013) [arXiv:1211.4799 [astro-ph.HE]].

[39] P. Blasi, EPJ Web Conf. **53**, 01002 (2013) [arXiv:1208.1682 [astro-ph.HE]].

[40] R. Aloisio, EPJ Web Conf. **53**, 06001 (2013) [arXiv:1207.2089 [astro-ph.HE]].

[41] R. Aloisio, V. Berezinsky and S. Grigorieva, Astropart. Phys. **41**, 94 (2013) [arXiv:1006.2484 [astro-ph.CO]].

[42] R. Aloisio, V. Berezinsky and S. Grigorieva, Astropart. Phys. **41**, 73 (2013) [arXiv:0802.4452 [astro-ph]].

[43] G. Colucci, M. Mannarelli and C. Manuel, Astrophys. **56**, 88 (2013) [arXiv:1007.2304 [hep-ph]].

[44] G. Colucci, M. Mannarelli and C. Manuel, Astrophys. **56**, 104 (2013) [Astrofiz. **56**, 117 (2013)].

[45] M. A. Escobedo, F. Giannuzzi, M. Mannarelli and J. Soto, Phys. Rev. D **87**, 114005 (2013) [arXiv:1304.4087 [hep-ph]].

[46] R. Anglani, R. Casalbuoni, M. Ciminale, R. Gatto, N. Ippolito, M. Mannarelli and M. Ruggieri, arXiv:1302.4264 [hep-ph].

[47] M. Mannarelli, PoS ConfinementX , 261 (2012) [arXiv:1301.6074 [hep-ph]].

165

[48] M. Mannarelli, C. Manuel and L. Tolos, Annals Phys. **336**, 12 (2013) [arXiv:1212.5152 [cond-mat.quant-gas]].

Conferences, seminars and other activities

CP3 origins, Sud-Denmark University, Odense, Denmark, March 18, 2013 (*"Dark World"*, distinguished lecture by Z. Berezhiani)

ESS Science Symposium on "Neutron Particle Physics at Long Pulse Spallation Sources", LSPC, Grenoble, France , March 22-25, 2013 (*"Neutron oscillations and implications in physics and astrophysics",* invited talk by Z. Berezhiani)

3rd Int. Workshop on Baryon and Lepton Number Violation (BLV 2013): "From the Cosmos to the LHC", MPIK, Heidelberg, Germany, Apr 8-11, 2013, (*"Baryon number violation and ultra high energy cosmic rays"*, invited talk by Z. Berezhiani)

DESY, Hamburg, Germany, July 1, 2013 (invited seminar by F.L. Villante)

Int. Workshop "Beyond the Standard Model after the first run of the LHC", GGI, Florence, Italy, June 24-July 14, 2013 (*"Millicharged Dark World: Cosmological Etudes",* seminar by Z. Berezhiani)

Int. Conference "Dark matter, dark energy and their detection", NSU, Novosibirsk, Russia, July 22-26, 2013 (*"Mirror Dark Matter",* invited talk by Z. Berezhiani)

Int. Conference on Topics in Astroparticle Physics and Underground Physics (TAUP2013) Asilomar, California, USA, Sept. 8-13, 2013 (*"Solar models and solar neutrinos: a quantitative analysis of the solar composition problem",* contributed talk by F.L. Villante)

First Autumn School & Workshop on Particle Phenomenology, Tbilisi, Georgia, Sept. 23-28, 2013 (*"Physics beyond Standard Model",* invited lectures by Z. Berezhiani)

Int. Workshop on "Precision Physics and Fundamental Physical Constants", (FFK 2013), Pulkovo Observatory, St. Petersburg, Oct. 7-11, 2013 (*"Dark matter and generation of galactic magnetic fields",* invited talk by Z. Berezhiani)

Laboratory of Theoretical Physics, JINR, Dubna, Russia, Oct. 10, 2013 (*"Dark matter and generation of galactic magnetic fields",* invited seminar by Z. Berezhiani)

Institut de Physique Théorique, CEA Saclay, France, Oct. 16, 2013 (*"Dark matter and generation of galactic magnetic fields",* invited seminar by Z. Berezhiani)

Fifth INFN International School on: "Architectures, tools and methodologies for developing efficient large scale scientific computing applications" ESC13 - Bertinoro, Italy 20-26

Oct. 2013 (R. Biondi participant)

PSI Kolloquium, Villingen, Switzerland, Dec. 5, 2013 (*"Neutron Oscilations: a window to parallel worlds?"*, invited colloquium by Z. Berezhiani)

"Passion for Physics", Riccardo Barbieri Fest, SNS, Pisa, Dec. 19-20, 2013 (Z. Berezhiani participant)

Tales of Lambda - Nottingham (UK), July 1-5 (M. Crisostomi and L. Pilo speakers)

GR20, 20th International conference on General Relativity and Gravitation 07-13 July 2013, Warsaw (Polland) (L. Pilo speaker).

COSMO 2013 @ DAMTP Cambridge (UK), September 2-6 (M. Crisostomi speaker).

7th Aegean Summer School "Beyond Einstein's theory of gravity", Paros (Greece), September 23-28 (M. Crisostomi speaker).

The Cosmological side of Massive Gravity, 26/11/2013, APC Paris; (L. Pilo invited speaker).

The Cosmological side of Massive Gravity, 27/11/2013, LPT Orsay; (L. Pilo invited speaker).

Int. Conference on Topics in Astroparticle Physics and Underground Physics (TAUP2013) Sept. 8-13, 2013, Asilomar, California, USA, (F.L. Villante, contributed talk)

DESY, Hamburg (Germany), July 1, 2013 (F.L. Villante, Invited Seminar)

33rd International Cosmic Ray Conference, July 2-9 2013, Rio De Janeiro, Brasil (R. Aloisio speaker)

16th Lomonosov Conference on Elementary Particle Physics, Moscow, August 22 -28, 2013 (V. Berezinsky, invited talk)

INFN-IHEP Meeting on Cosmic Ray Physics, LNGS, September 16 -17, 2013 (V. Berezinsky, introductory talk)

International Cosmic Ray Conference, Rio De Janeiro, Brasil, July 2-9 2013 (P. Blasi, invited plenary talk)

4th Workshop on Air Shower Detection at High Altitude, Naples, January 31- February 1, 2013 (F. Vissani, invited talk)

NuMass2013 workshop, The Future of Neutrino Mass Measurements: Terrestrial, Astrophysical, and Cosmological Measurements in the Next Decade. Milan, February 4-7, 2013 (F. Vissani, invited talk)

Activity in INFN and International organizations

R. Aloisio is a member of the GSSI Scientific Board.

Z. Berezhiani organized the Int. Workshop SW6 "Hot Topics in Modern Cosmology" in Cargese, is coordinator of the L'Aquila unit of PRIN biennal grant 20084ZCK5J-004 "Astroparticle Physics", is scientific Coordinator of the Russian Science and Education Ministry biennial Grant N. 14.U02.21.0913 "Physics of solar, reactor and geo-neutrinos" at JINR, Dubna (2012-2013), teaches Theoretical Physics (Quantum Field Theory), Gauge Theories, Relativity and Cosmology at the University of L'Aquila, is member of the Doctorate Collegium of the Physics Dept. University of L'Aquila.

V. Berezinsky is a member of Int. Advisory Board of JEM-EUSO. He was a member of Int. Advisory Committees of many conferences.

M. Mannarelli is the scientific secretary of the LNGS. Coordinator of the CFA and co-organizer of the LNGS seminars, teaches Weak and Strong Interactions II at the University of L'Aquila.

L. Pilo is member of the Doctorate Collegium of the Physics Dept. and of the Doctorate Commission, University of L'Aquila and teaches Weak and Strong Interactions I at the University of L'Aquila.

F.L. Villante is a member of the scientific board of the CFA, has been convener of the "Int. Neutrino Oscillation Workshop (NOW 2012)", of the Nat. Workshop: "Incontri di Fisica delle Alte Energie (IFAE 2012), member of the organizing committee of the Int. Workshop: "The Physics of the Sun and the Solar Neutrinos: 3rd", teaches Astrophysics at the University of L'Aquila.

F. Vissani is co-organizer of the LNGS seminars, observer in Comm.II on behalf of Comm.IV, referee for the INFN National Permanent Committees II on non-accelerator physics and IV on theoretical physics, LNGS representative in the Italian Physics Society, INFN representative in the Scientific Advisory Committee of ApPEC/ASPERA, member of the scientific committee for the ICRANet-INFN agreement, member of the scientific council of the Groupement de Recherche Neutrino (CEA and IN2P3), coordinator of the CFA, lecturer of two PhD neutrino courses, one at the University of Milan and one at the University of Catania.

The XENON experiments

E. Aprile[a]*, M. Alfonsi[b], K. Arisaka[c], F. Arneodo[d][†], C. Balan[e], L. Baudis[f],
B. Bauermeister[g], K. Bokeloh[i], A. Brown[j], E. Brown[i], S. Bruenner[n],
G. Bruno[d], R. Budnik[a], J. M. R. Cardoso[e], A. P. Colijn[b], H. Contreras[a],
J. P. Cussonneau[k], M. P. Decowski[b], E. Duchovni[h], S. Fattori[g],
A. D. Ferella[d,f], W. Fulgione[l], M. Garbini[m], L. W. Goetzke[a],
C. Grignon[g], E. Gross[h], W. Hampel[n], R. Itay[h], F. Kaether[n],
G. Kessler[f], A. Kish[f], H. Landsman[h], R. F. Lang[j], M. Le Calloch[k],
C. Levy[i], S. Lindemann[n], M. Lindner[n], J. A. M. Lopes[e],
T. Marrodán Undagoitia[n,f], F. V. Massoli[m], A. J. Melgarejo Fernandez[a],
Y. Meng[c], M. Messina[a], A. Molinario[l], J. Naganoma[o],
U. Oberlack[g], S. E. A. Orrigo[e][‡], R. Persiani[m], F. Piastra[f], G. Plante[a],
N. Priel[h], A. Rizzo[a], S. Rosendahl[i], J. M. F. dos Santos[e], G. Sartorelli[m],
J. Schreiner[n], M. Schumann[p,f], L. Scotto Lavina[k], M. Selvi[m],
P. Shagin[o], H. Simgen[n], A. Teymourian[c], A. Tiseni[b], D. Thers[k],
H. Wang[c], M. Weber[n] and C. Weinheimer[i]
(The XENON100 Collaboration)

---

*Spokesperson
†Present address: New York University in Abu Dhabi, UAE
‡Present address: IFIC, CSIC-Universidad de Valencia, Valencia, Spain

[a] Physics Department, Columbia University, New York, NY, USA

[b] Nikhef and the University of Amsterdam, Science Park, Amsterdam, Netherlands

[c] Physics & Astronomy Department, University of California, Los Angeles, CA, USA

[d] INFN, Laboratori Nazionali del Gran Sasso, Assergi (AQ), Italy

[e] Department of Physics, University of Coimbra, Coimbra, Portugal

[f] Physics Institute, University of Zürich, Zürich, Switzerland

[g] Institut für Physik & Exzellenzcluster PRISMA, Johannes Gutenberg-Universität Mainz, Mainz, Germany

[h] Department of Particle Physics and Astrophysics, Weizmann Institute of Science, Rehovot, Israel

[i] Institut für Kernphysik, Wilhelms-Universität Münster, Münster, Germany

[j] Department of Physics, Purdue University, West Lafayette, IN, USA

[k] SUBATECH, Ecole des Mines de Nantes, CNRS/In2p3, Université de Nantes, Nantes, France

[l] INFN-Torino and Osservatorio Astrofisico di Torino, Torino, Italy

[m] University of Bologna and INFN-Bologna, Bologna, Italy

[n] Max-Planck-Institut für Kernphysik, Heidelberg, Germany

[o] Department of Physics and Astronomy, Rice University, Houston, TX, USA

[p] Albert Einstein Center for Fundamental Physics, University of Bern, Bern, Switzerland

Abstract

The XENON collaboration has entered a new phase in 2013. After operating, analyzing and publishing data from the running XENON100 experiment for five years, the focus has shifted to the construction of the XENON1T experiment. This experiment, sited in Hall B of LNGS, will be two orders of magnitude more sensitive than XENON100. XENON1T will be completed during 2014 and start collecting data in 2015. While the design and construction of XENON1T was ongoing in 2013, the collaboration has also published several important papers based on XENON100 data.

1   Introduction

The XENON collaboration operates a series of direct detection experiments at LNGS to search for dark matter particles in our Milky Way. The experiments use dual-phase liquid xenon time-projection chambers (TPCs) and are particularly well-suited to search for one of the most compelling dark matter candidate particle, the Weakly Interacting Massive Particle (WIMP), over a broad range of parameters. Starting with the XENON10 experiment more than a decade ago, the collaboration has successively built larger and more sensitive detectors. The XENON100 experiment was the world's most sensitive direct detection dark matter experiment for a number of years, until late 2013. The collaboration is currently constructing the next experiment, XENON1T, which itself will be two orders of magnitude more sensitive than XENON100, with a sensitivity goal of $2 \times 10^{-47}\,\mathrm{cm}^2$. Much of the infrastructure and detector design for XENON1T is such that it can be reused for an even larger upgrade in the future.

2 XENON100

2.1 Operation status

The XENON100 detector continues operating and taking valuable data. After a maintenance period in 2012, the detector was filled again with liquid xenon (LXe) in late 2012. The maintenance period allowed also to lower the contamination of Rn and ^{85}Kr in the LXe, these are radioactive isotopes that can be a background in the dark matter search. A new dark matter search run was started in April 2013 and ended in January 2014, with more than 150 days of data collected. These data were complemented with a dedicated ^{241}AmBe neutron calibration run and regular calibrations using gamma sources. The detector remains healthy and continues to provide science data.

We anticipate to continue operating the detector for a fifth year, to improve the sensitivity of the search for annual modulation, and to test new calibration procedures that will be important both for assessing the performance of the detector at the lowest energies and to test new calibration strategies for XENON1T.

2.2 Published Data

The XENON collaboration continued to analyze and publish data in 2013, based on the same 225 day data-set used in Ref. [1]. However, we also published papers that provide further description of the neutron background and detector response to nuclear recoils and a long paper that provided a very detailed description of the dark matter analysis.

2.2.1 Spin-dependent interpretation of the XENON100 Dark Matter Data
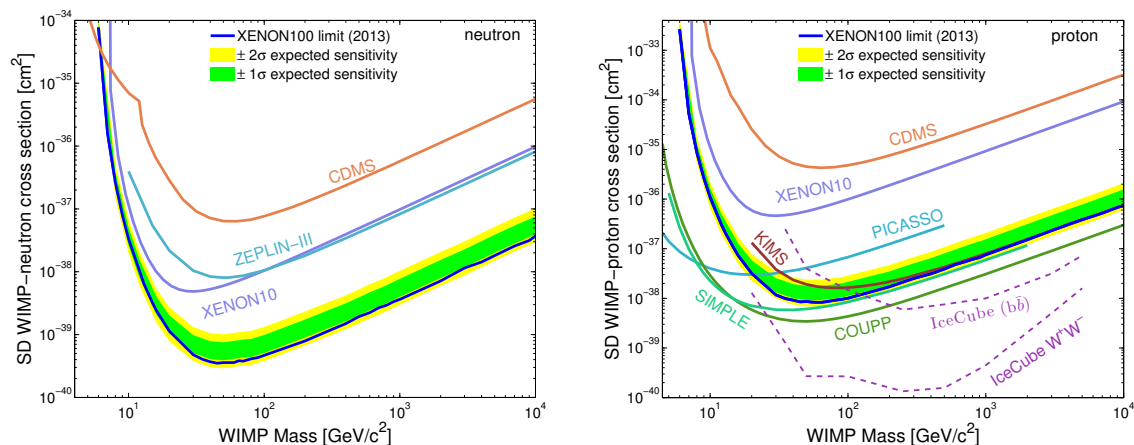
Figure 1: XENON100 90% C.L. upper limits on the WIMP spin-dependent cross section on neutrons (left) and protons (right). The 1σ (2σ) uncertainty on the expected sensitivity of this analysis is show as a green (yellow) band. The figures were published in Ref. [2].

Using the data collected between 2011 and 2012 comprising a total of 224.6 live days, we published a paper on the results for spin-dependent WIMP-nucleon interactions [2].

Sensitivity to spin-dependent interactions is possible due to the presence of two xenon isotopes, ^{129}Xe and ^{131}Xe, with an odd number of nucleons and a non-zero spin. The XENON100 results give the most stringent limit for WIMP-neutron scattering cross section for most WIMP masses, and are competitive with other experimental results for WIMP-proton scattering, as shown in Fig. 1.

2.2.2 Response of XENON100 to Nuclear Recoils
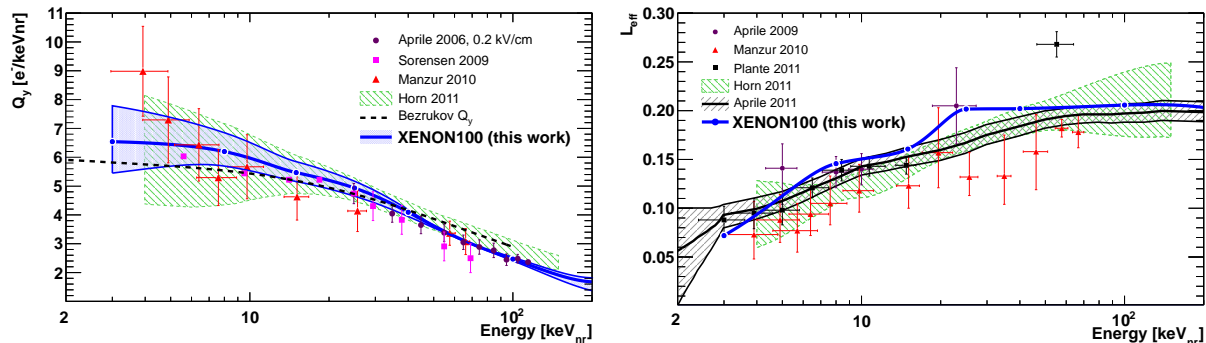
Figure 2: (left) Result on $\mathcal{Q}_y$ obtained from fitting the MC generated charge spectrum to neutron calibration data, allowing to extend $\mathcal{Q}_y$ to lower nuclear recoil energies than reported in dedicated measurements. (right) Similarly, $\mathcal{L}_{eff}$ obtained after absolute scintillation light matching. The blue lines show the obtained $\mathcal{Q}_y$ and $\mathcal{L}_{eff}$ relations in both cases, see Ref [3].
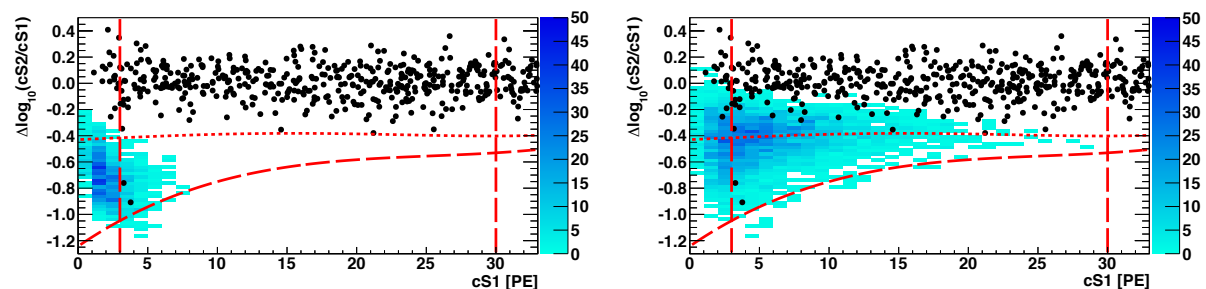
Figure 3: Simulation of the cS1 and cS2 signals based on the $\mathcal{Q}_y$ and $\mathcal{L}_{eff}$ curves presented in Fig. 2 for two different WIMP parameters. (left) The distribution for an $8\,\mathrm{GeV/c^2}$ WIMP and (right) the distribution for a $25\,\mathrm{GeV/c^2}$ WIMP with spin-independent WIMP-nucleon cross-sections of $3\times10^{-41}\,\mathrm{cm^2}$ and of $1.6\times10^{-42}\,\mathrm{cm^2}$, respectively. The vertical red lines represent the $3\,\mathrm{PE}$ analysis threshold and the upper $30\,\mathrm{PE}$ boundary, other analysis cuts defining the nuclear recoil region are also shown, see Ref. [3] for details. The black dots show the XENON100 data, with only two events in the nuclear recoil region, while hundreds would be expected for the two simulated WIMP parameters.

In this publication [3], data from measurements with an external ^{241}AmBe neutron source were compared with a detailed Monte Carlo simulation which was used to extract

the energy-dependent charge-yield $\mathcal{Q}_y$ and relative scintillation efficiency $\mathcal{L}_{\text{eff}}$ (see Fig. 2). The analysis showed an excellent level of absolute spectral matching in both observable signal channels (i.e., scintillation and ionization). The results provide a powerful confirmation of the validity of the derived signal acceptance in dark matter searches of the XENON100 experiment reported earlier. In particular, they also show that any low-mass WIMP signal with parameters reported by other dark matter experiments would give a convincing signal in the XENON100 experiment, see Fig. 3.

2.2.3 Estimate of the Neutron background in the XENON100 experiment

Ref. [4] presents a study on the nuclear recoil background of the XENON100 experiment, taking into account neutron backgrounds from (α,n) and spontaneous fission reactions due to natural radioactivity in the detector and shield materials, as well as muon-induced neutrons. Based on detailed Monte Carlo simulations, see Fig. 4, and using measured radioactive contaminations of all detector components, the paper predicts the nuclear recoil backgrounds for the WIMP search results published in the 2011 [5] and 2012 [1] XENON100 publications. In particular, we show that these nuclear backgrounds to do not limit the sensitivity of the experiment.
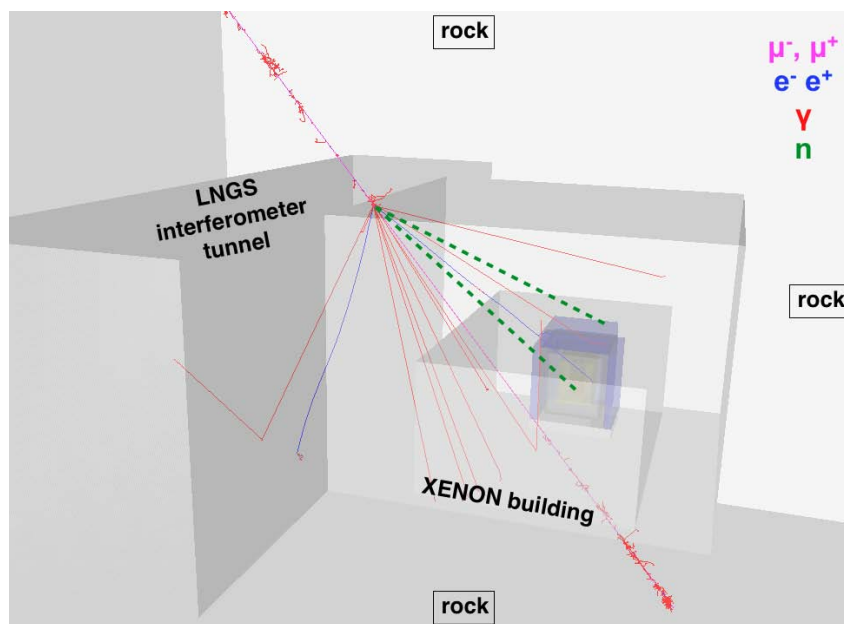
Figure 4: The GEANT4 model of the XENON100 experimental site for simulations of the cosmogenic neutron background, showing a muon interaction as an example. Two neutrons (dashed lines) and an electromagnetic shower are produced in the rock: one neutron is stopped by the shield, and another one penetrates into the detector volume [4].

2.2.4 Behavior of single Electrons in LXe

Finally, the collaboration also published a detailed study of the behavior of single electrons in XENON100 [6]. These single electrons are unrelated to WIMP interactions, but the

study is very important to understand the response of a two-phase xenon TPC to single electrons, enabling searches for low energy events based on the S2 signal alone. Ref. [6] discusses single-electron charge signals and explains them as being due to the photoionization of impurities in the liquid xenon and of the metal components inside the TPC. These signals can be used as a unique calibration source to characterize the detector.

3   XENON1T

XENON1T is the successor to the XENON100 experiment and 2013 was an important year for this phase of the XENON-series of experiments. With a design sensitivity two orders of magnitude better than XENON100, over a broad range of WIMP masses and interaction types, this first LXe TPC experiment at the tonne-scale will have significant discovery potential. In designing the experiment, we have built-in the possibility for a rapid sensitivity scale-up by another order of magnitude, by enabling a $\sim 2\times$ larger LXe detector to fit into the same cryostat while re-using most of the other systems developed for XENON1T.

3.1   Construction Status
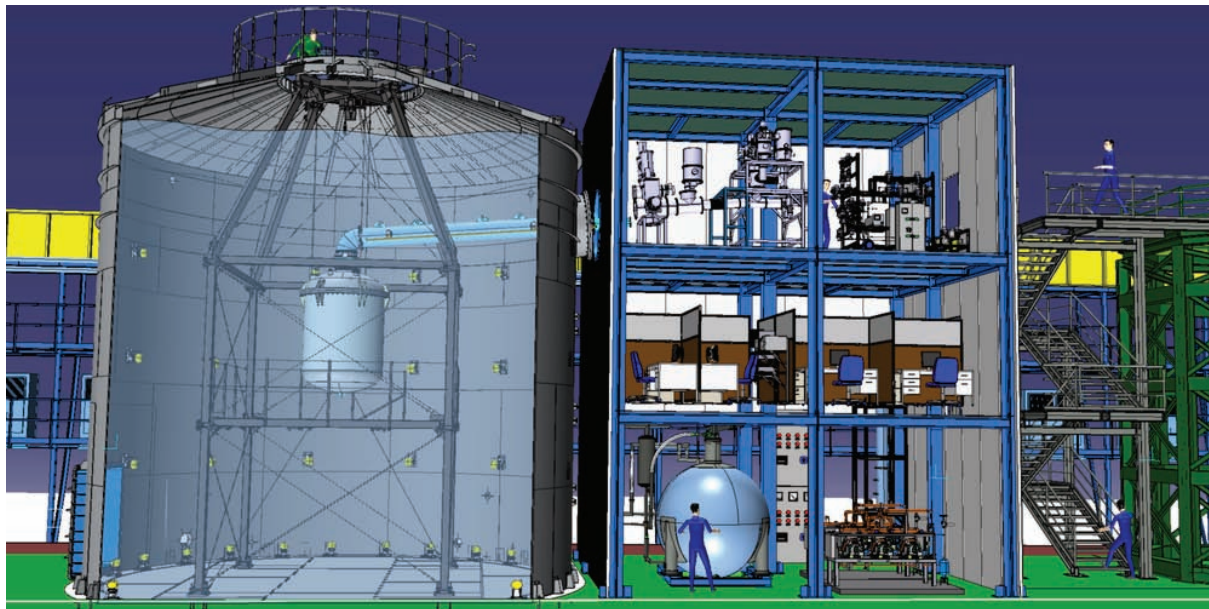
Figure 5: 3D rendering of XENON1T. The cryostat housing the dual-phase xenon TPC is hanging in the middle of the water tank (left). The service building with all equipment to support running the experiment, has three, fully packed, floors.

The construction of the XENON1T experiment is progressing rapidly at LNGS, on schedule to start taking science data in Summer 2015. Before the construction of the major items could start, a detailed safety analysis was completed and approved by the "Genio Civile" and by the LNGS SPP. Fig. 5 shows a CAD rendering of XENON1T. We

started the construction in the fall of 2013 with the erection of the Water Tank (WT), the largest structure of the experiment. The WT will be filled with $700\,\mathrm{m}^3$ of ultra-pure water and instrumented with PMTs for an active Cherenkov muon veto. It is a stainless steel cylinder, $9.6\,\mathrm{m}$ diameter and $9\,\mathrm{m}$ high, with a conical roof rising an additional $3.2\,\mathrm{m}$. The construction of the WT was completed on December 15th, 2013 after three months of underground assembly. During the WT construction, the muon veto group spent an intense weekend cladding the internal surface of the WT's roof with a reflective foil. This foil will later cover the entire surface of the WT and improve the muon veto efficiency.
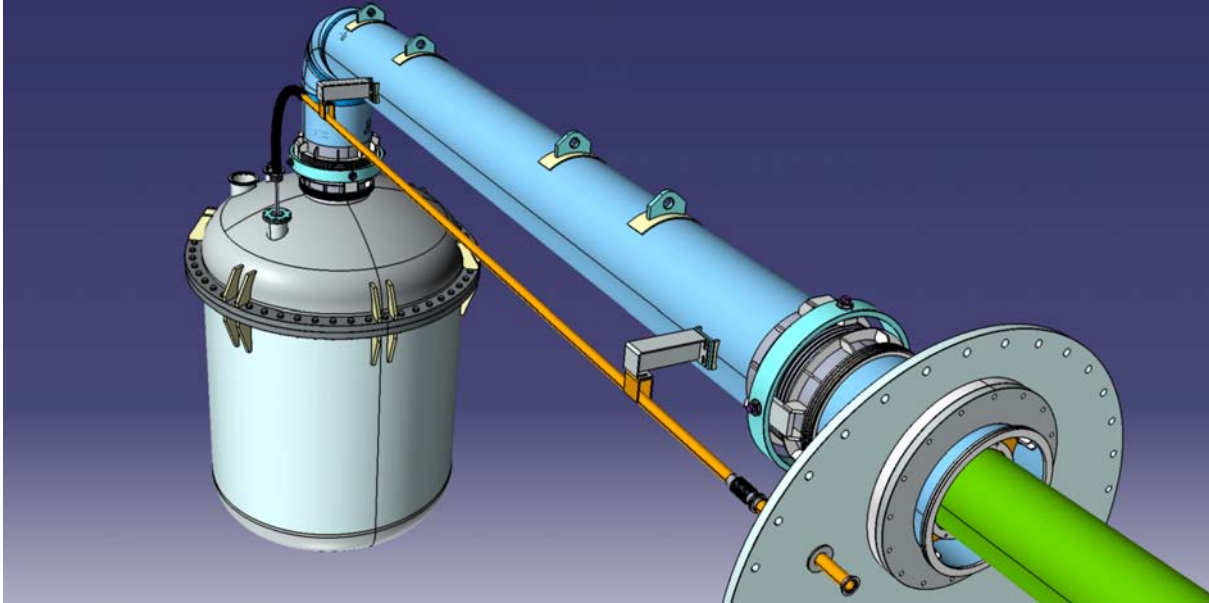
Figure 6: The cryostat, with an outer diameter of $1.6\,\mathrm{m}$, houses the dual-phase xenon TPC in the water tank. The thick cryogenic pipe contains the xenon and vacuum lines between the cryogenic system and the cryostat. It also carries the signal and high-voltage cables for the PMTs. The separate thin pipe carries the high-voltage cable for the cathode in the TPC.

All the photo-multiplier tubes (PMTs) for the muon veto system itself were purchased and tested during 2013. Two different calibration systems were tested and the reflective foil has been characterized (reflectivity curve versus wavelength, wavelength shifting power and radioactive content). In addition, the PMT mounting structures were also constructed.

The construction of the service building also began in the fall of 2013. This building, depicted in the middle of Fig. 5, will house all the systems and equipment necessary to operate the detector. The ground-level floor will be dedicated to ReStoX (Xe recovery and storage system) and cryogenic distillation column. The mid-level floor houses the electronics, and data acquisition (DAQ) system and has an operations room. Finally, the top-level floor is for the XENON1T cyrogenics system and purification system. The cryogenic pipe from the cryostat in the WT also enters the service building through the top-level floor. The single cryogenic pipe carries the xenon input and output lines and also has all the signal and high-voltage cables for the instrumentation in the cryostat.

Figure 7: Construction of the water tank in the fall of 2013.

The design of the cryostat and cryogenic pipe was finalized during 2013 (see Fig. 6) with manufacturing starting in early 2014. All the material necessary for the manufacturing of this device was procured and screened. The cryostat, like almost all the other systems of the experiment, was designed with an upgrade of XENON1T in mind. XENON1T is designed for 3.3 tons of LXe, with 248 PMTs in the TPC. The upgrade of XENON1T will roughly double the amount of xenon and the number of PMTs. We will be able to reuse the outer vessel of the cryostat and the cryogenic pipe for this upgrade. Since the cables carrying the PMT signals and high-voltage from the support building to the TPC have to be installed into the cryogenic pipe during manufacturing, we will already install sufficient cables for the upgrade as well. The construction of the vibration-free support structure holding the cryostat in the center of the water tank was started in September 2013. It is also designed to be able to hold a possible future upgrade of XENON1T. It has been installed in the WT during May 2014. The installation of the cryostat itself will take place in July 2014.

The design of the XENON1T TPC continued during 2013, with most design-aspects finalized. We spent time identifying, screening and procuring PTFE, stainless steel and OFHC copper, the main components of the TPC. A prototype of the anode electrode grid, which needs to fulfill strict requirements in terms of flatness, has been produced, as well as a prototype of the cathode grid, which needs to hold a voltage around -100 kV. Full-sized prototypes of the Cu-field-shaping-ring and the custom-made high-voltage feedthrough

Figure 8: (left)Completed water tank. (right) Raising of the service building.

were also constructed. About a third of the 248 3-inch Hamamatsu R11410-21 PMTs necessary for the construction of the TPC have been delivered and tested at cryogenic temperatures and screened for radioactivity with a HPGe detector.

The design of the cryogenic system, required for liquefaction of xenon, was largely completed in 2013 and most of the components purchased. The cryogenic system interfaces with the xenon purification system and forms the recirculation system during normal operations. Most of the construction of the purification system has also been completed. Both systems will be installed at LNGS during the summer of 2014. Similarly, the Kr distillation column was constructed and tested. Initial commissioning results look extremely promising, with indications that the Kr concentration in Xe will be much lower than the 0.5 ppt required for XENON1T.

The Xe recovery and storage system (ReStoX) was redesigned during 2013 to allow for a larger storage capacity, more optimal cooling power and safety redundancy. The system is now based on a 2-m-diameter spherical double-walled stainless steel pressure vessel which will be able to store up to 7.6 tonnes of Xe in supercritical, liquid or even solid state. The increased capacity will enable ReStoX to serve also for the upgraded XENON1T detector. The sphere is vacuum insulated and designed to have a maximum heat leak of about 50 W. The cooling system has been improved with two nitrogen-based systems: a 3 kW condenser, made of copper mounted inside the sphere, enables ReStoX to keep the xenon in liquid state for filling into the TPC; a system of cooling lines surrounding

177

Figure 9: Inspection of the water tank during construction.

the inner sphere keep its temperature well below the LXe triple point, enabling ReStoX to efficiently and rapidly recover the LXe from the detector if necessary.

Finally, a lot of progress has been made on the DAQ, slow control and computing efforts. The DAQ system consists of two main components, the trigger-less DAQreader that continuously reads and digitizes all PMTs, and the EventBuilder that selects and saves the relevant information from the data flow. A 40-channel prototype was constructed and is used to test the entire readout chain, from the raw data until disk storage and makes us confident that this novel readout system will preform well. The modular approach makes it very easy to adapt the system to the increased number of channels for the upgrade of XENON1T.

The XENON1T slow control system is based on a commercial system of controller units with a central supervisory control and data acquisition computer (SCADA). Almost all XENON1T sub-systems interface with the slow control system. Besides a formal technical requirements document, many of the necessary slow-component systems were purchased and customized for our use during 2013.

The computing group continued to refine the computing model for XENON1T. The amount of data, especially during calibration, will be significant and unprecedented at LNGS. We are therefore planning to use GRID resources in order to process this data.

We also further enhanced the detail of our GEANT4-based Monte Carlo simulations during 2013. This allows us to anticipate the effects on the XENON1T backgrounds for various design choices. With a design goal of less than one background event in a 2 ton-yr

exposure, the Monte Carlo has become an essential tool for XENON1T.

4 Conclusions

The construction of XENON1T started in 2013, on schedule to deliver science data in the second half of 2015. The LNGS laboratory support has been invaluable and exemplary during this time, from providing the engineering support and integration of various sub-systems, from water tank to cryostat to support building, to maintaining the safety of construction and operations. While the construction was ongoing, the XENON collaboration has also operated and analyzed data from XENON100, reported in several publications. We expect to still release a number of important publications based on data from this experiment in the coming years.

5 List of Publications

The XENON Collaboration published three papers in 2013:

- "Limits on spin-dependent WIMP-nucleon cross sections from 225 live days of XENON100 data", E. Aprile *et al.* [XENON100 Collaboration], Phys. Rev. Lett. **111**, 021301 (2013).

- "Response of the XENON100 dark matter detector to nuclear recoils", E. Aprile *et al.* [XENON100 Collaboration], Phys. Rev. **D 88**, 012006 (2013).

- "The neutron background of the XENON100 dark matter search experiment", E. Aprile *et al.* [XENON100 Collaboration], J. Phys. G: Nucl. Part. Phys. **40**, 115201 (2013). *This paper was also one of the Highlights of 2013 chosen by the J. Phys. G.'s Editors for presentation of outstanding research.*

The following paper was submitted in 2013 and published at the beginning of 2014:

- "Observation and applications of single-electron charge signals in the XENON100 experiment", E. Aprile *et al.* [XENON100 Collaboration], J. Phys. G: Nucl. Part. Phys. **41** (2014) 035201.

Finally, our long paper describing the details of the dark matter analysis, originally submitted in 2012, was significantly expanded. It describes not only the analysis methods in the 100 day dark matter exposure data-set [5], but also includes the analysis methods used in the 225 day data-set [1]. The manuscript was resubmitted in 2013 and published at the beginning of 2014.

- "Analysis of the XENON100 Dark Matter Search Data", E. Aprile *et al.* [XENON100 Collaboration], Astropart.Phys. **54** (2014) 11-24.

References

[1] E. Aprile *et al.* [XENON100 Collaboration], Phys. Rev. Lett. **109**, 181301 (2012) [arXiv:1207.5988 [astro-ph.CO]].

[2] E. Aprile *et al.* [XENON100 Collaboration], Phys. Rev. Lett. **111**, no. 2, 021301 (2013) [arXiv:1301.6620 [astro-ph.CO]].

[3] E. Aprile *et al.* [XENON100 Collaboration], Phys. Rev. D **88**, 012006 (2013) [arXiv:1304.1427 [astro-ph.IM]].

[4] E. Aprile *et al.* [XENON100 Collaboration], J. Phys. G **40**, 115201 (2013) [arXiv:1306.2303 [astro-ph.IM]].

[5] E. Aprile *et al.* [XENON100 Collaboration], Phys. Rev. Lett. **107**, 131302 (2011) [arXiv:1104.2549 [astro-ph.CO]].

[6] E. Aprile *et al.* [XENON100 Collaboration], J. Phys. G **41**, 035201 (2014) [arXiv:1311.1088 [physics.ins-det]].

[7] E. Aprile *et al.* [XENON100 Collaboration], Astropart. Phys. **54**, 11 (2014) [arXiv:1207.3458 [astro-ph.IM]].

Cosmic Silence

E. Fratini[a,b], M.F. Fischietti[a,c], G. Simone[a], E. Bortolin[b], G. Esposito[b], P. Fattibene[b], C. Nuccetelli[b], M.A. Tabocchini[a,b], E. Alesse[c], A. Tessitore[c], F. Zazzeroni[c], M. Balata[d], L. Ioannuci[d], A. Esposito[e], M.. Chiti[e], L. Satta[e]

[a] Museo Storico della Fisica e Centro Studi e Ricerche Enrico Fermi
[b] Istituto Superiore di Sanit, Technology and Health Department,
and INFN-Roma1 Gr. coll. Sanit, 00161 Roma, Italy
[c] L'Aquila University, Department of Biotechnological and Applied Clineical Sciences
[d] INFN - Gran Sasso National Laboratory
[e] INFN - Frascati National Laboratory

Abstract

Low radiation doses may have a modulation effect to the normal cell metabolism that can result in perturbations leading to resistance or sensitivity to damage induced by various stressors. In order to investigate the cellular mechanisms that take pace at environmental radiation exposure levels we have designed experiments consisting in twin set-up of different biological systems in a laboratory where the environmental radiation is reduced as possible and in a reference laboratory. To this purpose a cell culture laboratory has been set up underground LNGS several years ago. The results of recent in vitro studies carried out on pKZ1 A11 hybridoma cells are here reported. An animal housing facility has been designed for the planned in vivo studies.

1   Introduction

Environmental radiation represents a constant daily stimulus that has been incorporated in the biology of living organisms during evolution with the development of defense mechanisms well preserved during phylogeny.

In order to investigate if modulation of radiation environment can modify the biochemistry of biological systems and their response to genotoxic agents, *Satta et al* [1] designed an experiment consisting in twin set-up of yeast culture in a laboratory where the environmental radiation is reduced as possible and in a reference laboratory. They took advantage of the unique opportunity represented by the Gran Sasso National Laboratory (LNGS) of the Istituto Nazionale di Fisica Nucleare (INFN), where the cover of at least 1400 m of rock gives an excellent shielding against cosmic rays and neutrons, the former being reduced by a factor of 10^6 [2] and the latter by a factor of 10^3 [3, 4] respect to the external environment. Yeasts maintained for up to 120

generations under low radiation environment (LRE) were more susceptible to the toxic effects of methyl-methan-sulphonate respect to yeasts maintained in reference radiation environment (RRE).

Since then, further studies have been carried out on cells from higher eukaryotes, namely Chinese hamster V79 cells and TK6 human cells [5, 6, 7], cultured for several months, in order to reach a comparable number of generations as yeasts, in LRE and in RRE. The overall results have shown that cells maintained under LRE are less efficient in scavenging reactive oxygen species and more susceptible to radiation induced DNA damage compared to cultures maintained in RRE. The open question is if and how this behaviour is also occurring *in vivo*, being well know that not all the radiation induced damage has a local origin and that part of the biological response is due to non-cell-autonomous physiological mechanism that point to studies at organism level.

The Cosmic Silence Project aims to study the biochemical behaviour of living organisms in a reduced radiation environment by means of very sensitive biological in vitro and in vivo models: hybridoma cells derived from transgenic pKZ1 mouse model and pKZ1 mice.

The pKZ1 intrachromosomal recombination assay has been extensively used for studying *in vitro* and *in vivo* responses to low acute doses of DNA damaging agents [8, 9, 10, 11, 12]. In the framework of the collaboration with Prof. P. Sykes, Flinders University, Australia, and with Prof. Edoardo Alesse and co-workers, University of LAquila, Italy, in vitro experiments have been carried out using the hybridoma cell line A11, obtained by fusing pKZ1 spleen cells with a myeloma cell line and then selecting clones housing the pKZ1 transgene [9]. A11 cells were cultured for 1 month in both LRE (underground at LNGS) and RRE (at the Istituto Superiore di Sanit, ISS, in Rome). The results have shown that the concentration of poly (ADP-ribose) polymerase-1 (Parp-1), a key protein in DNA repair as well as in differentiation, proliferation, and tumour transformation, is drastically reduced in cells grown in LRE. Moreover, divergences have been observed in the expression of genes (among them CAT, SOD and GPX) involved in the protection from oxidative damage.

In the framework of the Cosmic Silence Project, an animal housing facility, satellite of the facility already existing at LAquila University, has been designed for the planned *in vivo* studies. For an accurate interpretation of the biological *in vitro* and *in vivo* results the characterization of the different components of the radiation environment will be carried out in the different experimental sites.

2 Characterization of the radiation field in the different experimental sites

The Cosmic Silence project requires a characterization of the radiation field in the environments where the *in vitro* and the *in vivo* experiments will be carried out. To this purpose new measurements have been planned in the different sites of interest, namely in the underground laboratories of Gran Sasso (INFN) and in the ground laboratories at LAquila University and at Istituto Superiore di Sanit (ISS). The details of the measurement plans have been widely discussed in the framework of the collaboration. Taking into account that the monitoring measurements will be carried out inside and outside the animal housing and cell incubators, 11 sites has been identified to be monitored: 2 at ISS, where only *in vitro* experiments will be performed, 4 at LAquila University where *in vitro* and *in vivo* experiments will be performed and 5 at LNGS underground laboratories, where both *in vivo* and *in vitro* experiments will be carried out.

At the LNGS underground cell culture laboratory two incubators have to be monitored, one of them located inside a 10 cm thick iron shield.

Thermoluminescence dosimeters (LiF), optically stimulated luminescent dosimeters (Al2O3), large dimension BF3 detector, high pressure ionization chambers (Reuter-Stokes), have been chosen to measure the dose, dose rate due to terrestrial radiation (gamma rays and Rn) and cosmic radiation (mainly neutrons). In particular, among the possible LiF based dosimeters, the TLD 700H have been selected as they are characterized by a high radiation sensitivity and signal stability. They cannot reveal the neutron component which, being low with respect to the other components (gamma), especially in the underground laboratories, will be better detected by using the more appropriate instrumentation mentioned above. A set of these dosimeters has been purchased, and the Al2O3 dosimeters are available at ISS.

Two high pressure ionization chambers Reuter-Stokes are also available and an inter-comparison between them has been planned in order to warrant the comparability of the results obtained in the different measurement sets/sites.

Gamma radiation energy spectrum, and activity concentration of gamma radiation emitting radionuclides, will be performed by gamma spectroscopy with an HpGe.

Neutron dose will be assessed by BF3 high sensitive detector.

A tentative neutron spectrometry will be also carried out by an extender range multi-spheres system.

Radon activity concentration in air will be measured and monitored using an Alfaguard instrument.

The described measurements will be performed in the ground laboratories at LAquila University and ISS and at the LNGS underground laboratory.

3   Experimental results on in vitro cell cultures

The hybridoma cell line (A11) was kindly donated by Prof. Pamela Sykes, Flinders University, Adelaide, Australia. A11 cells were cultured in parallel for up to 1 month at the ISS (reference radiation environment, RRE) and at the LNGS underground cell culture laboratory (low radiation environment, LRE). Afterwards, A11 cells grown at LRE were brought to RRE laboratory and cultured for additional 2 weeks, together with the 1 month-old RRE culture. Experiments were performed two times.

To evaluate gene expression of enzymes such as catalase (CAT), superoxide dismutase (SOD), and glutathione peroxidase (GPX), all of them involved in quenching the damage produced by Reactive Oxygen Species (ROS), mRNA was extracted weekly from the A11 parallel cultures. CAT is hydrogen peroxide scavenger and SOD is superoxide ion scavenger. GPX (with his 4 isoforms) has several function: Glutathione oxidation, scavenger of hydrogen peroxide intracellular (GPX1 and GPX2) and extracellular (GPX3) or lipid peroxide (GPX4) scavenger.

At the same time protein expression of poly (ADP-ribose) polymerase-1 (PARP-1), a key protein in DNA repair and physiological and pathological functions from cell survival to several forms of cell death, was evaluated. Analysis of gene expression of antioxidant enzymes was performed with real time quantitative PCR analysis (qPCR) and relative quantification was carried out with the $\Delta\Delta$CT method [13].

Gene expression analysis of ROS-Scavenger genes (Fig. 1) showed that the two Gpx mRNA isoforms (*Gpx1* and *Gpx3*) as well as *Cat* are less expressed in A11 cells grown at LRE respect to cells maintained at RRE as soon as after 1 week of culture. This under expression increases
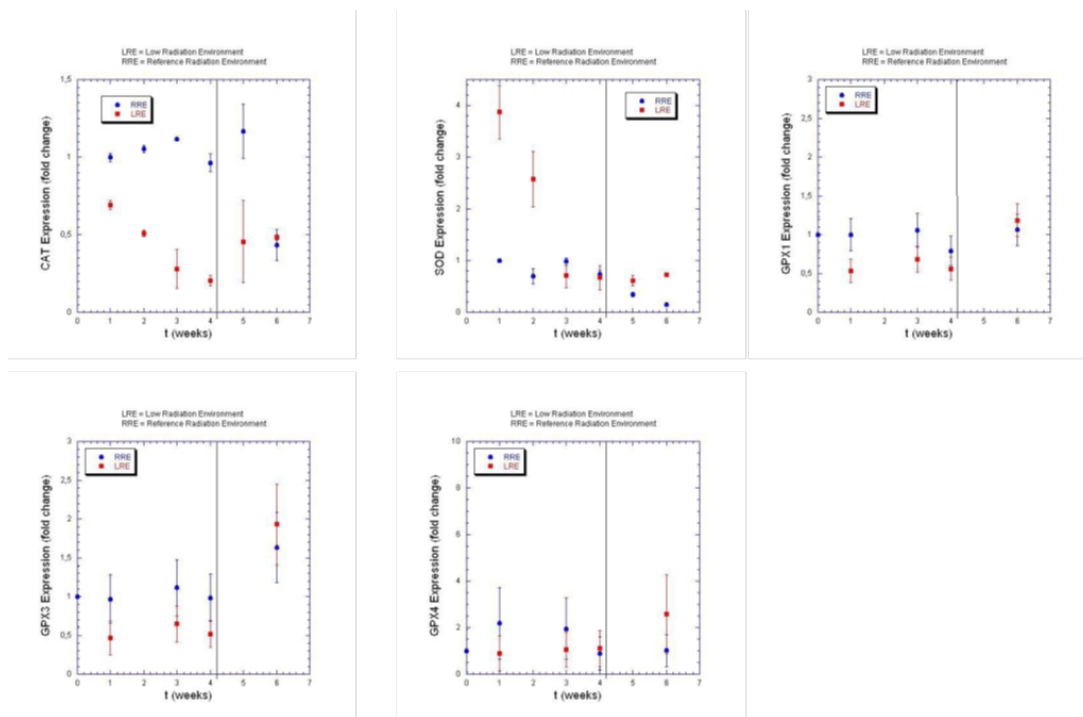
Figure 1: Gene expression of *Catalase (Cat), Superoxide dismutase (Sod), Glutathione peroxidase (Gpx1, Gpx3, Gpx4) evaluated by qPCR e normalized on the gene expression in A11 cells at time 0. ● Hybridoma cell line 9198 A11 growth in RRE; ◇ Hybridoma cell line 9198 A11 growth in LRE. The black vertical line indicate the time (4 weeks) in which the cells growth in LRE for 1 month have been taken back to RRE (the data from these experimental point are pictured in red as the cells in LRE).*

with time and it is maintained for up to 1 month. When cells grown at LRE were brought to RRE these gene expression were restored to the original level or even increased. It is worth note that the level of under *Sod* mRNA expression found after 1 week of growth at LRE is maintained during all the experiment duration: the minimum value is obtained as early as after 1 week of growth.

PARP-1 modulation was also evident after a very short period (1 week). A11 cells grown at LRE showed less protein modulation respect to cells grown at RRE and this finding was kept during the entire month of culture.

When A11 cells grown at LRE were brought to RRE laboratory and cultured for additional 2 weeks, together with the 1 month-old RRE culture, the protein modulation increases and showed an inversion between the two cultures (Fig. 2) [14, 15].

If, after further experiments already planned, PARP-1 modulation from the environmental radiation will be confirmed, this finding would open new scenario on the interaction between radiation environment and individual genotype, either on the incidence of DNA damage related diseases either on life span. Actually, literature data show a correlation among lifespan and PARP-1 modulated DNA repair [16, 17, 18, 19].
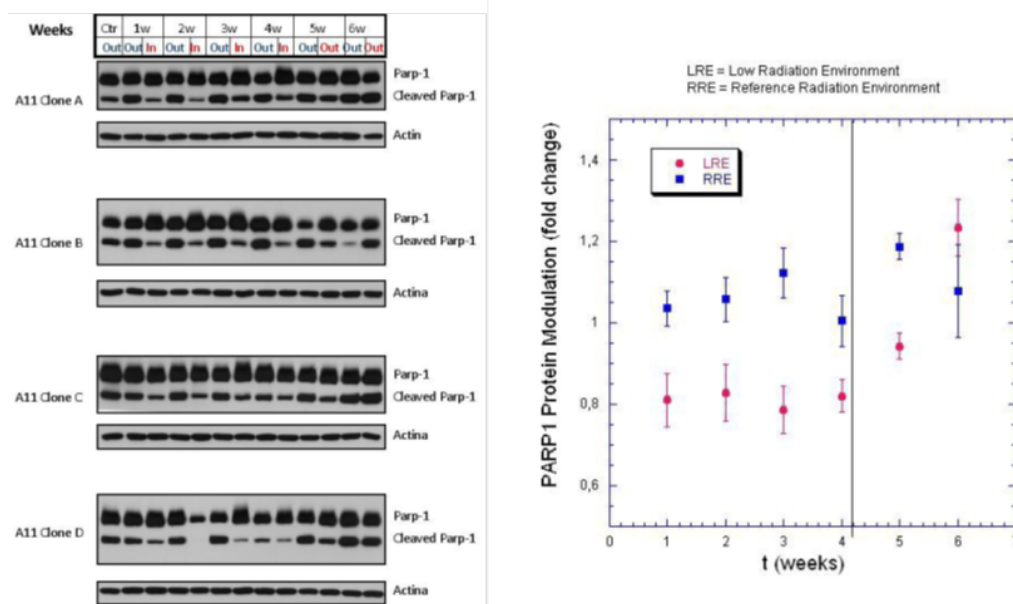
Figure 2: *Modulation of Poly [ADP-ribose] polymerase-1 protein both unprocessed (Parp-1) and cleaved (Cleaved PARP-1) compared to the internal standard -Actin evaluated by Western Blot on 4 clones of the hybridoma cell line 9198 A11growth in the two experimental condition. In the graph quantity differences of Parp-1 protein compared to the internal standard are normalized on the quantity of Parp-1 in A11 cells at time 0. ⋄ Hybridoma cell line 9198 A11growth in RRE; • Hybridoma cell line 9198 A11growth in LRE.*

4   Design of the underground LNGS mice housing facility

A mice housing facility, satellite of the facility already existing at LAquila University, has been designed. The set up is shown in Fig. 3. Mice will be kept inside closed cages in a rack located in a closed room. A further closed space is foreseen for storage and further isolation of the animal housing site from outside. It is important to underline that the underground mice housing satellite facility of LNGS will be used only for the maintenance of the pKZ1 mice colony in LRE. After different periods of time mice will be transferred to LAquila University (where a parallel mice colony will be established in reference conditions) for the planned biological tests. The colleagues of LAquila University will be in charge for the management and for all the authorization aspects (accordingly to the national rules for animal testing, ethical committee included) of the LNGS satellite mice housing facility.

Acknowledgements
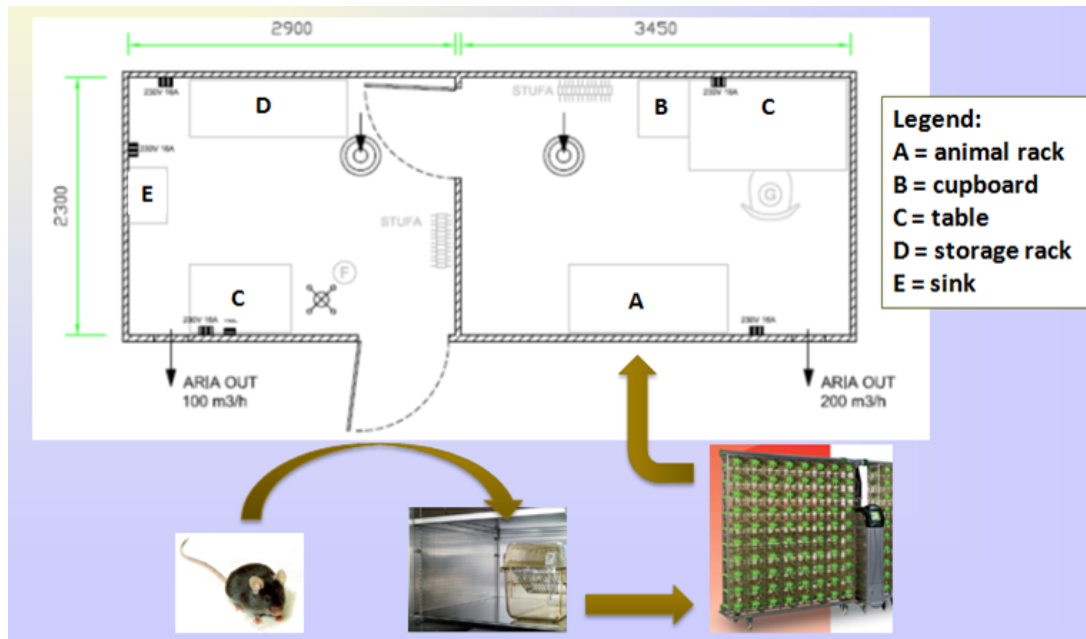
Figure 3: Possible configuration of the underground LNGS mice housing facility

References

[1] Satta L, Augusti-Tocco G, Ceccarelli R, Esposito A, Fiore M, Paggi P, Poggesi I, Ricordy R, Scarsella G, Cundari E *Low environmental radiation background impairs biological defence of the yeast Saccharomyces cerevisiae to chemical radiomimetic agents.* Mutat Res (1995) 347(3-4):129-33

[2] The MACRO Collaboration (1990) Study of penetrating cosmic ray muons and search for large scale anisotropies at the Gran Sasso Laboratory. Phys Lett B 249:149 156

[3] Rindi A, Celani F, Lindozzi M, Miozzi S. *Underground neutron flux measurement.* Nucl Inst Meth A (1998)272:871-874

[4] Belli P, Bernabei R, DAngelo S, De Pascale M, Paoluzi L, Santonico R, Taborgna NIN, Villoresi G *Deep underground neutron flux measurement with large BF3 counters.* Rivista del Nuovo Cimento A (1989) 101:959-966

[5] Satta L, Antonelli F, Belli M, Sapora O, Simone G, Sorrentino E, Tabocchini M A, Amicarelli F, Ara C, Cerú MP, Colafarina S, Conti Devirgiliis L, De Marco A, Balata M, Falgiani A, Nisi S. *Influence of a low background radiation environment on biochemical and biological responses in V79 cells.* Radiat Environ Biophys (2002) 41 (3):217-24

[6] Carbone M C, Pinto M, Antonelli F, Amicarelli F, Balata M, Belli M, Conti Devirgiliis L, Ioannucci L, Nisi S, Sapora O, et al (2009) *The Cosmic Silence Experiment: on the putative adaptive role of environmental ionizing radiation.* Radiat. Environ. Biophys. 48:189-196

[7] Carbone M C, Pinto M, Antonelli F, Amicarelli F, Balata M, Belli M, Conti Devirgiliis L, Sapora O, Simone G, Sorrentino E, Tabocchini M A, Satta L (2010) *Effects of deprivation of background environmental radiation on cultured human cells.* Il Nuovo Cimento 4:469-477

[8] Sykes P. J., Hooker A. M., Harrington C. S., Jacobs A. K., Kingsbury L., Morley A. A. *Induction of somatic intrachromosomal recombination inversion events by cyclophosphamide in a transgenic mouse model.* Mutat Res (1998) 397:209-219

[9] Hooker A M, Home R, Morley A A, Sykes P J, (2002) *Dose-dependent increase or decrease of somatic intrachromosomal recombination produced by etoposide.* Mut. Res. 500, 117-124.

[10] Hooker M., Bhat M., Day T. K., Lane J. M., Swinburne S. J., Morley A. A., Sykes P. J. *The linear no-threshold model does not hold for low-dose ionizing radiation.* Radiat Res (2004) 162:447-452

[11] Zeng G., Day T. K., Hooker A. M., Blyth B. J., Bhat M., Tilley W. D., Sykes P. J. *Non-linear chromosomal inversion response in prostate after low dose X-radiation exposure.* Mutat Res (2006) 602:65-73

[12] Day T. K., Zeng G., Hooker A. M., Bhat M., Scott B. R., Turner D. R., Sykes P. J. *Extremely low priming doses of X radiation induce an adaptive response for chromosomal inversions in pKZ1 mouse prostate.* Radiat Res (2006) 166:757-766

[13] Livak K J and Schmittgen T D (2001) *Analysis of Relative Gene Expression Data Using Real-Time Quantitative PCR and the 2-[Delta][Delta]CT Method.* Methods, 25(4):402-408

[14] Fratini E., Capece D., Simone G., Alesse E., Sykes P., Satta L., Tabocchini M.A. *Molecular mechanisms involved in the biological response of living systems to natural background radiation.* 40 Annual Meeting della European Radiation Research Society (ERRS), Dublin (Irland), 1-5 september 2013

[15] Fratini E., Capece D., Simone G., Alesse E., Sykes P., Satta L., Tabocchini M.A. *The Cosmic Silence experiment: modulation of stress response mechanisms in living systems exposed to different radiation environments.* 5th MELODI Workshop, October 7-10, 2013

[16] Grube K., Bürkle A. *Poly(ADP-ribose) polymerase activity in mononuclear leukocytes of 13 mammalian species correlates with species-specific life span.* Proc. Natl. Acad. Sci. U.S.A. (1992) 89 (24): 1175963. doi:10.1073/pnas.89.24.11759

[17] Muiras M.L., Müller M., Schächter F., Bürkle A. *Increased poly(ADP-ribose) polymerase activity in lymphoblastoid cell lines from centenarians.* J. Mol. Med. (1998) 76 (5): 34654. doi:10.1007/s001090050226

[18] Lebel M., Lavoie J., Gaudreault I., Bronsard M., Drouin R. *Genetic cooperation between the Werner syndrome protein and poly(ADP-ribose) polymerase-1 in preventing chromatid breaks, complex chromosomal rearrangements, and cancer in mice.* Am. J. Pathol. (2003) 162 (5): 155969. doi:10.1016/S0002-9440(10)64290-3

[19] Bernstein H., Payne C.M., Bernstein C., Garewal H., Dvorak K. *Cancer and aging as consequences of un-repaired DNA damage.* (2008) Kimura H, Suzuki A, ed. New York: Nova Science Publishers, Inc. pp.147

ERMES
Radioxenon monitoring in Darwin (Australia) and Fukushima Dai–Ichi Nuclear Power Plant Accident

Blake Orr[a], Michael Schöppner[b,c], Rick Tinker[a] Wolfango Plastino[b,c]

[a] Australian Radiation Protection and Nuclear Safety Agency (ARPANSA),
619 Lower Plenty Road, Yallambie, Victoria 3085, Australia
[b] University of Roma Tre, Department of Physics, Via della Vasca Navale 84,
I-00146 Roma, Italy
[c] National Institute of Nuclear Physics (INFN), Section of Roma Tre,
Via della Vasca Navale 84, I-00146 Roma, Italy

Abstract

A series of ^{133}Xe detections in April 2011 made at the Comprehensive Nuclear-Test-Ban Treaty Organisation (CTBTO) International Monitoring System noble gas station in Darwin, Australia, were analysed to determine the most likely source location. Forward and backwards atmospheric transport modelling simulations using FLEXPART were conducted. It was shown that the most likely source location was the Fukushima Dai-ichi nuclear power plant accident. Other potential sources in the southern hemisphere were analysed, including the Australian Nuclear Science and Technology Organisation (ANSTO) radiopharmaceutical facility, but it was shown that sources originating from these locations were highly unlikely to be the source of the observed ^{133}Xe Darwin detections.

1   Introduction

The Fukushima Dai-ichi nuclear power plant (NPP) accident, which occurred in the subsequent days after the earthquake and tsunami off the east coast of Japan on March 11 2011, released large amounts of radionuclides into atmosphere and the ocean. The magnitude of the atmospheric releases of radionuclides attached to particulates have been estimated to be as high as 43% of the Chernobyl accident, with estimates of total radioxenon activity released being more than twice that of Chernobyl [1][2]. In the days and weeks following the accident many radionuclide detection systems throughout the northern hemisphere, including the IMS network, experienced highly elevated detections of radioiodine, radio-caesium and radioxenon [3]-[6]. This study focusses on identifying the probable source

of radioxenon detections made in the southern hemisphere from the Darwin IMS station (130.9°E, 12.4°S) in April 2011 using atmospheric transport modelling [7].

2   Results and discussion

A series of ^{133}Xe detections were made by the Darwin IMS noble gas station in April 2011. Prior to April 2011, the Darwin IMS noble gas station had not recorded a detection of 1 mBq m^{-3} or greater. Quality assurance was performed for this detection period, to screen out false positive activity concentrations associated with either calibrations or detector problems. There were 17 consecutive detections greater than 1 mBq m^{-3} from 8 April to 16 April 2011. The number of consecutive detections is unique to the noble gas monitoring stations located in Australia. The IMS noble gas station in Melbourne has recorded detections greater than 1 mBq m^{-3}, which can be attributed to releases generated from the ANSTO radiopharmaceutical facility [8].

The location of the Hadley cells and the Intertropical Convergence Zone (ITCZ) typically acts as a barrier to limit interhemisphere atmospheric transport within the troposphere [9]. In March to April the location of the ITCZ in the Australian-Asia region is very close to the equator [10]. However the modelling shows that over a period of around a month, there would be some radioxenon plume movement across the ITCZ into the southern hemisphere.

The forward simulation shows that in late March there appeared to be some plume movement into southern Asia and Indonesia. In the subsequent days and weeks, the modelling shows this air mass had moved into the southern hemisphere through Indonesia into Darwin. There was also some plume movement across the equator through the central Pacific which moved across countries such as Fiji. According to [11], March to April is an optimum time of the year for transport across the equator from the northern to southern hemisphere in the central Pacific [7].

The predicted activity concentrations using forward simulations are sufficient to produce observed detections at the Darwin IMS noble gas station, even with the decay of the source, movement across hemispheres and the dilution due to the plume travel distance. The modelling results from backwards simulations also support detections of radioxenon in Darwin from the Fukushima Dai-ichi NPP accident [7].

3   Conclusion

In this study a series of ^{133}Xe detections made at the Darwin IMS noble gas station in April 2011 were analysed to determine the most likely source location. Due to the prolonged nature of the detections and the magnitude of the release, it is likely that the source originated from the Fukushima Dai-ichi NPP accident. Despite the position of the ITCZ close to the equator in the Australian-Asian region during March to April, the modelling predicted that radioxenon would migrate into the southern hemisphere and would be detectable at the Darwin IMS noble gas station. Other potential sources in the southern hemisphere were analysed, including the ANSTO radiopharmaceutical facility,

but it was shown that sources originating from these locations were highly unlikely to be the source of the ^{133}Xe Darwin detections.

References

[1] Stohl, A., Seibert, P., Wotawa, G., Arnold, D., Burkhart, J., Eckhardt, S., Tapia, C., Vargas, A., Yasunari, T., 2012. Xenon-133 and caesium-137 releases into the atmosphere from the Fukushima Dai-ichi nuclear power plant: determination of the source term, atmospheric dispersion and deposition. Atmospheric Chemistry and Physics 12, 2313-2343.

[2] Schoeppner, M., Plastino, W., Povinec, P.P., Nikkinen, M., Ruggieri, F., Bella, F., 2013. Estimation of the radioactive source dispersion from Fukushima nuclear power plant accident. Applied Radiation and Isotopes, 81, 358-361.

[3] Bolsunovsky, A., Dementyev, 2011. Evidence of the radioactive fallout in the center of Asia (Russia) following the Fukushima nuclear accident. Journal of Environmental Radioactivity 102, 1062-1064.

[4] Bowyer, T., Biegalski, S., Cooper, M., Eslinger, P., Hass, D., Hayes, J., Miley, H., Strom, D., Woods, V., 2011. Elevated radioxenon detected remotely following the Fukushima nuclear accident. Journal of Environmental Radioactivity 102, 681-687.

[5] Manolopoulou, M., Vagena, E., Stoulos, S., Ioannidou, A., Papastefanou, C., 2011. Radioiodine and radiocesium in Thessaloniki, Northern Greece due to the Fukushima nuclear accident. Journal of Environmental Radioactivity 102, 796-797.

[6] Pittauerova, D., Hettwig, B., Fischer, H., 2011. Fukushima fallout in northwest German environmental media. Journal of Environmental Radioactivity 102, 877-880.

[7] Orr, B., Schoeppner, M., Tinker, R., Plastino, W., 2013. Detection of radioxenon in Darwin, Australia following the Fukushima Dai-ichi nuclear power plant accident. Journal of Environmental Radioactivity, 126, 40-44.

[8] Tinker, R., Orr, B., Grzechnik, M., Hoffman, E., Saey, P., Solomon, S., 2010. Evaluation of radioxenon releases in Australia using atmospheric dispersion modelling tools. Journal of Environmental Radioactivity 101, 353-361.

[9] UNSCEAR (United Nations Scientific Committee on the Effects of Atomic Radiation), 2000. United Nations: Sources and Effects of Ionizing Radiation e Report to the General Assembly. In: Annex C, vol. 1. United Nations Sales Publications, United States, New York.

[10] Waliser, D., Gautier, C., 1993. A satellite-derived climatology of the ITCZ. Journal of Climate 6, 2162-2174.

[11] Avery, M., Westberg, D., Fuelberg, H., Newell, R., Anderson, B., Vay, S., Sachse, G., Blake, D., 2001. Chemical transport across the ITCZ in the central Pacific during an El Nino-Southern Oscillation cold phase event in MarcheApril 1999. Journal of Geophysical Research 106, 32539-32553.

THE VIP EXPERIMENT

S. Bartalucci[a], S. Bertolucci[b], M. Bragadireanu[a,c]

M. Cargnelli[d], A. Clozza[a], C. Curceanu[a],

S. Di Matteo[e], J-P. Egger[f], C. Guaraldo[a], M. Iliescu[a],

T. Ishiwatari[d], M. Laubenstein[g], J. Marton[d], E. Milotti[h], D. Pietreanu[a,c],

K. Piscicchia[a], M. Poli Lener[a], T. Ponta[c], A. Romero Vidal[a],

A. Scordo[a], H. Shi[d], D.L. Sirghi[a,c], F. Sirghi[a,c], L. Sperandio[a],

O. Vazquez Doce[a], E. Widmann[d], J. Zmeskal[d]

[a] INFN, Laboratori Nazionali di Frascati, CP 13, Via E. Fermi 40, I-00044, Frascati (Roma)-Italy

[b] CERN, CH-1211, Geneva 23-Switzerland

[c] "Horia Hulubei" National Institute of Physics and Nuclear Engineering, Str. Atomistilor no. 407, P.O. Box MG-6, Bucharest - Magurele-Romania

[d] The Stefan Meyer Institute for Subatomic Physics, Boltzmanngasse 3, A-1090 Vienna-Austria

[e] Institut de Physique UMR CNRS-UR1 6251, Université de Rennes1, F-35042 Rennes-France

[f] Institut de Physique, Université de Neuchâtel, 1 rue A.-L. Breguet, CH-2000 Neuchâtel-Switzerland

[g] INFN, Laboratori Nazionali del Gran Sasso, S.S. 17/bis, I-67010 Assergi (AQ)-Italy

[h] Dipartimento di Fisica, Università di Trieste and INFN– Sezione di Trieste, Via Valerio, 2, I-34127 Trieste-Italy

Abstract

The Pauli exclusion principle (PEP) and, more generally, the spin-statistics connection, is at the very basis of our understanding of matter and nature. The PEP spurs, presently, a lively debate on its possible limits, deeply rooted in the very foundations of Quantum Mechanics and Quantum Field Theory. Therefore, it is extremely important to test the limits of its validity. The VIP collaboration is considering as well the possibility to extend its scientific program towards the study of spontaneous x-ray radiation predicted in the framework of collapse models.

1   Introduction

The Pauli Exclusion Principle (PEP), which plays a fundamental role in our understanding of many physical and chemical phenomena, from the periodic table of elements, to the

electric conductivity in metals and to the degeneracy pressure which makes white dwarfs and neutron stars stable, is a consequence of the spin-statistics connection [1]. Although the principle has been spectacularly confirmed by the huge number and accuracy of its predictions, its foundation lies deep in the structure of quantum field theory and has defied all attempts to produce a simple proof [2]. Given its basic standing in quantum theory, it seems appropriate to carry out precise tests of the PEP validity and, indeed, mainly in the last 20 years, several experiments have been performed to search for possible small violations [3, 4, 5, 6, 7, 8, 9, 10, 11]. Moreover, many (if not all) of these experiments are using methods which are not obeying to the so-called Messiah-Greenberg superselection rule [12]. The indistinguishability and the symmetrization (or antisymmetrization) of the wave-function should be checked independently for each particle, and accurate tests were and are being done.

The VIP (VIolation of the Pauli Exclusion Principle) experiment has the goal to improve the limit on the probability of the violation of the PEP for electrons, (P < 1.7 x 10^{-26} established by E. Ramberg e G. A. Snow: *Experimental limit on a small violation of the Pauli principle*, Phys. Lett. **B 238** (1990) 438) by three-four orders of magnitude (P <$10^{-29 \div -30}$), exploring a region where new theories might allow for a possible PEP violation.

The experimental method, originally described in [13], consists in the introduction of electrons into a copper strip, by circulating a current, and in the search for X-rays resulting from the forbidden radiative transition that occurs if one of the new electrons is captured by a copper atom and cascades down to the 1s state already filled by two electrons with opposite spins. The energy of this transition would differ from the normal K_α transition by about 300 eV (7.729 keV instead of 8.040 keV) [14] providing an unambiguous signal of the PEP violation. The measurement alternates periods without current in the copper strip, in order to evaluate the X-ray background in conditions where no PEP violating transitions are expected to occur, with periods in which current flows in the conductor, thus providing "fresh" electrons, which might violate PEP. The rather straightforward analysis consists in the evaluation of the statistical significance of the normalized subtraction of the two spectra in the region of interest.

The experiment is being performed at the LNGS underground Laboratories, where the X-ray background, generated by cosmic rays, is reduced.

2   The VIP experimental setup

The first VIP setup was realized in 2005, using the CCD (Charge Coupled Devices) as X-ray detectors [15, 16, 17, 18, 19], and consisted as main elements of a copper cylinder, 4.5 cm in radius, 50 μm thick, 8.8 cm high, surrounded by 16 equally spaced CCDs of type 55.

The CCDs were at a distance of 2.3 cm from the copper cylinder, grouped in units of two chips vertically positioned. The setup was enclosed in a vacuum chamber, and the CCDs were cooled to about 165 K by the use of a cryogenic system. A schematic drawing of this setup is shown in Fig. 1.

The DAQ alternated periods in which a 40 A current is circulated inside the copper
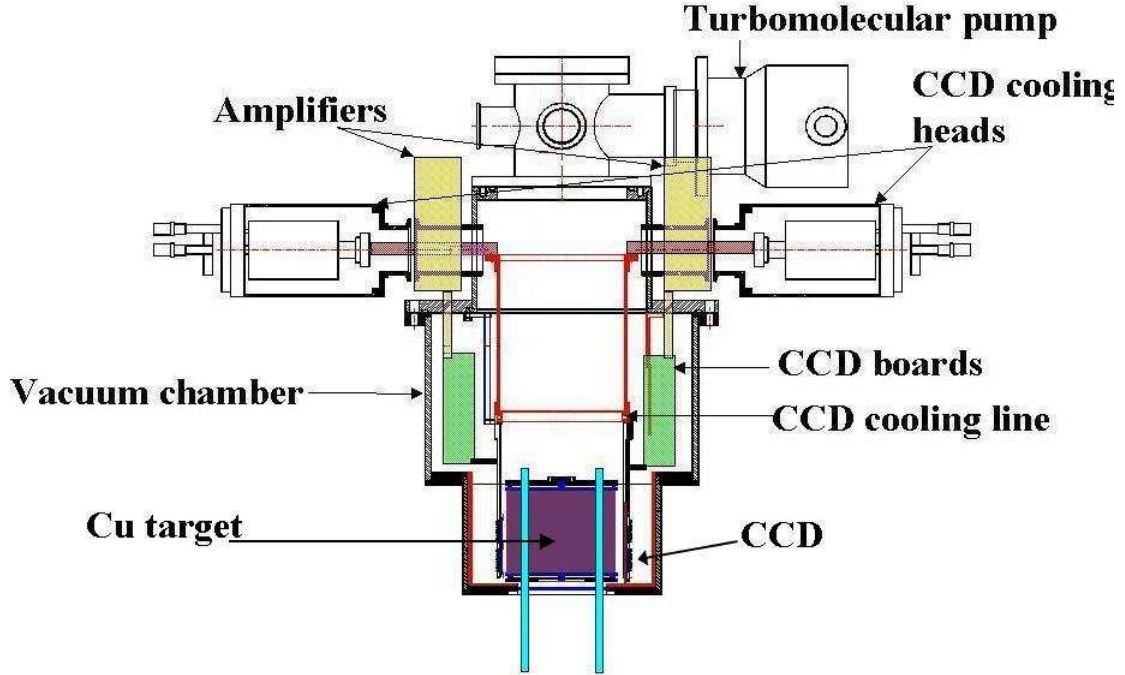
Figure 1: *The VIP setup. All elements af the setup are identified in the figure.*

target with periods without current, referred as background.

This was installed at the LNGS Laboratory in Spring 2006 and was taking data in this configuration until Summer 2010 (presently, see below, we are working on a new setup). The setup was surrounded by layers of copper and lead (as seen in the picture) to shield it against the residual background present inside the LNGS laboratory, see Fig. 2.

3   VIP results

3.1   VIP analyses results

Until summer 2010 the VIP experiment was in data taking, alternating periods of "signal" (I=40 A) with periods without signal (I=0 A). Data analyses were performed (energy calibration, sum of spectra, subtraction of background) and the probability of violation of PEP for electrons obtained in 2013 after a refined re-analysis of the data:

$$\frac{\beta^2}{2} < 2.8 \times 10^{-29} \tag{1}$$

3.2   Discussion of the results

We are attempting an interpretation of our results in the framework of quon-theory, which turned out to be a consistent theory of *small* violations of PEP. The basic idea of quon theory [20] is that (anti)commutators, are replaced by weighted sums

$$\frac{1-q}{2}\left[a_i, a_j^+\right]_+ + \frac{1+q}{2}\left[a_i, a_j^+\right]_- = a_i a_j^+ - q a_j^+ a_i = \delta_{i,j} \tag{2}$$

194
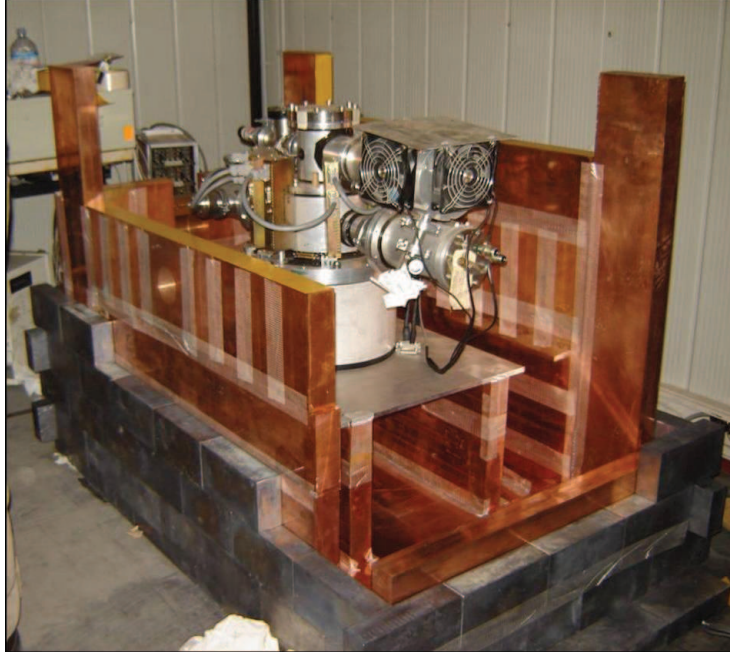
Figure 2: The VIP setup at the LNGS laboratory during installation.

where $q = -1$ ($q = 1$) gives back the usual fermion (boson) commutators. The statistical mixture in equation (2) also shows that the PEP violation probability is just $(1 + q)/2$ and thus our best experimental bound on q is

$$\frac{1 + q}{2} < 2.8 \times 10^{-29} \tag{3}$$

4 Future perspectives:VIP2, a high sensitivity setup

The VIP setup used CCD detectors, which are excellent X-ray detectors, but very slow. We plan to switch to a new type of detectors for precision X-rays measurements, the triggerable Silicon Drift Detectors (SSD) which have a fast readout time ($\simeq 1\mu s$) and large collection area (100 mm^2) in the framework of VIP2, a new high sensitivity setup. These detectors were successfully used in the SIDDHARTA experiment at LNF-INFN for measurements of the kaonic atoms transitions at the DAΦNE accelerator of LNF-INFN [21]; using a proper trigger system a background rejection factor of the order of 10^{-4} was achieved in SIDDHARTA. We built a new setup, much more compact, with higher current circulating and with a veto system against background coming from outside. A schematic layout of the new setup is shown in Fig. 3.

In 2013 we assembled and tested the VIP2 setup at LNF-INFN. In 2014 after end of testing at LNF, the setup will be transported, installed and debugged at LNGS.

We then expect to gain about 2 orders of magnitude in the limit of PEP violation in a data taking of 3-4 years. We are, as well, considering to extend the scientific program towards a feasibility study of limits on parameters of the collapse model (as a solution of the measurement problem, put initially forward by Ghirardi, Rimini and Weber) by
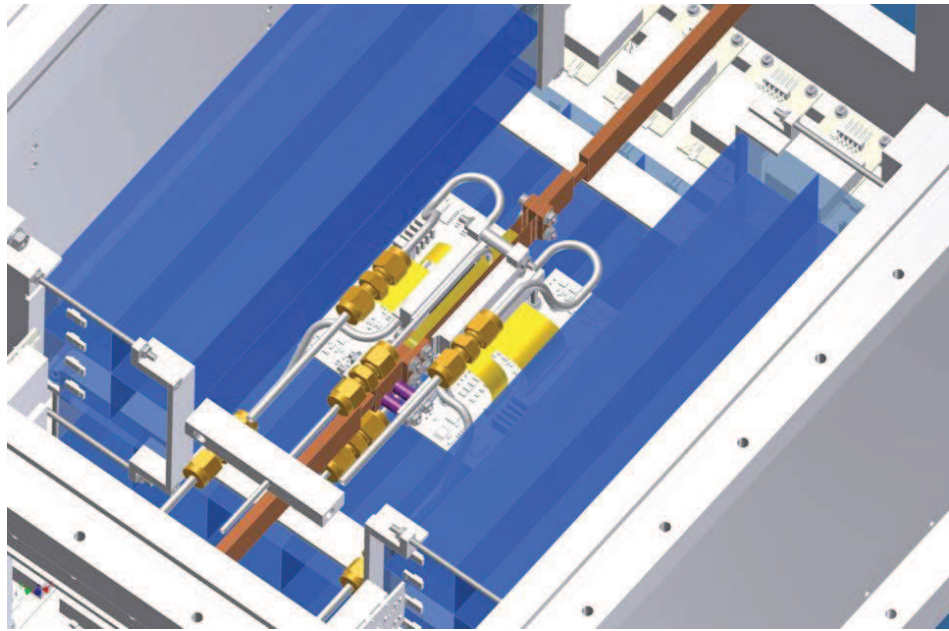
Figure 3: The VIP2 setup experiment using SDD detectors and an external veto-system.

measurements of X rays spontaneously emitted in the continuous spontaneous localization (CSL) model [22], [23] .

5 Acknowledgements

6 List of Publications in 2013

1. C. Curceanu *et al.* Evaluation of the X-ray transition energies for the Pauli-Principle-violating atomic transitions in several elements by using the Dirac-Fock method, LNF preprint, INFN-13-21/LNF, 21-11-2013.

2. S. Di Matteo, L. Sperandio *et al.* Evaluation of the anomalous X-ray energy in VIP experiment: some values from Dirac-Fock method, LNF preprint, INFN-13-20/LNF, 21-11-2013.

3. S. Di Matteo, L. Sperandio *et al.* Evaluation of the Anomalous X-ray energy in VIP Experiment, LNF preprint, INFN-13-19/LNF, 21-11-2013.

4. S. Donadi, A. Bassi, L. Ferialdi and C. Curceanu, The Effect of Spontaneous Collapses on Neutrino Oscillations, Found. Phys. **43**, (2013) 1066.

5. M. Bahrami, S. Donadi, L. Ferialdi, A. Bassi, C. Curceanu, A. Di Domenico and B. C. Hiesmayr, Are collapse models testable with quantum oscillating systems? The case of neutrinos, kaons, chiral molecules, Sci. Rep. **3**, (2013) 1952.

6. J. Marton, S. Bartalucci, S. Bertolucci, C. Berucci, M. Bragadireanu,M. Cargnelli, C. Curceanu and S. Di Matteo *et al.* Testing the Pauli Exclusion Principle for Electrons, J. Phys. Conf. Ser. **447** (2013) 012070

7. S. Donadi, A. Bassi, C. Curceanu, A. Di Domenico and B. C. Hiesmayr, Are Collapse Models Testable via Flavor Oscillations?, Found. Phys. **43** (2013) 813.

References

[1] W. Pauli, *Phys. Rev.* **58**, (1940), 716.

[2] R. P. Feynman, R. B. Leighton and M. Sands *The Feynman Lectures on Physics*, Addison-Wesley, Reading, MA (1963).

[3] R. Arnold, *et al.*, *Eur. Phys. J. A***6** (1999) 361.

[4] H.O. Back, *et al.*, *Eur. Phys. J. C***37** (2004) 421.

[5] A. Barabash, *Found. of Phys.* **40** (2010) 703.

[6] A.S. Barabash,*et al.*, *JETP Lett.* **68** (1998) 112.

[7] P. Belli, *et al.*, **460** (1999) 236.

[8] G. Bellini, *et al.*, *Phys. Rev. C* **81** (2010) 034.

[9] R. Bernabei, *et al.*, *Phys. Lett. B* **408** (1997) 439.

[10] R. Bernabei, *et al.*, *Eur. Phys. J. C* **62** (2009) 327.

[11] Y. Suzuki, *et al.*, *Phys. Lett. B* **311** (1993) 357.

[12] A.M.L. Messiah, O.W. Greenberg, *Phys. Rev.* **136** (1964) B248.

[13] E. Ramberg and G. A. Snow, *Phys. Lett. B* **238** (1990) 438.

[14] C. Curceanu *et al.* Evaluation of the X-ray transition energies for the Pauli-Principle-violating atomic transitions in several elements by using the Dirac-Fock method, LNF preprint, INFN-13-21/LNF, 21-11-2013.

[15] J. L. Culhane, *Nucl. Instrum. Methods A* **310** (1990) 1.

[16] J.-P. Egger, D. Chatellard and E. Jeannet, *Particle World* **3**, (1993) 139.

[17] G. Fiorucci, *et al. Nucl. Instrum. Methods A* **292** (1990) 141.

[18] D. Varidel, *et al.Nucl. Instrum. Methods A* **292** (1990) 147

[19] R. P. Kraft, *et al.Nucl. Instrum. Methods A* **372** (1995) 372.

[20] O. W. Greenberg *Phys. Rev. Lett.* **64** (1990) 705.

[21] C. Curceanu *et al. Eur Phys* **J A31** (2007) 537-539; M. Bazzi *et al. Phys. Lett.* **B681** (2009) 310; M. Bazzi *et al. Phys. Lett.* **B704** (2011) 113; Bazzi *et al. Phys. Lett.* **B697** (2011) 199; Bazzi *et al. Phys. Lett.* **B714** (2012) 40.

[22] Q. Fu *Phys. Rev* **A56** (1997) 1806.

[23] G.C. Ghirardi, A. Rimini and T. Weber *Phys. Rev.* **D34** (1986) 470: ibid. (1987) 3287: *Found. Phys.* **18** (1988) 1.

THE PIERRE AUGER OBSERVATORY

D. Boncioli[a], A. di Matteo[b], A.F. Grillo[a], S. Petrera[b,c], V. Rizi[b]

for the Pierre Auger Collaboration

[a] INFN Laboratori Nazionali del Gran Sasso, Assergi, Italy
[b] INFN and Physics Department, University of L'Aquila, L'Aquila, Italy
[c] GSSI, Gran Sasso Science Institute, L'Aquila, Italy

Abstract

The Pierre Auger Project is an international Collaboration involving over 400 scientists from 17 countries, with the objective of studying the highest energy cosmic rays. Recent results from the Collaboration as well as further developments in the detector are presented in this report.

1 Introduction

Ultra-high energy cosmic rays are of intrinsic interest as their origin and nature are unknown. It is quite unclear where and how particles as energetic as $\approx 10^{20}$ eV are accelerated. Over 40 years ago it was pointed out that if the highest energy particles are protons then a fall in the flux above an energy of about 4×10^{19} eV is expected because of energy losses by the protons as they propagate from distant sources through the CMB radiation. At the highest energies the key process is photo-pion production in which the proton loses part of its energy in each creation of a Δ resonance. This is the Greisen–Zatsepin–Kuzmin (GZK) effect. It follows that at 10^{20} eV any proton observed must have come from within about 50 Mpc and on this distance scale the deflections by intervening magnetic fields in the galaxy and intergalactic space are expected to be so small that point sources should be observed. Despite immense efforts in the period since the prediction, the experimental situation remains unclear. The main problem in examining whether or not the spectrum steepens is the low rate of events which, above 10^{20} eV, is less than 1 per km^2 per century so that the particles are only detectable through the giant air showers that they create.

These showers have particle footprints on the ground of ≈ 20 km^2 and suitably distributed detectors can be used to observe them. Also the showers excite molecules of atmospheric nitrogen and the resulting faint fluorescence radiation, which is emitted isotropically, can be detected from distances of several tens of kilometers.

The Pierre Auger Observatory has been developed by a team of over 400 scientists from 17 countries. The Observatory comprises about 1600 10 m$^2 \times 1.2$]m water-Cherenkov

detectors deployed over 3000 km^2 on a 1500 m hexagonal grid, plus a sub array, the Infill, with 71 water Cherenkov detectors on a denser grid of 750 m covering nearly 30 km^2. This part of the Observatory (the surface detector, SD) is over-looked by 24 fluorescence telescopes in 4 clusters located on four hills around the SD area which is extremely flat. The surface detectors contain 12 tonnes of clear water viewed by 3 × 9″ hemispherical photomultipliers. The fluorescence detectors (FD) are designed to record the faint ultra-violet light emitted as the shower traverses the atmosphere. Each telescope images a portion of the sky of 30° in azimuth and 1°–30° in elevation using a spherical mirror of 3 m^2 effective area to focus light on to a camera of 440 × 18 cm^2 hexagonal pixels, made of photomultipliers complemented with light collectors, each with a field of view of 1.5° diameter. 3 High Elevation Auger Telescopes (HEAT) located at one of the fluorescence sites are dedicated to the fluorescence observation of lower energy showers. The Observatory also comprises a sub array of 124 radio sensors (AERA, Auger Engineering Radio Array) working in the MHz range and covering 6 km^2, a sub Array of 61 radio sensors (EASIER, Extensive Air Shower Identification with Electron Radiometer) working in the GHz range and covering 100 km^2, and two GHz imaging radio telescopes AMBER and MIDAS with respectively 14° × 14° and 10° × 20° field of views.

An important feature of the design of the Observatory was the introduction of the hybrid technique as a new tool to study airshowers. It is used here for the first time. The hybrid technique is the term chosen to describe the method of recording fluorescence data coincident with the timing information from at least one surface detector. Employing these two complementary observation methods provides the Auger Observatory with high quality information about angular reconstruction, determination of the core position of the shower and of the types of particles in the primary cosmic rays. Comparing results from the different types of detectors also helps scientists reconcile the two sets of data and produce the most accurate results about the energy of primary cosmic rays.

2 Recent results from the Pierre Auger Observatory

2.1 The Energy Spectrum

The energy spectrum of ultra-high energy cosmic rays at energies greater than 3×10^{17} eV has been derived using data from the Pierre Auger Observatory [1]. This measurement provides evidence for the suppression of the flux above 4×10^{19} eV and is updated here. The combined energy spectrum scaled with E^3 is shown in Fig. 1. The dominant systematic uncertainty of the spectrum stems from that of the overall energy scale, which is estimated to be 14%.

The position of the ankle at $\log_{10}(E\text{ankle/eV}) = 18.72 \pm 0.01$ (stat.) ± 0.02 (sys.) has been determined by fitting the flux with a broken power law $E^{-\gamma}$. An index of $\gamma = 3.23 \pm 0.01 \pm 0.07$ is found below the ankle. Above the ankle the spectrum follows a power law with index $2.63 \pm 0.02 \pm 0.04$. In comparison to the power law extrapolation, the spectrum is suppressed by a factor two at $\log_{10}(E_{1/2}/\text{eV}) = 19.63 \pm 0.01 \pm 0.01$. The significance of the suppression is larger than 20σ. The suppression is similar to what is expected from the GZK effect for protons or nuclei as heavy as iron, but could in part also be related to a change of the shape of the average injection spectrum at the sources.

2.2 The mass composition

The atmospheric depth, X_{max}, at which the longitudinal development of a shower reaches its maximum in terms of the number of secondary particles is correlated with the mass of the incident cosmic ray particle. With the generalization of Heitlers model of electron–photon cascades to hadron-induced showers and the superposition assumption for nuclear primaries of mass A, the average depth of the shower maximum, X_{max}, at a given energy E is expected to follow [2]

$$\langle X_{max} \rangle = \alpha(\ln E \langle \ln A \rangle) + \beta \tag{1}$$

where $\langle \ln A \rangle$ is the average of the logarithm of the primary masses. The coefficients α and β depend on the nature of hadronic interactions, most notably on the multiplicity, elasticity and cross-section in ultra-high energy collisions of hadrons with air, see e.g. [3].

A recent analysis [4] based on high quality and high statistics hybrid data collected with the southern site of the Pierre Auger Observatory has been addressed to the $\langle X_{max} \rangle$ measurement and its energy dependence. The results of such measurements are presented in Fig. 2 together with predictions for proton and Fe primaries using different hadronic interaction models [4]. These models need to extrapolate the features of hadronic interactions well beyond the cms-energies accessible at man-made accelerators. Their uncertainties are correspondingly large and the wide distribution of predictions in the figure demonstrates that the systematic uncer- tainties in this analysis can be significant. With this caveat kept in mind, a transition from a light composition up to the ankle approaching the expectations for heavier nuclei up to 40 EeV is inferred from both the X_{max} values and from its RMS values.

2.3 The Cosmic Ray Anisotropy

Between January 2004 and December 2009 the Pierre Auger Observatory has detected 69 cosmic rays events with energy in excess of 55 EeV. Their arrival directions are reported in [5] This data set is more than twice as large as the one analyzed in [6], which provided evidence of anisotropy in CR arrival directions at the 99% confidence level. The anisotropy was tested with a priori parameters through the correlation between the arrival directions of CRs and the positions of nearby active galaxies from the 12th edition of the Veron-Cetty Veron catalog of quasars and active galactic nuclei. The degree of that observed correlation has decreased from $(69^{+11}_{-13})\%$ to $(38^{+7}_{-6})\%$, to be compared with the 21% expected to occur by chance if the flux were isotropic. More data are needed to determine this correlating fraction accurately. The evidence for anisotropy has not strengthened since the analysis reported in [6].

The correlation of recent data with objects in the VCV catalog is not as strong as that observed in 2007. If the evidence for anisotropy is substantiated by future data, then it should also become possible to discriminate between different astrophysical scenarios using techniques of the type that have been presented here to explore the compatibility of different models with the present set of arrival directions.

The time sequence of the correlations between events with energy exceeding 55 EeV and AGN in the VCV catalog is shown in Fig. 3. Period I is the exploratory period [6]
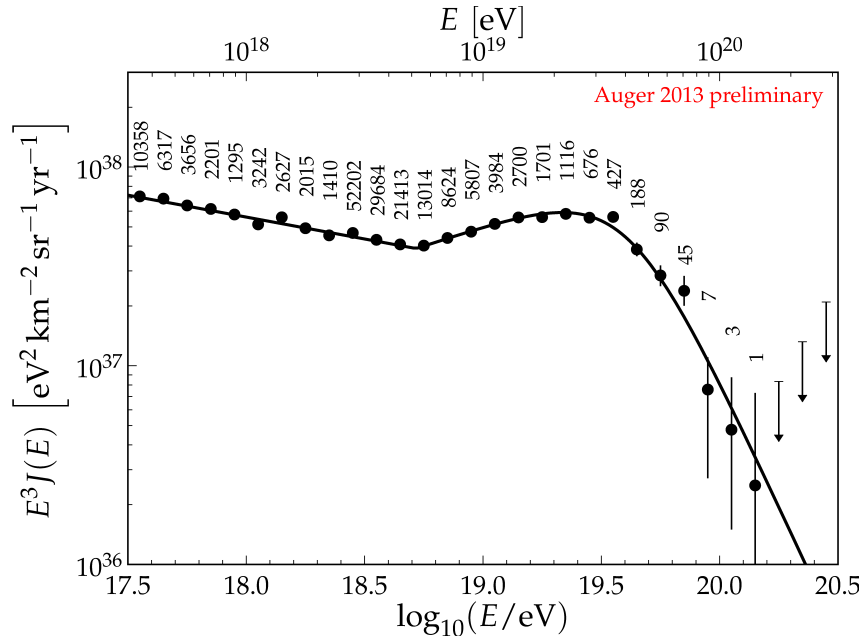
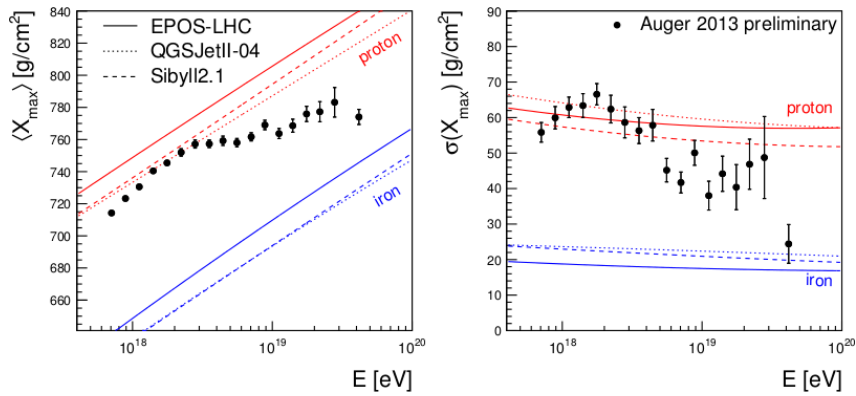Figure 1: The combined energy spectrum [1] measured by the Pierre Auger Observatory.

Figure 2: Measurements of $X_{\max}$ (left) and its RMS (right) as a function of energy [4].

from 1 January, 2004 through 26 May, 2006. The data collected during this period was scanned to establish the parameters which maximize the correlation. Period II is from 27 May, 2006 through 31 August, 2007 when the correlation paper [6] was published and period III includes data collected after, from 1 September, 2007 through 31 December, 2009. The time sequence is shown in terms of p_{data}, the degree of correlation with objects in the VCV catalog as a function of the total number of time-ordered events after the exploratory period.
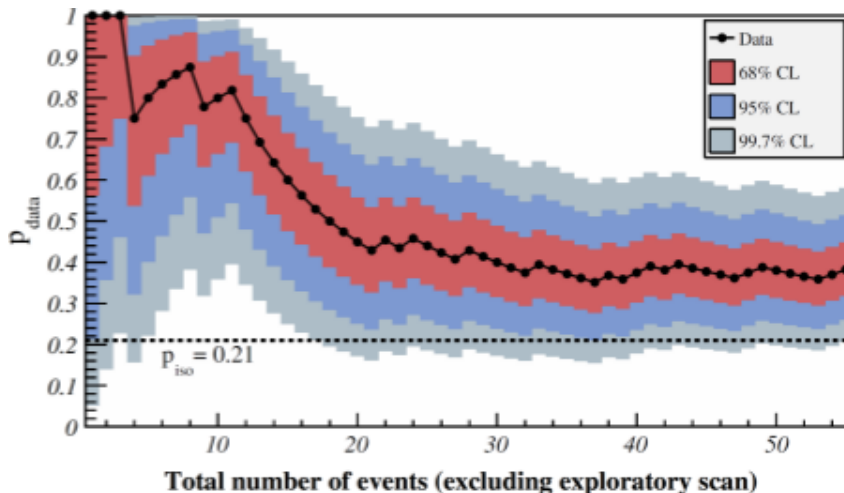
Figure 3: The most likely value of the degree of correlation $p_{data} = k/N$ is plotted with black circles as a function of the total number of time-ordered events (excluding those in period I). The 68%, 95% and 99.7% confidence level intervals around the most likely value are shaded. The horizontal dashed line shows the isotropic value $p_{iso} = 0.21$.

We have also compared the distribution of arrival directions with the positions of different populations of nearby extragalactic objects: galaxies in the 2MRS survey and AGNs detected in X-rays by Swift-BAT. These studies are a posteriori and do not constitute further quantitative evidence for anisotropy.

We have analyzed the region of the sky close to the location of the radiogalaxy Cen A, since this corresponds to the largest observed excess with respect to isotropic expectations. The region of Cen A is densely populated with different types of nearby extragalactic objects. From all the arrival directions of CRs with $E \geq 55$ EeV, 18.8% lie within 18° of Cen A, while 4.7% is the isotropic expectation. There are two arrival directions very close to the position of the Cen A nucleus. Aside from those two events, the excess is distributed rather broadly.

A knowledge of CR composition is important for deciding which of several source scenarios is more likely. The trajectories of highly charged nuclei are expected to undergo large deflections due to the Galaxys magnetic fields. While a correlation of arrival directions with nearby matter on small angular scales is plausible for protons above 55 EeV, it is puzzling if the CR are heavy nuclei. If the particles responsible for the measured excesses for example around Centaurus A at $E > 55$ EeV are heavy nuclei with charge Z, the proton component of the sources should lead to excesses in the same regions at

energies E/Z. In [7] the lack of anisotropies in the directions of the excesses at energies above E_{th}/Z is reported, setting constraints on the allowed proton fraction at the lower energies.

2.4   Searches for high-energy neutrinos and gamma rays

The limits on the fluxes of photons [8] and neutrinos [9] obtained from the Pierre Auger Observatory are shown in Fig. 4. Model scenarios for sources of UHECRs, in which the observed particles are produced by the decay of other particles (top-down models), lead to large secondary fluxes of photons and neutrinos. Some representative examples of predicted secondary fluxes of such models are shown in Fig. 4 (photons: GZK, TD, Z-burst, and SHDM; neutrinos: TD, Z-burst). The neutrino flux limit of the Auger Observatory is now lower than the Waxman-Bahcall flux. The current flux limits rule out or strongly disfavor that top-down models can account for a significant part of the observed UHECR flux. The bounds are reliable as the photon flux limits in Fig. 1.2 depend only on the simulation of electromagnetic showers and, hence, are very robust against assumptions on hadronic interactions at very high energy.
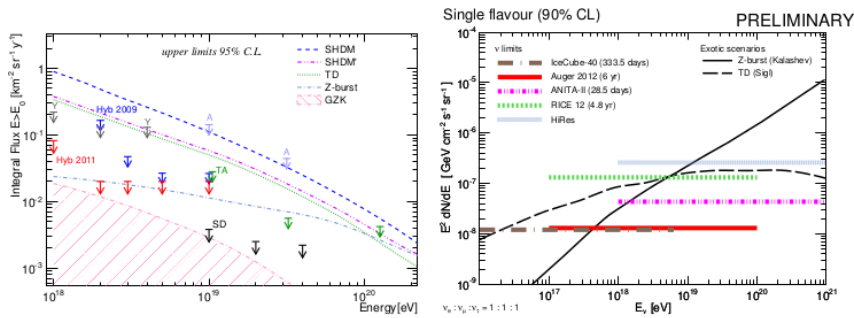
Figure 4: Limits on the flux of photons [8] and neutrinos [9] obtained from the Pierre Auger Observatory. The data are shown together with the current limits from other experiments and some examples of predicted fluxes.

The photon flux limits have further far-reaching consequences by providing important constraints on theories of quantum gravity involving Lorentz invariance violation (LIV). And, observing a single photon shower at ultra-high energy would imply very strong limits on another set of parameters of LIV theories. Similarly, observing cosmogenic neutrinos would allow to put constraints on LIV in the neutrino sector.

3   Activity of the L'Aquila–Gran Sasso Group

The activity of the group has followed two main lines:

- Developement of a Monte Carlo code (*SimProp*) for the propagation of UHECR nuclei in extragalactic space, and its use for the study of physical observables

- Developement and test of the Raman Lidar system for an enhanced atmospheric test beam within the Observatory.

Concerning the first item, the work has been the subject of the PhD thesis of D. Boncioli (PhD obtained in December 2011) and the MSc thesis of A. di Matteo (MSc obtained in October 2012). The code has been developed also in collaboration with F. Salamida (now at Paris-Orsay) and R. Aloisio (LNGS).

Using *SimProp*, several physical analyses are in progress, concerning mainly the mass composition of UHECRs detected in the Observatory and predictions for the fluxes of cosmogenic neutrinos from GZK interactions.

D. Boncioli has presented her work at the RICAP-13 conference held in Rome [10] and the CASPAR2013 held in Hamburg. A. di Matteo has presented related work at the 33rd International Cosmic Ray Conference conference held in Rio de Janeiro [11].

Concerning the second reserch argument, the Raman Lidar system has been run in coincidence with a lateral scattering facility in Lamar (Colorado). The whole system was moved last year to Malargue, to form part of the so-called Super Beam System [12].

4 List of Publications

1. The Pierre Auger Collaboration, "Constraints on the origin of cosmic rays above 10^{18} eV from large scale anisotropy searches in data of the Pierre Auger observatory", ApJL, 762 (2013) L13.

2. The Pierre Auger Collaboration, "The Interpretation of the Depths of Shower Maximum of Extensive Air Showers Measured by the Pierre Auger Observatory", JCAP 02 (2013) 026.

3. The Pierre Auger Collaboration, "Ultra-High Energy Neutrinos at the Pierre Auger Observatory", Advances in High Energy Physics, 2013 (2013) 708680.

4. The Pierre Auger Collaboration, "Techniques for Measuring Aerosols using the Central Laser Facility at the Pierre Auger Observatory", JINST 8 (2013) P04009.

5. The Pierre Auger Collaboration, "Bounds on the density of sources of ultra-high energy cosmic rays from the Pierre Auger Observatory", JCAP, 05 (2013) 009.

6. The Pierre Auger Collaboration, "Identifying Clouds over the Pierre Auger Observatory using IR Satellite Data", Astroparticle Physics, 50-52 (2013) 92-101.

References

[1] A. Schulz, for the Pierre Auger Collaboration, 33rd ICRC, Rio de Janeiro, Brazil, 2013, arXiv:1307.5059 [astro-ph.HE].

[2] W. Heitler, Oxford University Press, 1954;
J. Matthews, Astropart. Phys. 22 (2005), 387

[3] T. Wibig, Phys. Rev. D 79, 094008;
R. Ulrich et al. for the Pierre Auger Collaboration, Proc. 32th ICRC (Beijing, China)
2011

[4] E.J. Ahn, for the Pierre Auger Collaboration

[5] P.Abreu et al. [The Pierre Auger Collaboration], Astropart. Phys. 34, 314-326
(2010). ([arXiv:1009.1855])

[6] Pierre Auger Collaboration [J. Abraham et al.], Science 318 (2007) 938. Astropart.
Phys. 29 (2008) 188.

[7] Pierre Auger Collaboration [J. Abraham et al.], JCAP 1106 (2011) 022 and
arXiv:1106.3048 [astro-ph.HE].

[8] Pierre Auger Collab., J. Abraham et al., Astropart. Phys. 27, 155 (2007), astro-
ph/0606619.
Pierre Auger Collab., J. Abraham et al., Astropart. Phys. 29, 243 (2008),
arXiv:0712.1147.
Pierre Auger Collab., J. Abraham et al., Astropart. Phys. 31, 399 (2009),
arXiv:0903.1127.

[9] Pierre Auger Collab., P. Pieroni, Proc. of 33rd Int. Cosmic Ray Conf., Rio de Janeiro,
Brazil, #0697 (2013), arXiv:1307.5059.

[10] D. Boncioli for the Pierre Auger Collaboration, "Cosmic Ray Composition with the
Pierre Auger Observatory", Proceedings for the RICAP 2013, to appear in NIM A.

[11] R. Aloisio et al., "Propagation of UHECRs in cosmological backgrounds: some results
from SimProp", arXiv:1307.3895 [astro-ph.HE], to appear in Proc. 33rd ICRC, Rio
de Janeiro, Brazil, 2013

[12] L. Wiencke for the Pierre Auger Collaboration, Proc. 32nd ICRC, Beijing, China,
2011

The Pierre Auger Collaboration
A. Aab[42], P. Abreu[65], M. Aglietta[54], M. Ahlers[95], E.J. Ahn[83], I. Al Samarai[29], I.F.M. Albuquerque[17],
I. Allekotte[1], J. Allen[87], P. Allison[89], A. Almela[11, 8], J. Alvarez Castillo[58], J. Alvarez-
Muñiz[76], R. Alves Batista[41], M. Ambrosio[45], A. Aminaei[59], L. Anchordoqui[96], S. Andringa[65],
C. Aramo[45], F. Arqueros[73], H. Asorey[1], P. Assis[65], J. Aublin[31], M. Ave[76], M. Avenier[32],
G. Avila[10], A.M. Badescu[69], K.B. Barber[12], J. Bäuml[38], C. Baus[38], J.J. Beatty[89], K.H. Becker[35],
J.A. Bellido[12], C. Berat[32], X. Bertou[1], P.L. Biermann[39], P. Billoir[31], F. Blanco[73], M. Blanco[31],
C. Bleve[35], H. Blümer[38, 36], M. Boháčová[27], D. Boncioli[53], C. Bonifazi[23], R. Bonino[54],
N. Borodai[63], J. Brack[81], I. Brancus[66], P. Brogueira[65], W.C. Brown[82], P. Buchholz[42],
A. Bueno[75], M. Buscemi[45], K.S. Caballero-Mora[56, 76, 90], B. Caccianiga[44], L. Caccianiga[31],
M. Candusso[46], L. Caramete[39], R. Caruso[47], A. Castellina[54], G. Cataldi[49], L. Cazon[65],
R. Cester[48], A.G. Chavez[57], S.H. Cheng[90], A. Chiavassa[54], J.A. Chinellato[18], J. Chudoba[27],
M. Cilmo[45], R.W. Clay[12], G. Cocciolo[49], R. Colalillo[45], L. Collica[44], M.R. Coluccia[49],

206

R. Conceição[65], F. Contreras[9], M.J. Cooper[12], S. Coutu[90], C.E. Covault[79], A. Criss[90], J. Cronin[91], A. Curutiu[39], R. Dallier[34, 33], B. Daniel[18], S. Dasso[5, 3], K. Daumiller[36], B.R. Dawson[12], R.M. de Almeida[24], M. De Domenico[47], S.J. de Jong[59, 61], J.R.T. de Mello Neto[23], I. De Mitri[49], J. de Oliveira[24], V. de Souza[16], K.D. de Vries[60], L. del Peral[74], O. Deligny[29], H. Dembinski[36], N. Dhital[86], C. Di Giulio[46], A. Di Matteo[50], J.C. Diaz[86], M.L. Díaz Castro[18], P.N. Diep[97], F. Diogo[65], C. Dobrigkeit [18], W. Docters[60], J.C. D'Olivo[58], P.N. Dong[97, 29], A. Dorofeev[81], M.T. Dova[4], J. Ebr[27], R. Engel[36], M. Erdmann[40], M. Erfani[42], C.O. Escobar[83, 18], J. Espadanal[65], A. Etchegoyen[8, 11], P. Facal San Luis[91], H. Falcke[59, 62, 61], K. Fang[91], G. Farrar[87], A.C. Fauth[18], N. Fazzini[83], A.P. Ferguson[79], M. Fernandes[23], B. Fick[86], J.M. Figueira[8], A. Filevich[8], A. Filipčič[70, 71], B.D. Fox[92], E.D. Fraenkel[60], O. Fratu[69], U. Fröhlich[42], B. Fuchs[38], T. Fuji[91], R. Gaior[31], B. García[7], S.T. Garcia Roca[76], D. Garcia-Gamez[30], D. Garcia-Pinto[73], G. Garilli[47], A. Gascon Bravo[75], H. Gemmeke[37], P.L. Ghia[31], U. Giaccari[23], M. Giammarchi[44], M. Giller[64], C. Glaser[40], H. Glass[83], F. Gomez Albarracin[4], M. Gómez Berisso[1], P.F. Gómez Vitale[10], P. Gonçalves[65], J.G. Gonzalez[38], B. Gookin[81], A. Gorgi[54], P. Gorham[92], P. Gouffon[17], S. Grebe[59, 61], N. Griffith[89], A.F. Grillo[53], T.D. Grubb[12], Y. Guardincerri[3], F. Guarino[45], G.P. Guedes[19], P. Hansen[4], D. Harari[1], T.A. Harrison[12], J.L. Harton[81], Q.D. Hasankiadeh[36], A. Haungs[36], T. Hebbeker[40], D. Heck[36], P. Heimann[42], A.E. Herve[36], G.C. Hill[12], C. Hojvat[83], N. Hollon[91], E. Holt[36], P. Homola[42, 63], J.R. Hörandel[59, 61], P. Horvath[28], M. Hrabovský[28, 27], D. Huber[38], T. Huege[36], A. Insolia[47], P.G. Isar[67], K. Islo[96], S. Jansen[59, 61], C. Jarne[4], M. Josebachuili[8], A. Kääpä[35], O. Kambeitz[38], K.H. Kampert[35], P. Kasper[83], I. Katkov[38], B. Kégl[30], B. Keilhauer[36], A. Keivani[85], E. Kemp[18], R.M. Kieckhafer[86], H.O. Klages[36], M. Kleifges[37], J. Kleinfeller[9], R. Krause[40], N. Krohm[35], O. Krömer[37], D. Kruppke-Hansen[35], D. Kuempel[40], N. Kunka[37], G. La Rosa[52], D. LaHurd[79], L. Latronico[54], R. Lauer[94], M. Lauscher[40], P. Lautridou[34], S. Le Coz[32], M.S.A.B. Leão[14], D. Lebrun[32], P. Lebrun[83], M.A. Leigui de Oliveira[22], A. Letessier-Selvon[31], I. Lhenry-Yvon[29], K. Link[38], R. López[55], A. Lopez Agüera[76], K. Louedec[32], J. Lozano Bahilo[75], L. Lu[35, 77], A. Lucero[8], M. Ludwig[38], H. Lyberis[23], M.C. Maccarone[52], M. Malacari[12], S. Maldera[54], J. Maller[34], D. Mandat[27], P. Mantsch[83], A.G. Mariazzi[4], V. Marin[34], I.C. Mariş[31], G. Marsella[49], D. Martello[49], L. Martin[34, 33], H. Martinez[56], O. Martínez Bravo[55], D. Martraire[29], J.J. Masías Meza[3], H.J. Mathes[36], S. Mathys[35], A.J. Matthews[94], J. Matthews[85], G. Matthiae[46], D. Maurel[38], D. Maurizio[13], E. Mayotte[80], P.O. Mazur[83], C. Medina[80], G. Medina-Tanco[58], M. Melissas[38], D. Melo[8], E. Menichetti[48], A. Menshikov[37], S. Messina[60], R. Meyhandan[92], S. Mićanović[25], M.I. Micheletti[6], L. Middendorf[40], I.A. Minaya[73], L. Miramonti[44], B. Mitrica[66], L. Molina-Bueno[75], S. Mollerach[1], M. Monasor[91], D. Monnier Ragaigne[30], F. Montanet[32], C. Morello[54], J.C. Moreno[4], M. Mostafá[90], C.A. Moura[22], M.A. Muller[18, 21], G. Müller[40], M. Münchmeyer[31], R. Mussa[48], G. Navarra[54] ‡, S. Navas[75], P. Necesal[27], L. Nellen[58], A. Nelles[59, 61], J. Neuser[35], M. Niechciol[42], L. Niemietz[35], T. Niggemann[40], D. Nitz[86], D. Nosek[26], L. Nožka[28], L. Ochilo[42], A. Olinto[91], M. Oliveira[65], M. Ortiz[73], N. Pacheco[74], D. Pakk Selmi-Dei[18], M. Palatka[27], J. Pallotta[2], N. Palmieri[38], P. Papenbreer[35], G. Parente[76], A. Parra[76], S. Pastor[72], T. Paul[96], M. Pech[27], J. Pękala[63], R. Pelayo[55], I.M. Pepe[20], L. Perrone[49], R. Pesce[43], E. Petermann[93], C. Peters[40], S. Petrera[50, 51], A. Petrolini[43], Y. Petrov[81], R. Piegaia[3], T. Pierog[36], P. Pieroni[3], M. Pimenta[65], V. Pirronello[47], M. Platino[8], M. Plum[40], A. Porcelli[36], C. Porowski[63], P. Privitera[91], M. Prouza[27], V. Purrello[1], E.J. Quel[2], S. Querchfeld[35], S. Quinn[79], J. Rautenberg[35], O. Ravel[34], D. Ravignani[8], B. Revenu[34], J. Ridky[27], S. Riggi[52, 76], M. Risse[42], P. Ristori[2], H. Rivera[44], V. Rizi[50], J. Roberts[87],

W. Rodrigues de Carvalho[76], I. Rodriguez Cabo[76], G. Rodriguez Fernandez[46, 76], J. Rodriguez Rojo[9], M.D. Rodríguez-Frías[74], G. Ros[74], J. Rosado[73], T. Rossler[28], M. Roth[36], E. Roulet[1], A.C. Rovero[5], C. Rühle[37], S.J. Saffi[12], A. Saftoiu[66], F. Salamida[29], H. Salazar[55], F. Salesa Greus[90], G. Salina[46], F. Sánchez[8], P. Sanchez-Lucas[75], C.E. Santo[65], E. Santos[65], E.M. Santos[17], F. Sarazin[80], B. Sarkar[35], R. Sarmento[65], R. Sato[9], N. Scharf[40], V. Scherini[49], H. Schieler[36], P. Schiffer[41], A. Schmidt[37], O. Scholten[60], H. Schoorlemmer[92, 59, 61], P. Schovánek[27], A. Schulz[36], J. Schulz[59], S.J. Sciutto[4], A. Segreto[52], M. Settimo[31], A. Shadkam[85], R.C. Shellard[13], I. Sidelnik[1], G. Sigl[41], O. Sima[68], A. Śmiałkowski[64], R. Šmída[36], G.R. Snow[93], P. Sommers[90], J. Sorokin[12], R. Squartini[9], Y.N. Srivastava[88], S. Stanič[71], J. Stapleton[89], J. Stasielak[63], M. Stephan[40], A. Stutz[32], F. Suarez[8], T. Suomijärvi[29], A.D. Supanitsky[5], M.S. Sutherland[85], J. Swain[88], Z. Szadkowski[64], M. Szuba[36], O.A. Taborda[1], A. Tapia[8], M. Tartare[32], N.T. Thao[97], V.M. Theodoro[18], J. Tiffenberg[3], C. Timmermans[61, 59], C.J. Todero Peixoto[15], G. Toma[66], L. Tomankova[36], B. Tomé[65], A. Tonachini[48], G. Torralba Elipe[76], D. Torres Machado[34], P. Travnicek[27], E. Trovato[47], M. Tueros[76], R. Ulrich[36], M. Unger[36], M. Urban[40], J.F. Valdés Galicia[58], I. Valiño[76], L. Valore[45], G. van Aar[59], A.M. van den Berg[60], S. van Velzen[59], A. van Vliet[41], E. Varela[55], B. Vargas Cárdenas[58], G. Varner[92], J.R. Vázquez[73], R.A. Vázquez[76], D. Veberič[30, 70], V. Verzi[46], J. Vicha[27], M. Videla[8], L. Villaseñor[57], B. Vlcek[96], H. Wahlberg[4], O. Wainberg[8, 11], D. Walz[40], A.A. Watson[77], M. Weber[37], K. Weidenhaupt[40], A. Weindl[36], F. Werner[38], S. Westerhoff[95], B.J. Whelan[90], A. Widom[88], L. Wiencke[80], B. Wilczyńska[63] ‡, H. Wilczyński[63], M. Will[36], C. Williams[91], T. Winchen[40], D. Wittkowski[35], B. Wundheiler[8], S. Wykes[59], T. Yamamoto[91] a, T. Yapici[86], P. Younk[84], G. Yuan[85], A. Yushkov[42], B. Zamorano[75], E. Zas[76], D. Zavrtanik[71, 70], M. Zavrtanik[70, 71], I. Zaw[87] c, A. Zepeda[56] b, J. Zhou[91], Y. Zhu[37], M. Zimbres Silva[18], M. Ziolkowski[42]

[1] Centro Atómico Bariloche and Instituto Balseiro (CNEA-UNCuyo-CONICET), San Carlos de Bariloche, Argentina
[2] Centro de Investigaciones en Láseres y Aplicaciones, CITEDEF and CONICET, Argentina
[3] Departamento de Física, FCEyN, Universidad de Buenos Aires y CONICET, Argentina
[4] IFLP, Universidad Nacional de La Plata and CONICET, La Plata, Argentina
[5] Instituto de Astronomía y Física del Espacio (CONICET-UBA), Buenos Aires, Argentina
[6] Instituto de Física de Rosario (IFIR) - CONICET/U.N.R. and Facultad de Ciencias Bioquímicas y Farmacéuticas U.N.R., Rosario, Argentina
[7] Instituto de Tecnologías en Detección y Astropartículas (CNEA, CONICET, UNSAM), and National Technological University, Faculty Mendoza (CONICET/CNEA), Mendoza, Argentina
[8] Instituto de Tecnologías en Detección y Astropartículas (CNEA, CONICET, UNSAM), Buenos Aires, Argentina
[9] Observatorio Pierre Auger, Malargüe, Argentina
[10] Observatorio Pierre Auger and Comisión Nacional de Energía Atómica, Malargüe, Argentina
[11] Universidad Tecnológica Nacional - Facultad Regional Buenos Aires, Buenos Aires, Argentina
[12] University of Adelaide, Adelaide, S.A., Australia
[13] Centro Brasileiro de Pesquisas Fisicas, Rio de Janeiro, RJ, Brazil

[14] Faculdade Independente do Nordeste, Vitória da Conquista, Brazil
[15] Universidade de São Paulo, Escola de Engenharia de Lorena, Lorena, SP, Brazil
[16] Universidade de São Paulo, Instituto de Física, São Carlos, SP, Brazil
[17] Universidade de São Paulo, Instituto de Física, São Paulo, SP, Brazil
[18] Universidade Estadual de Campinas, IFGW, Campinas, SP, Brazil
[19] Universidade Estadual de Feira de Santana, Brazil
[20] Universidade Federal da Bahia, Salvador, BA, Brazil
[21] Universidade Federal de Pelotas, Pelotas, RS, Brazil
[22] Universidade Federal do ABC, Santo André, SP, Brazil
[23] Universidade Federal do Rio de Janeiro, Instituto de Física, Rio de Janeiro, RJ, Brazil
[24] Universidade Federal Fluminense, EEIMVR, Volta Redonda, RJ, Brazil
[25] Rudjer Bošković Institute, 10000 Zagreb, Croatia
[26] Charles University, Faculty of Mathematics and Physics, Institute of Particle and Nuclear Physics, Prague, Czech Republic
[27] Institute of Physics of the Academy of Sciences of the Czech Republic, Prague, Czech Republic
[28] Palacky University, RCPTM, Olomouc, Czech Republic
[29] Institut de Physique Nucléaire d'Orsay (IPNO), Université Paris 11, CNRS-IN2P3, France
[30] Laboratoire de l'Accélérateur Linéaire (LAL), Université Paris 11, CNRS-IN2P3, France
[31] Laboratoire de Physique Nucléaire et de Hautes Energies (LPNHE), Universités Paris 6 et Paris 7, CNRS-IN2P3, Paris, France
[32] Laboratoire de Physique Subatomique et de Cosmologie (LPSC), Université Joseph Fourier Grenoble, CNRS-IN2P3, Grenoble INP, France
[33] Station de Radioastronomie de Nançay, Observatoire de Paris, CNRS/INSU, France
[34] SUBATECH, École des Mines de Nantes, CNRS-IN2P3, Université de Nantes, France
[35] Bergische Universität Wuppertal, Wuppertal, Germany
[36] Karlsruhe Institute of Technology - Campus North - Institut für Kernphysik, Karlsruhe, Germany
[37] Karlsruhe Institute of Technology - Campus North - Institut für Prozessdatenverarbeitung und Elektronik, Karlsruhe, Germany
[38] Karlsruhe Institute of Technology - Campus South - Institut für Experimentelle Kernphysik (IEKP), Karlsruhe, Germany
[39] Max-Planck-Institut für Radioastronomie, Bonn, Germany
[40] RWTH Aachen University, III. Physikalisches Institut A, Aachen, Germany
[41] Universität Hamburg, Hamburg, Germany
[42] Universität Siegen, Siegen, Germany
[43] Dipartimento di Fisica dell'Università and INFN, Genova, Italy
[44] Università di Milano and Sezione INFN, Milan, Italy
[45] Università di Napoli "Federico II" and Sezione INFN, Napoli, Italy
[46] Università di Roma II "Tor Vergata" and Sezione INFN, Roma, Italy
[47] Università di Catania and Sezione INFN, Catania, Italy
[48] Università di Torino and Sezione INFN, Torino, Italy
[49] Dipartimento di Matematica e Fisica "E. De Giorgi" dell'Università del Salento and Sezione INFN, Lecce, Italy

[50] Dipartimento di Scienze Fisiche e Chimiche dell'Università dell'Aquila and INFN, Italy

[51] Gran Sasso Science Institute (INFN), L'Aquila, Italy

[52] Istituto di Astrofisica Spaziale e Fisica Cosmica di Palermo (INAF), Palermo, Italy

[53] INFN, Laboratori Nazionali del Gran Sasso, Assergi (L'Aquila), Italy

[54] Osservatorio Astrofisico di Torino (INAF), Università di Torino and Sezione INFN, Torino, Italy

[55] Benemérita Universidad Autónoma de Puebla, Puebla, Mexico

[56] Centro de Investigación y de Estudios Avanzados del IPN (CINVESTAV), México, Mexico

[57] Universidad Michoacana de San Nicolas de Hidalgo, Morelia, Michoacan, Mexico

[58] Universidad Nacional Autonoma de Mexico, Mexico, D.F., Mexico

[59] IMAPP, Radboud University Nijmegen, Netherlands

[60] Kernfysisch Versneller Instituut, University of Groningen, Groningen, Netherlands

[61] Nikhef, Science Park, Amsterdam, Netherlands

[62] ASTRON, Dwingeloo, Netherlands

[63] Institute of Nuclear Physics PAN, Krakow, Poland

[64] University of Łódź, Łódź, Poland

[65] Laboratório de Instrumentação e Física Experimental de Partículas - LIP and Instituto Superior Técnico - IST, Universidade de Lisboa - UL, Portugal

[66] 'Horia Hulubei' National Institute for Physics and Nuclear Engineering, Bucharest-Magurele, Romania

[67] Institute of Space Sciences, Bucharest, Romania

[68] University of Bucharest, Physics Department, Romania

[69] University Politehnica of Bucharest, Romania

[70] J. Stefan Institute, Ljubljana, Slovenia

[71] Laboratory for Astroparticle Physics, University of Nova Gorica, Slovenia

[72] Institut de Física Corpuscular, CSIC-Universitat de València, Valencia, Spain

[73] Universidad Complutense de Madrid, Madrid, Spain

[74] Universidad de Alcalá, Alcalá de Henares (Madrid), Spain

[75] Universidad de Granada and C.A.F.P.E., Granada, Spain

[76] Universidad de Santiago de Compostela, Spain

[77] School of Physics and Astronomy, University of Leeds, United Kingdom

[79] Case Western Reserve University, Cleveland, OH, USA

[80] Colorado School of Mines, Golden, CO, USA

[81] Colorado State University, Fort Collins, CO, USA

[82] Colorado State University, Pueblo, CO, USA

[83] Fermilab, Batavia, IL, USA

[84] Los Alamos National Laboratory, Los Alamos, NM, USA

[85] Louisiana State University, Baton Rouge, LA, USA

[86] Michigan Technological University, Houghton, MI, USA

[87] New York University, New York, NY, USA

[88] Northeastern University, Boston, MA, USA

[89] Ohio State University, Columbus, OH, USA

[90] Pennsylvania State University, University Park, PA, USA

[91] University of Chicago, Enrico Fermi Institute, Chicago, IL, USA

[92] University of Hawaii, Honolulu, HI, USA
[93] University of Nebraska, Lincoln, NE, USA
[94] University of New Mexico, Albuquerque, NM, USA
[95] University of Wisconsin, Madison, WI, USA
[96] University of Wisconsin, Milwaukee, WI, USA
[97] Institute for Nuclear Science and Technology (INST), Hanoi, Vietnam

(‡) Deceased
(a) Now at Konan University
(b) Also at the Universidad Autonoma de Chiapas on leave of absence from Cinvestav
(c) Now at NYU Abu Dhabi

PALXA Experiment
Design of a Microbeam in sub-keV region and an high voltage control system for high energy X-ray

Libero Palladino[a,b], Maurizio Di Paolo Emilio[a,b]

[a] Mesva Department of L'Aquila University
[b] INFN, Laboratorio Nazionale del Gran Sasso, Assergi (AQ)

Abstract

In this report, we present the activity of PLAXA Experiment in the year of 2013. The experiment that has resulted in the creation of an X-ray source with a spectrum of X-ray emission between 70 eV and 30 keV, is based on the generation of a plasma obtained by focusing a laser beam on a target of a different material. The activity can be divided in two parts:
- Development and characterization of soft X-rays Microbeam system in the range of energy 70 eV - 1 keV
- Improvement and simulation of High Voltage System for high energy X-rays emission.
In particular, we present the geometry of the optical system, the software/hardware control and the preliminary measures of the first configuration of soft x-ray Microbeam system (70 eV - 1 keV). Moreover, preliminary results of high energy x-rays emission, the design and simulation with p-spice of the high voltage system will be described.

1   Introduction

Different applications of soft X-rays ($\sim$70 eV - 2 keV) and hard x-rays ($\sim$3 keV - 25 keV) in biological, radiobiological and in medical imaging field, have encouraged the development of X ray sources based on the production of plasma. The x-rays emission is due to plasma obtained focalizing an high power Nd-YAG laser beam on different targets. Plasmas produced by focusing pulsed laser beams on solid targets are currently recognized as one of the most promising alternative to conventional (X-ray tubes) and to synchrotron X-ray sources. Optimization of pulsed x-rays sources ($\sim$3 keV - 25 keV), due to the

212

plasma electrons accelerated by an electric field, it is necessary to make x-rays source comparable with the most advanced current x-ray tubes (i.e. microfocus) for applications in the field of mammography and non-destructive inspection.

The microbeams plays an important role in the study of the biological effect of the ionizing radiation at low dose and low energy photons (100 eV - 1 keV). The microscopic size of the beam at the focus point allows to irradiate the cells or parts thereof. Using an x-ray microbeam single cell approach, it has been possible to study different implications, such as apoptosis of the bystander effect [1][2].

2 Soft x-rays: Microbeam

The x-ray micro-beams are important experimental tool due to two significant characteristics: the micrometer size of the focal spot and the high monocromaticity of the photon energy. The wavelength of soft x-rays selected is 2.48 nm. To collect and select soft x-rays at 2.48 nm we use a multilayer spherical mirror [3][4][5].

2.1 Experimental Layout

The choice of the 2.48 nm wavelength is related to the interaction, thought the photoelectric effect, with the biological structures as indicated in figure 1 and 2: where is shown the linear absorption coefficient and transmission profiles for different biological material.
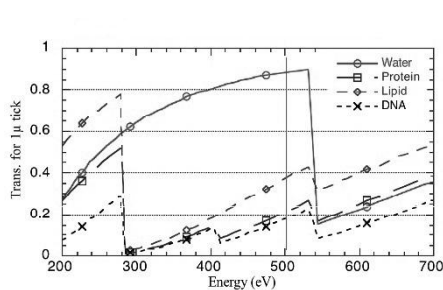
(a) Figure 1: transmission profile of the x-ray for different biological components (thick. 1 μm)
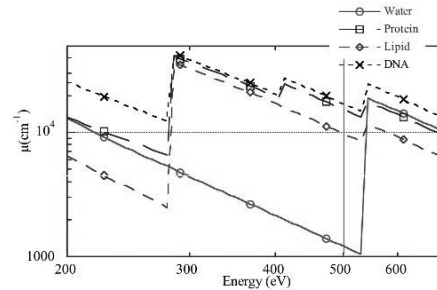
(b) Figure 2: linear absorption coefficients of the x-ray for different biological components.

The experimental layout is shown in figure 3 and 4 where is represented its outline. The interaction chamber is composed of lense (L), mirror (S), target (T): both, run on rails driven by step-by-step motors controlled by computer (4 stepper motors and 1 DC motor). The sensitivity of the whole movement is 1 μm. The centre of the chamber is indicated with C and biological sample position in B (figure 3 and 4). Moreover, is indicated the direction of focalized laser beam and x- ray emission from plasma. A single triangle SCT, togheter the biological sample position must satisfies the optical equation of the mirrors and the constancy of the incidence angle on the mirror simultaneously. The x ray plasma emission depends on the material: in our case we use the yttrium (Y 39)

that has a high x-ray conversion efficiency to 2.48 nm and will be used as target in the plasma source. To protect the mirror from the debris, produced during the formation of the plasma, we used a window of protection of 50 nm thick silicon nitride. The software used for management of the system is designed by high level programming language; the hardware is composed of 5 serials controllers, 4 stepper motors and 1 DC motor. The controller gives a number of features to achieve automation and handling tasks in research and industry in a very cost effective way. Programming is facilitated by the high- level mnemonic command language with macro and compound command functionality [5].
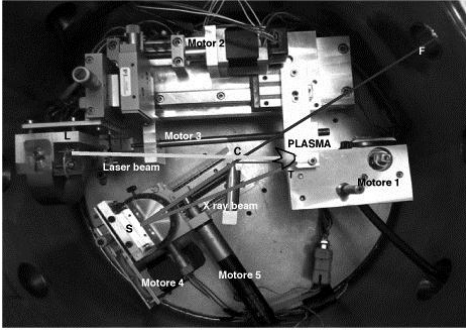
(c) Figure 3: inside of the interaction chamber
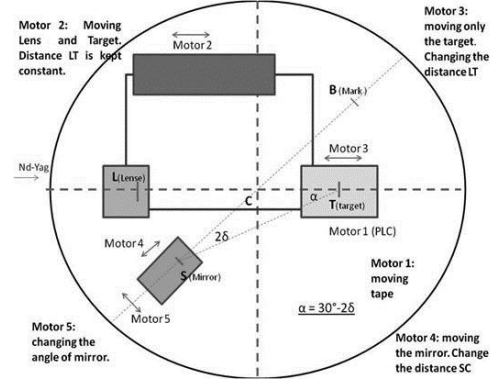
(d) Figure 4: general hardware and software setup

2.2 Measures and first configuration of Microbeam

In reference to figure 3 the target was placed at the center of the interaction chamber and the pin diode detector (by Emerge Corporation, 125 μm of intrinsic zone) was placed at distance of 84.5 cm from plasma. The detector was placed at an angle of 30 degrees in direction of the laser beam with a 7 mm diameter sensitive area. To measure the conversion efficiency in the range of about 300-510 eV and between about 450 and 800 eV, a 1 μm tick vanadium microfoil and a 1 μm tick nickel microfoil were placed in front of entrance window of the detector respectively. For the measurements of the radiation component of more than 800 eV, we used an 7.5 μm thick aluminum microfoil. In the table of figure 5 is shown analysis of x- ray efficiency at 3.7 J laser beam energy [5]. The charge represented in the following equations are the integrated signal of the detector filtered with Y, Ni and respectively:

$$Q_v^{tot} \propto \int S(E_x) T_{DL}(E_x) T_v^{t=1\mu m}(E_x) dE_x \tag{1}$$

$$Q_N^{tot} \propto \int S(E_x) T_{DL}(E_x) T_{Ni}^{t=1\mu m}(E_x) dE_x \tag{2}$$

$$Q_{Al}^{tot} \propto \int S(E_x) T_{DL}(E_x) T_{Al}^{t=7.5\mu m}(E_x) dE_x \tag{3}$$

T coefficients are the transmission profiles visualized in figure 6 for each filter and dead

Target MYLAR - E $_{laser}$ = 3.7 J +- 0.2 J

W (W/cm²)	Filter	Energy Interval (eV)	E$_X$ (mJ in 2π sr)	η% (in 2π sr)
1.6 x 10^{13}	V 1 μm tick	300 - 510	146.6	4.0
1.6 x 10^{13}	Ni 1 μm tick	450 - 850	83.6	2.3
1.6 x 10^{13}	Al 7.5 μm tick	> 800 eV	1.2	3 x 10^{-2}

Target Y - E $_{laser}$ = 3.7 J +- 0.2 J

W (W/cm²)	Filter	Energy Interval (eV)	E$_X$ (mJ in 2π sr)	η% (in 2π sr)
1.6 x 10^{13}	V 1 μm tick	300 - 510	413.4	11.2
1.6 x 10^{13}	Ni 1 μm tick	500 - 850	67.2	1.8
1.6 x 10^{13}	Al 7.5 μm tick	> 800 eV	1.6	4 x 10^{-2}

Figure 5: x-ray intensity measurements, $E_{laser} = 3.7$ J

layer (DL) of detector. From results we can noted a better x-ray efficiency for Yttrium than the Mylar (Figure 5).
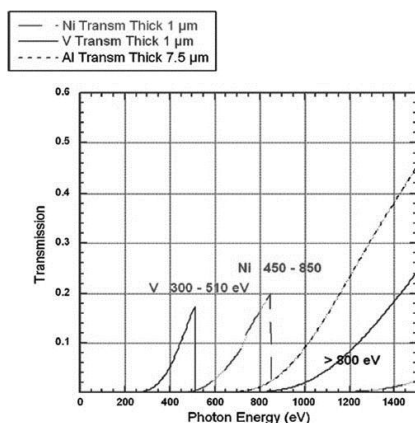
(e) Figure 6: transmission curves for three microfoils used
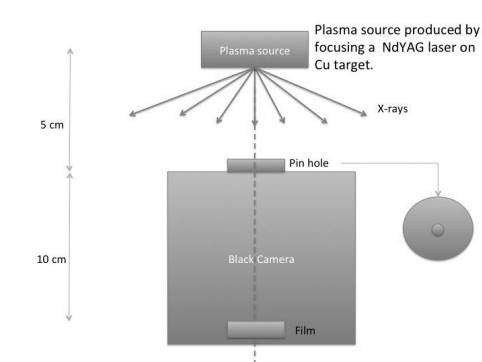
(f) Figure 7: Outline used to measure the spot size

First of characterization of x-ray microbeam optic, we have estimated the dimension of the source using a pin hole camera filtered with 3 μm thick aluminum foil. In the figure 7 is shown the outline used to measure the pot size where the distance of plasma source-pin hole is 5 cm and distance of pin hole - film is 10 cm. The dimension of pin hole in entrance windows is 25 μm and the image of source was captured by film kodak def.

The film image of the source is acquired at 4800 dpi resolution corresponding to 5.3 μm pixel dimension (Figure 8). The optical density of the system is up to 4. In the figure 8 we can observe a peak of image source with S/N ratio maximum about 3. In the figure 9 we report the profile of this peak and estimated the spot size to be around 27.5 μm at the FWHM. The microbeam setup (first configuration) is shown in figure 10

where is indicated the distances and materials filter used for the characterization of x-ray microbeam intensity at 2.48 nm. The 2.48 nm monochromatic microbeam is obtained by using a multilayer spherical mirror of 15 mm aperture radius and 256 mm of curvature radius which selects the wavelength of x-rays at an 8 degrees incidence angle from the normal of the mirror.
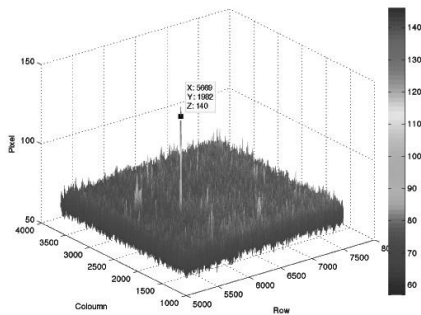
(g) Figure 8: density profile of the source image obtained by pin hole camera
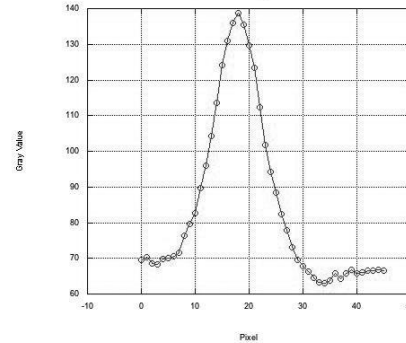
(h) Figure 9: Profile x-ray spot
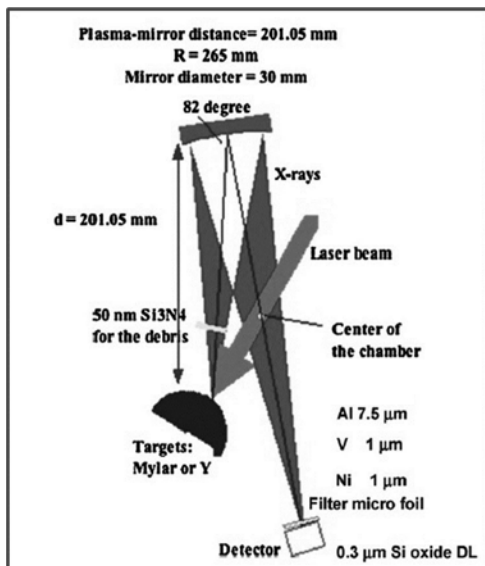
(i) Figure 10: Microbeam setup
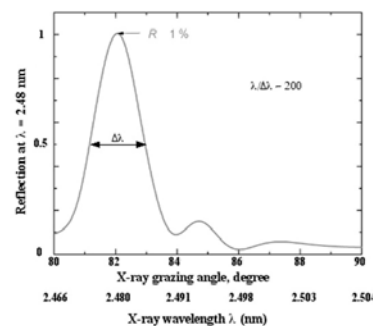
(j) Figure 11: Curve of the reflectivity

In the figure 11 is shown the curve of the reflectivity of the multilayer deposited on the substrate of the spherical mirror (Reflectivity is about 1% - Bragg angle of 82 @ 500 eV) and wavelength resolution of about 200. The focalized point of the beam was formed at a distance of 400.2 mm from the mirror.To analyze the x-ray intensity at 2.48 nm we used a Pin Diode placed in the proximity of the focus point of the monochromatic beam filtered with 1 μm Vanadium thick foil. The choice of vanadium filter is due to the good

216

transmission in this x-ray region (about 20%) and to separate the ultraviolet and visible window. The charge which we have collected by Pin diode was 4 nC.

3 High Voltage System for high energy X-rays emission

Optimization of pulsed x-rays sources ($\sim$ 3 keV - 25 keV) it is necessary to make x-rays source comparable with the most advanced current x-ray tubes. There are many variables that allow us to get this optimization but the electrical parameters are especially the basis of the choice for the high voltage system configuration. The reason to obtain a high voltage through a LC inverter is because of the system is working with high voltage in the discharge phase, but during the charge of the capacitors the system is isolated which is essential for the safety and average life of the electrical components [6] [7].

3.1 Experimental Apparatus

The x-rays of the higher energy region (about 25 keV) is produced for bremmsthralung effect. The relative configuration of the interaction chamber is shown in figure 12. The main feature is to apply the High voltage (30 - 50 kV) from the target, on which the laser is focalized, (cathode) to the anode (such as metallic materials Mo or W) where x-rays are produced. The mechanism of x-rays production is based on the generation of a plasma obtained by focusing a laser beam NdYag (5J per pulse, duration 6 ns, 0.3 mrad divergence, 536 nm wavelength) on a target metal.

The apparatus for the High Energy X-rays generation is composed of interaction chamber in the vacuum (10^{-6}mbar) and two main circuits systems: a power supply that provides a maximum voltage of 40 kV and an LC-inverter circuit. A Rogowsky loop is used to measure the intensity of the electronic current.

High Voltage System is composed of following sub-circuits:

- High Voltage Power Supply

- Trigger circuit for Spark-Gap

- Trigger circuit for Thyratron

- LC Inverter

A customize high power supply is applied to spark gap for generating a discharge to produces x-rays. The Maximum voltage is around 40 kV. Spark Gap is a high power three-terminal switch which is used to be activated the discharge. It is composed of 3 poles: two poles are connected to the power supply and the central pole is connected to the output of the trigger circuit for spark gap.

A trigger circuit for Spark Gap (Figure 13) consists in a LC inverter and a Thyratron,

217
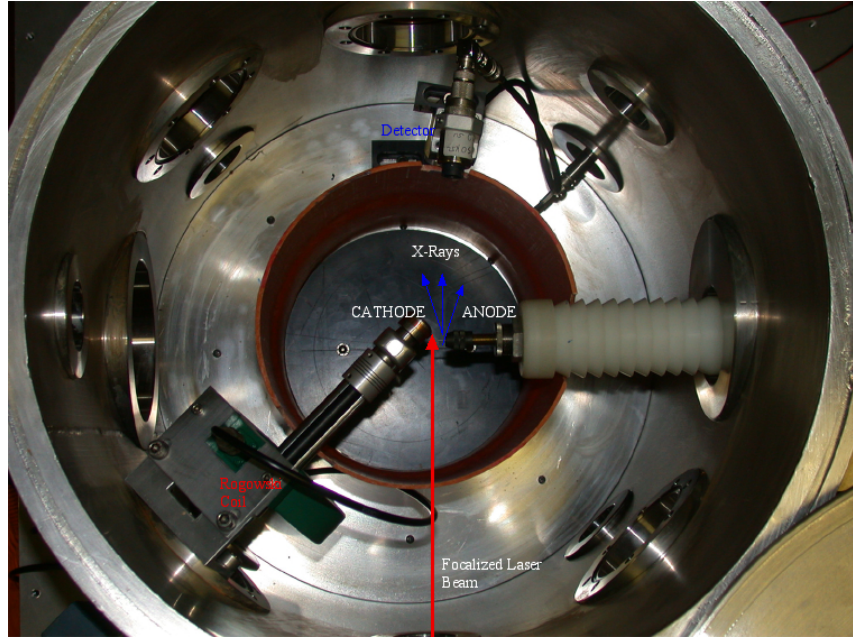
Figure 12: Interaction chamber (inside)

which is used as high electrical power switch. The trigger circuit for Thyratron is shown in figure 14 and is used to generate the peak voltage sent to the Thyratron (Figure 15). The control signal of the Silicon Controlled Rectifier (SCR) is obtained with a customize circuit as shown in figure 15. Moreover, a LC inverter (Figure 16) is used to activate the discharge by charging a couple of capacitors of 1.5 μF.

From the p-spice analysis we can observe a signal with the maximum value around 20kV in the output of the trigger circuit for spark gap (Figure 17): if this values is higher, it could damage the system, in oppositely, the discharge cant be activated. Its important that the intensity in the output of the trigger circuit for spark gap is about 20 kV.

The LC-Inverter (Figure 16) is the most important circuit in the high voltage system
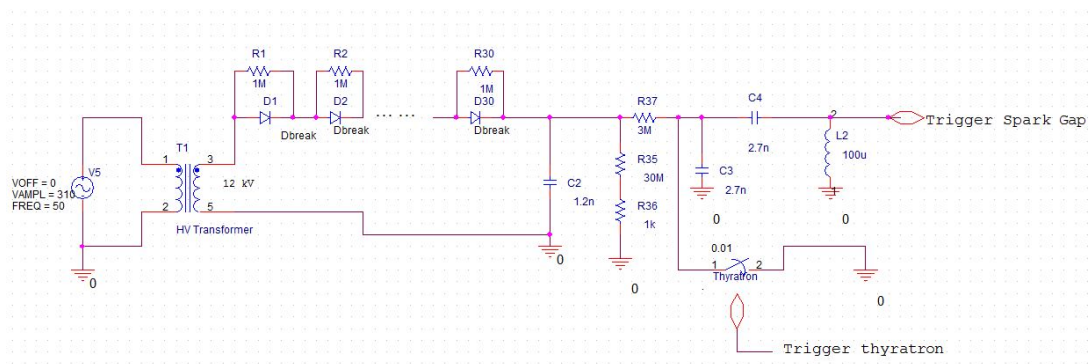
Figure 13: Trigger circuit for spark gap
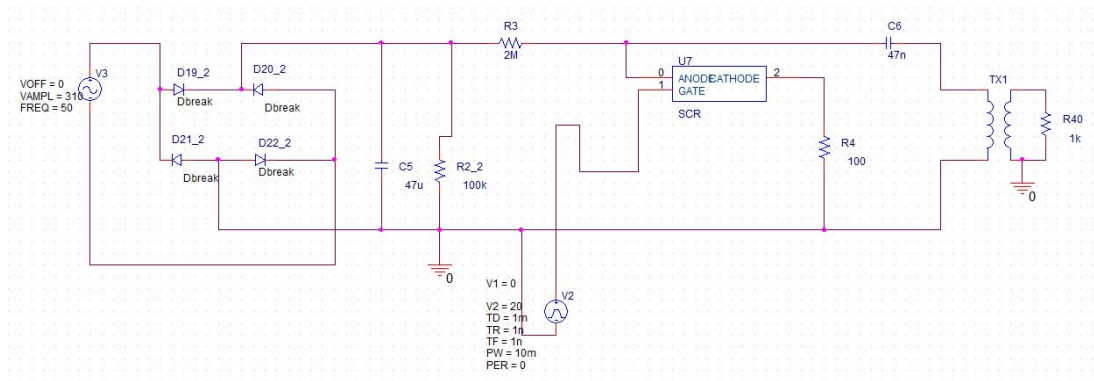
Figure 14: Trigger circuit for the Thyratron
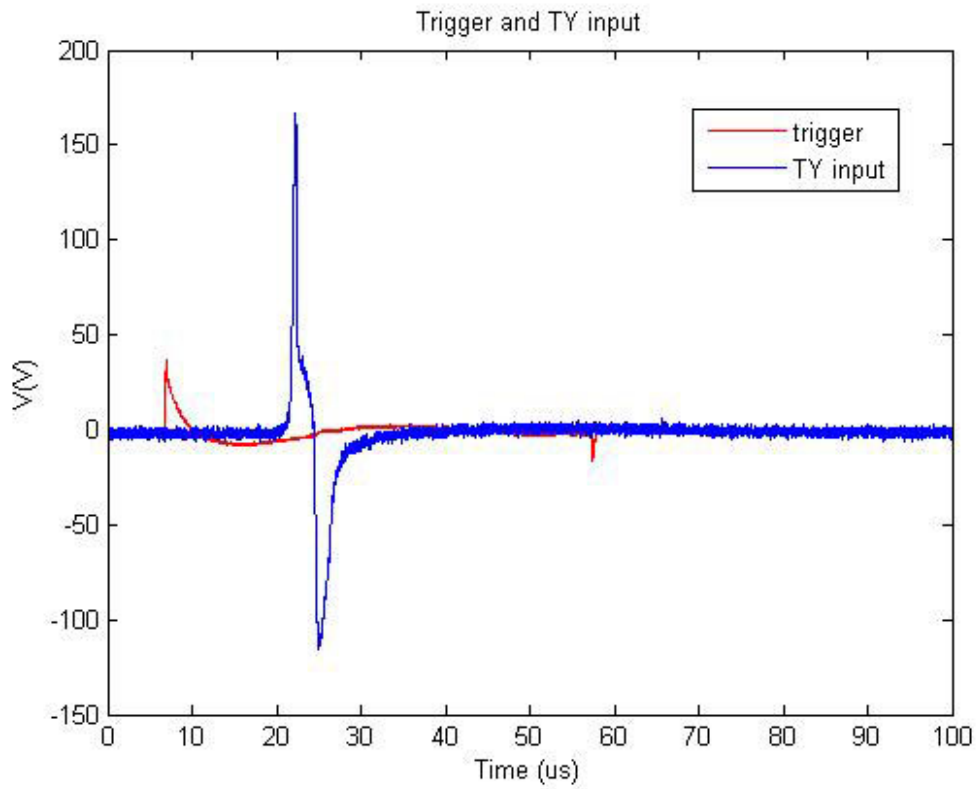
Figure 15: Output of the trigger circuit for thyratron (blu line). In red line the control signal of the SCR (Silicon Controlled Rectifier)
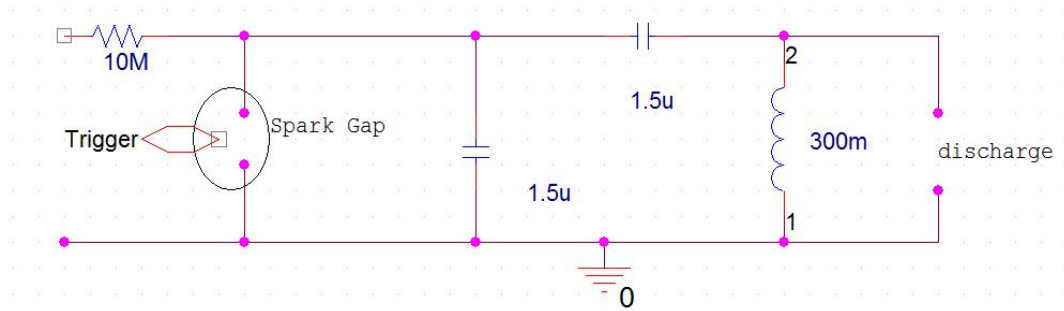
Figure 16: LC Inverter
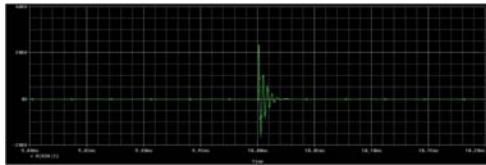
(k) Figure 17: output of the trigger circuit for spark gap
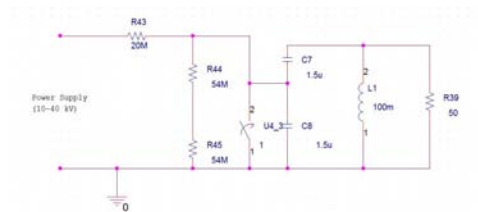
(l) Figure 18: LC Inverter Pspice model

to control the intensity of x-rays. In figure 18 the schematic representation of the p-spice model.

In figure 19 a typical voltage signal in output of LC inverter from P-spice simulation is shown. According to the experimental measurements (Figure 20), we obtained a similar signal with different damping due to the approximation of the model but with the same maximum value. All high voltage system is immersed in transformer oil (Figure 21) to isolate from the environment.

(m) Figure 19: output voltage of LC inverter (Model)
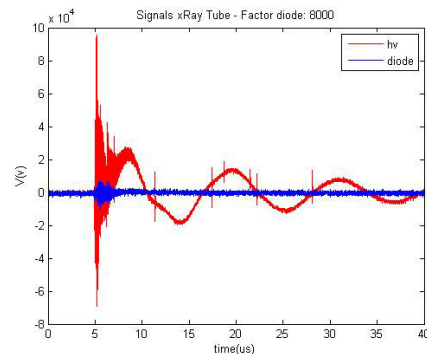
(n) Figure 20: output voltage of experimental LC inverter signal (red line)

220
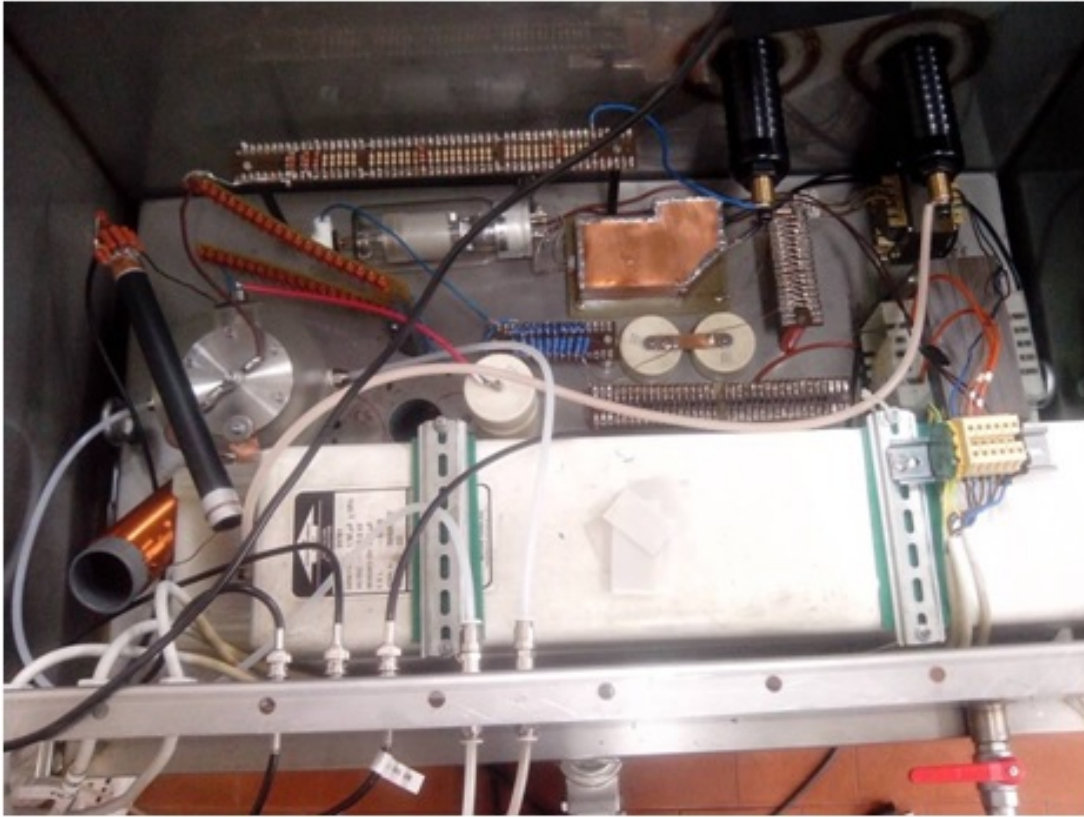
Figure 21: High Voltage system
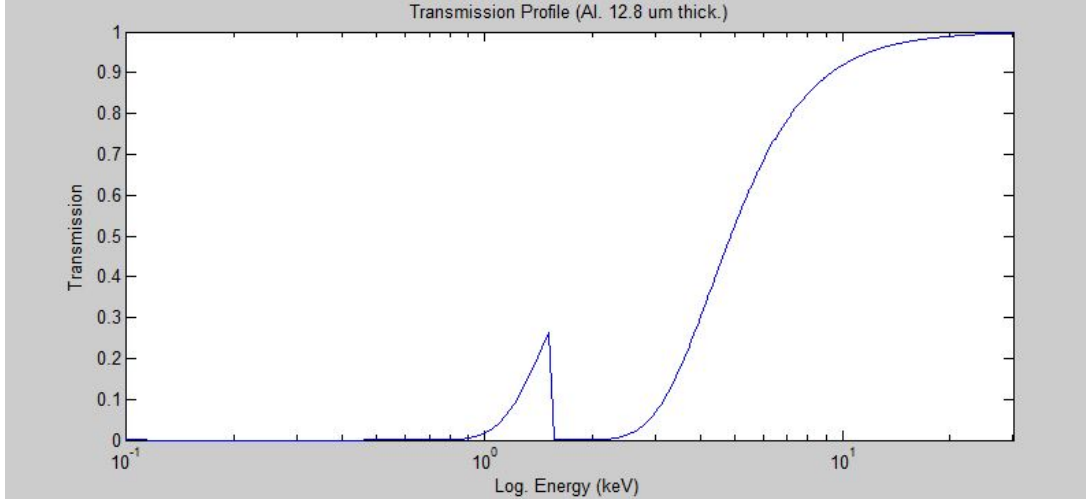
Figure 22: Profile transmission of aluminum (Thick. 12.8 μm) [7]

3.2   Preliminary results

From the results of p-spice model, we have tested the system by analyzing the emission of x- rays for iron target measured by photodetector from Quantrad system (diameter of 7.5 mm, absorption layer of 125 μm and dead layer of 0.3 μ). On the entrance window of photodetector, there is an aluminum foils of 12.8 μm thickness (Figure 22). The distance between photodector and cathode is 10.5 cm.

15 kV of power supply is applied in two poles of spark gap (which is the input of the circuit of figure 18); in according to the high voltage system the discharge voltage is around 25 kV. System Energy is estimated to be around 240 J. Inside the interaction chamber, we exposed films by Kodak (Film Dentaire ultra speed), to capture the sample of x-ray images (iron cross): one with aluminum foil of 12.8 μm thickness and another without aluminum foils. The x-ray images of iron cross are shown in Figure 23 where is noted a better image in the film with aluminum foil; in fact, in the film without filter, it has a blurring due to all x-rays energies components (around keV and greater than 5 keV). Since x-ray image is formed with all energies components that have a different absorption coefficient, the image of the film is not well defined. While in the film filtered is selected by a spectra where Kα and Kβ energies emission of iron are more intense. In figure 24 is shown the signal of the photodiode and current intensity.

According to the standard bremsstrahlung profile [8]:

$$I \propto Z((\frac{1}{\lambda_{mim}} - \frac{1}{\lambda})\frac{1}{\lambda^2}) \tag{4}$$

and taking into the consideration of the detector quantum efficiency, we have calculated the complete profile (Figure 25). From these values, we have estimated the number of photons in the input of the photodiode of $\sim 10^8$. Considering the emission of x-rays on a 4π sr solid angle, the total number of x-rays photons emitted is $\sim 10^{12}$. From these analysis we can see that the number of emitted photons is comparable with present X-ray tubes but with the difference that in our source, x-rays are emitted with a time of the
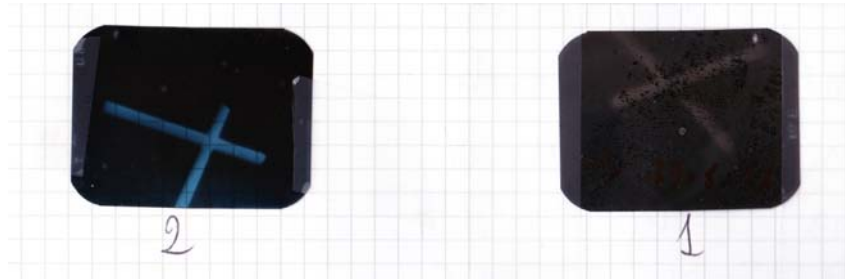
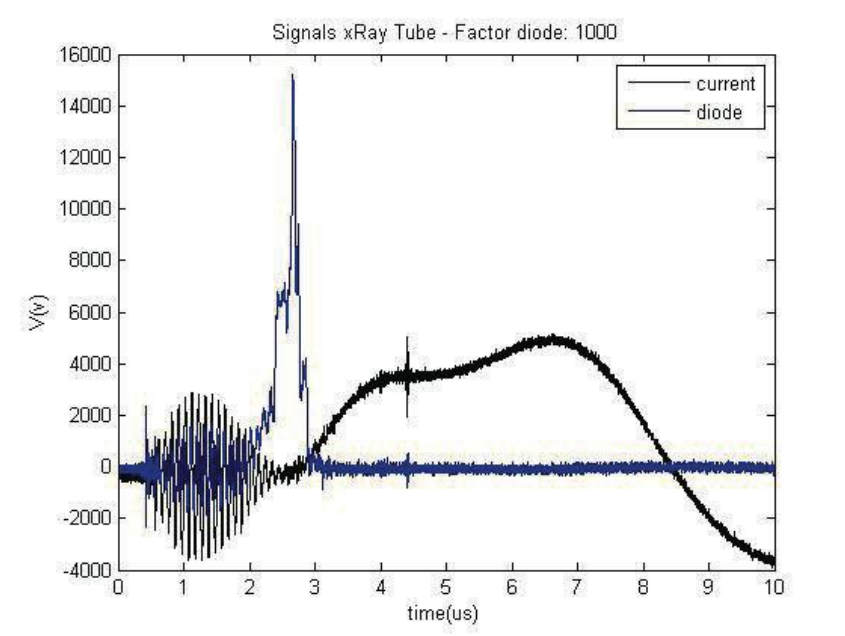Figure 23: X-ray images captured using Films Dentaire by Kodak. Film without aluminum (1), Film with Aluminum (2)

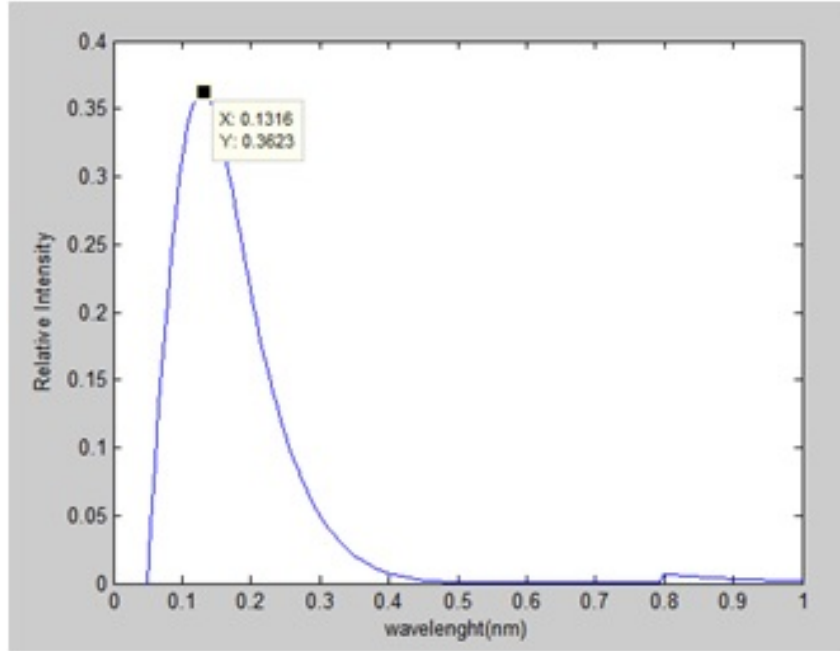Figure 24: Output of photodiode (blue line) and current intensity (black line)

Figure 25: Complete Bremsstrahlung profile

order of μs (figure 24), to be compared with the time of x-ray tubes traditional ranging from about 0.01 s to 10 s [9]. Another advantage of our High Voltage system is the LC-inverter; it allows to isolate the complete system during the charging phase which is essential for the safety of both people and electronic components.

4   Conclusions

In the preliminary measures about the Microbeam system, Yttrium conversion efficiency was sistematically 2 or 3 times larger than Mylar conversion efficiency in water window. The difference is due to the kind of spectrum emitted by the two materials used. The soft x-rays were generated from an yttrium target (energy of 3.7 J). Yttrium can be considered a good candidate for soft x- ray microbeam. The Microbeam setup will be be used in the future to obtain monochromatic beams with different optical configurations as parallel beam. We are planing to reduce the magnification of x-ray microbeam at value less or equal to 1, reconfiguring the optical mechanical layout. In the range of x-ray energy of 3 keV - 25 keV, we have studied a possible p-spice model to evaluate the electrical characteristics of the high voltage system to optimize the emission of x-rays. A possible future configuration will be to use an IGBT (Insulated Gate Bipolar Transistor) instead of Thyratron to compact the system and increase the energy [10]. In near future we will improve the synchronization of the system between trigger discharge with pulse laser beam. Moreover, we will examine x-rays emission by changing the distance from anode and cathode and power density of the laser.

5   Acknowledgements

References

[1] Gerardi S. (2009) **Ionizing radiation microbeam facilities for radiobiological studies in Europe**, *Journal of Radiation Research*, 50, A13- A 20.

[2] L. Palladino, **Annual Report 2010, INFN Laboratori Nazionali del Gran Sasso**, - *Link: http://www.lngs.infn.it/lngsinfn/contents/lngsit/research/experimentsscientificinfo/ librarypublications/preprintreports/report10/lasex.pdf*

[3] K.M. Prise, G. Schettino, et al. (2009), **Microbeam Studies of the Bystander Response.** , *Radiat. Res. (Tokyo) 50 (2009) A1-A6.*

[4] C. Van Oven et all, **An ultra x-ray multi- microbeam irradiation system for studies of DNA damage responses by fixed and live cell fluorescence microscopy**, *Springer European Biophysics Journal (2009) .*

[5] L. Palladino et all (2013) **X-ray emission analysis of a plasma source using an yttrium and a mylar target for the generation of 2.48 nm wavelength microbeam**, *Applied Surface Science, 272, 119-123.*

[6] Habetler, T.G. et all, **Design and implementation of an inverter output LC filter used for dv/dt reduction**, *Power Electronics, IEEE Transactions on (Volume:17 , Issue: 3)*

[7] Calculated from **http : //henke.lbl.gov/opticalconstants/filter2.html**,

[8] E. Bertin, **Introduction to x-ray spectrometric analysis**, *Springer Science+Business Media, LLC*

[9] **Data sheet of commercial X-ray Tube**, *http://www.varian.com/media/xray/products/pdf/m105sp.pdf Varian Medical System*

[10] S.L. Gold, Thyratron-PFN, **IGBT Hybrid, and Direct Switched Modulator R&D as it Effects**, *Klystron Protection SLAC-PUB-8475 June 2000*